

General Distribution
NEA/CSNI/R(92)17

OECD

NEA

ISP 28

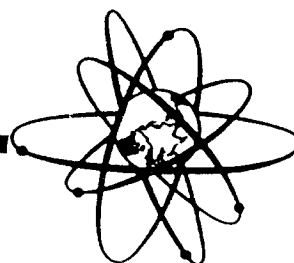
*OECD/NEA/CSNI
International Standard Problem N° 28*

*Phebus-SFD B9+ Experiment
on the Degradation of a PWR Type Core*

COMPARISON REPORT

Volume 1

December 1992



COMMITTEE ON THE SAFETY OF NUCLEAR INSTALLATIONS (CSNI)
OECD NUCLEAR ENERGY AGENCY
Le Seine Saint-Germain - 12, boulevard des Iles
92130 Issy-les-Moulineaux, France

LIBRARY
OECD Nuclear Energy Agency
12, Boulevard des Iles
92130 ISSY-LES-MOULINEAUX
FRANCE



DEPARTEMENT DE RECHERCHES EN
SECURITE

Cadarache, le 21/06/93

SERVICE D'ETUDES ET DE
MODELISATION
D'ACCIDENTS DE REACTEURS

BA/FT
Nb de Pages : 105

Laboratoire de Physique des Accidents
Groupe Physique Accidentelle des Matériaux

RAPPORT TECHNIQUE SEMAR 92/82
NOTE PHEBUS CSD 92/134
OECD/NEA/CSNI/R (92) 17

INTERNATIONAL STANDARD PROBLEM N°28

PHEBUS-SFD B9 + EXPERIMENT
ON THE DEGRADATION OF A PWR CORE TYPE

Comparison report - Volume 1

Authors
B. ADROGUER* - A. COMMANDE**
C. RONGIER* - M. MULET**

December 1992

*CEA/IPSN/DRS - CADARACHE
**CISI INGENIERIE - AIX EN PROVENCE

LABORATOIRE DE PHYSIQUE DES ACCIDENTS

 B. ADROGUER 28/06/93	 M. SCHWARZ 13/07/93	 G. HACHE 13/7/93
Rédaction : Nom/Visa/Date	Vérification : Nom/Visa/Date	Approbation : Nom/Visa/Date

This document, which contains proprietary or other confidential or privileged information, and any reproduction in whole or in part, shall not be disseminated outside the organization of the recipient without prior approval of the IPSN.



CONTENT

1 - INTRODUCTION	8
2 - OVERVIEW OF THE ISP 28 EXERCISE	9
3 - PHEBUS - SFD B9+ EXPERIMENT	10
3.1 - Outline of the facility	10
3.2 - Bundle description and measurements	11
3.3 - Objectives and experimental conditions of the B9+ test	12
3.3.1 - Objectives of the B9+ test	12
3.3.2 - Scenario and T/H boundary conditions	12
3.3.3 - Radial boundary conditions in the shroud	13
3.3.3.1 - Comments on the shroud	13
3.3.3.2 - Thermal radial boundary conditions	14
3.3.4 - Nuclear power history and distribution	16
3.3.4.1 - History	16
3.3.4.2 - Radial and axial distributions	16
3.3.5 - Experimental uncertainties	17
4 - MAIN PHENOMENA OBSERVED	18
4.1 - Thermal behaviour	18
4.2 - Oxidation behaviour	19
4.3 - Hydrogen release	20
4.4 - Inconel spacer grids	20
4.5 - UO ₂ dissolution by solid Zry	21
4.6 - UO ₂ dissolution by molten Zry	21
4.7 - ZrO ₂ dissolution by molten Zry	22
4.8 - Relocation of molten mixtures	22
4.9 - Bundle blockage	23
5 - OVERVIEW OF PARTICIPANTS' MODELS	25
5.1 - Physical models of degradation	25
5.2 - Nodalization of the PHEBUS bundle	26
5.3 - Shroud modelling	26
5.4 - Nuclear power	27
6 - COMPARISONS OF INDIVIDUAL RESULTS WITH THE EXPERIMENT	27
6.1 - FRA-SP (Annex 1) : ICARE2/V2p calculation	28
6.2 - SP-CSN (Annex 2) : SCDAP MOD1 Stand-alone code	29
6.3 - SP-UPM (Annex 3) : MELCOR V1.8.0 calculation	29
6.4 - CZECHOSLOVAKIA (Annex 4) : FRAS - SFD calculation	30
6.5 - GER-IKE1 and IKE2 (Annex 5a, Annex 5b) : KESS III calculation	30
6.6 - GER - GRS1 and GRS 2 (Annex 6a, Annex 6b) : ATHLET SA calculation	32
6.7 - HUNGARY (Annex 7) : MARCH3 calculation	33
6.8 - I-PISE (Annex 8) : SCDAP/RELAP5 MOD2 calculation	33
6.9 - ISPRA (Annex 9) : ICARE2 V1 calculation	34
6.10 - JAPAN (Annex 10) : SCDAP/R5 MOD1 calculation	35
6.11 - NETHER (Annex 11) : SCDAP/R5 MOD2.5 calculation	35
6.12 - SWEDEN (Annex 12) : SCDAP/R5 MOD2 calculation	36
6.13 - TAIWAN (Annex 13) : MELCOR V1.8.0 calculation	37
6.14 - UK (Annex 14) : SCDAP/R5 MOD2.5 Version 361SC	38
6.15 - U.S.A (Annex 15) : MELCOR V1.8EA calculation	39

7 - OVERVIEW OF THE COMPARISONS	40
7.1 - The Modelling of the B9+ transient	42
7.1.1 - Nodalization	42
7.1.2 - Difficulties	42
7.2 - Thermal behaviour	43
7.2.1 - Heat balance in the bundle	43
7.2.2 - Radial temperature profile	44
7.2.3 - Temperature escalation	45
7.2.4 - Fluid temperature at the bundle outlet	45
7.2.5 - Maximum temperature	45
7.3 - Oxidation and H2 production	46
7.3.1 - Cladding oxidation histories	46
7.3.2 - H2 production	47
7.3.3 - Experimental and modelling uncertainties	47
7.4 - Inconel spacer-grids	48
7.5 - Fuel dissolution by molten Zry	48
7.6 - Zirconia dissolution by molten Zry	50
7.7 - Relocation of molten materials and channel blockage	50
7.8 - Mixture compositions	54
7.9 - Code run time statistics	55
8 - CONCLUSIONS	56
- REFERENCES	61
- LIST OF ANNEXES (VOLUME 2)	63
- LIST OF TABLES (VOLUME 1)	64
- LIST FIGURES (VOLUME 1)	65
- LIST OF FIGURES FOR EACH CODE-T0-DATA ANNEX (VOLUME 2)	66
- TABLES	69
- FIGURES	84

<p align="center"><i>SERVICE D'ETUDES ET DE MODELISATION D'ACCIDENTS DE REACTEURS</i> <i>Laboratoire de Physique des Accidents</i></p>		
Nat. Document	RAPPORT TECHNIQUE SEMAR 92/82 NOTE PHEBUS CSD 92/134	
TITRE	INTERNATIONAL STANDARD PROBLEM ISP 28 PHEBUS-SFD B9 + EXPERIMENT ON THE DEGRADATION OF A PWR CORE TYPE Final comparison report - Volume 1	
Auteur(s)	B. ADROGUER - A. COMMANDE - C. RONGIER - M. MULET	
Type de Diffusion :	"Mots clés" : PHEBUS CSD B9+ ISP 28	Nbre pages: 105
	N° Fiche Action : 422 4110	Nbre annexes: 17
<p><i>Résumé :</i></p> <p>L'expérience PHEBUS CSD B9+ a été acceptée par l'OCDE/CSNI pour faire l'objet du Problème Standard International n° 28. L'objet de cet exercice était d'évaluer l'aptitude des codes à décrire la dégradation d'un coeur de type PWR et en particulier les principaux phénomènes observés dans l'essai B9+ : oxydation des gaines, émission d'H₂, dissolution de l'UO₂ par le Zr fondu et relocalisation des eutectiques formés. Ce problème organisé en condition semi-aveugle a fait l'objet de 15 calculs avec 7 codes différents. Les comparaisons calcul-expérience ont permis d'identifier les possibilités des codes, ainsi que des faiblesses et des manques, en particulier en ce qui concerne la liquéfaction de l'UO₂ et la relocalisation des eutectiques. Cet exercice illustre la nécessité d'améliorer et de compléter la modélisation des principaux phénomènes de dégradation d'un coeur et de mieux valider ces outils destinés aux calculs réacteur.</p> <p><i>Summary :</i></p> <p>The PHEBUS SFD B9+ test was accepted by OECD/CSNI as the International Standard Problem n° 28. The aim of this exercise was to assess the ability of the codes to describe the degradation of PWR-type cores and in particular to predict the main phenomena observed in B9+ : cladding oxidation H₂ production, fuel dissolution by molten Zr and relocation of melts resulting of chemical interaction. 15 calculations performed with 7 different codes were submitted in semi-blind conditions. Code to data comparisons enabled the current ability of the codes to be identified and to point out weaknesses and lacks regarding the UO₂ dissolution and melt relocation. Finally this exercise emphasized the need to improve and complete the modelling of the main degradation processes and to better assess these models to be used for reactor calculations.</p>		
Repère bureautique : RT1884.DOC		

OECD

In 1948, the United States offered Marshall Plan aid to Europe, provided the war-torn European countries worked together for their own recovery. This they did in the Organisation for European Economic Cooperation (OEEC). In 1960, Europe's fortunes had been restored ; her standard of living was higher than ever before. On both sides of the Atlantic the interdependence of the industrialised countries of the Western World was now widely recognised. Canada and the United States joined the European countries of the OEEC to create a new organisation, the Organisation for Economic Co-operation and Development. The Convention establishing the OECD was signed in Paris on 14th December 1960.

Pursuant to article 1 of the Convention, which came into force on 30th September 1961, the OECD shall promote policies designed :

- to achieve the highest sustainable economic growth and employment and a rising standard of living in Member countries, while maintaining financial stability, and this to contribute to the development of the world economy;
- to contribute to sound economic expansion in Member as well as non-member countries in the process of economic development; and
- to contribute to the expansion of world trade on a multilateral, non-discriminatory basis in accordance with international obligations.

The original Signatories of the Convention were Austria, Belgium, Canada, Denmark, France, the Federal Republic of Germany, Greece, Iceland, Ireland, Italy, Luxembourg, the Netherlands, Norway, Portugal, Spain, Sweden, Switzerland, Turkey, the United Kingdom and the United States. The following countries acceded subsequently to the Convention (the dates are those on which the instruments of accession were deposited) : Japan and New Zealand (29th May 1973).

NEA

The OECD Nuclear Energy Agency (NEA) was established on 20th April 1972, replacing the OECD's European Nuclear Energy Agency (ENEA established on 20th December 1957) on the adhesion of Japan as a full member.

The NEA now groups all the European Member countries of OECD and Australia, Canada, Japan and the United States. The Commission of the European Communities takes part in the work of the Agency. The primary objectives of NEA are to promote co-operation between its Member governments on the safety and regulatory aspects of nuclear development, and on assessing the future role of nuclear energy as a contributor to economic progress.

This is achieved by :

- encouraging harmonisation of government's regulatory policies and practices in the nuclear field, with particular reference to the safety of nuclear installations, protection of man against ionising radiation and preservation of the environment, radioactive waste management, and nuclear third party liability and insurance;
- keeping under review the technical and economic characteristics of nuclear power growth and of the nuclear fuel cycle, and assessing demand and supply for the different phases of nuclear power to overall energy demand;
- developing exchanges of scientific and technical information on nuclear energy, particularly through participation in common services;
- setting up international research and development programmes and undertakings jointly organised and operated by OECD countries.

In these and related tasks, NEA works in close collaboration with the International Atomic Energy Agency in Vienna, with which it has concluded a Co-operation Agreement, as well as with other international organisations in the nuclear field.

CSNI

The NEA Committee on the Safety of Nuclear Installations (CSNI) is an international committee made up of scientists and engineers. It was set up in 1973 to develop and coordinate the activities of the OECD Nuclear Energy Agency concerning the technical aspects of the design, construction and operation of nuclear installations insofar as they affect the safety of such installations. The Committee's purpose is to foster international co-operation in nuclear safety amongst the OECD Member countries.

CSNI constitutes a forum for the exchange of technical information and for collaboration between organisations which can contribute, from their respective backgrounds in research, development, engineering or regulation, to these activities and to the definition of its programme of work. It also reviews the state of knowledge on selected topics of nuclear safety technology and safety assessment, including operating experience. It initiates and conducts programmes identified by these reviews and assessments in order to overcome discrepancies, develop improvements, and reach international consensus on technical issues of common interest. It promotes the coordination of work in different Member countries, including the establishment of co-operative research projects and international standard problems, and assists in the feedback of the results to participating organisations. Full use is also made of traditional methods of co-operating, such as information exchanges, establishment of working groups, and organisation of conferences and specialist meetings.

The greater part of CSNI's current programme of work is concerned with the safety technology of water reactors. The principal areas covered are operating experience and human factors, reactor coolant system behaviour, various aspects of reactor component integrity, the phenomenology of radioactive releases in reactor accidents and their confinement, containment performance, risk assessment, and severe accidents. The Committee also studies the safety of the fuel cycle, conducts periodic surveys of reactor safety research programmes, and operates an international mechanism for exchanging reports on nuclear power plant incidents. In implementing its programme, CSNI establishes Co-operative mechanisms with NEA's Committee on Nuclear Regulatory Activities (CNRA), responsible for the activities of the Agency concerning the regulation, licensing and inspection of nuclear installations with regard to safety. It also co-operates with NEA's Committee on Radiation Protection and Public Health and NEA's Radioactive Waste Management Committee on matters of common interest.

ABSTRACT

The Nuclear Safety and Protection Institute (IPSN) of CEA proposed the PHEBUS Severe Fuel Damage B9+ test as the basis for an OECD/CSNI International Standard Problem. The objectives of the test were to study the following main phenomena occurring during the early phase of an SFD accident in a PWR : cladding oxidation, the mechanical behaviour of cladding with a ZrO_2 layer of variable thickness containing molten zircaloy, the simultaneous dissolution of UO_2 and ZrO_2 by molten Zry and melts relocation. These phenomena being crucial for a description of fuel behaviour during severe accidents, the B9+ test was accepted with semi blind conditions as International Standard Problem ISP 28.

Measured thermal-hydraulic conditions were supplied to help participants to calculate rod thermal behaviour as correctly as possible in order to evaluate the capabilities of the codes to calculate bundle degradation (blind part) using the appropriate thermal conditions. The calculations could be performed using two kinds of radial Boundary Conditions : a constant temperature applied on the external cold surface of the shroud (1st approach) or temperature evolutions versus time at different levels of the internal surface of the shroud (2nd approach). The first approach needed a fine modelling of all the layers of the shroud, in particular of the porous ZrO_2 layer which mainly determines the shroud insulation. The second approach, which was proposed to avoid modelling of the shroud, was "code dependent" because the thermal conditions were defined by a best estimate ICARE2 calculation.

The results of 17 calculations were submitted by 15 different organizations from 12 countries. Eight different codes were used and 4 calculations were performed using the second approach.

The calculated results were compared to measurements performed during the transient (fluid, rod and shroud temperatures, H_2 release) and to the final state of the bundle deduced from Post Test Examinations measurements (cladding oxidation, UO_2 dissolution, cladding dislocation, relocation of molten materials, flow blockage, ...).

Two groups of calculations can be distinguished. The first were performed with SCDAP Mod1, SCDAP/RELAP5 Mod1 and Mod2, MELCOR and ICARE2 and described the bundle degradation up to the final freezing of relocated materials. The second, including ATHLET SA, KESS III, FRAS-SFD and MARCH3 were limited to the calculation of thermal behaviour and to the first oxidation process of rod degradation.

All the calculations performed with the first approach using a recommended measured ZrO_2 porous conductivity value led to an overestimation of rod temperatures. Correct thermal and oxidation behaviours of the rods were only calculated when the thermal leakage through the shroud was increased and adjusted.

The capabilities of the advanced codes for calculating the main degradation phenomena when the thermal-hydraulic conditions are known were clearly illustrated. Areas with inadequate understanding and modelling weaknesses were identified. The most severe limitations concerned simultaneous UO_2 - ZrO_2 dissolution by molten Zry for which ZrO_2 dissolution was not modelled except in one code, UO_2 solubility limits in the resulting U-Zr-O mixture and cladding failure conditions by this molten mixture. There is also a general tendency to overestimate the relocation distance of these liquified mixtures. Finally, lacks were identified in the modelling of the Inconel spacer-grid interaction with both the rods and the relocated mixtures.

This first ISP on core degradation points out that more verification and validation work remains necessary for severe fuel damage computer codes which seem to be lagging behind current knowledge gained through experimental data on the early phase of core degradation.

The verification of reactor codes on small scale experiments needs more code versatility : power profile evolutions, surrounding structures with imposed boundary conditions, a pure non-condensable flow, more output convenience.

Finally this exercise also illustrates the importance of the code user, the need for improved user-guidelines with more detailed information and recommendations, as well as the need for experts in core degradation in order to make code utilization more effective with valuable judgements on predictions especially in these areas where code modelling deficiencies have been identified.

1 - INTRODUCTION

The Task Group on In-Vessel Degraded Core Behaviour was established by the Principal Working Group n°2 to address the physical processes that occur in the in-vessel phase of severe accidents in order to evaluate current code capabilities and to identify areas for further research.

In the field of severe accidents there remains a need to better understand and calculate core degradation and to check the ability of the codes to model main core degradation phenomena. The Institut de Protection et de Sûreté Nucléaire (I.P.S.N) of the Commissariat à l'Energie Atomique (C.E.A.) therefore proposed the PHEBUS SFD B9+ test as the basis for an OECD-CSNI International Standard Problem exercise.

The objectives of the B9+ test were to study the following main phenomena occurring during a SFD accident in a PWR : Cladding oxidation, the mechanical behaviour of the cladding with a ZrO₂ layer of variable thickness containing molten zircaloy, the simultaneous dissolution of UO₂ and ZrO₂ by molten Zr, and the relocation of the resulting melts.

These phenomena being crucial in the framework of code development and assessment, the test B9+ was accepted by the Principal Working Group n°2 with semi-blind conditions as exercise ISP28.

All the measured thermal-hydraulic conditions (open part) were supplied to help participants to calculate thermal conditions as correctly as possible in order to evaluate bundle degradation (blind-part) using appropriate conditions.

The results of 17 calculations were submitted by 15 different organizations from 12 countries indicating both the great interest and cooperative effort of the various institutions. Eight different codes were used.

A preliminary comparison report which compiled the 17 sets of comparison plots was sent to the participants in May 1991 in order to prepare the second workshop of this ISP which took place in June 1991 in Aix-en-Provence (France). During this meeting the participants' semi-blind predictions were discussed in detail. The present report includes these discussions and the conclusions drawn from this semi-blind exercise.

2 - OVERVIEW OF THE ISP 28 EXERCISE

PHEBUS-SFD B9+ was proposed by the Task Group on In-Vessel Degraded Core Behaviour and accepted by the Principle Working Group n°2 in October 1989. In order to better calculate correct thermal hydraulic behaviour which governs main degradation phenomena it was suggested that the problem be semi-open by giving the participants the thermal hydraulic measurements in order to calculate the degradation phase with correct initial conditions.

In other respects, this choice had the advantage of controlling radial thermal leakage through the surrounding shroud, which is difficult to calculate due to uncertainties at high temperature regarding the thermal conductivity on the porous ZrO₂ layer included in the shroud.

A first workshop was held in CADARACHE in April 1990 to give the technical specifications of the test. A detailed description of the B9+ test device and associated test instrumentation were given. The boundary conditions were specified with some recommendations. All the measured temperature evolutions within the test device were given to the participants [1]. The parameters to be calculated and the reporting format were also specified [4] and a schedule discussed. Participants had to submit the calculation by December 1st 1990, and the issue of this comparison report was scheduled for March 15, 1991.

Only four submissions were received by mid-December [the United Kingdom, Netherlands, Italy (Pise U), Germany (IKE)]. The remaining submissions were received at various times during the period December 15 - January 31, 1991. This delay can be explained by the fact that this exercise was the first ISP in the field of severe core degradation and constituted a pioneer effort for many participants who had to use severe accident codes for the first time. Some of these codes were not always available sufficiently soon to respect the ISP 28 agenda and some codes had to be modified to fit the PHEBUS test conditions. In other respects, some post-test examinations results concerning cladding oxidation, UO₂ dissolution and flow blockage were available late March and at the beginning of April. It was not possible therefore to release this comparison report as scheduled.

The results of 17 calculations were submitted by 15 different organizations from 12 countries indicating both the great interest and cooperative effort of the various institutions. Eight different codes were used : ATHLET SA, FRAS-SFD, ICARE2, KESS III, MARCH-3, MELCOR V 1.8.0 and V 1.8 EA, SCDAP (Mod1 stand-alone), SCDAP/RELAP5 Mod1 and Mod 2.

In agreement with the OECD, the CEA also invited non-OECD countries to calculate the PHEBUS SFD B9+ test in the framework of ISP28 and three calculations were submitted by HUNGARY, CZECHOSLOVAKIA and TAIWAN.

Other non-OECD countries also decided to perform this calculation but independently of ISP 28 (KOREA, POLAND, RUSSIA).

A preliminary comparison report which compiled the 17 sets of comparison plots was sent to the participants in May 1991 in order to prepare the second workshop of this ISP28 which took place in June 1991 in Aix-en-Provence [1]. During this meeting conclusions were drawn from this semi-blind exercise concerning the ability of the codes to predict the early phase of melt progression. Areas with inadequate understanding and modelling gaps and weaknesses were identified. The exercise also illustrated a significant code user effect.

Some participants proposed to perform new calculations in open conditions. Their submissions could be presented and analysed in an independent appendix report. This appendix comparison report could be released in 1992 in case of a sufficient participation with significant additional results.

3 - PHEBUS - SFD B9+ EXPERIMENT

The PHEBUS reactor is located at the CADARACHE Nuclear Centre.

3.1 - Outline of the facility

The PHEBUS SFD facility allowed a reproduction of thermal-hydraulic conditions that were relatively close to what would exist in a reactor core under beyond-design basis conditions. Careful attention was devoted to the monitoring of the bundle power and the thermal-hydraulic conditions. The principle of the tests consisted in supplying a bundle of 21 PWR-type fresh fuel rods with a flowrate mixture of overheated gases (steam-hydrogen or helium). The fuel power is adjusted in order to obtain the required temperature evolution.

The facility mainly consists of the PHEBUS driver core supplying the test fuel with nuclear power, a SFD loop (located on the vertical axis of the driver core) which reproduces the thermal-hydraulic conditions and a pressurized water loop (8 MPa, 533 K) working as an independent and external cooling circuit of the SFD loop.

A fairly flat axial profile of power (over 50 cm) is obtained with a neutronic filter of boron steel installed between the driver core and the test bundle.

The main component of the SFD loop is the test stringer (Fig. 1). It consists of three injection lines (steam, hydrogen, helium) for the gas supply, an electrical superheating device to increase the gas inlet temperature (max 1200 K) to the level required in the test scenario (not used during B9+), a test section, and an exit line which leads the gaseous flow to a pressure regulating system and then to a condenser and a storage tank.

3.2 - Bundle description and measurements

The test train cross-section and the longitudinal view show the bundle which consists of 21 unirradiated UO₂ fuel rods in a 12.6 mm pitch matrix (Fig. 2a and Fig. 2b). The total fissile height is 0.8 m. Two spacer-grids in Inconel 523 mm apart are located on either side of the mid plane at elevations 138 mm and 661 mm respectively from the bottom of the fissile column considered as the zero elevation. The implementation of fusible seals in the upper plugs of the rods (melting point : 1070 K) allows clad ballooning due to pressure effects during the tests to be avoided.

Rods are pressurized with helium at 0.7 MPa pressure in cold conditions.

The insulating shroud of the bundle is a multi-layer structure. The octagonal inner zircaloy liner 0.6 mm thick is surrounded by a thick porous ZrO₂ layer (94 mm ext. diameter and 69.5 mm between the faces of the inner octagonal surface), a dense ZrO₂ layer 1 mm thick and an external stainless steel tube 8 mm thick. Different kinds of thermocouples enable temperature measurements of the fuel centre, cladding, fluid and shroud at different radial locations and elevations (Fig. 3 and Fig. 4) to be made. The hydrogen concentration in the gas mixture at the loop outlet is measured continuously by means of a mass spectrometer. Detailed information on the facility is given in references [1], [2].

The rod numbering of the 21 rods bundle runs from 2 to 24 with omitted numbers 5 and 21 (Fig. 8).

3.3 - Objectives and experimental conditions of the B9+ test

3.3.1 - Objectives of the B9+ test

The objective of the PHEBUS SFD programme is to investigate the damage mechanisms acting on an uncovered PWR core. In order to avoid overly complicated integral experiments involving all the aspects of core degradation, the PHEBUS SFD tests have mainly been focussed on a few principal phenomena occurring during the core degradation [3].

In particular, the objectives of the B9+ test were to study the following phenomena.

- 1 - cladding oxidation.
- 2 - the mechanical behaviour of a variable thickness of the external zirconia layer of the cladding containing molten Zircaloy.
- 3 - the dissolution of UO_2 and ZrO_2 by molten Zircaloy.
- 4 - the relocation of the melt.

The test was performed with Inconel spacer-grids and also enables, under test conditions, the formation of low temperature eutectics with Zircaloy and the interaction with fuel pellets to be studied.

Absorber material rods were not included in the bundle and quenching effects on a hot bundle were not studied in this test.

3.3.2 - Scenario and T/H boundary conditions

The experimental scenario involves three parts (Fig. 5) :

- A first oxidation phase performed with a pure steam flow from 0 to 8370 s (closing time of steam injection). In fact steam probably remained present in the bundle up until 8378 s due to the delay between the closing time of the valve and the steam emptying of the bundle (Fig. 6).

The pressure, the mass flow rate and the inlet temperature were kept constant at the following values :

$$P = 1.9 \text{ MPa}$$

$$Q = 2 \cdot 10^{-3} \text{ kg/s}$$

$$T = 528 \text{ K}$$

Three power steps (4 KW, 8.8 KW and 11.5 KW) allowed rod temperature levels of 1000, 1350, 1600 K to be reached at the hottest level (Fig. 5). Then a slow power increase from 11.5 KW to 14.5 KW during about one hour resulted in slow heating from 1600 K to about 1800 K. A new power step from 14.5 KW to 18.0 KW allowed practically complete oxidation in the upper part of the bundle to be reached. The ballooning of the pressurized rods with He (0.7 MPa in cold conditions) was avoided by the low temperature melting of the fusible seal in the upper plug of each rod.

At the end of the oxidation phase the cooling gas was switched from steam to helium.

- The second heat-up phase was performed in pure helium starting at 8364 s (Fig. 6). A pressure of 1.9 MPa, a helium mass flow rate of 0.5 g/s and an inlet temperature of 528 K were maintained throughout this high temperature phase. Five power steps were performed leading to a maximum rod temperature of about 2750 K.
- During the final phase, which began at 13860 s, step reductions in nuclear power enabled a slow cooling down in order to keep the previous bundle geometry unchanged. The pressure was decreased to 0.4 MPa at 14135 s. During this phase a mean helium mass flow rate of 0.5 g/s with an inlet temperature of 528 K was maintained up to the final time of the test at 18000 s.

3.3.3 - Radial boundary conditions in the shroud

3.3.3.1 - Comments on the shroud

The analysis of previous PHEBUS-SFD tests showed that, due to the very low flow-rates used in these tests the main part of the power released in the bundle is transmitted to the external pressurized cooling loop through the shroud. The main parameter which controls this radial heat transfer is the thermal conductivity of the porous zirconia layer and uncertainties in this parameter dominates the uncertainty in calculating the temperature history of the fuel rods.

An effort was made in order to improve our knowledge of this parameter. The first PHEBUS-SFD tests showed a large change of thermal conductivity due to the progressive filling of the porosities with hydrogen arising from the oxidation of the inner Zry liner. This uncontrolled change was avoided in the B9+ test by the use of a continuous injection of helium in the porous zirconia during the first steam phase.

Laboratory tests were performed in order to measure the thermal conductivity of the porous ZrO₂ from different representative samples under a helium atmosphere, at atmospheric pressure and at temperatures in the range of 523 K to 2273 K. This conductivity was then extrapolated to the pressure conditions of the test (1.9 MPa) and this estimated value was recommended in the specifications [2] for the calculations.

$$\lambda = 0.302 \text{ W/m.K for } T < 1273 \text{ K}$$

$$\lambda = 0.374 - 1.31 \cdot 10^{-4} T + 5.85 \cdot 10^{-8} T^2$$

$$\text{for } 1273 < T < 2273 \text{ K}$$

As explained in section 7.2 this conductivity was non suitable due to an underprediction of the pressure effect.

3.3.3.2 - Thermal radial boundary conditions

Two kinds of radial Boundary Conditions (B.C.) were proposed in order to calculate the test.

1st approach :

It consists in representing as closely as possible the different layers of the shroud surrounding the 21 rod bundle (the internal octagonal liner in Zircaloy, a He gap, a porous ZrO₂ layer with a maximum thickness of 12.25 mm, a dense ZrO₂ layer 1 mm thick and the external stainless steel tube).

The external water cooling of the shroud maintained the steel tube surface at a constant temperature of 528 K all along the shroud for the entire test.

Grooves were provided in the porous ZrO₂ for the location of the thermocouples on the outer face of the Zry liner (Fig. 4) (Radius of the grooves 4 mm). Laboratory measurements on samples with a simulation of the grooves representative of the lower part of the insulator (- 27 cm to + 31 cm) showed that the heat flux increases by about 10 % at 1300 K, 20 % at 1800 K and 23 % at 2300 K due to the grooves.

2nd approach :

In order to avoid modelling of the actual shroud a simple surrounding structure involving only the internal octogonal liner was proposed. The following equivalent cylindrical geometry was proposed :

inner diameter	:	0.0733 m
outer diameter	:	0.0745 m
material	:	Zircaloy

Temperature histories were given at 10 different levels of the liner : 04/12/20/28/36/44/52/60/68/76 cm from the bottom of the fissile length [4].

These radial boundary conditions were defined by a best estimate ICARE2 calculation performed in modelling the actual shroud. This calculation was "adjusted" in order to find a correct thermal behaviour all along the bundle for the entire test. The parameter used so as to better match the measurements was the thermal conductivity of the porous zirconia.

It was pointed out that these radial boundary conditions were of course "ICARE 2 code dependent", for instance dependent on the physical models of the code. It was therefore recommended that the participants using a code able to represent the actual shroud, choose the 1st boundary conditions in making, if necessary, sensitivity studies on the shroud modelling (1st approach user-adjusted) to better fit the rod temperature measurements.

3.3.4 - Nuclear power history and distribution

3.3.4.1 - History

The nuclear power input in the test bundle is directly proportional to the neutron flux provided by the driver core. This latter is measured with two ionisation chambers which have been calibrated to directly indicate the driver core power level.

A comparison of the power signal as given by the ionisation chambers with a detailed thermal balance over the core cooling circuit showed very good linearity of the chambers' average signal (after correction for core inlet temperature) with the core power level.

The coupling factor between the driver core and the test bundle, that is the ratio between the chambers' signal and the actual power released in the bundle, was determined experimentally before each test. The average value is consistent with an analytical estimate of the same ratio.

Fig. 5 shows the bundle power evolution deduced from core power measurements as given by the ionisation chambers and the experimental coupling factor.

3.3.4.2 - Radial and axial distributions

Preliminary dosimetry tests on a PHEBUS SFD test bundle allowed the radial and axial power distributions to be determined. Fig. 8 gives the normalized radial distribution derived from dosimetry measurements.

Fig. 9 gives the axial power profile in the bundle at different times in the test transient corresponding to successive control rod positions.

This axial profile evolution results from a series of neutronic calculations with 4 successive control rod insertions, the zero power configuration being adjusted to the experimental dosimetry profile of the PHEBUS SFD bundle.

All of these curves refer to an intact bundle geometry. Neutronic calculations have shown that the coupling factor (ratio between driver core power and test bundle power) is very little dependent on the fuel mass distribution

in the test bundle. It means that the power axial profiles provided in Figure 9 may be considered as specific power profiles to be weighted by the UO₂ mass distribution at the different levels during fuel relocation (constant specific nuclear power for an unchanged control rod insertion).

3.3.5 - Experimental uncertainties

The following table summarizes the main estimated experimental uncertainties. More details are given in references [1] and [2].

Measurements	Uncertainties
Bundle Temperature	± 50 K above 2400 K
Pressure	3 %
Steam flow rate	5 %
Helium flow rate	5.10 ⁻⁶ kg/s
Nuclear Power	5 %
H ₂ mass generated	20 %

Among the 51 thermocouples which worked correctly at the beginning of the test, 31 failed sooner or later in the transient because they were exposed to too high a temperature or to material interactions. This was the case for all the fuel, cladding and liner thermocouples located between 30 cm and 75 cm, but the thermocouples located inside the porous ZrO₂ worked correctly up to the end of the test. These thermocouples have very similar histories to the one located at the same level in the bundle. This enabled the high temperature history of the rods to be evaluated with confidence by extrapolation from the temperature measurements inside the shroud. The consistency between the axial temperature profiles for each kind of structures enabled this extrapolation to be checked and confirmed.

4 - MAIN PHENOMENA OBSERVED

In this section a summary of the results related to the open part are given as well as the results from post test examinations [5] related to the blind part of ISP 28.

Figure 11 shows the two halves of the axial cutting of the bundle between 10 cm and 40 cm. Figures 12 to 16 show radial cutting at respectively 76, 58, 52, 44, 26, 17, 14, 5 cm from the bottom of the fissile length.

4.1 - Thermal behaviour

The first oxidation phase was characterized between 4000 and 8000 s by a mean slow heat-up of 0.06 K/s. At the end of this oxidation phase a rapid temperature increase was measured (> 3 K/s) at the hot zone (60-70 cm). The fuel temperature of an external rod reached about 2400 K at 60 cm. This temperature escalation was stopped by switching the cooling gas from steam to helium at 8364 s. Our analysis of this escalation showed that it was mainly due to enhancement of the oxidation kinetics at the temperature of the zirconia phase transition from a tetragonal to a cubic phase around 1850 K.

A detailed analysis of the thermal behaviour of the bundle at the 70 and 75 cm levels indicates that temperature escalations also occurred at these elevations on some cladding tubes.

It was deduced from ICARE2 sensitivity studies that the temperature peaks observed both on the liner and inside the shroud at the 70 and 75 cm levels could only be due to rod escalations occurring at the same levels in the bundle and not to a heat transfer from the 60 cm. Only the rods with a sufficient amount of remaining metallic Zry before the end of the oxidation phase were able to undergo a temperature escalation. Due to non-homogeneous oxidation observed on different rods at the same level, some other rods with less metallic Zry were not affected by an escalation, as shown by the only fuel TC01 located at 70 cm in the outer ring rods.

This escalation up to 75 cm was also confirmed by the limited fluid peak temperature observed on each of the 3 thermocouples (TC35, 75, 76) located at the outlet of the bundle at the 80 cm level.

On the whole, the oxidation escalation was limited either by the total oxidation of the remaining non-oxidized Zry or by the steam to helium switch injection. The melting temperature of the oxygen stabilized alpha Zry was reached for about 150 s, just before this injection switch. Then the resulting rapid stopping of the related oxidation power led to a local cooling of the rods with a temporary refreezing of the remaining non-oxidized Zry.

The second heat-up phase with He was characterized by pure steam starved conditions and melting or re-melting of the remaining Zry.

Thermocouple readings became unreliable at different times following the oxidation excursion due to interaction between the cladding sheaths and the molten materials. The unreliable part of the measurements has not been considered in this report.

A maximum temperature of about $2750 \text{ K} \pm 50 \text{ K}$ was reached at the hot zone at 13860 s. This value was estimated by extrapolation from the shroud and the lower bundle part temperature measurements (see § 3.3.5). Furthermore this value was confirmed by PIE results.

4.2 - Oxidation behaviour

Post-test examinations were performed on radial cuts of the bundle. Measurement of the cladding oxide thickness at different elevations was very difficult. At some levels the cladding had disappeared, at others the ZrO_2 layer was sometimes impossible to identify due to complex and non-uniform interaction between molten U-Zr-O materials and the remaining ZrO_2 layers (Fig. 13, 14).

In the upper part of the bundle, beyond 0.60 m, the cladding oxidation was complete or nearly complete and UO_2 dissolution was low. The general aspect of the bundle remained unchanged. However a strong distorsion of the array pitch due to the melting of the Inconel upper spacer grid (1650 K) at around 5500 s (Fig. 12) could be observed.

Between 25 and 60 cm, the cladding oxidation was partial (Fig. 13, 14). ZrO_2 dissolution by molten Zry occurred due to the diffusion of the oxygen from the oxide layer to the melt. This diffusion process appeared to have been localized near the Zr- ZrO_2 interface and led to a particular radial oxygen concentration profile inside the cladding.

At the lower levels where the metallic Zry remained solid during the He phase, an oxygen diffusion process also occurred at the levels characterized by a poor oxygen Zry sublayer. This process also led to a non-homogeneous radial oxygen profile which "kept in mind" the location of the initial ZrO₂ layer. The combination of visual examinations of micrographs and of the microprobe measurements of the local oxygen concentration profiles allowed an evaluation of the thickness of the ZrO₂ layer at the end of the oxidation phase. Uncertainties are believed to be less than the experimental range of the oxidation corresponding to the temperature differences between rods at the same elevation.

The axial profile (figure 25 of the individual comparisons) increased from a few percents (10 μm) below 20 cm to 40 % (350 μm at mid plane elevation) and complete (or nearly complete) oxidation in the upper part (60 to 70 cm).

4.3 - Hydrogen release

Hydrogen concentration in the gas mixture at the loop outlet was measured continuously with a mass spectrometer. The pressure evolution of uncondensable gases in a temporary storage tank also allowed the hydrogen produced to be measured. These two methods gave similar results. The measured total H₂ mass and production rate are given in figures 28 of the individual comparisons.

A total of 39,5 g of H₂ was released during the test. The uncertainty on this measurement was evaluated at 20 %.

4.4 - Inconel spacer grids

The two spacer-grids were located at 13.8 and 66 cm from the bottom of the active length. Post-test examinations on radial cuts performed at these elevations showed that the upper grid located in the hot bundle zone totally disappeared. Local interaction between Inconel and Zry cladding was not observed on the corresponding radial cut. The relocation of this grid occurred during the steam phase. Loss of thermocouple measurements just below this upper spacer-grid could indicate relocation temperatures of around 1550 K.

The lower spacer grid remained partially in place (Fig. 15b). Only the central part corresponding to the CR and 1R rods nearly disappeared and showed evidence of local Inconel-Zry interaction. The resulting melt led to local cladding failures followed by limited UO₂ dissolution during the He phase. Radial cutting of the bundle just above the lower spacer-grid (Fig. 15a) showed no evidence of any

significant catcher effect. Only little solid debris of oxidized Zry was observed on this grid. No evidence of refrozen melts was found on the remaining part of the grid. Visual observations of the radial cutting at 9.8 cm and 17.2 cm showed some gaps inside the cladding extending all over the Zry-UO₂ interface. These cavities could be due to local Inconel-Zry interaction. Globally no significant interaction was observed, probably on account of the protective effect of the ZrO₂ layer of the cladding.

4.5 - UO₂ dissolution by solid Zry

Due to the melting of the upper plug of the rods above 1070 K no differential pressure was applied across the cladding, enabling good UO₂ - solid Zry contacts. Nevertheless, due to a greater thermal expansion of the fuel than of the cladding, the PIE showed some evidence of local UO₂-solid Zry interactions on a few rods (level 26 cm, Fig. 14-b). Some (U, Zr) O₂-x globules were identified inside the cladding with an area-fraction less than 10 % of the total cladding section. But this interaction was very limited and did not lead to significant UO₂ dissolution (and relocation) that could be identified by a measurable fuel surface area decrease.

4.6 - UO₂ dissolution by molten Zry

Fuel dissolution was observed in radial cuts separated by about 2 cm in the zones of interest. Fuel dissolution was estimated from photographs by measuring the surface of the remaining fuel pellets.

$$D (\%) = 100 \cdot \frac{S_o - S}{S_o}$$

S : final surface area of the fuel
S_o : initial surface area of the fuel

These measurements were identified as the weight fraction of fuel dissolution. The uncertainty on these measurements was evaluated at 1.5 %. Only a mean value at each elevation seemed to be significant. At some elevations there was considerable spreading of the dissolution between the different rods particularly near the hot point - Figure 13-a - (from a few wt % up to 40 wt % at 56 cm). Visual observations of the different cuts showed that external rods (2nd ring rods) tended to be dissolved more than the internal ones.

The mean UO₂ dissolution profile is given in figures 29 of the individual comparisons. The dissolution was mainly limited to the zone between 28 and 60 cm. Limited mean dissolutions were found with a maximum of 14 wt % at 52 cm, in spite of considerable local dissolution on some rods. Between 60 and 70 cm only some particular rods were observed with significant local dissolution.

It was thought that local dissolutions could have occurred at the end of the oxidation phase during the 150 s period of the temperature escalation during which the remaining metallic Zry was molten and able both to dissolve the fuel and to be oxidized by the external steam. A second explanation concerned the Zry remaining at the end of the oxidation phase in the colder upper part of the rods. After melting during the He phase, this Zry could relocate internally into the slightly ballooned cladding of some rods, enabling more efficient local dissolution in pure steam-starved conditions, than during the first oxidation phase (Fig. 13 - Rod 6).

4.7 - ZrO₂ dissolution by molten Zry

Visual examinations of the cuts in the upper part of the bundle where oxidation exceeded 50 % showed significant azimuthal ZrO₂ layer thickness differences on some inner rods (minimum thickness about 3 times lower than the maximum thickness). Local ZrO₂ dissolution could partially explain these differences, but no quantitative evaluation could be made due to the difficulty of determining what was due to the azimuthal temperature differences, and what was due to ZrO₂ dissolution. The latter effect which seemed the more significant was mainly observed under the hot zone in the upper part of the cladding failure zone.

4.8 - Relocation of molten mixtures

Visual observations of the axial cuts of the bundle showed two main plugs. The lower one was very localized at the 5 cm level between rods 8, 9, 10, 13, 14, 15, 18. It was a metallic plug with Inconel (Fig. 16). Microprobe analysis of this frozen mixture gave the following mean atomic content :

55.4 % Zr ; 7.5 % U ; 23.6 % Ni ; 7 % Fe ; 1.5 % Cr ; 5 % O.

The external oxidation of this plug at the locations where microprobe analyses were performed was similar to that of the local cladding (~ 10 μm). This showed that relocation began during the steam phase from the liquefaction of the upper

spacer-grid. Part of the lower spacer-grid could also have been relocated in this zone later on during the He phase. At the level of the plug no evidence was found of interaction between the Inconel mixture with the surrounding rods.

The upper plug was larger and localized between 20 cm and 28 cm (Fig. 11, 14). It was a ceramic plug with two α -Zr(O) and (U, Zr) O₂ - x phases which formed during the cooling. Microprobe analysis gave the following mean atomic content :

$$65 \% \text{ Zr ; } 4 \% \text{ U ; } 31 \% \text{ O}$$

PIE observations showed that the ceramic phase (22 % of the surface area of the melt) was dispersed inside the α -Zr(O) phase.

Apart from these two plugs, local deposits on some external rod surfaces of small amounts of mixtures were mainly found between 28 and 40 cm. A few small deposits were also found locally on external rods as far as 60 cm.

The analysis of some of these small amounts of refrozen mixtures showed greater oxide phases. At level 40 cm the [α -Zr(O) ; (U, Zr) O₂ - x] two phase mixture had the following mean atomic content :

$$56 \% \text{ Zr ; } 6 \% \text{ U ; } 38 \% \text{ O}$$

The ceramic phase, richer in U (57 %) than the previous one, represented 33.5 % of the total surface area of the melt.

4.9 - Bundle blockage

Bundle blockage was determined from photographs by measuring all the surfaces of the different mixtures and sections of rods located inside the initial surface of the octogonal liner. This blockage was defined for the ISP 28 as the ratio between the solid surfaces and the internal surface of the liner.

$$B \% = 100 \frac{S_{oct} - S(t)}{S_{oct}}$$

S_{oct} = initial surface inside the octogonal liner (4000 mm²)

$S(t)$ = flow area section at the current time t

This definition had the advantage of giving a bundle blockage equal to 0 % in case of total dislocation of rods at one level and to 100 % in case of total flow blockage. This bundle blockage is equal to 38 % at time zero, due to undeformed rods. The blockage profile measured is given in figures 30 of the individual comparisons. The maximum blockage of 51 % was found in the upper plug zone at the 26 cm level in the upper plug zone. The minimum of 35 % was found at the 46 cm level. These bundle blockages corresponded respectively to hydraulic flow blockages of 21 % and - 4 %.

The cladding disappearance zone occurred for inner rods between 28 cm and 50 cm and up to 56 cm for external rods.

The fusible plug prevented fuel rod ballooning due to a pressure effect. No significant cladding "flowering" was observed, due to oxidation, as was observed in some CORA tests with unpressurized rods. Only a little deformation (a few %) was observed in the totally oxidized upper part of the bundle in the zone 70/80 cm (Fig. 12). These deformations could facilitate local zones of molten Zry relocation and accumulation with further local UO₂ dissolution (see § 4.6).

The liner configurations can be summarized as follows :

80 cm - 75 cm	:	in place - marked deformations nearly in contact with some rods. (Fig.12)
75 cm - 55 cm	:	partially in place - marked deformation - non-oxidized part relocated. (Fig.13)
56 cm - 34 cm	:	total disappearance. (Fig.13)
34 cm - 25 cm	:	partially in place - marked deformation. Some liner-rod contacts with frozen relocated mixtures are observed. (Fig.14)
25 cm - 0 cm	:	totally in place - slight deformation. (Fig.15,16)

5 - OVERVIEW OF PARTICIPANTS' MODELS

The 15 submissions to the ISP 28 are given in table 1 together with the names of the codes used for the analysis.

Eight codes with very different possibilities were used. SCDAP Mod1 stand-alone, SCDAP-RELAP5 Mod2 and Mod1, ICARE 2 V1 and V2p and MELCOR V 1.8.0 and V 1.8EA were able to take into account the main core degradation phenomena and the corresponding material relocation. KESS III, ATHLET SA, FRAS-SFD are under development concerning degradation - relocation processes and their calculations were mainly limited, as well as the MARCH3 calculation, to the prediction of the thermal and oxidation behaviour of the bundle.

The modifications of the codes carried out in order to calculate the PHEBUS B9+ test are summarized in table 2.

It must be pointed out that the ICARE2 modifications were mainly carried out in the framework of its development, and that the SCDAP Mod1 modifications were also carried out in the more general framework of its verification on the PHEBUS SFD experiments.

5.1 - Physical models of degradation

Some participants sent a short code description as was requested for this ISP concerning the physical models of the degradation phenomena involved during the B9+ test. Details of some of the implemented codes can be found in [6].

Tables 3 and 4 summarize the degradation models giving the user-specified parameters chosen by the participants. It must be noted that no specific spacer-grid involving a chemical interaction model exists in the eight codes used.

ZrO₂ dissolution by molten Zry is only considered by the ICARE2 code. The Hofmann kinetics law of ZrO₂ dissolution is used with the solubility of UO₂ deduced from an approximation of the ternary U-Zr-O phase diagram.

Great consistency is found as regards the oxidation kinetics correlations used. Cathcart up to 1853 K and Urbanic Heidrick correlations at higher temperature were the most often used.

Other differences between the codes involved cladding failure criteria (failure of the external ZrO_2 layer of the cladding) when the non oxidized Zry of the cladding melted and simultaneously dissolved the UO_2 pellets and the external ZrO_2 layer of the cladding. The resulting U-Zr-O mixture contained within a ZrO_2 shell was most often supposed to flow down after this ZrO_2 failure. Failure was supposed in the codes when an user specified temperature was reached ($2200\text{ K} < T_{\text{user limit}} < 2673\text{ K}$) provided that the oxide shell was not considered sufficiently thick to hold in the molten mixture. The user failure thickness limit was spread between $60\text{ }\mu\text{m}$ (USA) and $540\text{ }\mu\text{m}$ depending on the calculation.

5.2 - Nodalization of the PHEBUS bundle

There also existed a high degree of homogeneity between the different calculations concerning the total number of axial meshes for the active length of rods (80 cm). Most often eight to eleven meshes were chosen and 3 kinds of rods were selected representing respectively the Central Rod (CR), the 8 first Ring Rods (1R) and the 12 Second Ring Rods (2R). The 21 rods were put in one hydraulic channel except for SP-CSN and FRA-SP which chose 3 independent channels for each representative rod (Table 5). A typical modelling of the bundle is shown in Fig. 10.

5.3 - Shroud modelling

Shroud modelling was an important point because, as explained in the next section, the major heat loss from the fuel rods was through the multi-layering of the shroud to the subcooled surrounding cooling water (528 K). The most insulating layer was the porous ZrO_2 with an external cylindrical form and with an internal octogonal form (maximum thickness 12.25 mm). Table 6 summarizes the shroud modelling chosen by participants.

Four calculations were performed using the 2nd radial boundary condition approach : CZECHO, GER-IKE2, GER-GRS2 and TAIWAN.

Others calculations used different shroud modelling most often with the actual 4 shroud layers (Zr, porous ZrO_2 , dense ZrO_2 , SS) but FRA-SP and USA took into account a helium gap representing the 9 external liner thermocouple grooves which were made in the internal face of the porous ZrO_2 layer. This led to a variable porous ZrO_2 thickness with elevation [1].

It must be pointed out that each participant was free to choose the axial meshing in the bundle. Only 10 levels over the 80 cm of active length were required to give the calculational results - On the basis of our experience this choice which requires at least 10 meshes ensures numerical converged results even as regards melt relocations.

The conductivity of the porous ZrO_2 layer chosen by the participants is summarized in Table 6 and in Fig. 7. This point is discussed in the next sections.

5.4 - Nuclear power

Table 7 summarizes the modelling of the nuclear power for each submission.

6 - COMPARISONS OF INDIVIDUAL RESULTS WITH THE EXPERIMENT

Due to the important amount of data it was decided to compare in a first step each individual calculation with the experiment. The predictive capabilities of the codes involved in ISP 28 were analysed. The following parameters were chosen and are drawn in different Annexes given in volume 2 :

- UO_2 temp. versus time : lower and upper part : Fig. 1, 2
- Clad. temp. versus time : lower and upper part : Fig. 3, 4
- Fluid temp. versus time : lower and upper part : Fig. 5, 6
- Liner and shroud temp. versus time : Fig. 7, 8
- Temperature histories for different components at levels 50, 70 : Fig. 9, 10
- Axial temp. profiles at 7700 s, 9000 s, 12000 s, 14000 s : Fig. 11
- Heat flux through the shroud : Fig. 12
- Oxide, UO_2 , ZrO_2 dissolution profiles (CR) 9000 s and 14000 s : Fig. 13, 14, 15, 16
- Oxide, UO_2 , ZrO_2 dissolution profiles (1R) 9000 s and 14000 s : Fig. 17, 18, 19, 20
- Oxide, UO_2 , ZrO_2 dissolution profiles (2R) 9000 s and 14000 s : Fig. 21, 22, 23, 24
- Mean oxide profile / experiment : Fig. 25
- Oxidation and ZrO_2 dissolution versus time (cladding of 1R rods) : Fig. 26
- Oxidation profiles for the liner at 9000 s and 14000 s : Fig. 27
- H_2 release / experiment : Fig. 28
- Mean UO_2 dissolution profile / experiment : Fig. 29
- Flow blockage profile / experiment : Fig. 30
- Relocated material profile : Fig. 31

- Final picture of the bundle : Fig. 32
- Total UO_2 , ZrO_2 , Zry profiles at 9000 s : Fig. 33
- Total UO_2 , ZrO_2 , Zry profiles at 14000 s : Fig. 34

Annexes 1 to 15 contain, for each participation, the previous set of 34 figures. The plot identifiers used in these figures are described in Annex 17.

It must be pointed out that fourteen submissions were performed in SEMI BLIND conditions. The FRA-SP submission (joint CEA-Phebus Espana Consortium) was performed in OPEN conditions. This participant had to calculate the "2nd approach" boundary conditions on the shroud liner and was involved in the definition and the analysis of the post-test examinations. This submission, therefore, should be considered only as a reference calculation.

6.1 - FRA-SP (Annex 1) : ICARE2/V2p calculation

A good prediction of the rod temperatures was obtained in tuning the porosity of the porous ZrO_2 governing the heat conductivity. The temperature escalation (8200 s) was predicted at 60 and at 70 cm (as in the test). The maximum temperature was well predicted (2750 K) (A1 - Fig. 1 to 12). Total (CR, 1R) or near total oxidation (89 % is reached on 2R rods) was predicted at hot levels (60/70). Complete oxidation was not found in the upper part. These results are in agreement with the oxidation measurements (A1 - Fig. 25). The enhancement of oxidation when the temperature reaches 1853 K explains the temperature escalation at the hot level and the rapid ZrO_2 attaining nearly complete oxidation.

Limited ZrO_2 dissolution was calculated at levels 50 and 60 (maximum 13 % of the oxide layer calculated at the end of the steam phase. A1 - Fig. 26) but more significant ZrO_2 dissolution was found up to 60 % in the cladding failure zone. This important local reduction of the ZrO_2 thickness enabled the ZrO_2 failure thickness limit chosen by the user (300 μm) to be reached and contributed to a correct calculation of the cladding failure between 32 and 48 cm as observed in the test (A1 - Fig. 32). In spite of the correct oxidation prediction, H_2 production was slightly overestimated. The calculated fuel dissolution was limited to 12 % as in the test (A - Fig. 29). The bundle blockage profile showed a good prediction of the voiding and filling zones due to material relocation (A1 - Fig. 30).

The overall correct prediction of the fuel degradation was facilitated by the satisfactory prediction of the rod temperatures and by a correct calculation of the oxidation profile.

6.2 - SP-CSN (Annex 2) : SCDAP MOD1 Stand-alone code

The thermal behaviour of the bundle was greatly overestimated in spite of the use of a conductivity of the porous ZrO_2 (Fig. 7) calculated using the Missenard correlation (70 % constant porosity and He filled insulator). The temperature escalation was not calculated at 8200 s (as observed in the test) probably because the calculated oxidation was already complete at that time. The maximum rod temperature was overestimated, 2900 K instead of 2750 K in the test. Oxidation was overestimated : 100 % between 40 and 80 cm (A2, Fig. 25).

Extensive cladding deformation was calculated before the melting of the fusible seals in the upper plugs of the rods (1100 K) leading to a maximum blockage of 64 % at 60/70 cm.

Fuel dissolution was overpredicted (60 %) at lower levels only, between 16 cm and 40 cm, where cladding rupture was calculated. The relocation of the U-Zr-O mixture was partially frozen in the same zone and part of the molten material was predicted to flow down and to escape from the bundle.

6.3 - SP-UPM (Annex 3) : MELCOR V1.8.0 calculation

Temperatures were strongly overestimated mainly in the lower part of the bundle but cladding oxidation (A3 - Fig. 15, 19, 23, 25) and H_2 production (A3 - Fig. 28) were underestimated. (max oxidation of 62 %, 50 %, 27 % for CR, 1R, 2R rods). These contradictory results could be due to incorrect oxidation kinetics for $T > 1850$ K. The heat flux through the shroud (A3 - Fig. 12) was significantly underestimated during the He phase. This could be due to incorrect He properties. The heat exchange coefficients calculated by MELCOR in case of a pure He flow are to be checked.

Cladding failure by molten Zry occurred at level 20 cm on the 2R rods. When the melting point of ZrO_2 ($T > 2990$ K) was reached at 13500 s cladding failure occurred in the 48-64 cm zone for the CR and at the 60 cm level for 1R rods leading to a UO_2 debris bed formation. Part of the UO_2 was transported from the 20 cm and 60 cm levels. The ZrO_2 debris and the spacer-grids were relocated and

accumulated below the fissile length and at the 4 cm level. The total mass of relocated mixture (A3 - Fig. 31) represented in fact the total amount of dislocated UO_2 which had been produced at the 20 and 60 cm elevations when cladding failed. It did not represent a plug due to refrozen materials. Moreover, at these locations the bundle blockage decreased (A3 - Fig. 30).

6.4 - CZECHOSLOVAKIA (Annex 4) : FRAS - SFD calculation

ISP 28 was the first attempt made with the FRAS-SFD code to describe the severe fuel damage transient. No relocation can be calculated with the present version of the code and the calculation was stopped when cladding failure occurred.

The calculation was performed up to the steam-He switch at 8320 s where numerical instabilities were observed. Only one rod was calculated using a kind of 2nd BC approach applied to a surrounding rod instead of on the shroud liner. For this submission, therefore, all the 1R and 2R values corresponded in fact to the CR values.

Temperatures were overestimated mainly in the upper part. This led to an overestimation of the final oxidation profile (A4 - Fig. 25). At the upper levels a rapid oxidation versus time was anticipated (A4 - Fig. 26). The total oxidation was reached at 6000 s instead of 8000 s in the test. The H_2 produced for the central rod was converted to a complete bundle release (55 g) taking into account the ICARE2 calculated H_2 proportion between CR, 1R, 2R and liner (A4 - Fig. 28). Dissolution at the 80 cm level was calculated between 8200 and 8240 s (A4 - Fig. 14 and Fig. 29) just before the end of the calculation. Consequently the resulting molten mixture continued to be oxidized. A local dissolution of 10 wt % of UO_2 was calculated at 80 cm at the final time of the computation (8320 s).

6.5 - GER-IKE1 and IKE2 (Annex 5a, Annex 5b) : KESS III calculation

With the KESS III code, which is still being developed, IKE performed two calculations of ISP28. These calculations mainly focussed on the heat-up and oxidation processes.

IKE1 : 1st BC approach on the external face of the shroud :

The recommended heat conductivity values for the porous ZrO_2 resulted in a stronger temperature increase all along the whole length of the bundle than was

measured. This non-realistic prediction led to the use of the "first user-adjust BC approach" method with a ZrO_2 conductivity twice greater than the one measured. Under these conditions the overall calculation of the thermal behaviour was more correct but a general overestimation of the temperatures was still found during the oxidation phase. Just after the steam/He switch, the fluid temperature at the outlet (80 cm) (A5 - Fig. 6) was significantly underestimated. By comparison with the IKE2 calculation (2nd BC approach) it seems that this local trend was due to a local overestimation of the radial thermal leakage to the shroud. Oscillations of calculated temperatures were due to the use of too large time steps.

Oxidation and H_2 production (55 g) were also overestimated (A 5a - Fig. 25, 26). The temperature escalation at 60 cm was not predicted because oxidation was already calculated as complete at 8000 s, (A 5a - Fig 26) (The escalation was measured at 8200 s).

Due to the lack of the corresponding models in the current version of the KESS code no fuel dissolution results were transmitted and no relocation was allowed to occur in choosing a high value for the cladding failure (2673 K).

IKE 2 : 2nd BC approach on the shroud liner :

The application of the 2nd thermal BC on the liner led to a better prediction of the fuel rod temperature history but with a local underestimation by 75° at the hot level.

This was sufficient to prevent the calculation of the temperature escalation during which oxidation developed very fast. The total oxidation at hot levels, therefore, was not predicted due to the delayed threshold effect of the oxidation kinetics near 1850 K. The H_2 production was also too low (32 g instead of 39 g) (A 5b - Fig. 25 and 28).

In general, fluid temperatures seem to have been underpredicted but it must be pointed out that the fluid thermocouples were probably affected by the considerable radiative transfer in the bundle [A 5b - Fig. 5, 6]. Outlet fluid temperature was more correct than in the IKE1 case. Numerical instabilities on temperatures during the He phase were also reduced.

6.6 - GER - GRS1 and GRS 2 (Annex 6a, Annex 6b) : ATHLET SA calculation

With the ATHLET-SA code, which is still being developed, GRS performed two calculations of ISP28. These calculations mainly focussed on the core heat-up and oxidation processes.

GRS 1 : 1st BC approach on the external face of the shroud :

This calculation was performed after a first calculation run using the 2nd approach boundary condition (see the following GRS 2 calculation).

Results of this first calculation were used to calculate the porous ZrO_2 heat conductivity of the shroud composed of the main 3 layers (dense ZrO_2 omitted) versus time. Temperatures were overestimated in the lower part (up to 50 cm during the oxidation phase and up to 40 cm during the He phase). The reason for that could be an inadequate heat transfer coefficient in the shroud or the use of a constant power profile during the transient. Satisfactory agreement was obtained in the hot zone for the 2R rod (A 6a - Fig. 2) but the thermal radial gradient seems to have been overestimated between the 2R rods and the liner at 70 cm (A 6a - Fig. 10). In spite of very good 2R rod thermal behaviour, the temperature escalation was not predicted. Correct oxidation was obtained at the hot levels but overestimated under 40 cm. This explains the overestimation of H_2 by about 30 %. No fuel dissolution and no relocation results were available with the current version of the code.

GRS 2 : 2nd BC approach on the shroud liner :

GRS 2 and GRS 1 calculations were very similar because they are in fact two equivalent methods. Small differences were mainly due to the approximation performed to calculate the equivalent porous ZrO_2 conductivity from the GRS2 calculation (Fig. 6). This value was similar with the mean conductivity calculated with the Missenard model of ICARE2.

The final temperature plateau observed in Figs. 1 to 4 of Annex 6b corresponds to the formation of a U-Zr-O mixture which had to remain at its liquidus temperature of 2400 K up until the ZrO_2 layer was estimated to have melted.

6.7 - HUNGARY (Annex 7) : MARCH3 calculation

The calculation performed with MARCH3 was limited to the first oxidation phase. The He phase could not be calculated directly with the code. The shroud was taken into account by a fourth surrounding ring of 8 rods with zero nuclear power. The liner oxidation was taken into account by the cladding of these equivalent rods. Their properties were defined in order to find on these rods temperatures which could be used as reasonable boundary conditions for the inner 21 rods of the bundle. This method was presented as equivalent to the 1st BC approach.

The general behaviour of the rod temperature was correct, escalation was predicted at 8200 s (A7 - Fig. 2) but temperatures were overestimated in the hot zone where total oxidation was predicted from 45 cm to 80 cm. The H₂ production was 57 g instead of 39 g in the test.

The MARCH-3 code does not allow UO₂ and ZrO₂ dissolution. The calculation was stopped too soon to calculate rod relocation.

6.8 - I-PISE (Annex 8) : SCDAP/RELAP5 MOD2 calculation

A complete calculation was done with the SCDAP/RELAP5 MOD2 code. A correct thermal behaviour was obtained after adjustment of the heat conductivity of the porous ZrO₂ (Fig. 7) at a value about 3 times greater than the one measured.

A general slight overestimation was found except at the 70 and 80 cm levels where calculated temperatures fitted the measurements (A 8 - Fig. 2, 4, 6 and 10) very satisfactorily. A temperature escalation was found at level 70 cm on 2R rods but not at the 60 cm level as observed in the test, because oxidation was already nearly finished when the oxidation transition temperature of 1850 K was reached at this level. The calculated oxidation fitted the experiment (A8 - Fig. 25) very satisfactorily. The H₂ prediction was within the experimental uncertainty range (20 %). The non-active upper end of the fuel rods (7.3 cm long) gave an appreciable contribution to the oxidation (about 20 % of the cladding was oxidized at this level).

Fuel dissolution was obtained above and under the total oxidation zone. Dissolution was significantly overestimated (A8 - Fig. 29), 100 % was reached at

40 cm for the 3 kinds of rods instead of the 10 % in the test. Dissolution in the higher section of the active length (75/80 cm) was also calculated (45 %). In the test, only some local and weak UO₂ dissolution was also found above the hot zone.

The cladding oxide layer was correctly calculated to break, in the 35 - 55 cm zone at about 13050 s for the CR and 1R rods. But no cladding failure was calculated on the 2R rods which showed evidence of failure in the test.

Relocated U-Zr-O mixture was calculated to freeze at too low an elevation near the entrance of the bundle (5 cm) and below the active fuel column (52 % blockage at 5 cm) (A8 - Fig. 30) instead of the 20 - 28 cm zone in the test. Figure 32 summarizes the final bundle degradation. When the ZrO₂ cladding layer was calculated to break it was predicted not to relocate and remained in place.

The eutectic relocation at the 40 and 50 cm levels resulted in a reduction of the amount of fissile material and then of the nuclear heat generation. Temperature histories and profiles at these levels showed evidence of relocation (A8 - Fig. 1, Fig. 3, Fig. 11).

6.9 - ISPRA (Annex 9) : ICARE2 V1 calculation

The ICARE2 calculation was performed with a porous ZrO₂ conductivity greater than the one measured by a factor of three (Fig. 7). The overall thermal transient was correct with a slight underestimation of the rod temperatures in the hot zone (60 - 70 cm) (A9 - Fig. 11). Some parameters on the transmittal tape were incorrect due to writing errors and have not been given in the figures. (The shroud temperature, the heat flux through the shroud, the oxidation histories). Probably the non-prediction of the escalation at the hot level explains the too low oxidation value obtained (A9 - Fig. 25).

Fuel dissolution was found mainly between 15 and 25 cm where temperatures remained lower than the temperature failure criteria chosen by the user (2300 K). In the central zone where the cladding temperature exceeded 2300 K, the failure criteria was probably reached quickly because the oxide layer was always lower than the failure ZrO₂ thickness limit (500 μm). Molten Zry, therefore, could not be maintained in contact with the fuel for sufficiently long to lead to extensive UO₂ dissolution. All the rod cladding between 35 cm and 75 cm was relocated (A9 - Fig. 34). This led to an overestimated blockage in the lower part (93 % between

10 and 25 cm). Dissolution and relocation results were not in agreement with the experimental results mainly due to the considerable underestimation of the oxidation.

6.10 - JAPAN (Annex 10) : SCDAP/R5 MOD1 calculation

The first calculations performed with SCDAP/RELAP5/MOD1 led to cladding melt in the early phase of the test. The inner perimeter of the liner was therefore assumed to be three times longer than the real shroud, but the real geometry was kept unchanged for the flow area. Moreover it was not possible to take into account the pressure reduction during the final cooling phase.

The calculated thermal behaviour was greatly underestimated all along the bundle mainly during the oxidation phase (175 to 200° lower at the hot level just before the end of the oxidation phase). In these conditions oxidation and H₂ production were significantly underestimated.

A maximum of 40 % of oxidation at the hot level and 26 g of H₂ were calculated at the end of the steam phase. The code does not allow pure He, so during the helium phase a residual steam was maintained which explains the slow increase of oxidation and of H₂ production up to the end of the transient (A 10 - Fig. 26 and 28).

Fuel dissolution and molten mixture relocation did not appear in the results. The overestimation of the bundle blockage (A 10 - Fig. 30) could be due to the overestimation of the clad deformations.

6.11 - NETHER (Annex 11) : SCDAP/R5 MOD2.5 calculation

Due to an overestimation of the rod temperatures with the recommended thermal conductivity of the porous ZrO₂, sensitivity studies led to an increase of this value by a factor of 2. More correct temperatures were calculated, but still overestimated (A 11 - Fig. 1, 2, 10, 11). In particular the temperature escalation was predicted too early at 60, 70 and 80 cm (6800 s instead of 8200 s in the test) (A11 - Fig. 2, Fig. 7).

This early escalation was characterized by a run-away on the oxidation (A 11 - Fig. 26) and on the H₂ production (A 11 - Fig. 28). After this escalation, when the available zircaloy at hot level was fully oxidized the temperature decreased. The last peak in the H₂ rate was mainly due to the increase of the nuclear power which

led to an increase of the rod temperatures and of the oxidation at lower levels. After the steam/He switch a residual fraction of steam was maintained in order to avoid the code failure obtained when pure He is used. This explained the slow increase of oxidation in the He phase. Unexpected high oxidation was also found on the Zry liner at 70/80 cm. The strong oxidation run-away predicted on the rods in this zone explained the peak temperature calculated at the same elevation on the liner (A11 - Fig. 7). The overestimation of the temperature of the liner was also increased by a local run-away. This explained the overestimation of the liner oxidation in the upper part of the bundle.

A considerable overprediction of the fuel dissolution was found on the 3 kinds of rods between 25 and 55 cm (100 % at 40 cm) where non-oxidized Zr remained. (A 11 - Fig. 16, 20, 24, 29). Cladding failure of the CR and 1R rods was calculated as in the test at levels 30/40 cm when the failure temperature of 2500 K was reached at 13560 s. This was characterized by a loss of symmetry between the two total mass profiles of ZrO₂ and Zry at 14000 s (A 11 - Fig. 34). The corresponding U-Zr-O mixture was relocated and partially refrozen at level 5 cm. Second ring rod failure was not predicted because the temperature at the end of the He phase did not reach the chosen failure temperature of 2500 K. This indicates that this user-specified value was too large.

Around 13600 s the cladding of the 3 kinds of rods reached the melting temperature of ZrO₂ (2950 K) in the totally oxidized zone between 50 and 70 cm and a cohesive debris bed was predicted leading to a considerable 95 % bundle blockage at this level (A 11 - Fig. 30). This debris bed formation at 13600 s led to local unrealistic high temperatures (A 11 - Fig. 2, 4, 11) and to a code failure at 14000 s.

6.12 - SWEDEN (Annex 12) : SCDAP/R5 MOD2 calculation

The recommended heat conductivity of porous ZrO₂ was multiplied by about a factor 2 to obtain more reasonable predictions (Table 6). Rod temperatures were slightly overestimated under 30 cm, well-calculated between 30 and 50 cm and underestimated at the upper levels in the hot zone (A 12 - Fig. 2, 4, 11). The underprediction of the rod temperature was consistent with the underprediction of the liner temperature in spite of the SCDAP/R5 trend to overestimate the temperature difference between the outer row of rods and the liner. The temperature escalation observed at 60 cm, therefore, was not predicted, the oxidation of the 3 kinds of rods and the H₂ production were underestimated. A

maximum oxidation of 64 % was calculated on the central rod instead of the near 100 % observed and 27 g of H₂ was predicted instead of the 39 g measured in the test. The use of residual steam in the He phase explained the slow oxidation increase up to the end of the test (A 12 - Fig. 25, 26).

Due to the oxidation underestimation more non-oxidized Zr was available for the fuel dissolution which was overestimated (95 wt % instead of 14 wt % at 50 cm).

The overall underprediction of the fuel temperature and the choice of a high cladding temperature failure (2500 K - Table 4) prevented the prediction of a cladding rupture zone. The 2500 K limit was only exceeded at level 60 (A 12 - Fig. 2) where the calculated oxide layer thickness was greater than the ZrO₂ failure thickness limit (430 μm) chosen. No relocation occurred therefore and the bundle blockage (A 12 - Fig. 30) was only due to thermal rod deformations.

6.13 - TAIWAN (Annex 13) : MELCOR V1.8.0 calculation

The 2nd radial BC approach on the liner was chosen for this MELCOR calculation. In order to take into account the oxidation and relocation of the Zry liner, this structure was modelled as a canister (of a fuel BWR bundle) plus a surrounding heat structure. Radial heat flux was transmitted from rods to canister and then from the canister to this heat structure. The radiative steam absorption model was not used.

Very satisfactory agreement was obtained between the calculated and the measured temperatures (A 13 - Fig. 1 to 11). In spite of this accurate prediction, the temperature escalation observed at the 60 cm level was not calculated (A 13 - Fig. 2) and consequently the oxidation in the hot zone was underestimated (about 70 % instead of 100 %) and the calculated H₂ production was 32 g instead of the 39 g measured (inside the uncertainty experimental range) (A 13 - Fig. 25 and 28).

It must be pointed out that a constant mean axial power profile was used in the calculation. This could explain that the maximum temperature calculated was about 2600 K instead of about 2700 K in the test (the power profile was peaked in the hot zone due to the rising of the driver core control rods during the transient). No cladding failure was predicted due to the choice of a high failure temperature (2600 K) and due to an underprediction of the maximum temperature. Consequently no UO₂ and ZrO₂ material was transported.

The Zry liner (A 13 - Fig. 27) was calculated as melted and relocated. The corresponding failure criteria seemed different from those of the rods. All levels above 25 cm disappeared at 14000 s and liner relocation led to a maximum bundle blockage of 60 % at 20 cm. Refreezing location was correct (it must be pointed out that the Zry liner was equivalent concerning the initial mass of Zry to 8 rods).

The total mass profiles of UO₂, ZrO₂ and Zry material in the bundle also took into account the relocated materials (A 13 - Fig. 34). In the specifications [4] only non-relocated materials were required for the drawing of the total mass profiles.

6.14 - UK (Annex 14) : SCDAP/R5 MOD2.5 Version 361SC

The thermal conductivity recommended for the porous ZrO₂ gave rod temperatures in excess of those found in the test. Much better agreement was found when the much higher MATPRO values (Fig. 6) were used. The general thermal behaviour was well predicted for all the components, in particular at the hot 60 cm level (A 14 - Fig. 2). No further tuning of the shroud conductivity was made to better fit the measurements. The temperature escalation was well predicted at 60 cm and also at 70 cm.

Rod temperature histories at the 50 - 60 cm levels showed evidence of liquefied UO₂ relocation (A 14 - Fig. 1 to 3) in some upper axial nodes between 12000 s and 14000 s. The same evidence also appeared in the temperature profiles at 12000 s and 14000 s (A 14 - Fig. 11). Taking into account the evolution of the 5 power profiles versus time the maximum calculated temperature was about 2700 K as was estimated in the test. The fluid temperatures drawn at the 0 and 80 cm levels were in fact those at levels 4 and 76 cm (A 14 - Fig. 5,6).

At 60 cm, rapid oxidation during the run-away led to total oxidation on the CR and 1R rods and to 93 % on the 2R rods (A 14 - Fig. 15, 19, 23, 25). Oxidation was not complete in the upper part (70 - 80 cm) as measured in the test. Total H₂ production was also well calculated (36.8 g instead of 39 g in the test). Oxidation modelling was stopped during the He phase to avoid non-realistic oxidation due to residual steam (0.2 % imposed by the SCDAP/R5 code).

The fuel dissolution was excessive (100 % predicted at level 40 cm instead of 10 % in the test) (A 14 - Fig. 16, 20, 24, 29). It occurred where the Zry had not been completely oxidized, particularly at the upper level (70 - 80 cm) where dissolution was observed on some rods.

Cladding failure occurred on 2R rods at level 52 cm (11800 s) and later (13200/13640 s) at 44 cm (CR, 1R) and 36 cm (CR, 1R) roughly in the zone where failures were observed.

Relocated materials were calculated to freeze too far below the active fuel length. Only a small amount was located between 0 and 15 cm (A 14 - Fig. 30, 31). The shroud liner failure temperature was set to a high value so that no failure could occur.

A model for the hold-up of melt at the spacer-grids existed in the version of the code used but was effectively disabled due to an error of logic.

6.15 - U.S.A (Annex 15) : MELCOR V1.8EA calculation

The MELCOR calculation overestimated the rod temperatures with the recommended porous ZrO₂ conductivity. Sensitivity studies led to an improvement of the shroud modelling (Table 6) and an adjustment of the ZrO₂ conductivity in order to better fit the measurements (Fig. 6). The inlet steam flowrate (+ 5 %) and power (- 5 %) were changed in the experimental uncertainty range. Others parameters, in particular the flow distribution in the bundle, were also adjusted. Mixture properties were corrected (high quality of non-condensable gas) and cladding emissivity at high temperature imposed at 0.99 in order to improve rod temperature behaviour in the He phase.

In these conditions good thermal agreement was found and correct radial temperature gradients were calculated (A 15 - Fig. 9, 10). The temperature escalation was well predicted at 60 cm and also at 70 cm leading to the prediction of a temperature peak on the liner at 70 and 80 cm (A 15 - Fig. 2, 7, 8). Rod temperature dropped to zero at relocation because the cladding component relocated and was no longer present at 60 cm and 70 cm (A 15 - Fig. 4 and 10). Due to the use of a constant power profile, the maximum temperature was underestimated (2550 K instead of 2750 K in the test).

Oxidation run-away at hot levels (60 - 70 cm) led to a total oxidation on CR and on 1 R rods (78 % is reached on 2R rods) (A 15 - Fig. 13, 17, 21, 25). Oxidation was not found complete in the upper part as measured in the test. The total H₂ production was also well calculated (43 g instead of 39 g in the test).

No rod relocation was predicted until shortly before 14000 s. The CR failed at 50 and 60 cm (A 15 - Fig. 15) and the 1R rods failed at 60 cm (A 15 - Fig. 19) when the temperature reached the user-specified failure limit of 2500 K since the thickness of the oxide layer at these elevations was greater than the chosen limit of 60 μm . Due to the lack of support the remaining upper part of CR failed to form a debris bed. This rod failure process was not observed in the test.

No true UO_2 and ZrO_2 dissolution was calculated but a very small amount of UO_2 was transported as specified by the user in the input data deck when cladding failed at 50 and 60 cm (A 15 - Fig. 33 and 34). In a clad failure zone all the ZrO_2 was relocated with the remaining non oxidized Zr.

The axial profile of relocated materials (A 15 - Fig. 31) was characterized by 3 zones : a lower Inconel plug, a Zr - ZrO_2 - UO_2 plug at 20 cm and a pure UO_2 debris bed in the upper part (50 - 60 cm). The maximum bundle blockage of 45 % at 20 cm was mainly due to the freezing of cladding materials. This location was nearly in agreement with the test but the blockage was underestimated. All the grid spacers were relocated when the Inconel melting temperature of 1533 K was reached. They relocated on the core plate just below the active length and under the actual Inconel plug. The pure UO_2 debris bed in the upper part was not considered as a plug with a resulting blockage.

7 - OVERVIEW OF THE COMPARISONS

The aim of this section is to compare code predictions and to analyse the differences found using the same code. The ability to calculate the PHEBUS-SFD transient and the different thermal and degradation phenomena involved in the B9+ test will be examined in particular with regard to the choice of some user-specified input data. Modelling weaknesses and gaps will be identified and code performances with regard to the code running times will be discussed. A summary and an overview of the comparisons are given in [9].

Due to the large number of participants and to the difficulty in clearly showing the participants' results together, the submissions were classified into the following three groups :

GROUP I	GROUP II	GROUP III
FRA-SP SP-UPM ISPRA TAIWAN USA Measurements	FRA-SP I-PISE NETHER SWEDEN UK Measurements	FRA-SP SP CSN CZECHO GER IKE 1 GER GRS 1 HUNGARY JAPAN Measurements

The criteria for the classification were :

- Same code or same kind of codes :

- GROUP I - ICARE2 and MELCOR
- GROUP II - SCDAP/RELAP 5 Mod 2
- GROUP III - SCDAP Mod1 Stand Alone
- SCDAP/R5 Mod 1
- KESS III, ATHLET SA
- FRAS SFD, MARCH3

- Same phenomena calculated in the transient :

Degradation aspects are found mainly in GROUPS I and II.

The FRA-SP calculation with ICARE2 was quoted in the three groups in order to be used as a reference calculation (totally open submission).

For these comparisons a limited number of parameters were chosen.

- TU2RZZ : Fuel temperature versus time at different elevations (30, 50, 60, 70 cm).
- TSR160 and TSR360 : Liner and inner shroud temperatures
- OX1RZZ : Oxidation histories at different levels (40, 50, 60, 70 cm).

HYDTOT	:	Total H2 release.
OX1RZZ	:	Oxidation profile on the first ring rods just after the end of the first steam phase
DUMEAN	:	The mean fuel dissolution profile for the 1R rods at 14000 s.
COBKZZ	:	The channel blockage profile at 14000 s showing material relocation with the main plugs. This parameter is defined as being equal to 38 % at the initial conditions of the transient due to the 21 intact rods inside the initial inner section of the octagonal Zr liner (see section 4.9).

All the comparisons are given in the Annex 16.

7.1 - The Modelling of the B9+ transient

7.1.1 - Nodalization

In general, a more or less common approach was used for the nodalization of the different components of the bundle (see section 5 and Fig. 10). One hydraulic channel and three different rods were often used. Two participants made use of 3 parallel and independent channels (FRA - SP, SP-CSN).

7.1.2 - Difficulties

The main problem encountered concerned the shroud modelling. Some codes were not able to directly take into account the multilayer shroud, therefore some modifications (MELCOR) or modelling compromises (FRAS-SFD, MARCH-3) had to be made by some participants even when the simplified 2nd BC approach was chosen. It must be pointed out that these codes were developed for reactor studies and have not been intensely used up to now for modelling small scale experiments.

A second difficulty encountered by some participants concerned the modelling of the pure He phase and the transition from steam to He. In general codes do not allow He as a cooling gas. H₂, air, or steam were therefore used in place

of He in conserving the enthalpy flow rate or in redefining gas properties in input. He gas was directly taken into account by some codes after modification of the fluid properties (MELCOR V 1.8EA, ICARE2 V2).

A pure non-condensable gas was not allowed by MELCOR V1.8.0 and SCDAP/R5 and a small fraction of steam (0.2 %) was necessary to avoid a code failure or inconsistencies. This led some participants who could not modify the code to calculate continuous weak oxidation during the He phase (I-PISE, JAPAN, NETHER, SWEDEN).

Some participants using MELCOR and SCDAP/R5 could not take into account the 5 specified power profiles due to the codes being limited respectively to 1 and 3 profiles. This limitation, which is only a problem for calculations of in-pile tests, can explain part of the underprediction of rod temperature during the He phase.

Others limitations were also mentioned concerning rod axial meshing (maximum 10 meshes) which could not be checked so as to study the effect on the results.

The majority of the users had difficulties as regards to printed outputs and drawing possibilities, particularly in representing the radial heat flux at some elevations or parameters related to material relocation (fuel dissolution and flow blockage profiles, profiles of non-relocated materials such as Zry, ZrO₂, UO₂ or profiles of relocated mixtures).

Lastly, during the switch from steam to He and afterwards, some numerical instabilities led to severe time step reductions (MELCOR, SCDAP/R5 Mod2, FRAS-SFD). Run statistics will be examined at the end of this section.

7.2 - Thermal behaviour

7.2.1 - Heat balance in the bundle

The thermal behaviour is controlled by the heat balance in the bundle. A calculated energy balance was given by some participants. (Fig. 17a, 17b, 17c). These curves show approximately that 70 % (during the steam phase) to 90 % (during the He phase) of the total nuclear power is transferred to the shroud.

The remaining energy is transferred to the fluid by convection and radiation absorption by steam. Rod temperatures therefore are mainly dependent on the prediction of the radial heat flux through the shroud [7].

The use of the recommended thermal conductivity of the porous ZrO_2 layer [2] always gave bundle temperatures in excess of those found in the experiment. All the participants who used the first approach had to choose higher conductivity, two to three times greater than the experimental recommended value (Fig. 7). The tuning of this parameter was performed by some participants (USA, I-PISE, FRA-SP) in order to fit the temperature measurements and obtain correct cladding oxidation conditions which have significant effect for later rod degradation at high temperature.

In particular, FRA-SP adjusted the conductivity of the porous ZrO_2 at each level by tuning the porosity calculated by the Missenard model. The dotted line in figure 7 shows the conductivity calculated by the Missenard model, assuming 70 % porosity and He-filled pores.

A detailed analysis of the heat transfer in a porous medium showed that the pressure effect was underestimated when the atmospheric pressure measurements of the conductivity were extrapolated to 1.9 MPa. This effect led to an increase of the conductivity by a factor consistent with the tuning factor of the participants.

Overall satisfactory agreement was generally obtained with the different codes concerning the thermal behaviour of the bundle (A16 - Fig. 1/1 to 6/3). The significant discrepancies are due to incorrect calculation of the shroud thermal leakage, underestimated by SP-CSN, NETHER and SP-UPM (only in the He phase) and overestimated by JAPAN and SWEDEN.

7.2.2 - Radial temperature profile

Table 8 summarizes the radial temperature gradients calculated at 7800 s at the hot point (60 cm). There was a general tendency to underestimate the temperature difference between 1 R and 2 R rods - Reasonable predictions were obtained with ICARE2V2p, SCDAP/RELAP5 Mod2 and ATHLET SA. Radial temperature differences in the shroud were in general well calculated. The overestimation by GER-IKE is due to too early a prediction of the temperature escalation. It must be pointed out that the use of a mean hydraulic

channel tends to reduce radial differences while the use of three independent channels (FRA-SP, USA) tends to increase them. Radial differences are also a function of cladding emissivity and decrease when the emissivity increases. From these comparisons performed with different cladding emissivities and different radiative heat transfer models it is therefore difficult to conclude as to the best hydraulic modelling. Degradation differences between each kind of rod result from the calculated radial temperature profile in the bundle.

7.2.3 - Temperature escalation

A rapid heat-up rate (> 3 K/s) occurred in the hot zone (60/70 cm) just after 8000 s. This resulted both in a rapid oxidation increase above 1850 K (tetragonal to cubic change of the ZrO_2 structure) and to a simultaneous nuclear power increase.

In general, participants who correctly calculated the heat balance and rod temperatures before 8000 s also predicted this temperature escalation : USA, UK, FRA-SP, I-PISE, HUNGARY (A16 - Fig. 3/2). In spite of an overall correct temperature prediction GER-GRS1 and GRS2, GER-IKE2, and TAIWAN did not predict this escalation. Due to the overprediction of the temperatures at the hot level, SP-CSN, GER-IKE1, NETHER and CZECHO calculated the escalation sooner than in the test (A16 - Fig. 3/3).

7.2.4 - Fluid temperature at the bundle outlet

The 3 fluid outlet thermocouples located at 80 cm indicated very similar temperature responses. They are suspected to have given a lower temperature than the local fluid temperature. This trend, which could be due to thermocouple heat losses by radiation towards the upper colder region of the test train, is confirmed by a general overestimation of the outlet fluid temperatures, mainly in the He phase (Figures 6 of Annexes 1 to 15).

7.2.5 - Maximum temperature

With a correct prediction of the heat flux through the shroud and by taking into account the specified evolution of the axial power profile in time, I-PISE, UK and FRA-SP with SCDAP/R5 and ICARE2 made a correct calculation of the maximum temperature estimated at 2750 K. This value was extrapolated from the internal shroud lower temperatures which could be measured

throughout the test (see section 3.3.5). This maximum temperature was underestimated by the MELCOR calculations (TAIWAN, USA) which were performed with a constant power profile less peaked in the hot zone than in the real case at 14000 s.

7.3 - Oxidation and H₂ production

The prediction of these parameters resulted directly from the prediction of the rod temperature (except for SP-UPM, see section 6-3).

7.3.1 - Cladding oxidation histories

These are shown at different elevations : 40, 50, 60, 70 cm (A16 - Fig. 7/1 to 10/3).

No prediction of steam starved conditions was mentioned during the steam phase but this could have occurred in the hot zone during the final and short oxidation escalation.

During this escalation at 8200 s, the remaining non oxidized Zry of the cladding in the hot zone (about 50 % of the initial value) was quickly consumed reaching nearly complete oxidation (A16 - Fig. 9/1 to 10/3). In these conditions a correct calculation of the oxidation excursion requires a very accurate calculation of the temperatures and energy balance in the bundle.

The considerable spreading of the cladding oxidation histories at 50 and 60 cm is mainly due to the temperature differences between the calculations. This spreading is greater at 50 cm in the axial "transition zone" of the escalation both in the experimental and calculation results.

Calculated axial oxidation profiles of the 1st ring rods were compared with the ZrO₂ measurements (A16 - Fig. 12/1 to 12/3). The minimum and maximum measurements of the outer and inner rods given in these figures are representative of oxidation at the end of the steam phase. Axial oxidation profiles were correctly predicted by ICARE2, MELCOR and SCDAP/R5 when both temperature histories and escalation were correctly predicted.

The total oxidation in the hot zone (60-70 cm) was found by nearly all the participants except for ISPRA, TAIWAN, SP-UPM, SWEDEN and JAPAN. Prediction of total oxidation does not necessarily indicate good thermal calculations but can be due to temperature overestimations (NETHER,

SP-CSN). Inversely, the non-prediction of total oxidation can result from a slight underestimation of the temperature which overly delays the beginning of the escalation (TAIWAN).

When a cladding failure is predicted with MELCOR and ICARE2, the dislocated ZrO₂ layer slumps with the molten Zry but is kept in place with SCDAP/R5. The ZrO₂ slumping which explains the sudden reductions of the calculated ZrO₂ layers (A16 - Fig. 7/1, 8/3, 9/1 and 9/3) occurs, in the B9+ test, during the He phase.

7.3.2 - H₂ production

Comparisons between calculations and measurements are shown in figures 11/1 to 11/3 (Annex 16). Only 4 calculations are within the experimental uncertainty range [32/47 g]. Hydrogen prediction results directly from the global calculation of the oxidation of the cladding tubes and liner, and the spreading of the calculated H₂ release sums up the uncertainties related to the release from these two structures.

In some calculations (FRA-SP, I-PISE, IKE1) part of the H₂ overestimation could be due to an overestimation of the liner temperature which results from an underestimation of the temperature difference between the external rods and the liner. (About 20 % of the total H₂ is produced by oxidation of the liner which is equivalent to about eight rods).

7.3.3 - Experimental and modelling uncertainties

Experimental uncertainties are related to different difficulties such as non-homogeneous cladding temperatures in the bundle and identification of a ZrO₂ thickness representative of the oxidation at the end of the steam phase. This ZrO₂ layer was in fact affected during the second He phase by the following interactions depending on the elevation : ZrO₂ reduction due to O₂ diffusion during the He phase (see section 4), ZrO₂ dissolution by molten Zry, strong UO₂-cladding chemical interaction, complete relocation for some levels. The spreading of the ZrO₂ thickness measurements results from these uncertainties (A16 - Fig. 12/1 to 12/3).

Modelling uncertainties are also related to different factors. During a significant oxidation phase as observed in B9+, the underlying metallic Zry is totally transformed into α -Zr(O) and then to ZrO₂. In these conditions the ZrO₂ layer increase kinetics leads to an underestimation of the oxidation. On the other hand, local α -Zr(O) melting during the escalation could lead to a relocation and/or simultaneous UO₂-ZrO₂ dissolution which could decrease oxidation. Most of the time these last limiting factors are not taken into account in the codes.

Finally, in spite of all these uncertainties and drawbacks, comparisons between calculations and data show that the oxidation prediction with the current models are within the experimental range when temperatures are correctly estimated.

7.4 - Inconel spacer-grids

There are no spacer-grid models in the code versions used able to take into account clad - Inconel spacer-grid interaction (see section 4.4). Only the MELCOR calculations (USA, SP-UPM) mentioned grid liquefaction and relocation predicted by a simple parametric model.

7.5 - Fuel dissolution by molten Zry

The second heat-up phase is characterized by extreme steam-starved conditions in order to facilitate simultaneous UO₂ and ZrO₂ dissolution by molten Zry. This phenomenon is significantly dependent on the temperature but also the oxidation profile which determines the mass of molten Zry available and its oxygen content. The UO₂ and ZrO₂ dissolutions are limited by the temperature dependent UO₂ solubility in the local U-Zr-O mixture or by the failure of the external ZrO₂ layer of the cladding (named in the following sections "cladding failure") which governs the flow-down of the mixture and the end of the dissolution.

Tables 3 and 4 summarize respectively the fuel dissolution models used and the conditions of cladding failure by molten Zry chosen by the users. Comparisons are shown in figures 13/1 to 13/3 of Annex 16.

Only ICARE2, SCDAP Mod1 and SCDAP/R5 Mod2 gave final results for the fuel dissolution. The FRAS-SFD code began a calculation of the UO₂ dissolution at the very end of the steam phase at 0.75 m, but the calculation could not be

continued in the He phase. There is no true dissolution model in MELCOR but a parametric model allows removal and transport of a user-specified fraction of the UO_2 when cladding failure by molten Zry is predicted.

Only ICARE2 V2p predicted a fuel dissolution in agreement with the test. In general, fuel dissolution was significantly overpredicted by SCDAP/R5 at each elevation where the non-oxidized Zry melted.

The ISPRA submission with ICARE2 V1 (with a different model) did not predict significant dissolution at the upper part of the bundle due to the failure criteria chosen ($500\ \mu\text{m}$, $2300\ \text{K}$) and due to oxidation underprediction. The oxide thickness calculated was always lower than the failure ZrO_2 thickness chosen ($500\ \mu\text{m}$) to maintain the molten Zry in place at a temperature greater than $2300\ \text{K}$. As a result, early cladding failure prevented significant duration of the fuel dissolution in the upper part of the bundle due to an early flow-down of the molten mixture.

SCDAP/R5 Mod2 and SCDAP Mod1 predicted considerable UO_2 dissolution at each elevation where some non-oxidized Zry remained and melted after the end of the oxidation phase. All the participants using these codes (SP-CSN, I-PISE, NETHER, SWEDEN and UK) chose the same cladding failure temperature of $2500\ \text{K}$ (and a failure thickness limit between 435 and $540\ \mu\text{m}$), so similar results were obtained. Due to a significant underestimation of the oxidation, particularly in the hot zone, SWEDEN over-predicted the fuel dissolution at these levels compared with the other SCDAP/R5 calculations.

Three main reasons related to the code models might explain the differences between ICARE2 V2p and SCDAP/RELAP5 Mod2 calculations, the cladding failure temperature ($2300\ \text{K}$ for ICARE2 and $2500\ \text{K}$ for SCDAP/R5), a lower solubility limit of UO_2 in the U-Zr-O mixture and a ZrO_2 dissolution by molten Zry considered in ICARE2. The first in the ICARE2 prediction tends to limit UO_2 dissolution in the central zone ($40\ \text{cm}$) due to early cladding failure, the second also tends to limit the prediction of UO_2 dissolution by ICARE2 due to a lower UO_2 solubility chosen as being the liquidus boundary of the U-Zr-O mixture. The third reason is related to the ZrO_2 dissolution discussed below.

7.6 - Zirconia dissolution by molten Zry

Only FRA-SP gave a calculation of the ZrO₂ dissolution. The ICARE2 V2p code simultaneously took into account UO₂ and ZrO₂ dissolution by molten Zry. This second dissolution phenomenon tends both to increase the oxygen content in the mixture (which decreases UO₂ solubility) and to reduce the ZrO₂ thickness. The calculated ZrO₂ dissolution calculated in the failure zone was able to attain up to 60 % of the ZrO₂ layer calculated at the end of the oxidation phase. When the melting temperature of α-Zr (O) was reached at about 10600 s, the calculated ZrO₂ thickness reduction observed in the oxidation histories at 50 cm (A.16 - Fig. 8/3) was due to this ZrO₂ dissolution. PIE showed local ZrO₂ reduction of up to 50 % in the upper part of the bundle, but it is not sure that this reduction resulted only from the ZrO₂ dissolution (see section 4.7).

7.7 - Relocation of molten materials and channel blockage

Nine submissions gave calculated results concerning material relocation

FRA-SP and ISPRA	with ICARE2
SP-UPM, TAIWAN, USA	with MELCOR
SP-CSN	with SCDAP Mod 1
I-PISE, NETHER, UK	with SCDAP/RELAP5 Mod2.

Predictions of the general trend of the relocation and the cladding failure zones are summarized in figure 15 of A16. The channel blockage calculated by the different codes is given in A16 - Fig. 14/1, 14/2, 14/3 (see definition in section 4.9).

There is considerable spreading of the calculated results even when calculations were performed with the same code. Relocation behaviour is in fact very sensitive to the following parameters :

- The final oxidation profile at the end of the steam phase. This profile determines the amount of non-oxidized Zry for the UO₂ and ZrO₂ dissolution and the thickness of the ZrO₂ shell which maintain the molten Zry in place,

- The thermal histories during the high temperature heat-up of the He phase. These histories determine the melting zone of the non-oxidized Zry, the UO_2 solubility limit in the U-Zr-O mixture (ternary phase diagram) and also the failure zone where the cladding failure temperature limit is exceeded,
- Cladding failure by molten Zry is governed by simple criteria. The user-specified failure parameters of these criteria are very important for relocation [7] [8]. Criteria usually include two parameters, a failure temperature limit and a ZrO_2 thickness limit. The axial failure zone increases when both the temperature limit decreases and when the ZrO_2 thickness limit increases. Additional criteria also govern debris bed formation (e.g. the melting temperature of ZrO_2).
- With the same conditions of oxidation, temperature and cladding failure, the amount of U-Zr-O mixture which can be formed before the cladding failure depends on the UO_2 dissolution model (UO_2 and ZrO_2 dissolution kinetics plus the UO_2 solubility limit).
- The final freezing of relocated material depends on the melt progression model and also on some user specified parameters such as the heat exchange (heat transfer coefficient and contact surface) between the molten material and the solid support or the mixture properties (solidus temperature).

Taking into account all the parameters involved in relocation prediction, it is very difficult to make an accurate analysis of the relocation and blockage results. This is a classic example of a domain in which compensation errors can lead to acceptable results.

The following comments can be made concerning the relocation predictions.

Only the reference calculation (ICARE2 V2p) which correctly predicted the UO_2 dissolution gave reasonable results concerning both the cladding failure zones and the bundle blockage (A16 - Fig. 15).

Whatever the prediction of the cladding failure zones, in general SCDAP/R5 and MELCOR predicted the refreezing zones at elevations that are either too low in the bundle or under the lower end of the rods. This trend was particularly followed by I-PISE and UK in spite of a correct prediction of the cladding failure zones. This disagreement with the test is mainly due to an overestimation of the UO_2 dissolution.

Using MELCOR V 1.8EA, the USA predicted a cladding failure zone by molten Zry (45 cm to 65 cm) for the inner rods higher than the experimental zone (28 cm to 50 cm) and a non-observed debris formation with cladding embrittlement between 65 and 80 cm on the central rod. A cladding failure criterion based on a temperature limit of 2500 K when the oxide layer thickness is greater than $60 \mu\text{m}$ was applied to a transient which underestimated the temperature during the He phase (power profile constant). This explains the incorrect prediction of the failure zone above the actual one. The use of a different failure condition based on the usual ZrO_2 thickness limit condition would have avoided the failure prediction in the upper part of the bundle, and the prediction of higher temperatures would have led to a failure prediction lower in the bundle.

The location of the blockage near 20 cm is in agreement with the test but the corresponding bundle blockage (ZrO_2 -Zr mixture with 0.3 % of UO_2) is slightly underestimated and too poor in UO_2 . It results from the first cladding failure process by molten Zry. The cladding failure of the CR therefore spreads up to 80 cm due to lack of support from below. This leads to a UO_2 debris bed formation which remains located in the 50/60 cm zone. A solid debris bed was not observed in the B9+ test where the complete oxidized cladding maintained the UO_2 pellets in place.

No liner relocation was predicted.

The SP-UPM calculation with MELCOR V 1.8 predicted incorrect cladding failure and relocation zones. Two kinds of cladding failure were calculated. The first was due to molten material when the ZrO_2 thickness limit was lower than $100 \mu\text{m}$ whatever the temperature of the molten Zry. Due to this too low a value corresponding to an oxidation of only 11 %, the lower zone of the bundle could fail (zone 16 to 24 cm for 2R rods) whereas no failure could be predicted in the zone where clad failures were observed in the test. A second kind of cladding failure occurred in the 48-64 cm region to form a pure UO_2 debris bed. The corresponding criteria were based on the melting of ZrO_2 ($T > 2990 \text{ K}$) which

was reached at the end of the heating phase (just before 14000 s) because the rod temperatures were significantly overpredicted in spite of a power profile that was kept constant. (Maximum temperature estimated in the test : 2750 K). No debris bed formation would have been calculated with a more correct prediction of the rod temperatures. The main part of the relocated molten materials dripped outside the active fuel length (including all the spacer grids and the molten Zry and ZrO₂). These results are not in agreement with the test. The percentage of UO₂ and ZrO₂ transported by means of the molten Zry relocated after the cladding failure was imposed at 20 % by the user.

No cladding relocation was predicted by MELCOR V 1.8 in the TAIWAN submission due to the choice of too high a failure temperature of 2600 K, greater than the maximum temperature calculated (underestimation of the temperatures due to the use of a constant power profile). Only the Zry liner was relocated but the failure zone was overestimated (25-80 cm instead of 25-56 cm in the test). The freezing zone of the liner was well calculated with a blockage of 60 % instead of 52 % in the test (A16 - Fig. 14/1).

The UK and I-PISE calculations performed with SCDAP/RELAP5 Mod2 were similar, the rod temperatures were well predicted and the cladding failure parameters were the same (2500 K and about 520 μm). The results are in agreement with the test concerning the CR and the 1 R rods. In the two calculations, the cladding failure results were different as regards the 2R rods which were only predicted to fail in the UK calculation at 52 cm. The non-prediction of the 2 R rod failure in the I-PISE calculation was due to the cladding temperatures which remained below the failure temperature of 2500 K. The excessive amount of eutectic resulting from the UO₂ dissolution could explain part of the overestimation of the melt relocation distance (too large an amount of energy in the melt). Only part of the melt was therefore refrozen within the test train in the lower 0-8 cm zone leading to a limited bundle blockages (41 % in the UK submission and 52 % for I-PISE) in spite of the overestimation of the UO₂ dissolution.

The NETHER calculation was performed with the same cladding failure criteria as the UK, but the relocation results were very different. The overprediction of the temperatures led to an overestimation of the oxidation in the central 40-56 cm zone which prevented cladding failure. With overestimated temperature and oxidation conditions, the CR and 1R rods could only fail in the lower zone

30-40 cm. The melting temperature of ZrO_2 was also reached in the upper part (50-65 cm). This led to cladding failure with a debris bed formation around 60 cm and a nearly complete blockage of 96 % (A16 - Fig. 14/2) not observed in the test. The mixture resulting from the fuel dissolution was frozen too far, as in the UK and I-PISE calculations, in spite of a smaller amount of mixture. Only part of this mixture was refrozen in the lower 0-8 cm zone in the bundle.

The SCDAP-Mod1 calculation of SP-CSN was characterized by an overestimation of the rod temperatures and the oxidation (nearly complete oxidation above 40 cm). In spite of an overprediction of the fuel dissolution zone under 40 cm (A16 - Fig. 13/3), part of the predicted cladding failure zone and the frozen material distribution is in agreement with the test (A16 - Fig. 15). With cladding failure criteria based only on a temperature limit of 2500 K, and with overestimated temperature and oxidation conditions, the failure zone could only be found in the upper part of the remaining not completely oxidized zone (24 - 40 cm for CR and 1R rods). This calculated zone corresponds to the cladding failure zone observed in the test but is characterized by different temperature and oxidation conditions. The first part of the molten material was frozen in the failure zone in spite of the too high temperatures obtained in this zone and led to a correct channel blockage of 54 %. The second part was dripped outside the active fuel length (not observed in the test). Only compensation effects between the different degradation models can explain the noted agreements. The maximum flow blockage of 62 % at 60 cm (A16 - Fig. 14/3) was due to the prediction of considerable cladding deformation before rod plug melting (not observed in the test).

In the SWEDEN submission, no cladding failure was predicted because the cladding temperatures were always below the failure temperature limit (2500 K) chosen by the user.

For JAPAN, the same reason probably explains the non-prediction of cladding failure (too large a failure temperature of 2700 K was chosen). The calculated channel blockage of more than 50 % above 20 cm (A16 - Fig. 14/3) could be due to the prediction of considerable cladding deformation.

7.8 - Mixture compositions

The few mixture compositions which were transmitted are summarized in Table 9. These compositions are given in percentage of UO_2 , Zr_y , ZrO_2 and steel or

Inconel. The codes have no models that take into account chemical reactions in the mixtures except molten Zry oxidation. The final composition results only from the addition of the different relocated melts. There is poor agreement except with the ICARE2 code as regards the main plug at 20 - 28 cm.

7.9 - Code run time statistics

Table 10 summarizes the information concerning the computational times needed for the B9+ calculations. The lack of relative computer speeds for all the computers used does not allow a correct code performance comparison. Nevertheless the following comments can be made :

- The average time step size can give a rough idea of code performance. There is considerable spreading of this value. The largest time steps of about 1 to 10 s were used by ICARE2, FRAS, KESS, ATHLET and MELCOR (USA and TAIWAN). The SCDAP/R5 Mod 1 and Mod 2 and MARCH 3 codes were run with very small time steps in the range of 10^{-1} to 10^{-2} s. The CPU time of the MELCOR calculation performed by SP-UPM was also very long (8 times the MELCOR calculations of TAIWAN and USA). The main reason for this is that two control volumes in the core region were used, with too small a volume for the entrance of the rods which control the time step throughout the Courant condition. It must be pointed out that the KESS, ATHLET and FRAS codes did not perform dissolution and relocation calculations which are time consuming.
- The same trend is observed as regards the CPU-time per second problem time and per cell. The number of cells was deduced from Table 5 using the number of rods and the axial meshing for the total rod length or active length. (The shroud was considered as a rod). The largest minimum step (5 s) was used with KESS and this could explain the temperature oscillations found in the He phase. (A5a - Fig. 5, 6).
- The transition period from steam to helium and the following pure helium phase was CPU time consuming due to numerical instabilities. The minimum time step was often divided by a factor greater than 5 or 10 (MELCOR, SCDAP/RELAP5) No reduction was really necessary with SCDAP Mod1, ICARE2, ATHLET and KESS,

- Whatever the computer used, excessive CPU times are a real handicap for sensitivity studies. In particular it was indicated that the CPU times needed with SCDAP/RELAP5 Mod2 or SCDAP Mod1 ranged from 36 h (CRAY XMP14) to 75 h (SUN4/330). These very long CPU times were mainly due to numerical instabilities in the He phase calculation which took up 80 % to 90 % of the total CPU time. The first pure vapour phase was less time-consuming (more than 5 hours) but the CPU time still remained significant.

8 - CONCLUSIONS

The PHEBUS SFD B9+ test, selected as International Standard Problem n° 28 was calculated by a large number of participants using the main existing SFD codes. In spite of experimental uncertainties, unavoidable for tests performed with severe thermal-hydraulic conditions, the ability of these codes to predict the main governing phenomena of the early phase of a PWR core degradation was able to be assessed.

Above all, the semi-blind nature of ISP 28 must be considered as regards the comparisons with the experiment. The thermal-hydraulic behaviour was given to the participants. The degradation aspect of the bundle was the blind part of the exercise, so "user-tuning" to better predict degradation was not performed. One exception concerned the FRA-SP submission (joint CEA - Phebus Espana Consortium) which was performed in open conditions. These participants were closely involved in the PHEBUS Programme and their submission was considered as a reference calculation.

Substantial experimental data were obtained from the PHEBUS B9+ test. Different axial oxidation states, UO_2 and ZrO_2 dissolutions and relocations of the liquefied mixtures on the lower part of the bundle were characterized. Experimental boundary conditions such as the nuclear power, the thermal-hydraulic conditions at the bundle entrance, and the sink temperature on the outer surface of the shroud were well defined.

Thermal behaviour :

The main uncertainty of the test concerned the radial thermal leak through the shroud. Participants could not calculate correct rod temperatures using the recommended thermal conductivity of the porous ZrO_2 layer of the shroud. The porous ZrO_2 conductivity value deduced from laboratory measurements performed at 0.1 MPa

was extrapolated to the pressure condition of B9+ (1.9 MPa). This extrapolated value, recommended for performing the exercise was not suitable due to an underestimated pressure effect. Consequences on the thermal rod prediction were as follows.

- Using the 1st approach for the radial BC, all the calculations showed that to obtain a correct general tendency of the rod temperatures it was required a "user-adjusted" ZrO₂ conductivity value greater than the one recommended by a factor 2 to 3. Few participants seem to have performed accurate tuning of this very sensitive parameter for calculating the thermal conditions of the bundle.
- Using the 2nd approach for the radial BC, all the participants found correct rod temperatures with the MELCOR, ATHLET SA and KESS III codes.

In general, participants who performed a correct calculation of the thermal behaviour of the first steam phase were able to calculate the final oxidation and temperature escalations : the UK and I-PISE with SCDAP/R5-MOD2, the USA with MELCOR, FRA-SP with ICARE2. A slight tendency to overestimate oxidation in the upper part of the bundle and the corresponding H₂ release was observed. Only four participants predicted H₂ production inside the experimental uncertainty range.

In spite of the difficulty in predicting cladding oxidation with a local and strong escalation suddenly stopped by steam starved conditions, code to data comparisons show that the current models based on kinetics correlations of Cathcart up to 1853 K and Urbanic Heidrick at higher temperature are sufficient to predict oxidation within the experimental uncertainty range providing that a correct calculation of the energy balance in the bundle is performed.

UO₂-Cladding interactions and resulting melts relocation :

Except for the reference calculation with ICARE2V2p, degradation processes such as UO₂ and ZrO₂ dissolutions, cladding failure by molten Zry, and relocation and freezing of molten mixtures were not well predicted. Nearly all the codes showed the same trend in the deviation with the PTE. Discrepancies in rod temperatures and related sensitive effects on melt progression cannot totally explain the discrepancies found for rod degradation. Discrepancies also resulted from areas with weaknesses and gaps in the following aspects of core damage modelling.

UO₂ dissolution by molten Zry and solubility limit

- Fuel dissolution by molten Zry was significantly overestimated except with version V2p of ICARE2. The maximum mean dissolution observed in B9+ test was in fact

limited to 14 %. This chemical interaction is highly dependent on the temperature and oxidation conditions. In addition, a correct prediction needs correct modelling of UO_2 solubility in the resulting U-Zr-O mixture. This limiting factor of the interaction is given by rough models of the ternary phase diagram of the mixture which should be verified, particularly at high temperature.

ZrO₂ dissolution by molten Zry

- ZrO_2 dissolution by molten Zry, which could not be quantified in the PIE, determines the chemical effect on the cladding failure process (reduction of the ZrO_2 layer) and increases the O_2 content in the U-Zr-O melt resulting from the simultaneous UO_2 and ZrO_2 dissolutions. These two effects tend to limit UO_2 dissolution by molten Zry. Modelling of ZrO_2 dissolution by molten Zry is recommended.

External ZrO₂ cladding layer failure

- Mechanistic models of mechanical failure of the external ZrO_2 cladding layer by molten Zry are currently lacking. Only simple parametric models based on one or two criteria using parameters defined by the user are available. These important user-specified conditions determine the end of UO_2 dissolution at the failure location, and the flow-down and relocation of the U-Zr-O mixture. The diversity of the conditions and parameters used clearly shows a lack of data in this field and modelling deficiencies. From the B9+ experimental results, the failure criteria which would have defined a better cladding failure zone in the case of a correct thermal and oxidation prediction are :

$$T_{\text{clad}} > 2300 \text{ K and } e^{\text{OX}} < 400 \text{ to } 500 \mu\text{m.}$$

These criteria remain applicable for a code which does not have a cladding ZrO_2 dissolution model. For codes modelling ZrO_2 dissolution, the oxide thickness limit related to mechanical effects only is reduced.

Melts relocation

- Calculated melts relocate and refreeze too far or out of the bundle (SCDAP/RELAP5 - Mod2, MELCOR, SCDAP Mod1). In addition to an overestimated amount of melts resulting from UO_2 dissolution, which leads to an overestimated amount of transported energy and relocation distance, incorrect relocation parameters or incorrect mixture material properties are also suspected.

Inconel spacer-grid

- Effective Inconel spacer-grid models including interaction with rods do not exist or are not able to work. Only MELCOR described spacer-grid melting and relocation. Modelling of spacer-grid effects is recommended.

User effects :

As shown in previous ISP exercises different results were produced by different participants using the same code. In this ISP28, user influence on the predicted results mainly originated from the possibility of defining degradation parameters in the input data deck. The main ones are the cladding failure parameters which can have tremendous effects on relocation going from a total relocation to no relocation at all with similar thermal and oxidation conditions. Some parametric models allow relocation of fuel and ZrO₂ in quantities specified by user input parameters (MELCOR). In that case, final relocation results, particularly flow blockage, are therefore user-dependent.

Degradation results were calculated using different nodalizations and representations. The resulting differences could not be identified except as regards multi channel modelling which tended to increase radial temperature gradients and differences between the second ring rods and the inner rods for degradation prediction.

User effects could be reduced if more mechanistic models were available, or if more detailed information and recommendations were given in the user guide-lines, including the sensitivity of some user-specified parameters strongly affecting rod degradation (cladding failure limits).

Results also depend to a large extent on user experience and on the time and means devoted to performing the necessary sensitivity studies. Some participants acknowledged that they were not familiar with the code used and with the sensitivity of some of the parameters for degradation. A good knowledge of the phenomena governing rod degradation and of the related physical models of the codes would help the user to better prepare code input data with relevant values assigned to the more sensitive user-specified parameters.

Finally this exercise illustrates the importance of the code user, the need for improved user-guidelines, as well as the need for experts in core degradation in order to make code utilization more effective with valuable judgements on predictions especially in these areas where code modelling deficiencies have been identified.

Running times :

Excessive running times were communicated by some participants, well in excess of a few hours (SCDAP/RELAP5 Mod2). Whatever the computer used, such long computing times are a real handicap for sensitivity studies. Efficient calculations were performed with MELCOR and ICARE2 with more reasonable CPU times.

Codes validation :

In addition to the modelling improvements suggested above, code validation efforts must be maintained. The significant differences obtained in the code-to-data, or code-to-code comparisons illustrate a considerable need for SFD code validation focussing on core degradation phenomena which govern major aspects of safety studies : H₂ release and quantification of the remaining non oxidized Zry, early UO₂ dissolution with change of core geometry, core channel blockage, high temperature and fuel morphology histories which are key parameters governing the release of fission products.

Codes versatility :

Codes have been developed for reactor calculations, but verification and validation need more code versatility so as to take into account some peculiarities of small-scale experiments : power profiles versus time, surrounding structures with imposed boundary conditions, pure non-condensable flow, models to calculate view factors - in particular experimental geometries - and more output and drawing convenience.

Recommendation for reactor calculations :

Complete validation of degradation models for reactor plant calculations should take into account code-to-data comparison results obtained from a larger set of conditions, e.g. irradiated and cracked fuel concerning the UO₂ dissolution. Similarly, different conditions, from a steam-rich atmosphere to pure steam-starved conditions, as in the B9+ test, including different heating rates should be considered as regards cladding failure conditions before final recommendations for plant calculations are given.

Next ISPs on SFD experiments like CORA13 and FLHT-6 should provide a complementary and valuable contribution to SFD code validation.

REFERENCES

- [1] C. GRANDJEAN - C. GONNIER
Preliminary specifications for the International Standard Problem ISP 28.
C.E.A report - PHEBUS CSD 112/90 - March 1990.
- [2] C. GRANDJEAN - C. GONNIER
Technical specifications - Complementary report.
C.E.A report - PHEBUS CSD 117/90 - September 1990.
- [3] C. GONNIER - G. GEOFFROY - B. ADROGUER
PHEBUS Severe Fuel Damage Programme - Main results.
A.N.S. meeting - Portland - 21, 25 July 1991.
- [4] B. ADROGUER
International Standard Problem ISP 28.
SFD PHEBUS test B9+ - Final specifications for calculations and reported results.
C.E.A report - PHEBUS CSD 115/90 - September 1990.
- [5] R. GEOFFROY - J.M. BOYER - M. PERROT
PHEBUS B9+ . Examens après essais.
C.E.A report - DMT 91/346 - Juillet 1991.
- [6] S.R. KINNERSLY and al.
State-of-the-Art Report (SOAR) on In-Vessel Core. Degradation in LWR Severe Accidents.
OECD/CSNI report. NEA/CSNI/R (91) 12-NOV. 1991.
- [7] S. BOURDON - P. VILLALIBRE - B. ADROGUER - G. GEOFFROY
Analysis of the severe fuel damage test PHEBUS B9+ using ICARE code.
27th National Meeting, AIChE Minneapolis (1991).

- [8] B. ADROGUER, S. BOURDON, R. GONZALEZ.
Analysis of the fuel-cladding chemical interaction in PHEBUS SFD tests using ICARE2 Code.
AIEA meeting on "Behaviour of Core Materials and Fission Product Release in Accident Conditions in LWRs".
Aix-en-Provence - March 1992.
- [9] B. ADROGUER, S. BOURDON, C. RONGIER.
Results of the International Standard Problem 28 on the PHEBUS SFD test B9+.
AIChE meeting on Heat Transfer and Fuel Behaviour in Nuclear Reactor Accidents.
San Diego - August 1992.

LIST OF ANNEXES (VOLUME 2)

All these annexes are given in the volume 2 of this report.

- Annex 1 : FRA-SP. Joint CEA-Phebus España submission
- Annex 2 : SP-CSN submission
- Annex 3 : SP-UPM submission
- Annex 4 : CZECHOSLOVAKIA-NRI submission
- Annex 5a : GER-IKE 1 submission (1st BC approach)
- Annex 5b : GER-IKE2 submission (2nd BC approach)
- Annex 6a : GER-GRS1 submission (1st BC approach)
- Annex 6b : GER-GRS2 submission (2nd BC approach)
- Annex 7 : HUNGARY-CRIP submission
- Annex 8 : I-PISE UNIVERSITY submission
- Annex 9 : ISPRA submission
- Annex 10 : JAPAN-JAERI submission
- Annex 11 : NETHERLANDS-ECN submission
- Annex 12 : SWEDEN-SN submission
- Annex 13 : TAIWAN-AEC submission
- Annex 14 : UK-AEA Technology submission
- Annex 15 : USA-NRC submission
- Annex 16 : Comparisons between codes
- Annex 17 : Plot identifiers

LIST OF TABLES (VOLUME 1)

Table 1	:	List of participants and codes
Table 2	:	Code modifications
Table 3	:	Physical models used
Table 4	:	Cladding failure criteria and relocation models used
Table 5	:	Nodalization schemes
Table 6	:	Shroud modelling
Table 7	:	Nuclear power
Table 8	:	Radial temperature differences at 60 cm - Time 7800 s
Table 9	:	Mixture composition at 18000 s
Table 10	:	Run statistics.

LIST OF FIGURES (VOLUME 1)

- Fig. 1 : Test stringer
- Fig. 2a : Bundle cross section
- Fig. 2b : Longitudinal view of the bundle
- Fig. 3 : Thermocouple locations
- Fig. 4 : Shroud thermocouples
- Fig. 5 : Experimental scenario
- Fig. 6 : Steam to helium switch
- Fig. 7 : Porous ZrO₂ conductivity
- Fig. 8 : Radial power profile
- Fig. 9 : Axial power profiles
- Fig. 10 : Bundle modelling
- Fig. 11 : Axial cut of the lower end of bundle
- Fig. 12 : Cross cutting at elevation 0.76 m
- Fig. 13a : Cross cutting at elevation 0.58 m
- Fig. 13b : Cross cutting at elevation 0.52 m
- Fig. 14a : Cross cutting at elevation 0.44 m
- Fig. 14b : Cross cutting at elevation 0.26 m
- Fig. 15a : Cross cutting at elevation 0.17 m
- Fig. 15b : Cross cutting at elevation 0.14 m
(Lower spacer - grid location)
- Fig. 16 : Cross cutting at elevation 0.05 m
- Fig. 17a : Bundle power distribution
SCDAP/R5/Mod2 calculation (USA)
- Fig. 17b : Bundle power distribution
SCDAP/R5/Mod2 calculation (UK)
- Fig. 17c : Bundle power distribution
ICARE2 V2p calculation (FRA-SP)

**LIST OF FIGURES FOR EACH CODE-TO-DATA ANNEX
ANNEX 1 TO ANNEX 15 (VOLUME 2)**

Page 1 : UO₂ temperature

- Fig. 1 : UO₂ temperature of the second ring rods versus time at levels 20, 30, 40 and 50 cm (TU2R20, TU2R30, TU2R40, TU2R50).
- Fig. 2 : UO₂ temperature of the second ring rods versus time at levels 60 and 70 cm (TU2R60, TU2R70).

Page 2 : Cladding temperature

- Fig. 3 : Cladding temperature of the first ring rods versus time at levels 20, 30, 40 and 50 cm.
- Fig. 4 : Cladding temperature of the first ring rods versus time at levels 60 and 70 cm.

Page 3 : Fluid temperature

- Fig. 5 : Fluid temperature of the mean channel versus time at levels 0, 30 and 40 cm.
- Fig. 6 : Fluid temperature of the mean channel versus time at levels 50 and 80 cm.

Page 4 : Liner and shroud temperature

- Fig. 7 : Liner temperature versus time at levels 40, 60 and 80 cm.
- Fig. 8 : Shroud temperature versus time at levels 30, 40, 60 and 70 cm.

Page 5 : Radial temperature histories at 50 and 70 cm

- Fig. 9 : Temperature versus time at level 50 cm.
- Fig. 10 : Temperature versus time at level 70 cm.

Page 6 : Axial temperature profiles and radial heat flux

Fig. 11 : Axial temperature profiles at 7700, 9000, 12000 and 14000 s.

Fig. 12 : Heat flux to the shroud versus time at levels 20, 40 and 60 cm.

Page 7 : Central rod : Oxidation, UO₂ and ZrO₂ dissolution profiles

Fig. 13 : ZrO₂ profile at 9000 s.

Fig. 14 : UO₂ and ZrO₂ dissolution profiles at 9000 s.

Fig. 15 : ZrO₂ profile at 14000 s.

Fig. 16 : UO₂ and ZrO₂ dissolution profiles at 14000 s.

Page 8 : First ring rods : Oxidation, UO₂ and ZrO₂ dissolution profiles

Fig. 17 : ZrO₂ profile at 9000 s.

Fig. 18 : UO₂ and ZrO₂ dissolution profiles at 9000 s.

Fig. 19 : ZrO₂ profile at 14000 s.

Fig. 20 : UO₂ and ZrO₂ dissolution profiles at 14000 s.

Page 9 : Second ring rods : Oxidation, UO₂ and ZrO₂ dissolution profiles

Fig. 21 : ZrO₂ profile at 9000 s.

Fig. 22 : UO₂ and ZrO₂ dissolution profiles at 9000 s.

Fig. 23 : ZrO₂ profile at 14000 s.

Fig. 24 : UO₂ and ZrO₂ dissolution profiles at 14000 s.

Page 10 : Clad oxidation profiles and ZrO₂ layer histories

Fig. 25 : Clad oxidation profiles for central rod and second ring rods at 9000 s.

Fig. 26 : ZrO_2 layer increase and dissolution versus time for the first ring rods at levels 20, 30, 40, 50, 60, 70 and 75 cm.

Page 11 : ZrO_2 profile in the liner and total H_2 production

Fig. 27 : ZrO_2 mass fraction versus level for the liner at 9000 and 14000 s.

Fig. 28 : Total H_2 production and H_2 mass flow rate.

Page 12 : Mean profiles of UO_2 dissolution and bundle blockage

Fig. 29 : Mean UO_2 dissolution profile at 18000 s.

Fig. 30 : Blockage (defined as being equal to 38 % at initial conditions).

Page 13 : Bundle pictures

Fig. 31 : Total mass of relocated mixtures at 9000 s and 18000 s.

Fig. 32 : Final picture of the bundle.

Page 14 : Axial distribution of core materials

Fig. 33 : Total mass of UO_2 , ZrO_2 , Zr at 9000 s.

Fig. 34 : Total mass of UO_2 , ZrO_2 , Zr at 18000 s.

TABLE 1 : LIST OF PARTICIPANTS AND CODES

INSTITUTION	COUNTRY	EXPERT	CODE	IDENTIFIER (*)
Spanish PHEBUS Consortium and CEA	SPAIN and FRANCE	P. VILLALIBRE S. BOURDON	ICARE2 V2p	FRA-SP
Spanish PHEBUS Consortium - CSN	SPAIN	A. ALVAREZ J. MARTINEZ	SCDAP MOD1	SP-CSN
Universidad Politecnica de Madrid C.T.N. - UPM	SPAIN	S.A. ENCISO JV.L MONTERO J.G. PINDADO C.S. SANTAMARINA	MELCOR V 1.8.0	SP -UPM
Nuclear Research Institute N.R.I. - REZ	CZECHOSLOVAKIA	F. PAZDERA M. VALACH L. BELOVSKY	FRAS - SFD	CZECHO
IKE, University of Stuttgart	GERMANY	K.D. HOCKE S. KRETSCHMER K. MULLER	KESS - III	GER-IKE1 GER-IKE2 (**)
GRS, Garching	GERMANY	A. BALL K. TRAMBAUER	ATHLET-SA	GER-GRS1 GER-GRS2 (***)
Central Research Institute for Physics C.R.I.P.	HUNGARY	G. GYENES B. TOTH P. VERTES	MARCH 3	HUNGARY
Pise University and ENEA	ITALY	G. FRUTTUOSO F. ORIOLO	SCDAP/RELAP5 MOD2	I-PISE
ISPRA J.R.C.	ISPRA	J.A. CAPITAO I. SHEPHERD	ICARE 2 V1	ISPRA

TABLE 1 : LIST OF PARTICIPANTS AND CODES (continued)

INSTITUTION	COUNTRY	EXPERT	CODE	IDENTIFIER (*)
JAERI CSK Corp.	JAPAN	K. HASHIMOTO K. SODA E. MATSUMOTO (*)	SCDAP/RELAP5 MOD1/C22	JAPAN
Energ. Centrum Nederland E.C.N.	NETHER- LANDS	L.WINTERS	SCDAP/RELAP5 MOD2-V3F1	NETHER
STUDSVIK NUCLEAR	SWEDEN	J. ERIKSSON	SCDAP/RELAP5 SRL-C/V3f	SWEDEN
Institute of Nuclear Energy Research A.E.C.	TAIWAN	SHIH-KUEI CHENG LAINSU KAO	MELCOR V 1.8.0	TAIWAN
AEA Technology WINFRITH	UK	T.J. HASTE J.N. LILLINGTON A.J. LYONS	SCDAP/RELAP5 MOD2.5 SRL-C/V 361sc	U.K.
SANDIA Nat. Lab. and NRC	USA	G.M. MARTINEZ	MELCOR V 1.8. EA	U.S.A

(*) IDENTIFIER for comparisons between the different codes and the measurements

(**) IKE 1 : identifier for the calculation performed in using the 1st shroud boundary condition approach

IKE 2 : for the 2nd shroud boundary condition approach

(***) GRS1 : identifier for the calculation performed using the 1st shroud boundary condition approach

GRS2 : for the 2nd shroud boundary condition approach

TABLE 2 : CODE MODIFICATIONS

PARTICIPANT	CODE	ORIGINAL CODE OR MODIFICATIONS
FRA-SP	ICARE 2 V2p	<ul style="list-style-type: none"> - New UO₂ dissolution model - New ZrO₂ dissolution model - Solubility limits in U-Zr-O mixtures - Oxidation when β-Zr is consumed
SP-CSN	SCDAP MOD1 stand alone	<ul style="list-style-type: none"> - Modelling of the melting seal of rod plenum - He as coolant gas - Fuel gap model for fresh fuel - Oxidation release energy at the steam temp. - Missenard model for conductivity of porous ZrO₂
SP-UPM	MELCOR V 1. 8. 0	No
CZECHO	FRAS-SFD	Adaptation for the B9+ calculation and for SFD conditions
GER-IKE	KESS III	<ul style="list-style-type: none"> - Oxidation of the shroud liner - Adaptation for the 2nd approach B.C
GER-GRS	ATHLET-SA	No
HUNGARY	MARCH3	<ul style="list-style-type: none"> - Imposed steam flow rate at the entrance instead of steam controlled by a water level - Modelling of the shroud with 2 methods (core barrel and fictitious outer ring rods)
I. PISE	SCDAP/RELAP5	No

TABLE 2 : CODE MODIFICATIONS (continued)

PARTICIPANT	CODE	ORIGINAL CODE OR MODIFICATIONS
ISPRA	ICARE 2 V1	No
JAPAN	SCDAP/RELAP5 MOD1	No
NETHER	SCDAP/RELAP5 MOD2	<ul style="list-style-type: none"> - Imposed cladding failure at 1073 K to avoid overpressurization of rods - Remove double side oxidation - Setting He void fraction to 0.998 to avoid code failure during the steam/He switch
SWEDEN	SCDAP/RELAP5 SRL	Increase the number of points of the axial power profile
TAIWAN	MELCOR V 1.8.0	No
U.K.	SCDAP/RELAP5 MOD2	<ul style="list-style-type: none"> - Increase the number of different axial power profiles and the total number of points - Melt temp. of ZrO₂ imposed to 3000 K to avoid debris bed formation (has no effect in the base case)
U.S.A.	MELCOR V 1.8. EA	<ul style="list-style-type: none"> - Time dependant pressure as boundary condition - Failure temperature versus elevation for structures - Fluid viscosities corrections for non condensable gas - Add a conduction transfer in the helium gap between the shroud liner and porous ZrO₂ - Correction of radiation transfer between components and liner instead of a canister structure - Correction of the mixture gas viscosity

TABLE 3 : PHYSICAL MODELS USED

PARTICIPANT	CODE	RADIATIVE MODEL	OXIDATION AND TRANSITION T	UO ₂ DISSOLUTION BY MOLTEN Zr SOLUBILITY LIMITS (SL) IN THE U-Zr-O MIXTURE	ZrO ₂ DISSOLUTION BY MOLTEN Zr	SPACER GRID MODEL
FRA-SP	ICARE2 V2p	- Hotel method - Fij per rod (*) - absorption by H ₂ O	Urbanic-H 1853 K	Kim diffusion model SL : Liquidus Temp. from a ternary U-Zr-O phase diagram model	Hofmann diffusion model	No
SP-CSN	SCDAP Mod1	- Net radiative method - Fij per rod - absorption by H ₂ O	Cathcart-Pawel Urbanic-H 1850 K	Turk dissolution model SL : pseudo-binary Politis diagram	No model	No
SP-UPM	MELCOR V 1.8.0	- Fij per adjacent representative rod (constant) - absorption by steam - axial Fij	Cathcart-Pawel Urbanic-H 1853 K modified constant	- No specific model - User parametric model to impose the fraction of UO ₂ transported when candling occurs (20 %)	Same comment than for UO ₂ (20 %)	Relocation when melting
CZECHO	FRAS-SFD (1 rod)	Simple model Fij between cylinders	Diffusion model for solid and liquid Zr	Time-independent model SL : a ternary U-Zr-O phase diagram model	Same comment than for UO ₂	
GER-IKE	KESS III	Fij = f (pinch, rod \emptyset) Fij = 0.45 (rod/rod)	Urbanic-H	Not used	No	No
GER-GRS	ATHLET-SA	- Fij per rod - no absorption by steam	Cathcart Urbanic-H 1853 K	Not used	No	

TABLE 3 : PHYSICAL MODELS USED (continued)

PARTICIPANT	CODE	RADIATIVE MODEL	OXIDATION AND TRANSITION T	UO ₂ DISSOLUTION BY MOLTEN Zr SOLUBILITY LIMITS (SL) IN THE U-Zr-O MIXTURE	ZrO ₂ DISSOLUTION BY MOLTEN Zr	SPACER GRID MODEL
HUNGARY	MARCH-3	Fij between cylinders	Urbanic-H	No model	No	No
I-PISE	SCDAP/ RELAP5 Mod2	- Net radiative approach - Fij per rod calculated by the code - absorption by H ₂ O	Cathcart-Pawel Urbanic-H (1850 K)	Hofmann-Uetsuka diffusion model SL : liquidus limit given by MATPRO model	No specific model	No
ISPRA	ICARE2 V1	See FRA-SP	Urbanic-H 1853 K	Time-independent model SL : pseudo binary diagram of Politis	No	No
JAPAN	SCDAP/ RELAP5 Mod1		Cathcart-P Urbanic-H 1820 K	See I-PISE	No	No
NETHER	SCDAP/ RELAP5 Mod2	See I-PISE	See I-PISE	See I-PISE	No	No
SWEDEN	SCDAP/ RELAP5 SRL	Fij given by a Studsvik code (8 zones per rod)	"	"	"	"

TABLE 3 : PHYSICAL MODELS USED (continued)

PARTICIPANT	CODE	RADIATIVE MODEL	OXIDATION AND TRANSITION T	UO ₂ DISSOLUTION BY MOLTEN Zr SOLUBILITY LIMITS (SL) IN THE U-Zr-O MIXTURE	ZrO ₂ DISSOLUTION BY MOLTEN Zr	SPACER GRID MODEL
TAIWAN	MELCOR V 1. 8. 0	Fij between representative rods imposed to 1	Urbanic-H	See SP-UPM	See SP-UPM	No
U.K.	SCDAP/RELAP5 Mod2	Fij given by the view code (true geometry)	See I-PISE	See I-PISE	No	No
U.S.A	MELCOR V 1. 8. EA	Fij between components (axial $F_{ij} = 0.25$) (radial $F_{ij} = 1.0$) absorption by H ₂ O	Urbanic-H 1853 K	See SP-UPM 20 % of UO ₂ transport when candling occurred	See SP-UPM 100 % of ZrO ₂ transport	See SP-UPM

(*) Fij view factor between 2 surfaces i and j

**TABLE 4 : CLADDING FAILURE CRITERIA (CFC)
AND RELOCATION MODEL USED**

PARTICIPANT	CFC due to molten Zr Tc, eOX, eZr (*)	CFC for solid debris formation	Relocation model for molten mixtures
FRA-SP (ICARE2 V2p)	Tc > 2300 K eOX < 300 μm	Criteria to define dislocated mate- rial (not used)	Candling model with an user specified velocity (0.6 m/s). Mass and energy equations.
SP-CSN (SCDAP MOD1)	Tc > 2500 K (criteria only tempera- ture dependent)		Mechanistic candling model with calcula- tion of velocity and Temp. of the mix- ture.
SP-UPM (MELCOR V 1. 8. 0)	2200 K < Tc < 2990 K and eOX < 100 μm or T > 2990 K	eZr < 100 μ m (gravitational setting by logical processes)	Candling model with user imposed heat transfer (1000 W/m ² K) and based on mass/energy equations.
CZECHO (FRAS-SFD)	Tc > 2400 K eOX < 300 μm		No model Calculations stops when clad failure occurs
GER-IKE (KESS III)	Tc > 2673 K eOX has no retention effect		Not used
GER-GRS (ATHLET SA)	no explicit criteria based on Tc and eOX		Not used
HUNGARY (MARCH 3)	Melting temp. of α-Zr (O)		Not used
I. PISE (SCDAP/RELAP5)	Tc > 2500 K eOX < 540 μm		Model based on mass momentum and energy equations

**TABLE 4 : CLADDING FAILURE CRITERIA (CFC)
AND RELOCATION MODEL USED (continued)**

PARTICIPANT	CFC due to molten Zr T_c, e^{OX}, e_{zr} (*)	CFC for solid debris formation	Relocation model for molten mixtures
ISPRA (ICARE2 V1)	T _c > 2300 K e ^{OX} < 500 μm		See FRA-SP
JAPAN (SCDAP/R MOD1)	T _c > 2700 K e ^{OX} < 360 μm	T _c > 2950 K (melting T of ZrO ₂)	
NETHER (SCDAP/R. MOD2)	T _c > 2500 K e ^{OX} < 520 μm	T _c > 2950 K	Model based on mass momentum and energy equations.
SWEDEN (SCDAP/R. SRL)	T _c > 2500 K e ^{OX} < 435 μm	T > 2950 K	See NETHER
TAIWAN (MELCOR V 1. 8. 0)	T _c > 2600 K e ^{OX} < 100 μm	e _{zr} = 0	See SP-UPM h = 1000 W/m ² .K
U.K. (SCDAP/R. MOD2)	T _c > 2500 K e ^{OX} < 520 μm	T > 2950 K	See NETHER
U.S.A. (MELCOR V 1. 8. EA)	if e ^{OX} < 60 μm T _c > 2200 K if e ^{OX} > 60 μm T _c > 2500 K	e _{zr} < 0.1 μm (not used)	See SP-UPM Candling heat transfer coefficient = 300 W/m ² K

- (*) T_c : failure cladding temperature
e^{OX} : failure ZrO₂ thickness limit
e_{zr} : failure Zr thickness limit

TABLE 5 : NODALIZATION SCHEMES

PARTICIPANT	NUMBER OF HYDRAULIC CHANNELS	NUMBER OF DIFFERENT KIND OF RODS	AXIAL MESHING (active length)	AXIAL MESHING (total rod)	RADIAL MESHING OF RODS
FRA-SP	3	3	10 Cst	13	2
SP-CSN	3	3	10 Cst		4
SP-UPM	1	3	10 Cst	12	
CZECHO	1	1	40 ≠		17
GER-IKE	1	3	20 Cst	22	
GER-GRS1	1	3	9 ≠	11	
GER-GRS2	1	3	10 Cst	12	
HUNGARY	1	3	10 Cst		1
I-PISE	1	3	8 ≠	10	5
ISPRA	1	5	16 Cst		2
JAPAN	1	3	10 Cst		
NETHER	1	3	11 ≠	13	3
SWEDEN	1	3	8 Cst		5
TAIWAN	1	3	9 ≠	10	
U.K.	1	3	10 Cst	10	5
U.S.A.	1	3	9 ≠	11	

Cst : constant meshing

≠ : different ΔZ

TABLE 6 : SHROUD MODELLING

PARTICIPANT	RADIAL DIFFERENT LAYERS	POROUS ZrO ₂ RADIAL MESHING	POROUS ZrO ₂ THICKNESS (mm)	CONDUCTIVITY OF THE POROUS ZrO ₂ LAYER
FRA-SP	5 Zr/He/pZrO ₂ dZrO ₂ /SS	4 (bottom) 6 (top)	8.3 (bottom) 9 (top)	Missenard model - pure helium Porosity tuned : 40 % < p < 80 %
SP-CSN	4 Zr/pZrO ₂ / dZrO ₂ /SS	5		Missenard model - pure helium Porosity constant : p = 70 %
SP-UPM	4	12	10.72	$\lambda' = 2 \times \lambda_{mes}$
CZECHO	2nd BC way			non used
GER-IKE1		11		$\lambda' = 2 \times \lambda_{mes}$
GER-IKE2	2nd BC way			non used
GERf-GRS1	3 Zr/pZrO ₂ /SS	4	10.7	λ deduced from the 2nd approach case
GER-GRS2	2nd BC way			non used
HUNGARY				fictitious shroud with λ adjusted
I-PISE	4	10	11.65	$\lambda' > 2 \times \lambda_{mes}$ - see Fig. 6
ISPRA	4	3		$\lambda' = 3 \times \lambda_{mes}$
JAPAN	4	3	10	$\lambda' \sim 3 \times \lambda_{mes}$
NETHER	4	5	10.7	$\lambda' = 2 \times \lambda_{mes}$
SWEDEN	4 same SP-CSN		9.23	$\lambda' = 2 \times \lambda_{mes} \times (1 + 0.0005 (T - 300))$
TAIWAN	2nd BC way			non used
U.K.	4 Zr/ZrO ₂ / dZrO ₂ /SS	10	11.65	MATPRO - see Fig. 6
U.S.A.	5 Zr/He/pZrO ₂ dZrO ₂ /SS	3	9.72 (bottom) 10.69 (top)	Similar to the Missenard model - see Fig. 6

λ_{mes} : measured heat conductivity (recommended)

pZrO₂ : porous ZrO₂ - dZrO₂ : dense ZrO₂ - SS : Stainless Steel

TABLE 7 : NUCLEAR POWER

PARTICIPANT	CODE	AXIAL PROFILE VERSUS TIME / POWER
FRA-SP	ICARE 2 V2p	- 5 recommended axial profiles - Recommended radial profile on 3 rods
SP-CSN	SCDAP MOD1	- 3 recommended axial profiles (B, C, D) - Recommended radial profiles on 3 rods
SP-UPM	MELCOR V 1. 8. 0	- One mean axial profile (based on A and E profiles) - Recommended radial profile on 3 rods - + 5 % on the Nuclear Power
CZECHO	FRAS-SFD	- 5 recommended axial profiles - central rod
GER-IKE	KESS III	- 4 interpolated axial profiles - Recommended radial profile on 3 rods
GER-GRS	ATHLET SA	- One axial profile (D profile at 11940 s) - Recommended radial profile on 3 rods
HUNGARY	MARCH 3	- Mean axial profile - Recommended radial profile on 3 rods
I-PISE	SCDAP/RELAP5 MOD2	- 3 recommended axial profiles (C, D, E) - Recommended radial profile on 3 rods
ISPRA	ICARE2 V1	- Mean axial profile - Recommended radial profile on 5 rods
JAPAN	SCDAP/RELAP5 MOD1	- 3 recommended axial profile (A, B, D) - Recommended radial profile on 3 rods
NETHER	SCDAP/RELAP5 MOD2	- 5 recommended axial profiles - Recommended radial profile on 3 rods
SWEDEN	SCDAP/RELAP5 SRL	- 3 recommended axial profiles (A, C, E) - Recommended radial profile on 3 rods
TAIWAN	MELCOR V 1. 8. 0	- One axial mean profile - Recommended radial profile on 3 rods
U.K.	SCDAP/RELAP5 MOD2	- 5 recommended axial profiles - Recommended radial profile on 3 rods
U.S.A.	MELCOR V 1.8.0 EA	- One axial profile (C profile at 9370 s) - Recommended radial profile on 3 rods - - 5 % on the Nuclear Power

TABLE 8 - RADIAL TEMPERATURE DIFFERENCES AT 60 cm - TIME 7800 s

PARTICIPANT	TUIR-TCIR	TUCR-TUIR	TUIR-TU2R	TC2R-TSRI	TSRI-TSR3
EXPERIMENT	50 to 60	<10	60 to 90	150 to 180	650
FRA-SP (ICARE V2p)	54	5	66	151	600
SP-CSN (SCDAP Mod1)	50	5	115	220	600
SP-UPM (MELCOR V1.8.0)	70	72	160	219	450
CZECHO (FRAS-SFD)	50	-	-	-	-
GER-IKE (KESS III)	25	7	26	68	1000
GER-GRS (ATHLET SA)	25	17	58	200	620
HUNGARY (FRAS-SFD)	Same	~	25	-	-
I-PISE (SCDAP/R5/M2)	50	10	50	~ 190	600
ISPRA (ICARE2V1)	50	1	16	136	640
JAPAN (SCDAP/R5/M1)	42	7	24	100	600
NETHER (SCDAP/RD/M2)	42	25	40	193	560
SWEDEN (SCDAP/R5/M2)	41	5	40	195	575
TAIWAN (MELCOR V1.8.0)	44	13	50	100	-
UK (SCDAP/R5/M2)	45	10	20	155	550
USA (MELCOR V1.8EA)	40	42	113	143	660

TABLE 9 : MIXTURE COMPOSITION AT 18000 s

PARTICIPANTS	ELEVATION (cm)	UO2 (WT %)	ZrO2 (WT %)	Zr (WT %)	INCONEL (WT %)	U (A %)	O (A %)	Zr (A %)	INCONEL Ni Fe Cr
Experiment	40 20-28 5	(U, Zr) O2-x (U, Z) O2-x	ZrO2 ZrO2	α -Zr(O) α -Zr(O)		6 4 7.44	38 31 4.9	56 65 55.4	23.6 7. 1.5
FRA-SP (ICARE2)	28 (1R) 20 (1R) 12 (2R)	13.5 23.9 23.3	43.8 29.9 24.4	42.7 46.2 52.2	0 0 0	3 6 6	48 44 40	49 50 54	-- -- --
SP-UPM (MELCOR V 1.8.0)	- 7 - 16 - 26	10.5 68.1 33.4	6.6 0.4 7.5	83.2 0 0.9	0 31.5 58.1	3.3	15.5	81.2	
USA (MELCOR V 1.8EA)	60/50 20 5 0	100 0.3 3 0.5	98 76.9 7.4	1.7 20.1 7.8	0 0 0 84.3	~ 0 0.52	66.2 59.75	33.8 39.73	

TABLE 10 : RUN STATISTICS

PARTICIPANT	CODE	TIME CALCULATED (s)	COMPUTER	CPU TIME (s)	Δt min (s)		Δt max (s)		MEAN Δt (s)	NUMBER TIME STEPS	CPU / Cell / Problem time (ms)
					p1	p2	p1	p2			
FRA-SP	ICARE2 V2p	18000	SUN 4/60	6340	10	5	20	10	11.3	1593	6.8
SP-CSN	SCDAP MOD1	18000	CDC Cyber 180	432918	0.1		20	0.1			600
SP-UPM	MELCOR V1.8.0	18000	VAX STATION 3100	376200	0.6	0.03	1	0.6	0.1	178614	435
CZECHO	FRAS-SFD	8320	PC-INTEL 386/7	18000	3.410 ⁻⁴		40		7	1200	27
GER-IKE1	KESS III	18000	VAX 6000-410	7200	5	5	20	10	6.4	2800	4.5
GER-GRS1	ATHLET SA	18000	Amdahl 5870	7240	2	1	2	1	1.3	13828	8.4
HUNGARY	MARCH 3	8364	mVAX TPA-11	52200	0.12		3		1.45 10 ⁻²	575000	72
I-PISE	SCDAP/RELAP5/2	18000	CRAY MXP 14	131623		0.01	0.5		1.45 10 ⁻²	1243002	114
ISPRA	ICARE2 V1	18000	SUN Sparcl	7610	0.5	0.5	50	50	15.9	1133	7
JAPAN	SCDAP/RELAP5/1	18000	FACOM M780	25800	0.12	0.03	1	0.12	0.07	256023	36
NETHER	SCDAP/RELAP5/2	14000	CONVEX C220S	222000	0.025	.01	0.3	0.05	2.85 10 ⁻²	491912	237
SWEDEN	SCDAP/RELAP5/2	18000	SUN 4/330	100800		0.025		0.5	0.14	125755	176
TAIWAN	MELCOR V1.8.0	18000	VAX 6310	21260	0.5	0.4	1	1	0.94	19160	39
U.K.	SCDAP/RELAP5/2	18000	SUN 4/330	270000	0.2	.025	1	0.025	0.043	416721	416
U.S.A.	MELCOR/V1.8EA	18000	VAX 8700	22197	1.5	0.3	5	1.5	0.8	22119	28

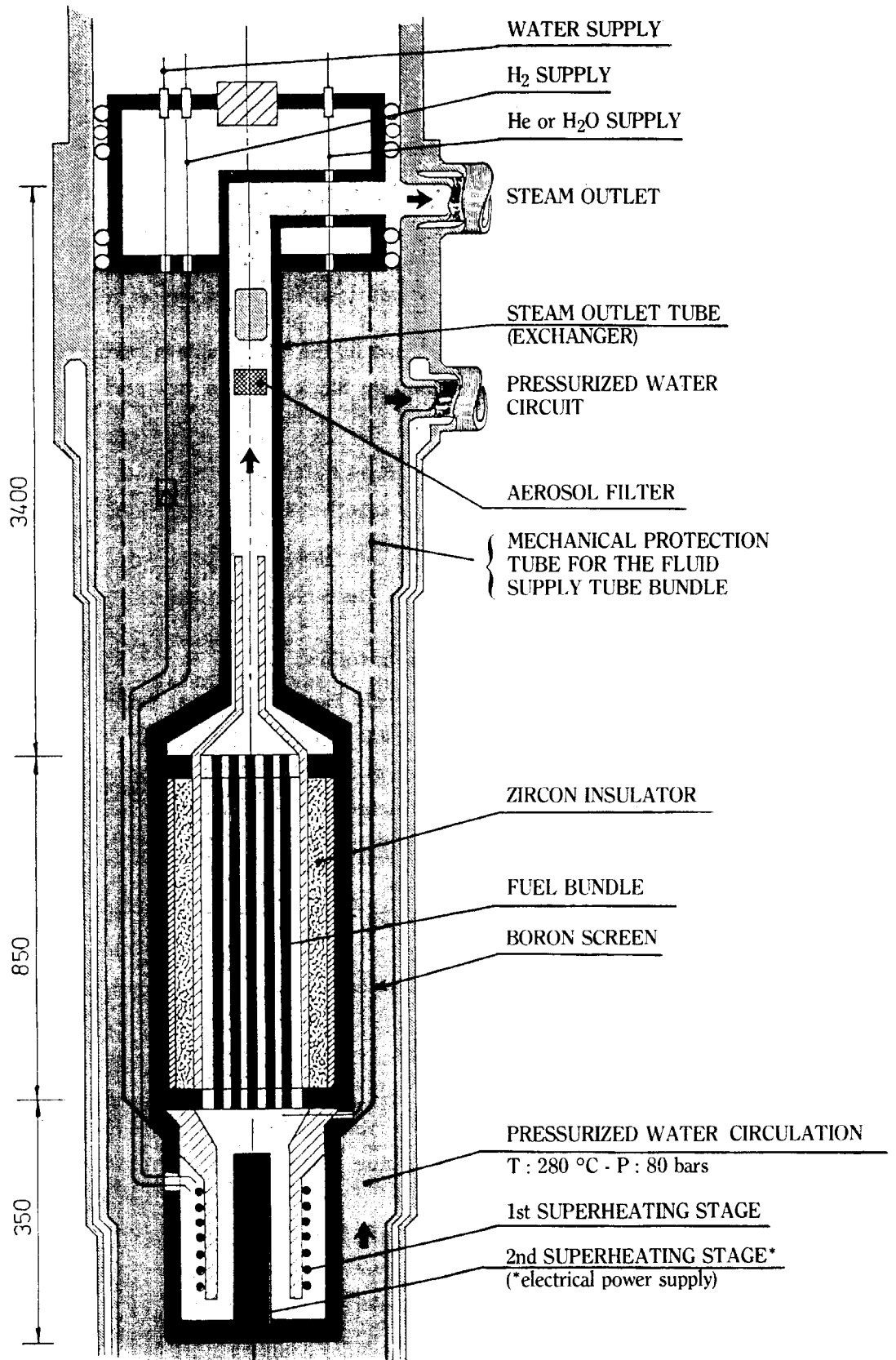
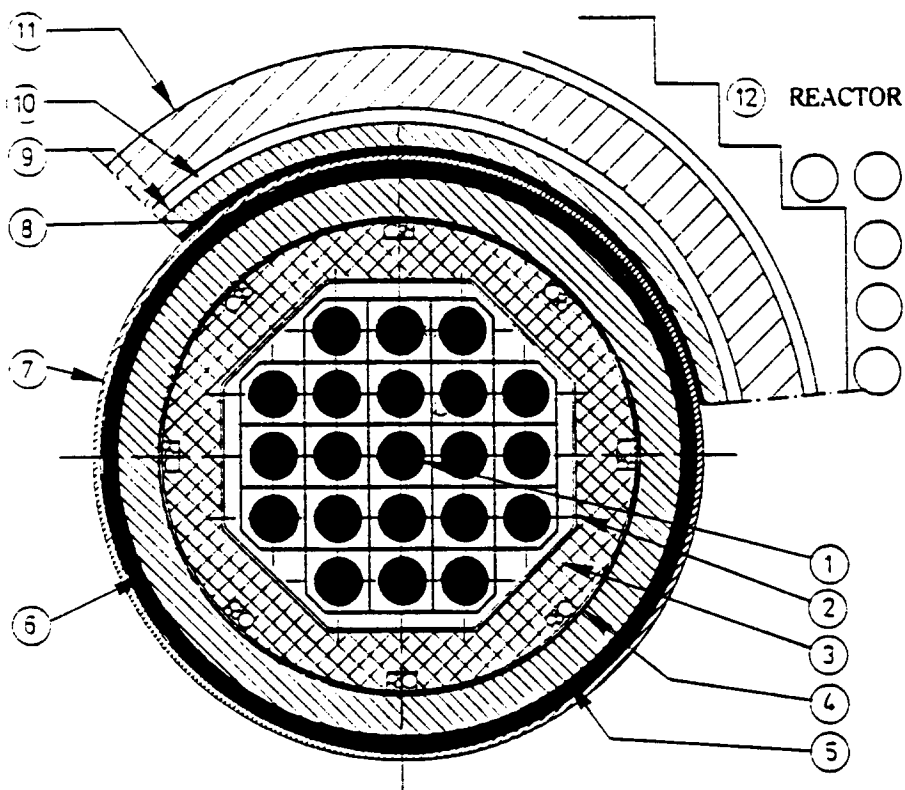


FIG. 1 : TEST STRINGER



	DESIGNATION (materials)	Int. radius (mm)	Ext. radius (mm)	Thickness (mm)
Test device pressurized water loop	1 21 pins test bundle : UO ₂ , Zr			
	2 Octagonal tube : Zircaloy	34.75	35.35	0.6
	3 Thermal insulation : porous ZrO ₂	35.35	47.	
	4 Dense zirconia flame sprayed layer	47.	48.	1.
	5 Test device tube : stainless steel	48.	56.	8.
	6 Pressurized water : - H ₂ O, 80 bar, 260°C	56.	59.25	3.25
	7 Neutronic screen : boron steel	59.25	60.75	1.5
	8 Pressurized water : - H ₂ O, 80 bar, 260°C	60.75	62.	1.25
Cell in pile	9 Inconel pressure tube	62.	67.	
	10 Vacuum	67.	70.	3.
	11 Zircaloy safety tube	70.	82.	12.
Reactor	12			

FIG. 2a : BUNDLE CROSS SECTION

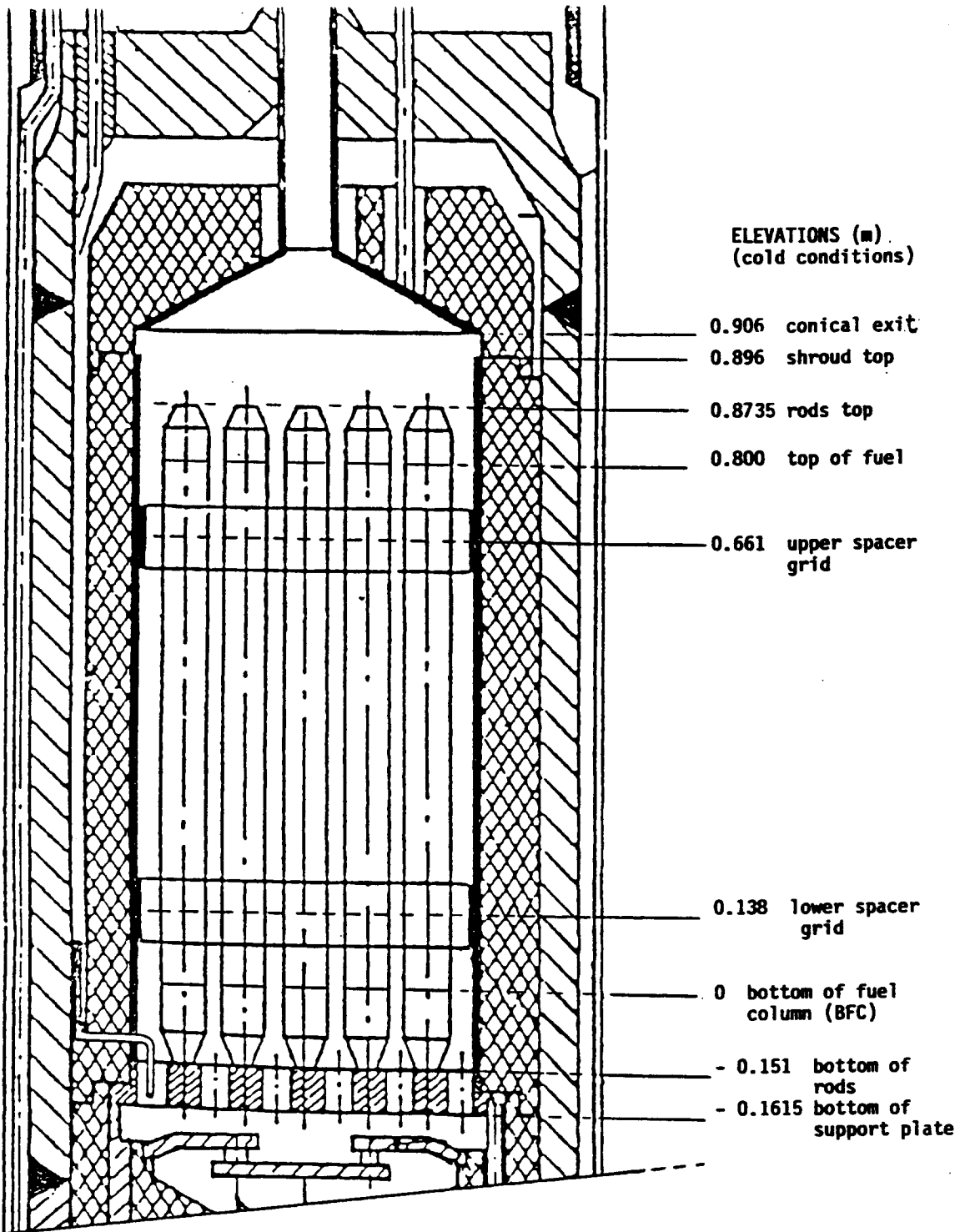


FIG. 2b : LONGITUDINAL VIEW OF THE BUNDLE

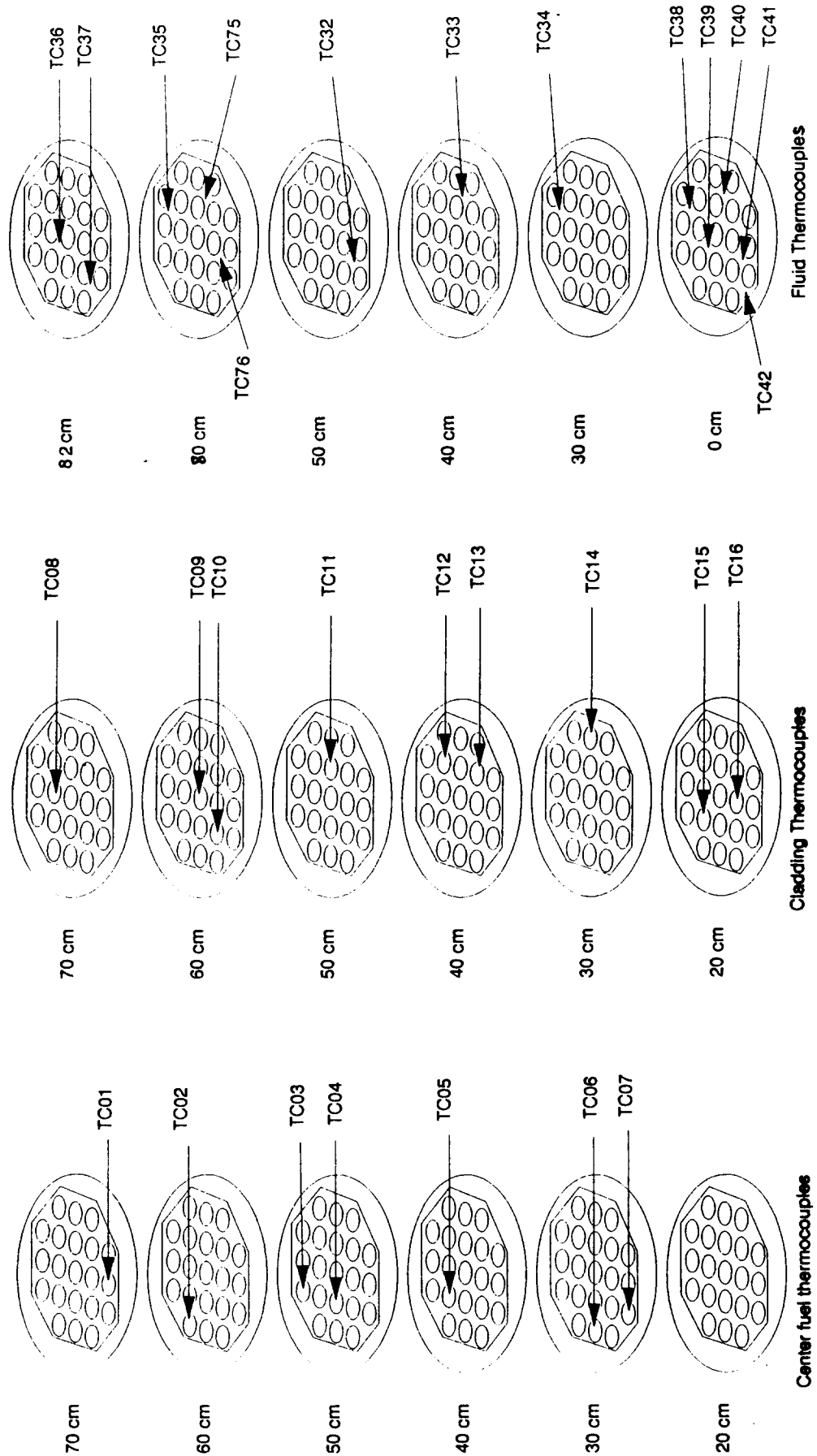


FIG. 3 : THERMOCOUPLE LOCATIONS

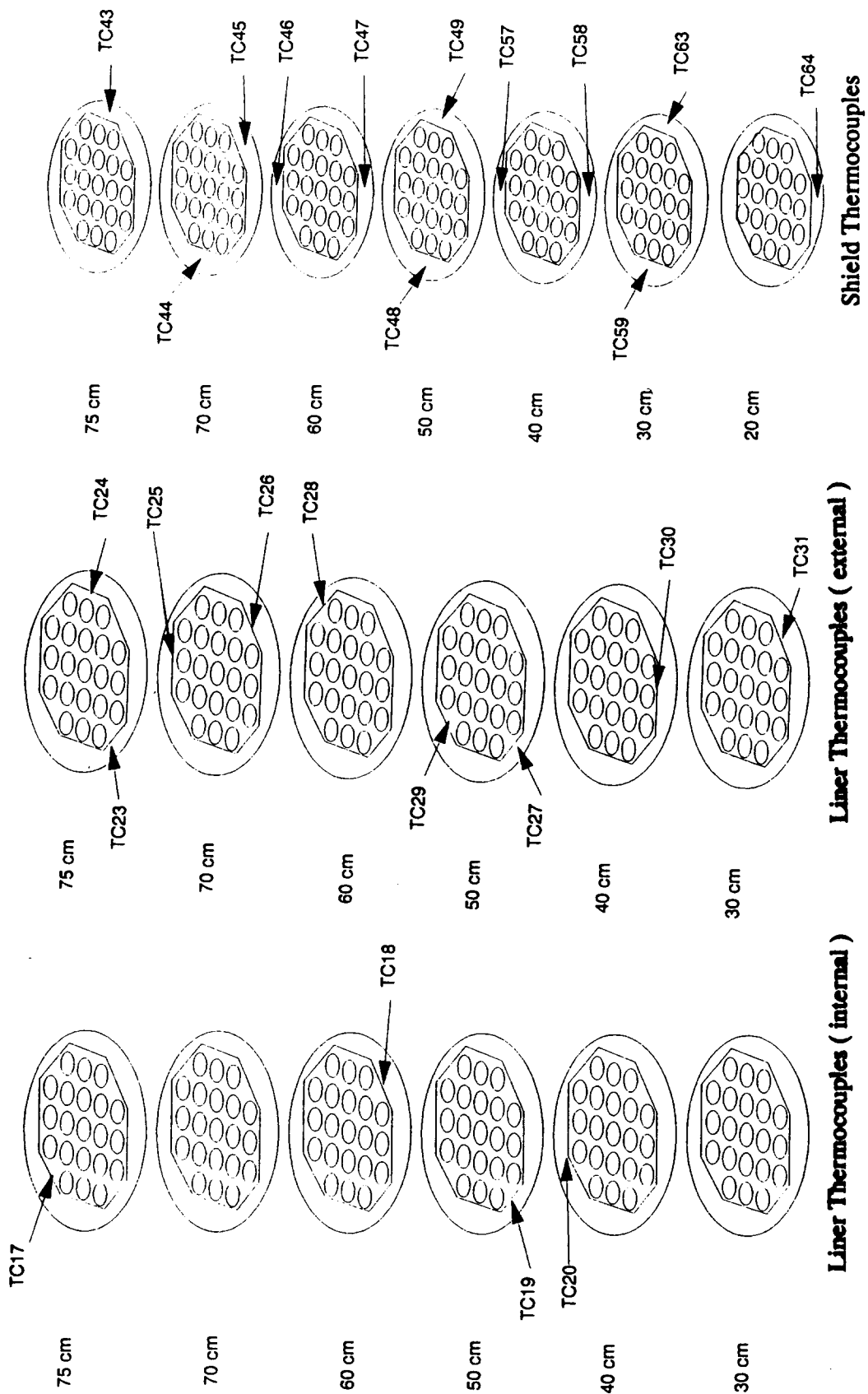


FIG. 4 : SHROUD THERMOCOUPLES

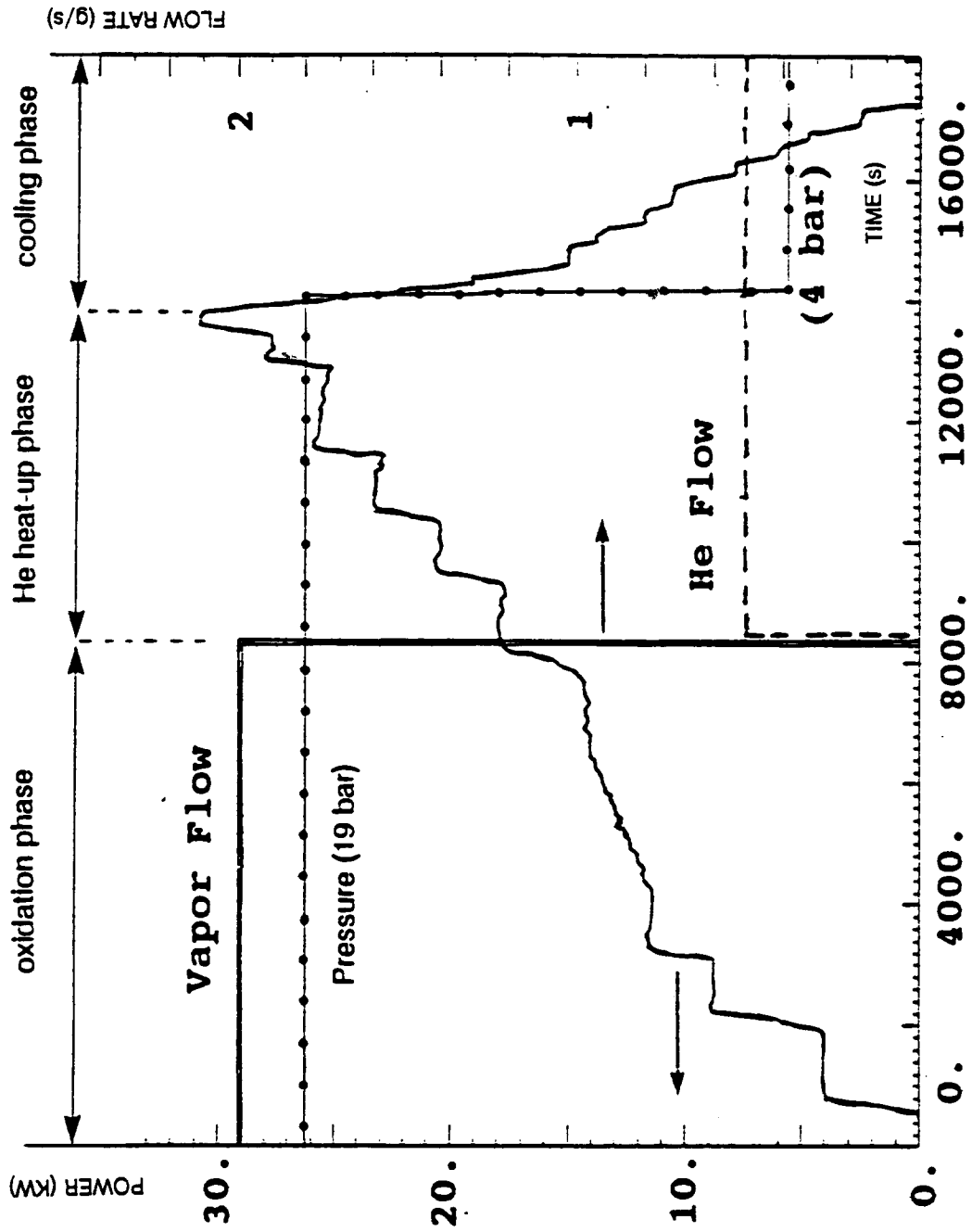


FIG. 5 : EXPERIMENTAL SCENARIO

**PHEBUS SFD B9+
SWITCH H2O/HE**

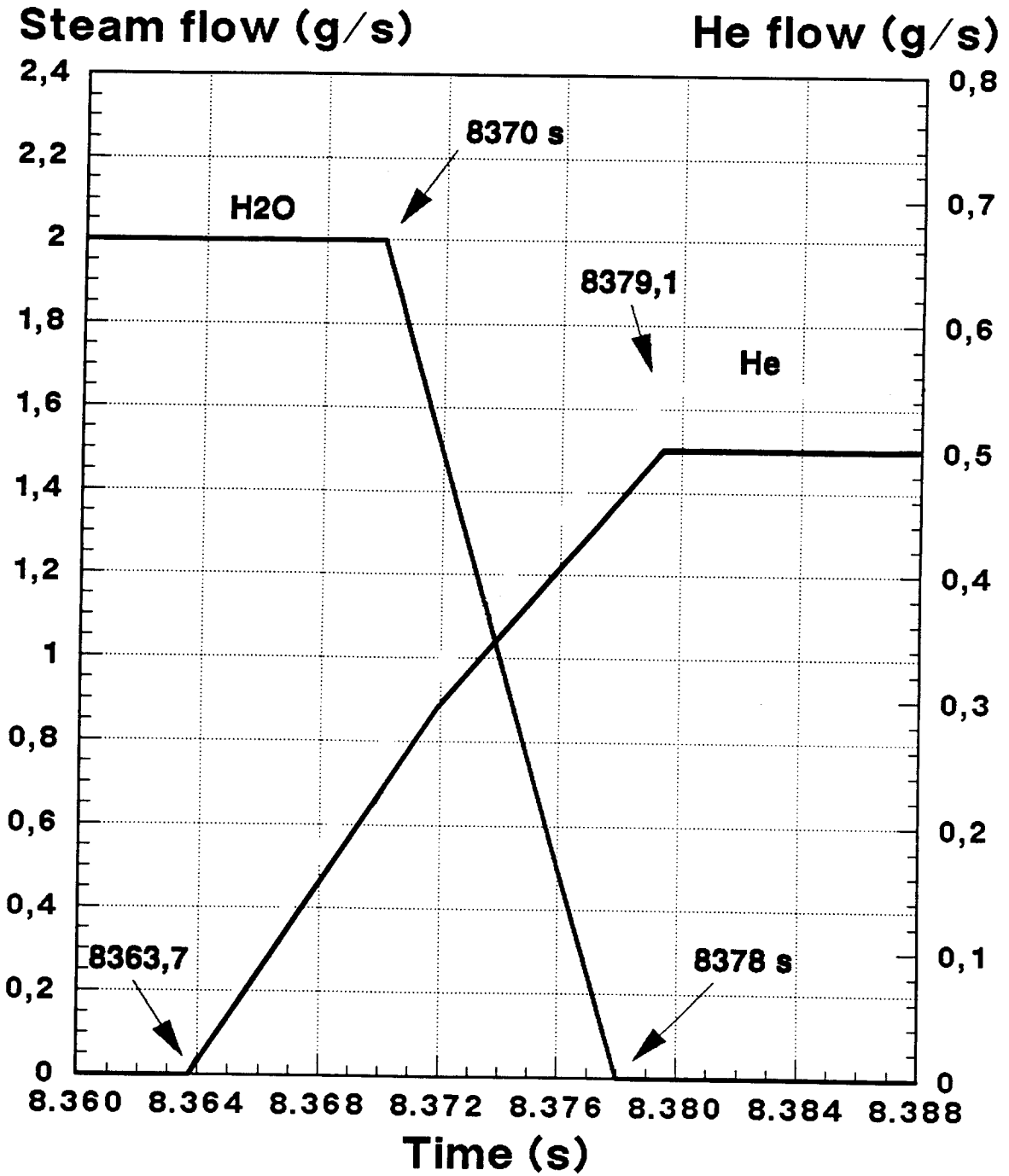


FIG. 6 : STEAM TO HELIUM SWITCH

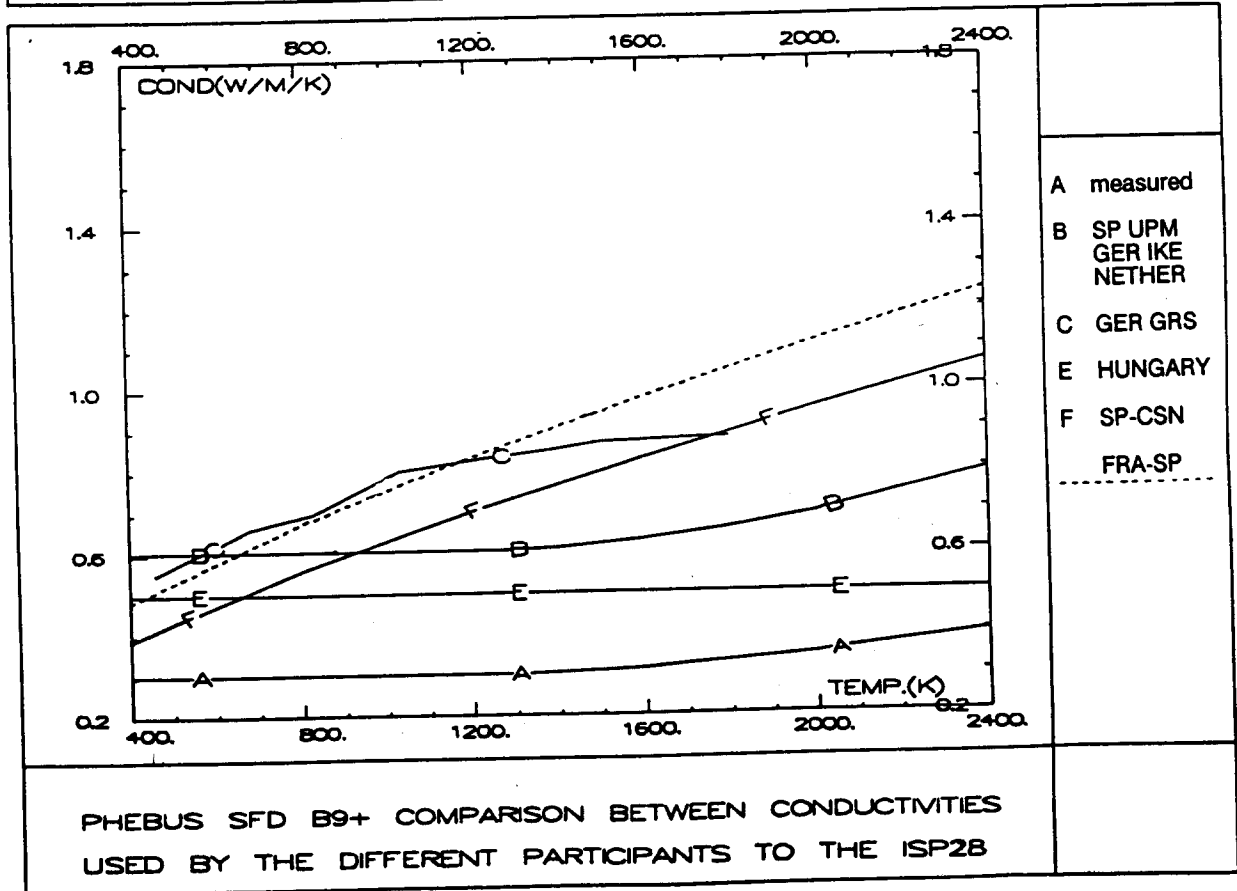
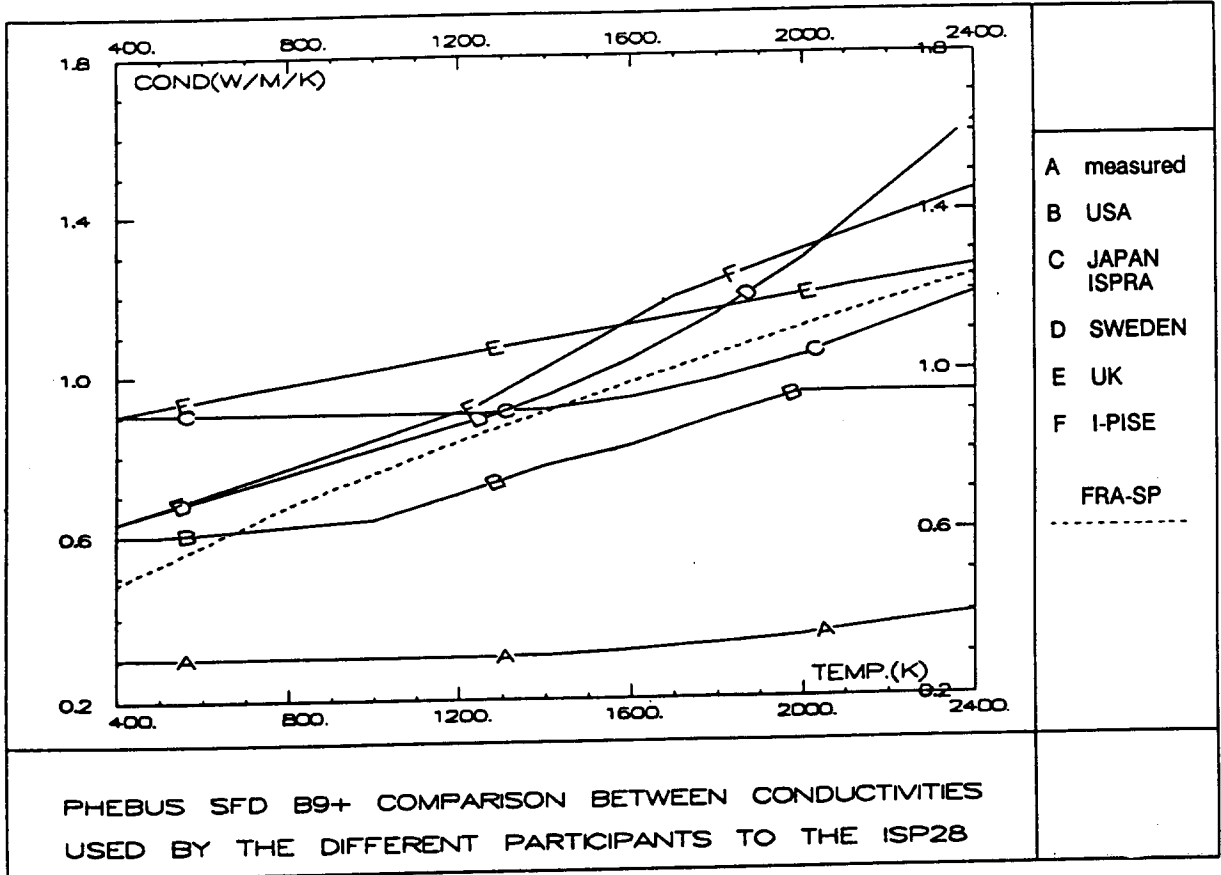


FIG. 7 : POROUS ZRO2 CONDUCTIVITY

Rod numbering and radial power distribution in the bundle

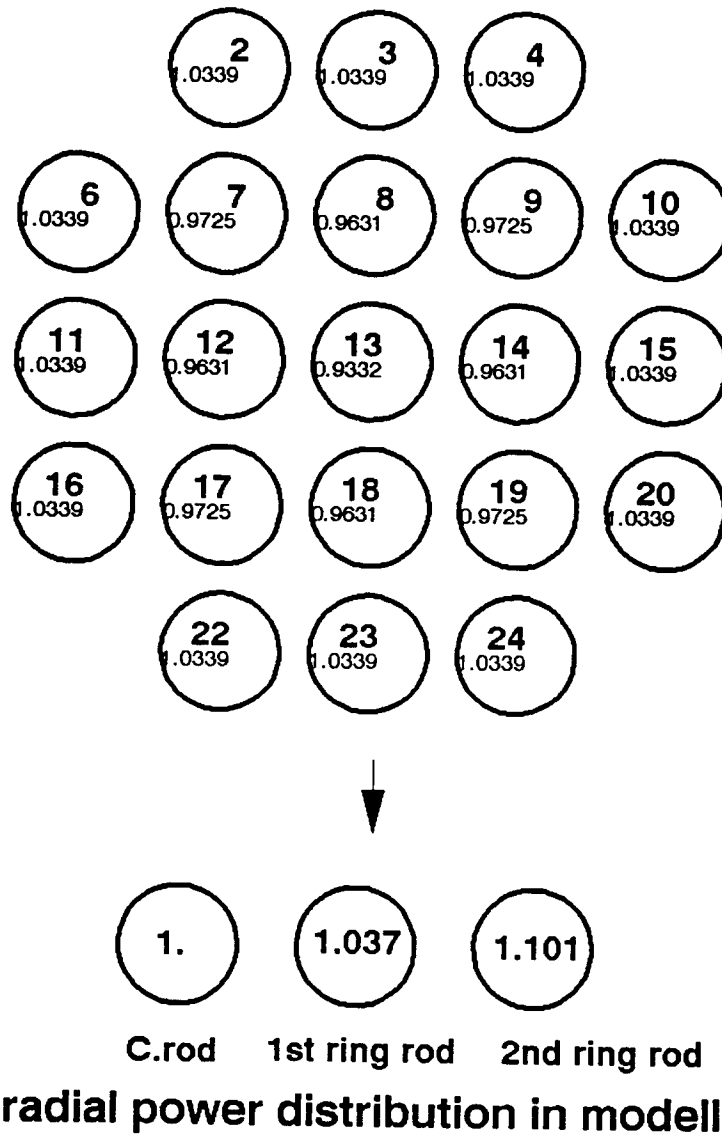


FIG. 8 : RADIAL POWER PROFILE

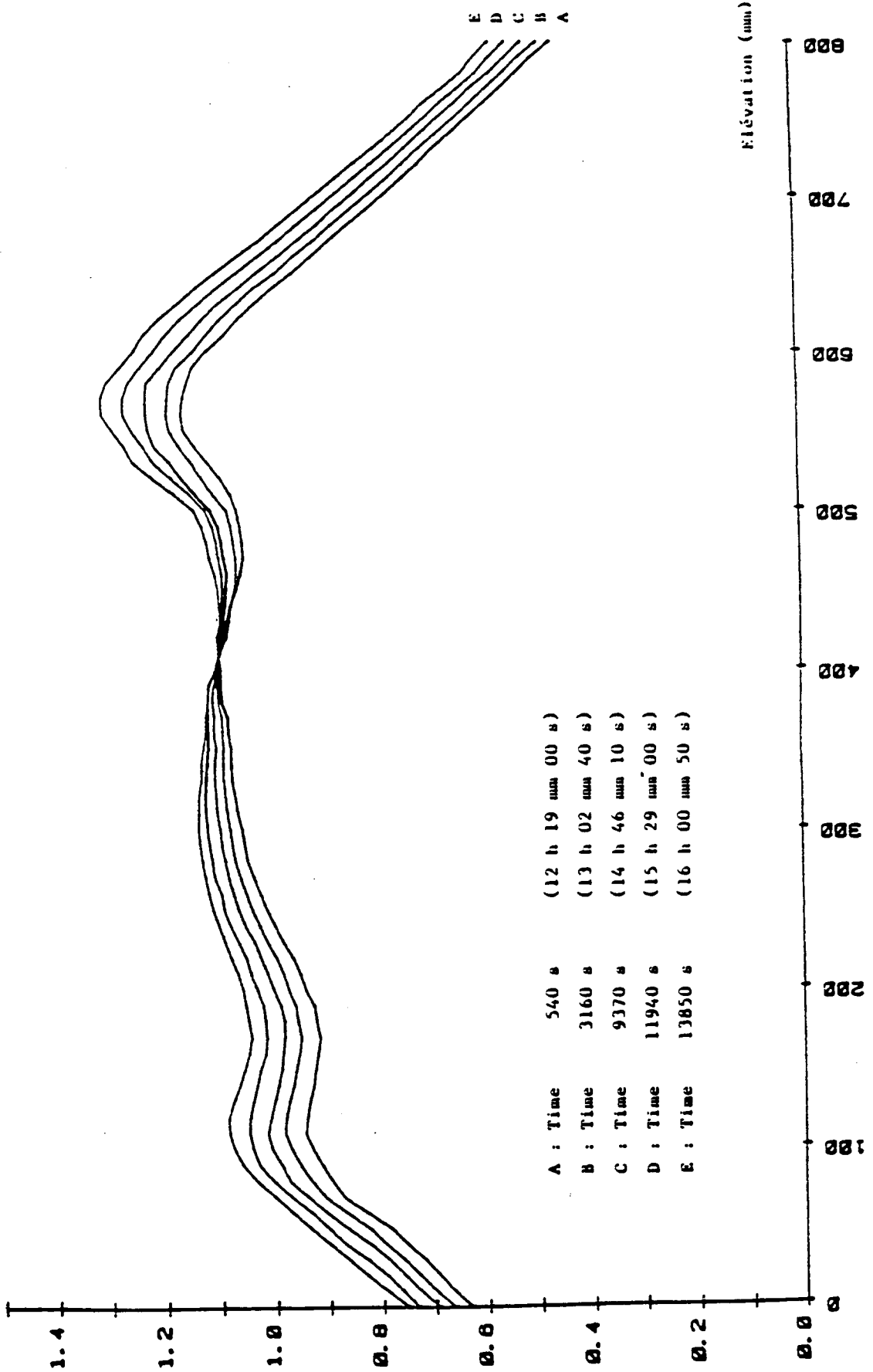


FIG. 9 : AXIAL POWER PROFILE

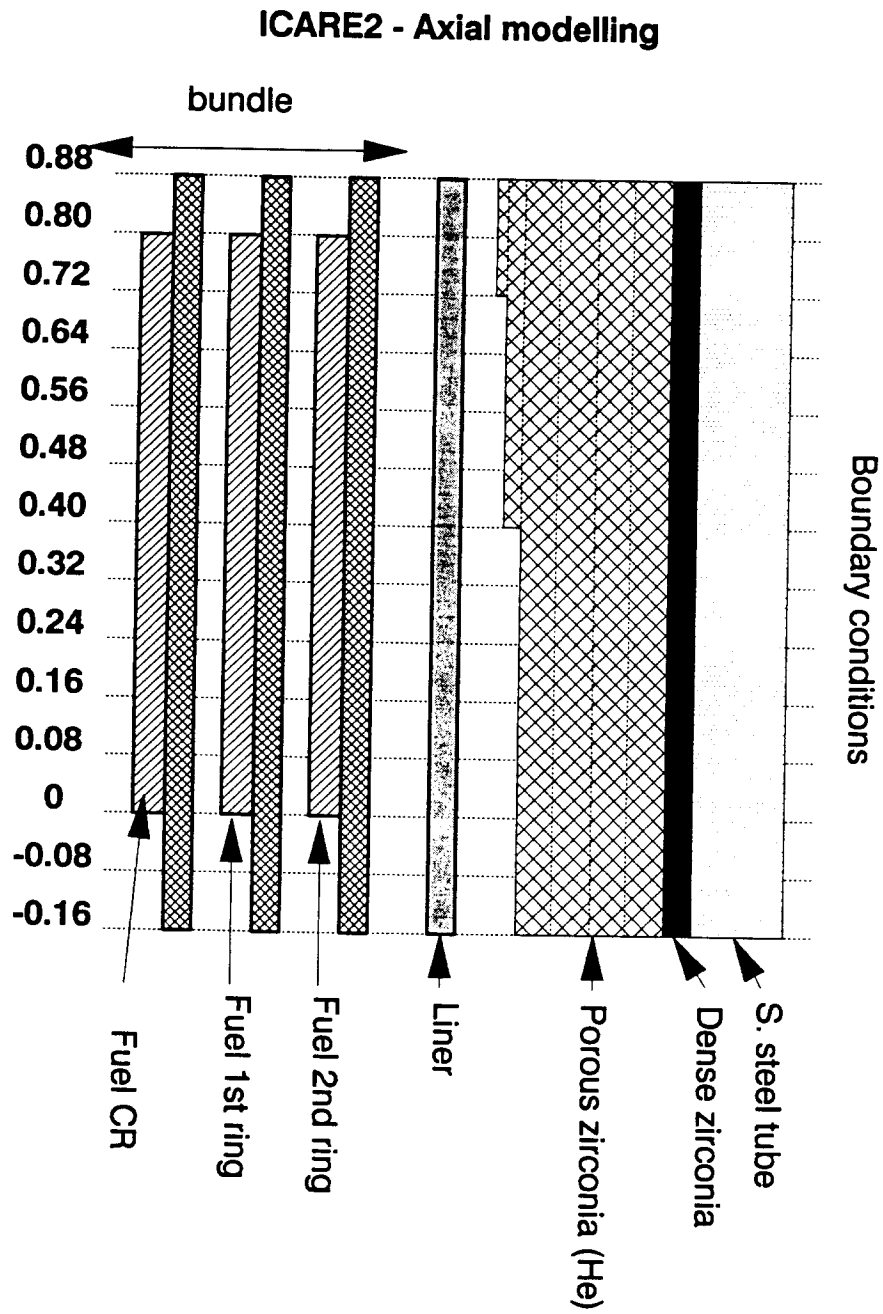


FIG. 10 : BUNDLE MODELLING

PHEBUS TEST B9+

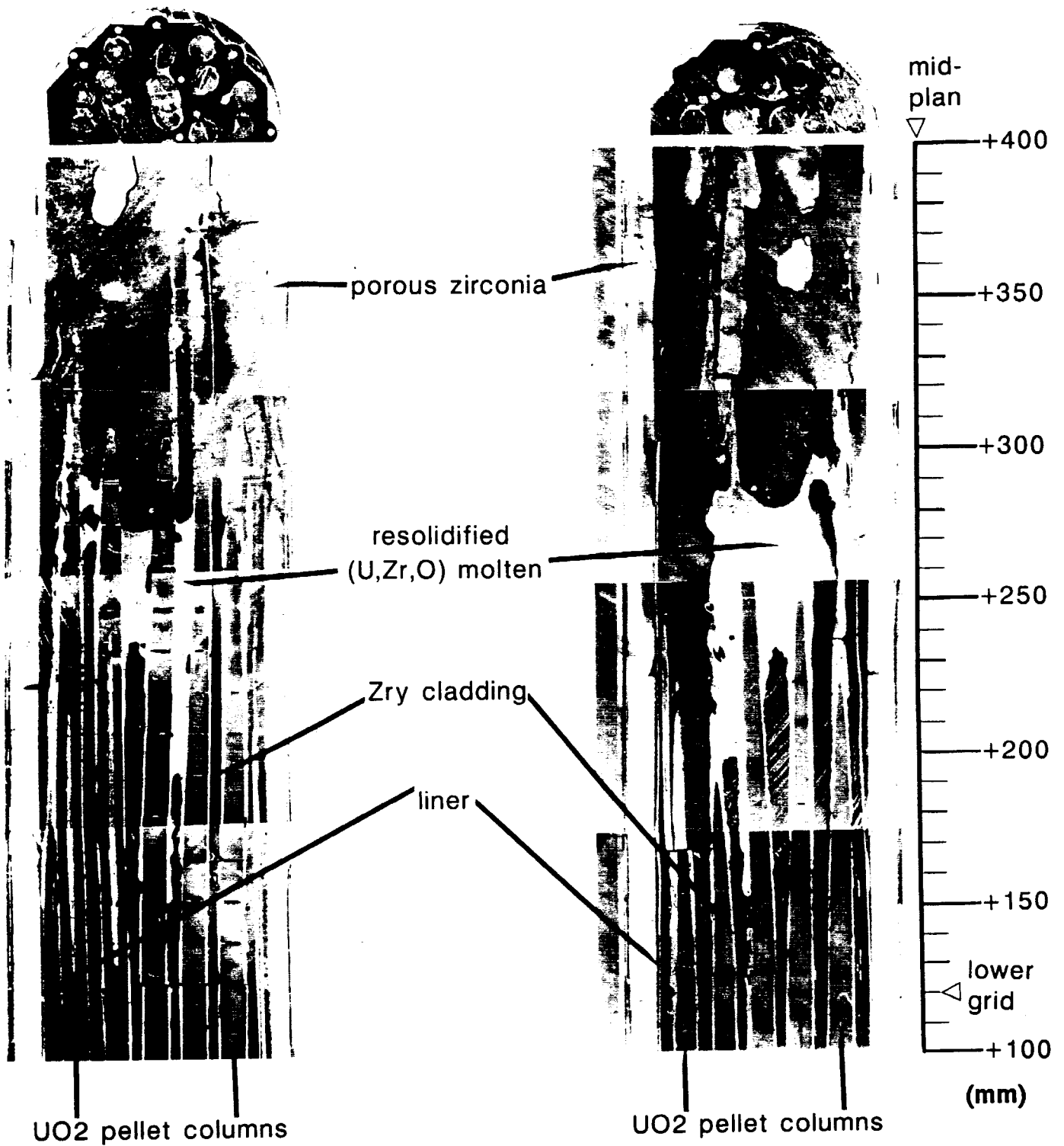


Fig. 11 : Axial cut of the lower end of bundle

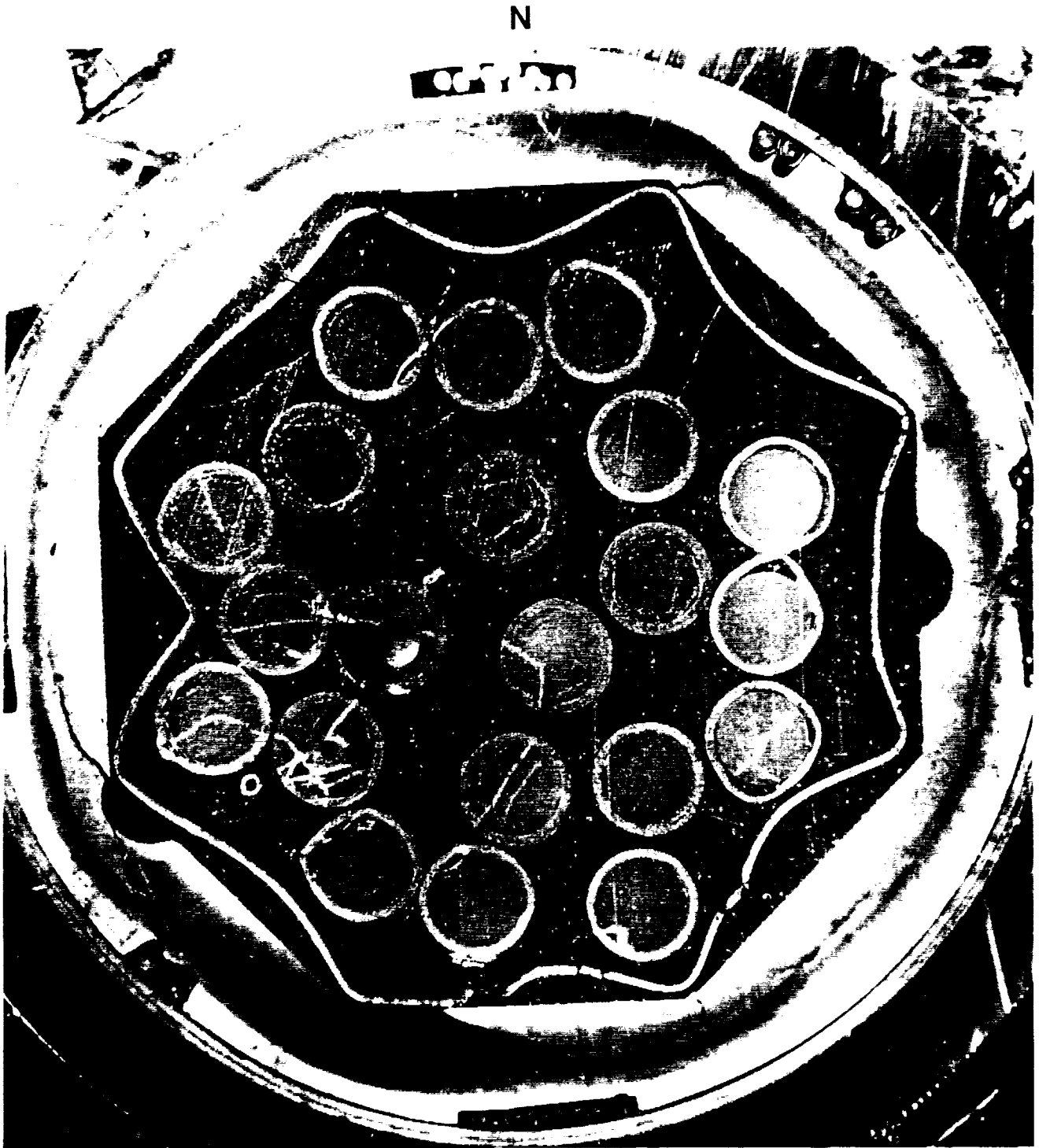


Fig. 12 : Cross cutting at elevation 0.76m

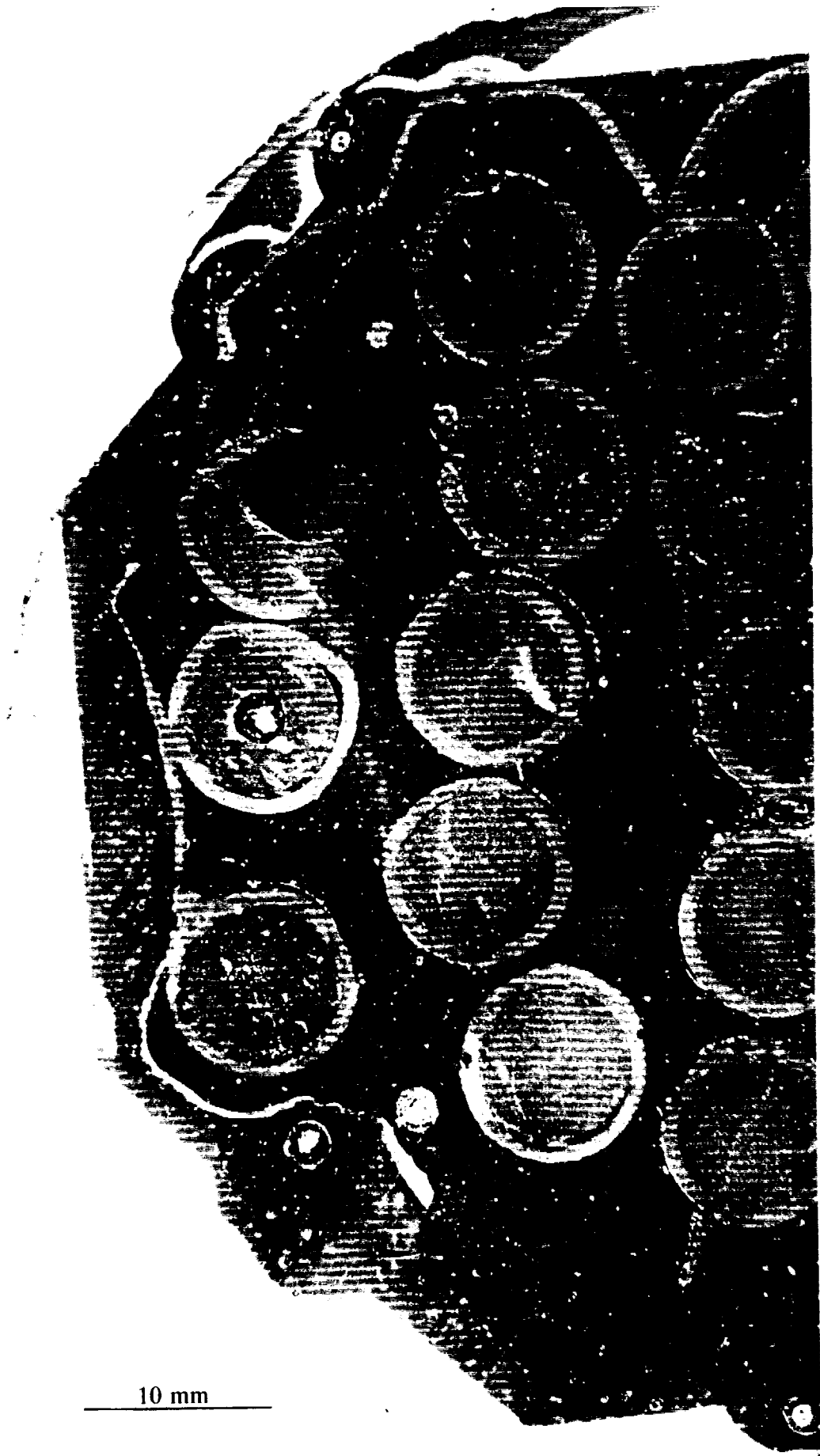


Fig. 13a : Cross cutting at elevation 0.58m

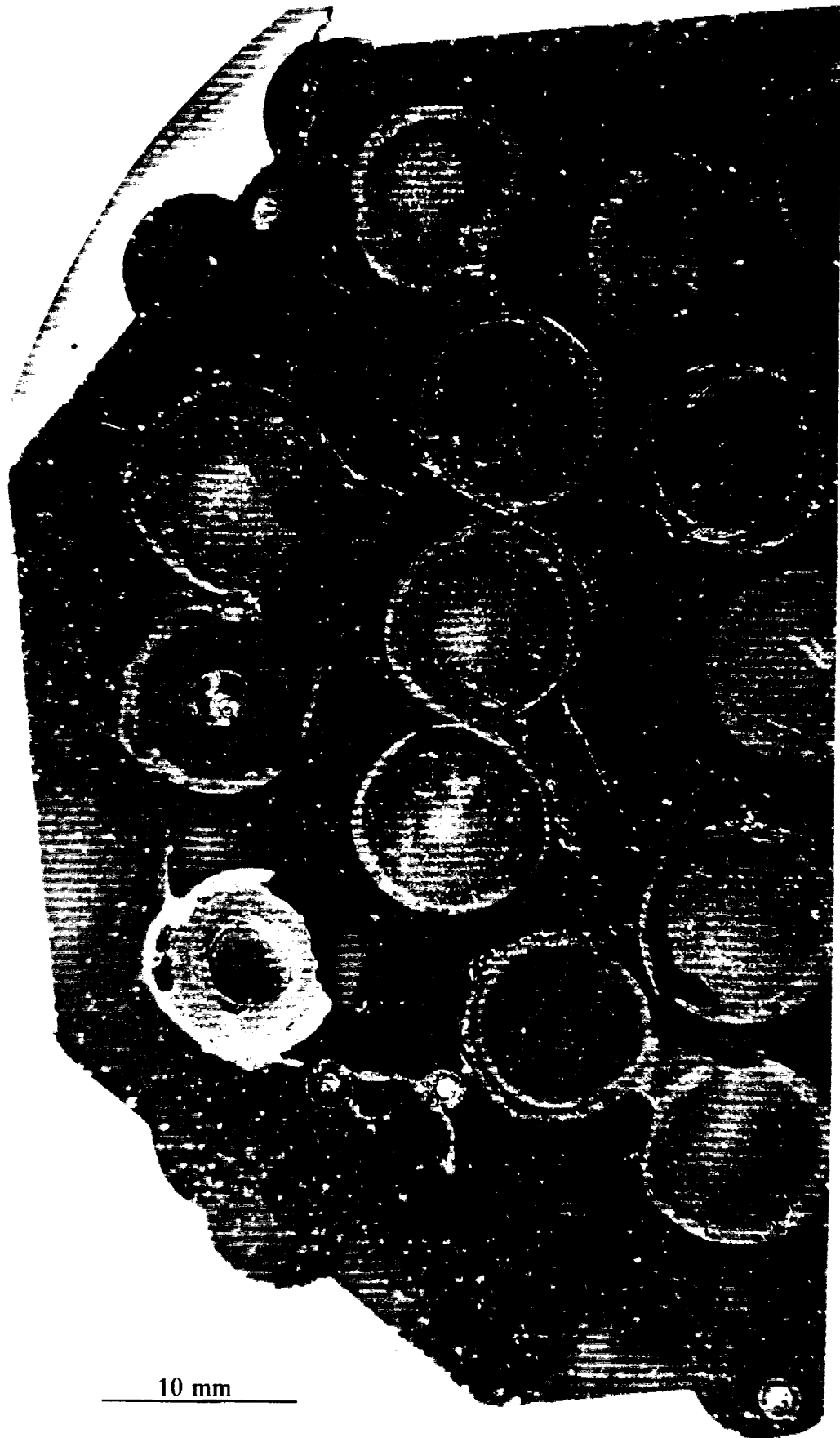


Fig. 13b : Cross cutting at elevation 0.52m

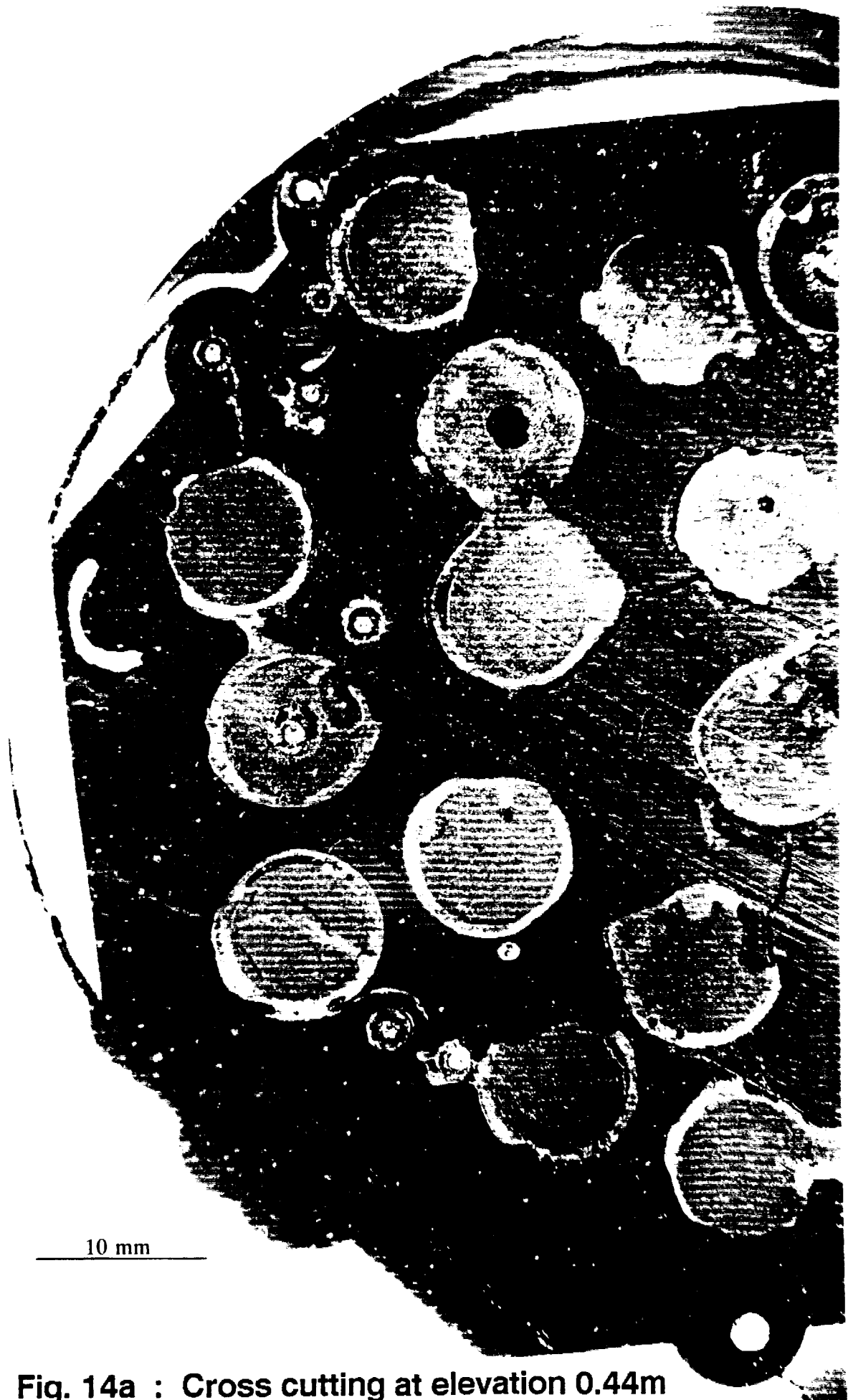


Fig. 14a : Cross cutting at elevation 0.44m

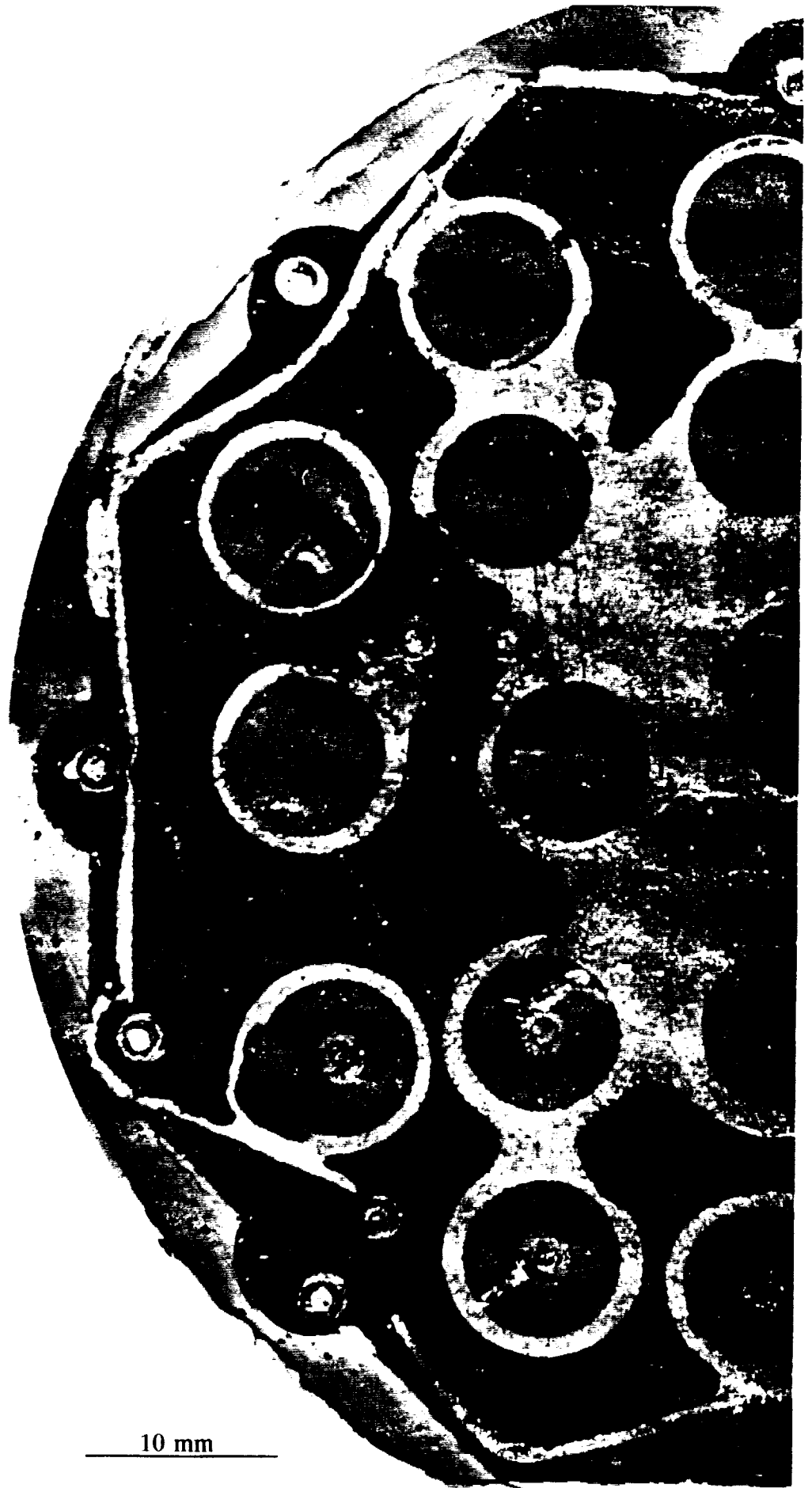


Fig. 14b : Cross cutting at elevation 0.26m

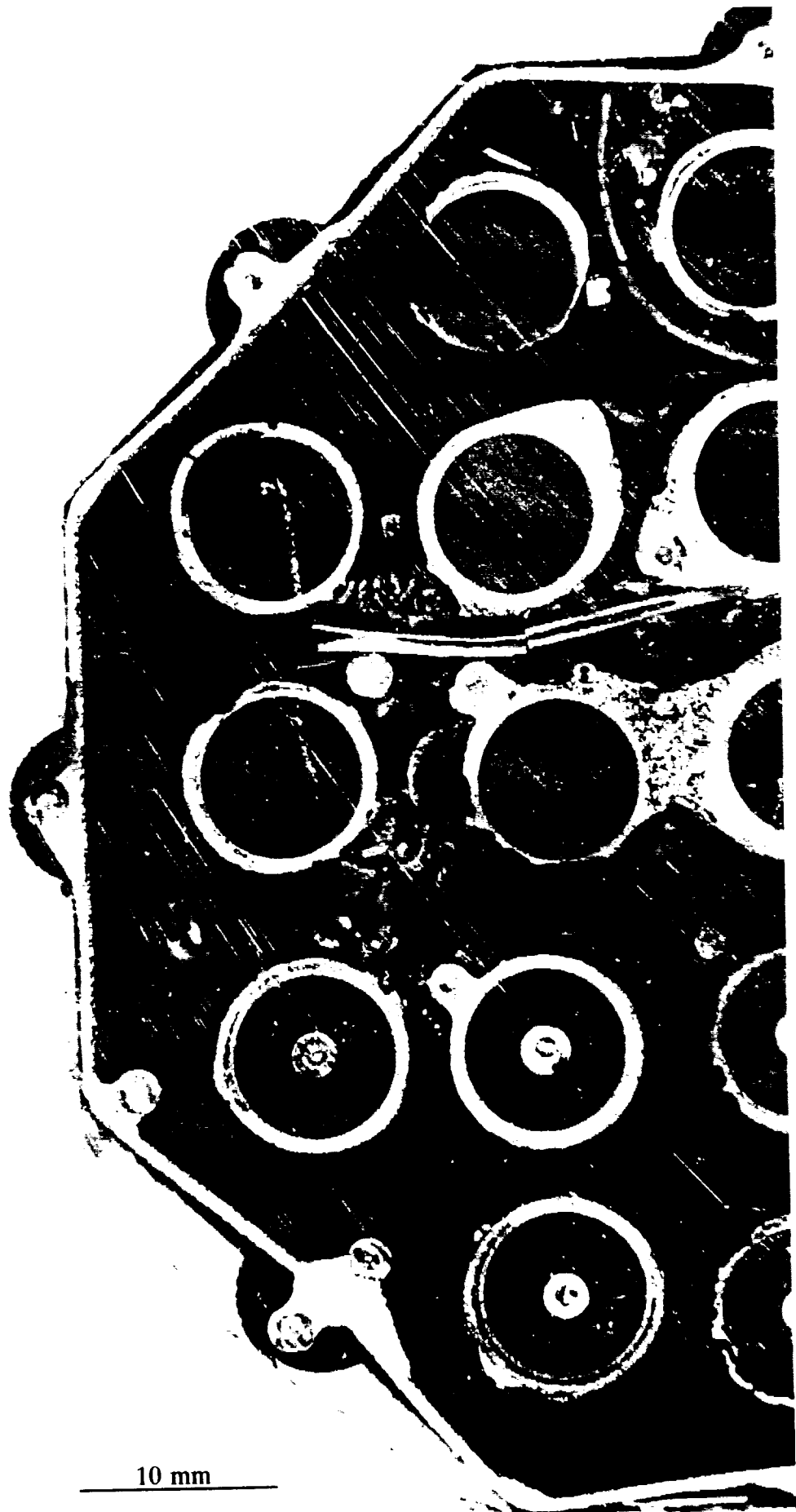
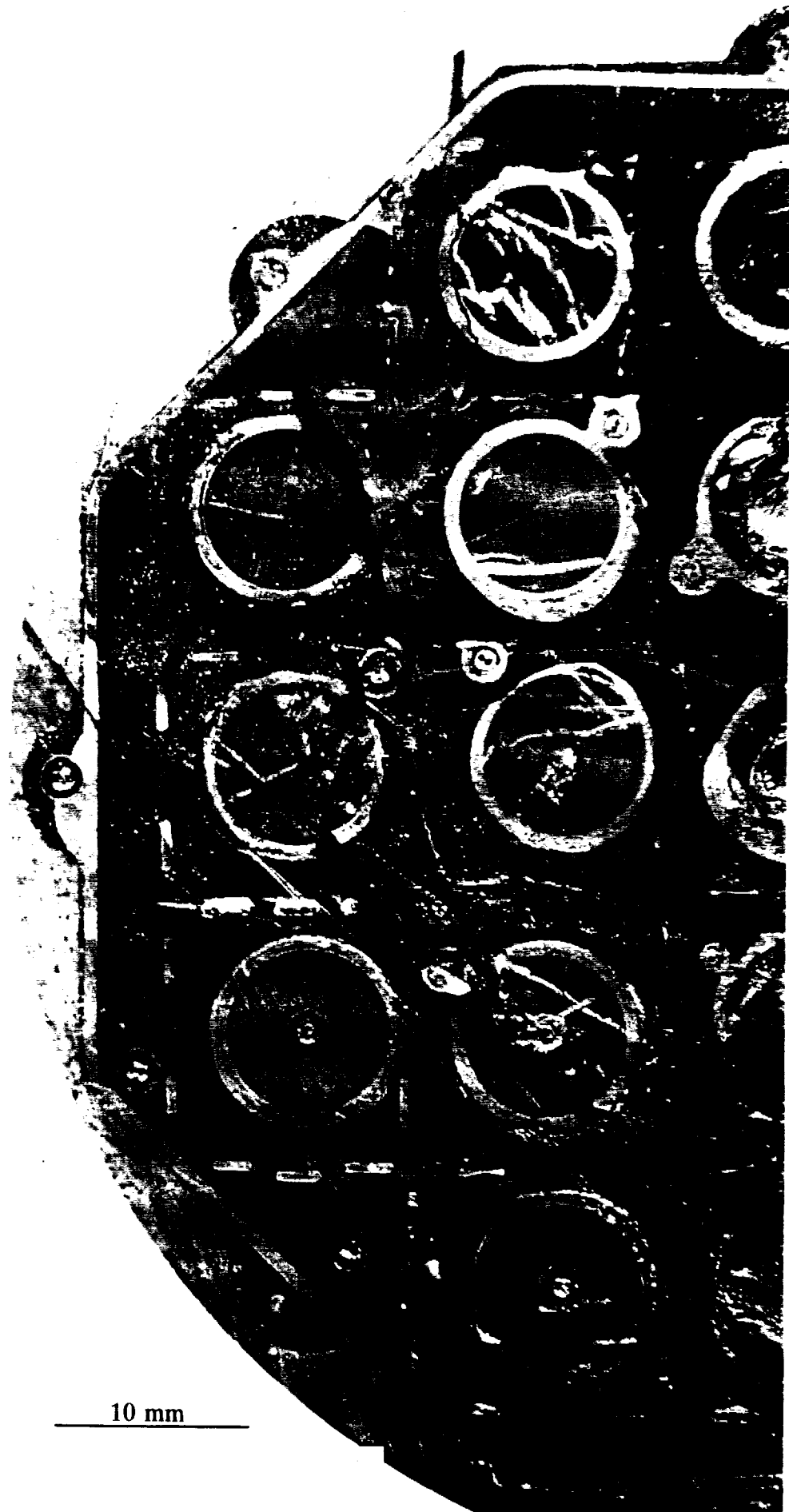
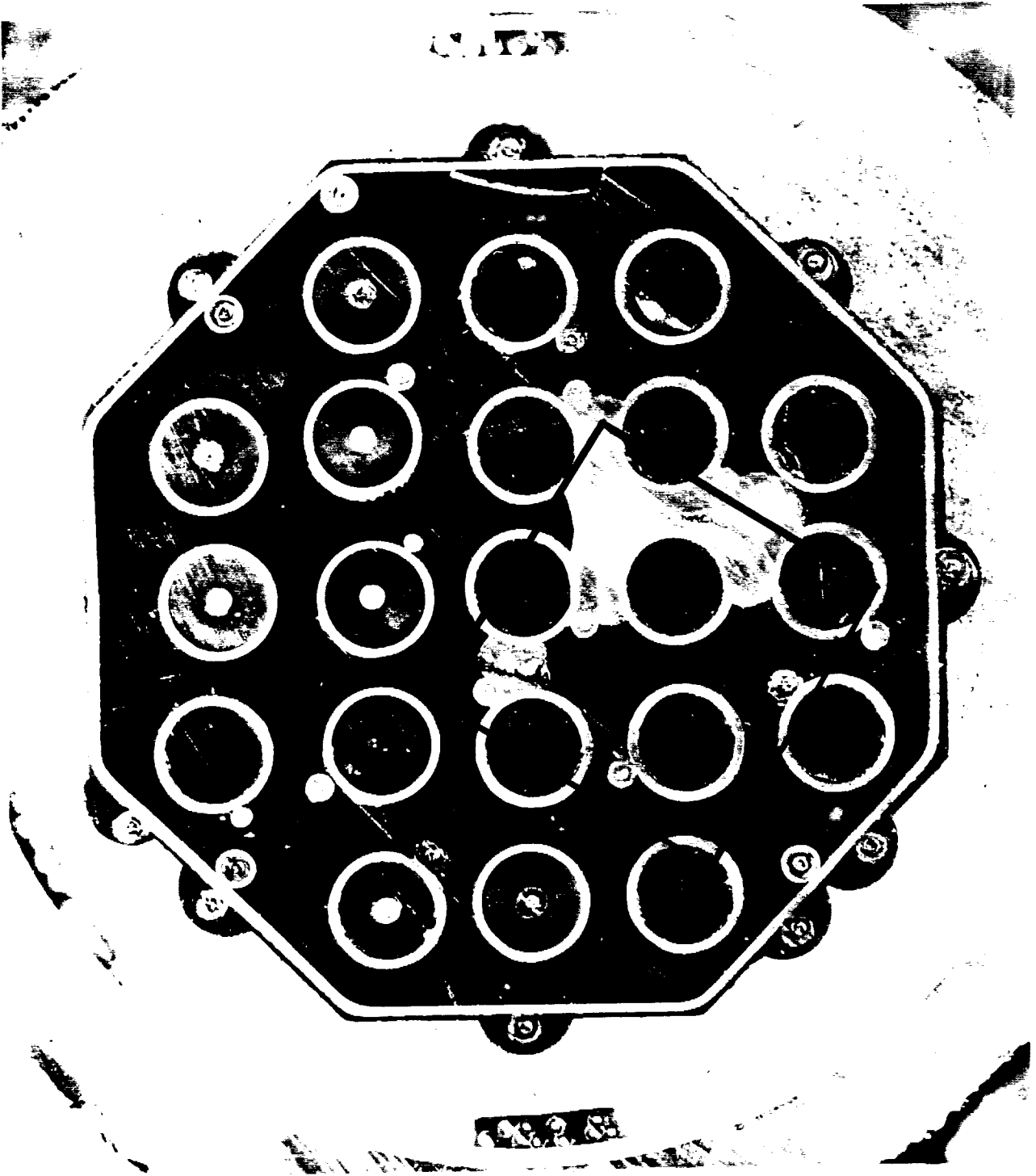


Fig. 15a : Cross cutting at elevation 0.17m



**Fig. 15b : Cross cutting at elevation 0.14m
(Lower Spacer-Grid Location)**

N



10mm

Fig. 16 : Cross cutting at elevation 0.05m

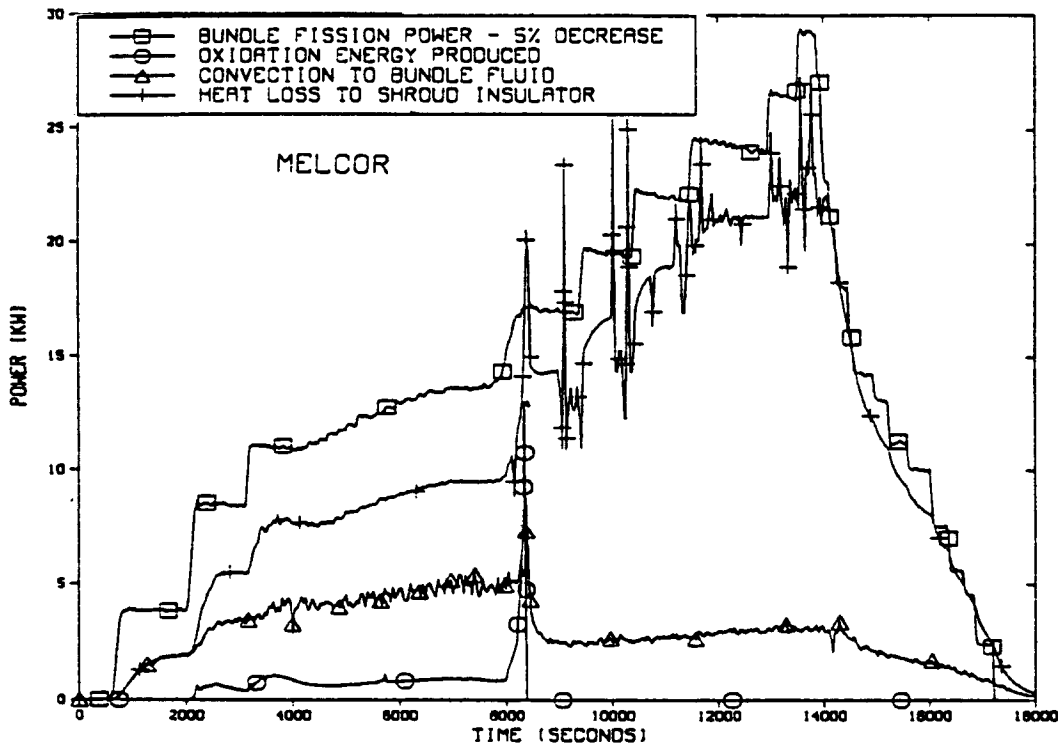


FIG. 17a : BUNDLE POWER DISTRIBUTION
MELCOR CALCULATION (USA).

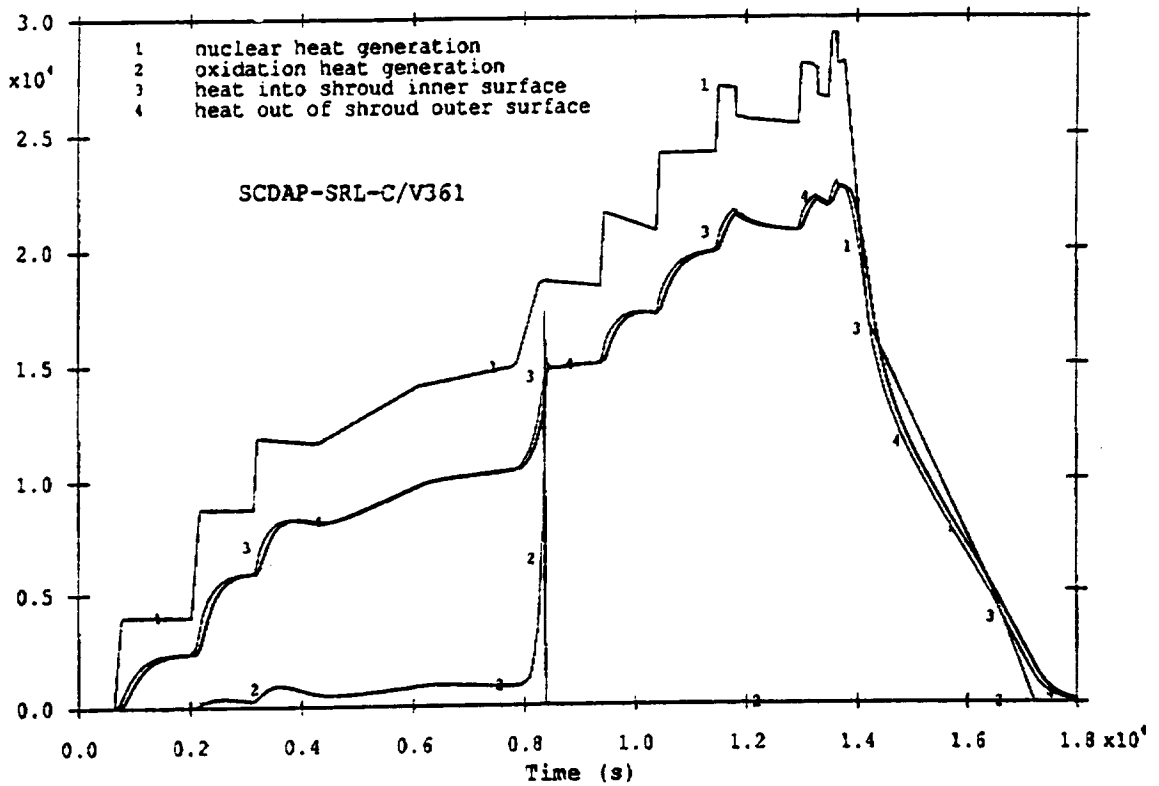
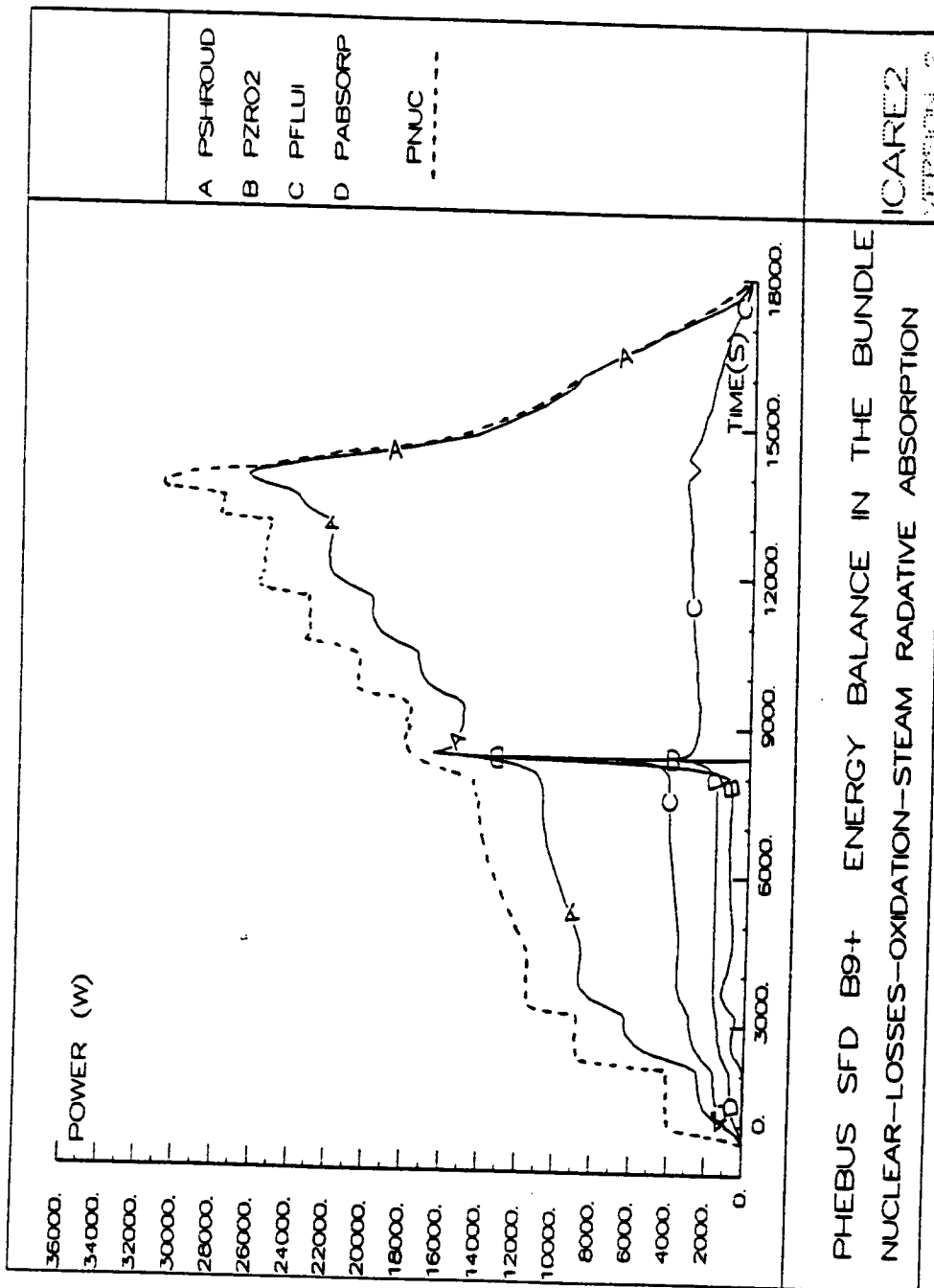


FIG. 17b : BUNDLE POWER DISTRIBUTION
SCDAP/R5/Mod 2 CALCULATION (UK)



PHEBUS SFD B9+ ENERGY BALANCE IN THE BUNDLE
 NUCLEAR-LOSSES-OXIDATION-STEAM RADATIVE ABSORPTION

ICARE2
 VERSION 2

FIG. 17c : BUNDLE POWER DISTRIBUTION
 ICARE2V2p CALCULATION (FRA-SP)

DISTRIBUTION LIST
ISP 28 PARTICIPANTS

ISP 28 PARTICIPANTS	ORGANIZATION	NAME
CZECHOSLOVAKIA	NRI/REZ	F. PAZDERA M. VALACH L. BELOVSKY
FRANCE and SPAIN	CEA/IPSN Spanish PHEBUS Consortium	S. BOURDON P. VILLALIBRE
GERMANY	GRS/GARCHING	A. BALL K. TRAMBAUER
GERMANY	IKE/STUTT GART	K.D. HOCKE S. KRETSCHMER K. MULLER
HUNGARY	C.R.I.P./BUDAPEST	G. GYENES B. TOTTH P. VERTES
E.C.	ISPRA/JRC	J.A. CAPITAO I. SHEPHERD
ITALY	ENEA and PISE Univ.	G. FRUTTUOSO F. ORIOLO
JAPAN	JAERI and CSK Corp.	K. HASHIMOTO K. SODA E. MATSUMOTO
NETHERLANDS	E.C.N./PETTEN	L. WINTERS
SPAIN	U.P. Madrid - C.T.N.	S.A. ENCISO J.V.L. MONTERO J.G. PINDADO C.S. SANTAMARINA
SPAIN	Spanish PHEBUS Consortium and CSN	A. ALVAREZ J. MARTINEZ
SWEDEN	Studsvik Nuclear/NYOPKING	J. ERIKSSON
TAIWAN	INER/AEC/LUNG-TAN	S.K. CHENG L. KAO
UNITED KINGDOM	AEA-Tech./WINFRITH	T.J. HASTE J.N. LILLINGTON A.J. LYONS
UNITED STATES	SANDIA Nat. Lab. and NRC	G.M. MARTINEZ

PARTICIPANTS OUT OF THE FRAMEWORK OF ISP 28

KOREA	KAERI/DAEDUK-DANJI	H.P. PARK Y. JIN C.K. PARK
POLAND	IAE/OTWOCK/SWIERK	S. STEMPNIEWICZ P. MARKS
RUSSIA	IBRAE/NSI	A. KIESELEV G. SAMOLIOVA



DEPARTEMENT DE RECHERCHES EN
SECURITE

Cadarache, le 21/06/93

SERVICE D'ETUDES ET DE
MODELISATION
D'ACCIDENTS DE REACTEURS

BA/FT
Nb de Pages : 105

Laboratoire de Physique des Accidents
Groupe Physique Accidentelle des Matériaux

RAPPORT TECHNIQUE SEMAR 92/82
NOTE PHEBUS CSD 92/134
OECD/NEA/CSNI/R (92) 17

INTERNATIONAL STANDARD PROBLEM N°28

**PHEBUS-SFD B9 + EXPERIMENT
ON THE DEGRADATION OF A PWR CORE TYPE**


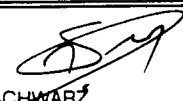
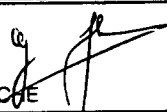
Comparison report - Volume 1

Authors
B. ADROGUER* - A. COMMANDE**
C. RONGIER* - M. MULET**

December 1992

*CEA/IPSN/DRS - CADARACHE
**CISI INGENIERIE - AIX EN PROVENCE

LABORATOIRE DE PHYSIQUE DES ACCIDENTS

 B. ADROGUER 28/06/93	 M. SCHWARZ 13/07/93	 G. HACHE 13/7/93
Rédaction : Nom/Visa/Date	Vérification : Nom/Visa/Date	Approbation : Nom/Visa/Date

This document, which contains proprietary or other confidential or privileged information, and any reproduction in whole or in part, shall not be disseminated outside the organization of the recipient without prior approval of the IPSN.



CONTENT

1 - INTRODUCTION	8
2 - OVERVIEW OF THE ISP 28 EXERCISE	9
3 - PHEBUS - SFD B9+ EXPERIMENT	10
3.1 - Outline of the facility	10
3.2 - Bundle description and measurements	11
3.3 - Objectives and experimental conditions of the B9+ test	12
3.3.1 - Objectives of the B9+ test	12
3.3.2 - Scenario and T/H boundary conditions	12
3.3.3 - Radial boundary conditions in the shroud	13
3.3.3.1 - Comments on the shroud	13
3.3.3.2 - Thermal radial boundary conditions	14
3.3.4 - Nuclear power history and distribution	16
3.3.4.1 - History	16
3.3.4.2 - Radial and axial distributions	16
3.3.5 - Experimental uncertainties	17
4 - MAIN PHENOMENA OBSERVED	18
4.1 - Thermal behaviour	18
4.2 - Oxidation behaviour	19
4.3 - Hydrogen release	20
4.4 - Inconel spacer grids	20
4.5 - UO ₂ dissolution by solid Zry	21
4.6 - UO ₂ dissolution by molten Zry	21
4.7 - ZrO ₂ dissolution by molten Zry	22
4.8 - Relocation of molten mixtures	22
4.9 - Bundle blockage	23
5 - OVERVIEW OF PARTICIPANTS' MODELS	25
5.1 - Physical models of degradation	25
5.2 - Nodalization of the PHEBUS bundle	26
5.3 - Shroud modelling	26
5.4 - Nuclear power	27
6 - COMPARISONS OF INDIVIDUAL RESULTS WITH THE EXPERIMENT	27
6.1 - FRA-SP (Annex 1) : ICARE2/V2p calculation	28
6.2 - SP-CSN (Annex 2) : SCDAP MOD1 Stand-alone code	29
6.3 - SP-UPM (Annex 3) : MELCOR V1.8.0 calculation	29
6.4 - CZECHOSLOVAKIA (Annex 4) : FRAS - SFD calculation	30
6.5 - GER-IKE1 and IKE2 (Annex 5a, Annex 5b) : KESS III calculation	30
6.6 - GER - GRS1 and GRS 2 (Annex 6a, Annex 6b) : ATHLET SA calculation	32
6.7 - HUNGARY (Annex 7) : MARCH3 calculation	33
6.8 - I-PISE (Annex 8) : SCDAP/RELAP5 MOD2 calculation	33
6.9 - ISPRA (Annex 9) : ICARE2 V1 calculation	34
6.10 - JAPAN (Annex 10) : SCDAP/R5 MOD1 calculation	35
6.11 - NETHER (Annex 11) : SCDAP/R5 MOD2.5 calculation	35
6.12 - SWEDEN (Annex 12) : SCDAP/R5 MOD2 calculation	36
6.13 - TAIWAN (Annex 13) : MELCOR V1.8.0 calculation	37
6.14 - UK (Annex 14) : SCDAP/R5 MOD2.5 Version 361SC	38
6.15 - U.S.A (Annex 15) : MELCOR V1.8EA calculation	39

7 - OVERVIEW OF THE COMPARISONS	40
7.1 - The Modelling of the B9+ transient	42
7.1.1 - Nodalization	42
7.1.2 - Difficulties	42
7.2 - Thermal behaviour	43
7.2.1 - Heat balance in the bundle	43
7.2.2 - Radial temperature profile	44
7.2.3 - Temperature escalation	45
7.2.4 - Fluid temperature at the bundle outlet	45
7.2.5 - Maximum temperature	45
7.3 - Oxidation and H2 production	46
7.3.1 - Cladding oxidation histories	46
7.3.2 - H2 production	47
7.3.3 - Experimental and modelling uncertainties	47
7.4 - Inconel spacer-grids	48
7.5 - Fuel dissolution by molten Zry	48
7.6 - Zirconia dissolution by molten Zry	50
7.7 - Relocation of molten materials and channel blockage	50
7.8 - Mixture compositions	54
7.9 - Code run time statistics	55
8 - CONCLUSIONS	56
- REFERENCES	61
- LIST OF ANNEXES (VOLUME 2)	63
- LIST OF TABLES (VOLUME 1)	64
- LIST FIGURES (VOLUME 1)	65
- LIST OF FIGURES FOR EACH CODE-T0-DATA ANNEX (VOLUME 2)	66
- TABLES	69
- FIGURES	84

<p align="center"><i>SERVICE D'ETUDES ET DE MODELISATION D'ACCIDENTS DE REACTEURS</i> <i>Laboratoire de Physique des Accidents</i></p>		
Nat. Document	RAPPORT TECHNIQUE SEMAR 92/82 NOTE PHEBUS CSD 92/134	
TITRE	INTERNATIONAL STANDARD PROBLEM ISP 28 PHEBUS-SFD B9 + EXPERIMENT ON THE DEGRADATION OF A PWR CORE TYPE Final comparison report - Volume 1	
Auteur(s)	B. ADROGUER - A. COMMANDE - C. RONGIER - M. MULET	
Type de Diffusion :	"Mots clés" : PHEBUS CSD B9+ ISP 28	Nbre pages: 105
	N° Fiche Action : 422 4110	Nbre annexes: 17
<p><i>Résumé :</i></p> <p>L'expérience PHEBUS CSD B9+ a été acceptée par l'OCDE/CSNI pour faire l'objet du Problème Standard International n° 28. L'objet de cet exercice était d'évaluer l'aptitude des codes à décrire la dégradation d'un coeur de type PWR et en particulier les principaux phénomènes observés dans l'essai B9+ : oxydation des gaines, émission d'H₂, dissolution de l'UO₂ par le Zr fondu et relocalisation des eutectiques formés. Ce problème organisé en condition semi-aveugle a fait l'objet de 15 calculs avec 7 codes différents. Les comparaisons calcul-expérience ont permis d'identifier les possibilités des codes, ainsi que des faiblesses et des manques, en particulier en ce qui concerne la liquéfaction de l'UO₂ et la relocalisation des eutectiques. Cet exercice illustre la nécessité d'améliorer et de compléter la modélisation des principaux phénomènes de dégradation d'un coeur et de mieux valider ces outils destinés aux calculs réacteur.</p> <p><i>Summary :</i></p> <p>The PHEBUS SFD B9+ test was accepted by OECD/CSNI as the International Standard Problem n° 28. The aim of this exercise was to assess the ability of the codes to describe the degradation of PWR-type cores and in particular to predict the main phenomena observed in B9+ : cladding oxidation H₂ production, fuel dissolution by molten Zr and relocation of melts resulting of chemical interaction. 15 calculations performed with 7 different codes were submitted in semi-blind conditions. Code to data comparisons enabled the current ability of the codes to be identified and to point out weaknesses and lacks regarding the UO₂ dissolution and melt relocation. Finally this exercise emphasized the need to improve and complete the modelling of the main degradation processes and to better assess these models to be used for reactor calculations.</p>		
Repère bureautique : RT1884.DOC		

OECD

In 1948, the United States offered Marshall Plan aid to Europe, provided the war-torn European countries worked together for their own recovery. This they did in the Organisation for European Economic Cooperation (OEEC). In 1960, Europe's fortunes had been restored ; her standard of living was higher than ever before. On both sides of the Atlantic the interdependence of the industrialised countries of the Western World was now widely recognised. Canada and the United States joined the European countries of the OEEC to create a new organisation, the Organisation for Economic Co-operation and Development. The Convention establishing the OECD was signed in Paris on 14th December 1960.

Pursuant to article 1 of the Convention, which came into force on 30th September 1961, the OECD shall promote policies designed :

- to achieve the highest sustainable economic growth and employment and a rising standard of living in Member countries, while maintaining financial stability, and this to contribute to the development of the world economy;
- to contribute to sound economic expansion in Member as well as non-member countries in the process of economic development; and
- to contribute to the expansion of world trade on a multilateral, non-discriminatory basis in accordance with international obligations.

The original Signatories of the Convention were Austria, Belgium, Canada, Denmark, France, the Federal Republic of Germany, Greece, Iceland, Ireland, Italy, Luxembourg, the Netherlands, Norway, Portugal, Spain, Sweden, Switzerland, Turkey, the United Kingdom and the United States. The following countries acceded subsequently to the Convention (the dates are those on which the instruments of accession were deposited) : Japan and New Zealand (29th May 1973).

NEA

The OECD Nuclear Energy Agency (NEA) was established on 20th April 1972, replacing the OECD's European Nuclear Energy Agency (ENEA established on 20th December 1957) on the adhesion of Japan as a full member.

The NEA now groups all the European Member countries of OECD and Australia, Canada, Japan and the United States. The Commission of the European Communities takes part in the work of the Agency. The primary objectives of NEA are to promote co-operation between its Member governments on the safety and regulatory aspects of nuclear development, and on assessing the future role of nuclear energy as a contributor to economic progress.

This is achieved by :

- encouraging harmonisation of government's regulatory policies and practices in the nuclear field, with particular reference to the safety of nuclear installations, protection of man against ionising radiation and preservation of the environment, radioactive waste management, and nuclear third party liability and insurance;
- keeping under review the technical and economic characteristics of nuclear power growth and of the nuclear fuel cycle, and assessing demand and supply for the different phases of nuclear power to overall energy demand;
- developing exchanges of scientific and technical information on nuclear energy, particularly through participation in common services;
- setting up international research and development programmes and undertakings jointly organised and operated by OECD countries.

In these and related tasks, NEA works in close collaboration with the International Atomic Energy Agency in Vienna, with which it has concluded a Co-operation Agreement, as well as with other international organisations in the nuclear field.

CSNI

The NEA Committee on the Safety of Nuclear Installations (CSNI) is an international committee made up of scientists and engineers. It was set up in 1973 to develop and coordinate the activities of the OECD Nuclear Energy Agency concerning the technical aspects of the design, construction and operation of nuclear installations insofar as they affect the safety of such installations. The Committee's purpose is to foster international co-operation in nuclear safety amongst the OECD Member countries.

CSNI constitutes a forum for the exchange of technical information and for collaboration between organisations which can contribute, from their respective backgrounds in research, development, engineering or regulation, to these activities and to the definition of its programme of work. It also reviews the state of knowledge on selected topics of nuclear safety technology and safety assessment, including operating experience. It initiates and conducts programmes identified by these reviews and assessments in order to overcome discrepancies, develop improvements, and reach international consensus on technical issues of common interest. It promotes the coordination of work in different Member countries, including the establishment of co-operative research projects and international standard problems, and assists in the feedback of the results to participating organisations. Full use is also made of traditional methods of co-operating, such as information exchanges, establishment of working groups, and organisation of conferences and specialist meetings.

The greater part of CSNI's current programme of work is concerned with the safety technology of water reactors. The principal areas covered are operating experience and human factors, reactor coolant system behaviour, various aspects of reactor component integrity, the phenomenology of radioactive releases in reactor accidents and their confinement, containment performance, risk assessment, and severe accidents. The Committee also studies the safety of the fuel cycle, conducts periodic surveys of reactor safety research programmes, and operates an international mechanism for exchanging reports on nuclear power plant incidents. In implementing its programme, CSNI establishes Co-operative mechanisms with NEA's Committee on Nuclear Regulatory Activities (CNRA), responsible for the activities of the Agency concerning the regulation, licensing and inspection of nuclear installations with regard to safety. It also co-operates with NEA's Committee on Radiation Protection and Public Health and NEA's Radioactive Waste Management Committee on matters of common interest.

ABSTRACT

The Nuclear Safety and Protection Institute (IPSN) of CEA proposed the PHEBUS Severe Fuel Damage B9+ test as the basis for an OECD/CSNI International Standard Problem. The objectives of the test were to study the following main phenomena occurring during the early phase of an SFD accident in a PWR : cladding oxidation, the mechanical behaviour of cladding with a ZrO_2 layer of variable thickness containing molten zircaloy, the simultaneous dissolution of UO_2 and ZrO_2 by molten Zry and melts relocation. These phenomena being crucial for a description of fuel behaviour during severe accidents, the B9+ test was accepted with semi blind conditions as International Standard Problem ISP 28.

Measured thermal-hydraulic conditions were supplied to help participants to calculate rod thermal behaviour as correctly as possible in order to evaluate the capabilities of the codes to calculate bundle degradation (blind part) using the appropriate thermal conditions. The calculations could be performed using two kinds of radial Boundary Conditions : a constant temperature applied on the external cold surface of the shroud (1st approach) or temperature evolutions versus time at different levels of the internal surface of the shroud (2nd approach). The first approach needed a fine modelling of all the layers of the shroud, in particular of the porous ZrO_2 layer which mainly determines the shroud insulation. The second approach, which was proposed to avoid modelling of the shroud, was "code dependent" because the thermal conditions were defined by a best estimate ICARE2 calculation.

The results of 17 calculations were submitted by 15 different organizations from 12 countries. Eight different codes were used and 4 calculations were performed using the second approach.

The calculated results were compared to measurements performed during the transient (fluid, rod and shroud temperatures, H_2 release) and to the final state of the bundle deduced from Post Test Examinations measurements (cladding oxidation, UO_2 dissolution, cladding dislocation, relocation of molten materials, flow blockage, ...).

Two groups of calculations can be distinguished. The first were performed with SCDAP Mod1, SCDAP/RELAP5 Mod1 and Mod2, MELCOR and ICARE2 and described the bundle degradation up to the final freezing of relocated materials. The second, including ATHLET SA, KESS III, FRAS-SFD and MARCH3 were limited to the calculation of thermal behaviour and to the first oxidation process of rod degradation.

All the calculations performed with the first approach using a recommended measured ZrO_2 porous conductivity value led to an overestimation of rod temperatures. Correct thermal and oxidation behaviours of the rods were only calculated when the thermal leakage through the shroud was increased and adjusted.

The capabilities of the advanced codes for calculating the main degradation phenomena when the thermal-hydraulic conditions are known were clearly illustrated. Areas with inadequate understanding and modelling weaknesses were identified. The most severe limitations concerned simultaneous UO_2 - ZrO_2 dissolution by molten Zry for which ZrO_2 dissolution was not modelled except in one code, UO_2 solubility limits in the resulting U-Zr-O mixture and cladding failure conditions by this molten mixture. There is also a general tendency to overestimate the relocation distance of these liquified mixtures. Finally, lacks were identified in the modelling of the Inconel spacer-grid interaction with both the rods and the relocated mixtures.

This first ISP on core degradation points out that more verification and validation work remains necessary for severe fuel damage computer codes which seem to be lagging behind current knowledge gained through experimental data on the early phase of core degradation.

The verification of reactor codes on small scale experiments needs more code versatility : power profile evolutions, surrounding structures with imposed boundary conditions, a pure non-condensable flow, more output convenience.

Finally this exercise also illustrates the importance of the code user, the need for improved user-guidelines with more detailed information and recommendations, as well as the need for experts in core degradation in order to make code utilization more effective with valuable judgements on predictions especially in these areas where code modelling deficiencies have been identified.

1 - INTRODUCTION

The Task Group on In-Vessel Degraded Core Behaviour was established by the Principal Working Group n°2 to address the physical processes that occur in the in-vessel phase of severe accidents in order to evaluate current code capabilities and to identify areas for further research.

In the field of severe accidents there remains a need to better understand and calculate core degradation and to check the ability of the codes to model main core degradation phenomena. The Institut de Protection et de Sûreté Nucléaire (I.P.S.N) of the Commissariat à l'Energie Atomique (C.E.A.) therefore proposed the PHEBUS SFD B9+ test as the basis for an OECD-CSNI International Standard Problem exercise.

The objectives of the B9+ test were to study the following main phenomena occurring during a SFD accident in a PWR : Cladding oxidation, the mechanical behaviour of the cladding with a ZrO_2 layer of variable thickness containing molten zircaloy, the simultaneous dissolution of UO_2 and ZrO_2 by molten Zr, and the relocation of the resulting melts.

These phenomena being crucial in the framework of code development and assessment, the test B9+ was accepted by the Principal Working Group n°2 with semi-blind conditions as exercise ISP28.

All the measured thermal-hydraulic conditions (open part) were supplied to help participants to calculate thermal conditions as correctly as possible in order to evaluate bundle degradation (blind-part) using appropriate conditions.

The results of 17 calculations were submitted by 15 different organizations from 12 countries indicating both the great interest and cooperative effort of the various institutions. Eight different codes were used.

A preliminary comparison report which compiled the 17 sets of comparison plots was sent to the participants in May 1991 in order to prepare the second workshop of this ISP which took place in June 1991 in Aix-en-Provence (France). During this meeting the participants' semi-blind predictions were discussed in detail. The present report includes these discussions and the conclusions drawn from this semi-blind exercise.

2 - OVERVIEW OF THE ISP 28 EXERCISE

PHEBUS-SFD B9+ was proposed by the Task Group on In-Vessel Degraded Core Behaviour and accepted by the Principle Working Group n°2 in October 1989. In order to better calculate correct thermal hydraulic behaviour which governs main degradation phenomena it was suggested that the problem be semi-open by giving the participants the thermal hydraulic measurements in order to calculate the degradation phase with correct initial conditions.

In other respects, this choice had the advantage of controlling radial thermal leakage through the surrounding shroud, which is difficult to calculate due to uncertainties at high temperature regarding the thermal conductivity on the porous ZrO₂ layer included in the shroud.

A first workshop was held in CADARACHE in April 1990 to give the technical specifications of the test. A detailed description of the B9+ test device and associated test instrumentation were given. The boundary conditions were specified with some recommendations. All the measured temperature evolutions within the test device were given to the participants [1]. The parameters to be calculated and the reporting format were also specified [4] and a schedule discussed. Participants had to submit the calculation by December 1st 1990, and the issue of this comparison report was scheduled for March 15, 1991.

Only four submissions were received by mid-December [the United Kingdom, Netherlands, Italy (Pise U), Germany (IKE)]. The remaining submissions were received at various times during the period December 15 - January 31, 1991. This delay can be explained by the fact that this exercise was the first ISP in the field of severe core degradation and constituted a pioneer effort for many participants who had to use severe accident codes for the first time. Some of these codes were not always available sufficiently soon to respect the ISP 28 agenda and some codes had to be modified to fit the PHEBUS test conditions. In other respects, some post-test examinations results concerning cladding oxidation, UO₂ dissolution and flow blockage were available late March and at the beginning of April. It was not possible therefore to release this comparison report as scheduled.

The results of 17 calculations were submitted by 15 different organizations from 12 countries indicating both the great interest and cooperative effort of the various institutions. Eight different codes were used : ATHLET SA, FRAS-SFD, ICARE2, KESS III, MARCH-3, MELCOR V 1.8.0 and V 1.8 EA, SCDAP (Mod1 stand-alone), SCDAP/RELAP5 Mod1 and Mod 2.

In agreement with the OECD, the CEA also invited non-OECD countries to calculate the PHEBUS SFD B9+ test in the framework of ISP28 and three calculations were submitted by HUNGARY, CZECHOSLOVAKIA and TAIWAN.

Other non-OECD countries also decided to perform this calculation but independently of ISP 28 (KOREA, POLAND, RUSSIA).

A preliminary comparison report which compiled the 17 sets of comparison plots was sent to the participants in May 1991 in order to prepare the second workshop of this ISP28 which took place in June 1991 in Aix-en-Provence [1]. During this meeting conclusions were drawn from this semi-blind exercise concerning the ability of the codes to predict the early phase of melt progression. Areas with inadequate understanding and modelling gaps and weaknesses were identified. The exercise also illustrated a significant code user effect.

Some participants proposed to perform new calculations in open conditions. Their submissions could be presented and analysed in an independent appendix report. This appendix comparison report could be released in 1992 in case of a sufficient participation with significant additional results.

3 - PHEBUS - SFD B9+ EXPERIMENT

The PHEBUS reactor is located at the CADARACHE Nuclear Centre.

3.1 - Outline of the facility

The PHEBUS SFD facility allowed a reproduction of thermal-hydraulic conditions that were relatively close to what would exist in a reactor core under beyond-design basis conditions. Careful attention was devoted to the monitoring of the bundle power and the thermal-hydraulic conditions. The principle of the tests consisted in supplying a bundle of 21 PWR-type fresh fuel rods with a flowrate mixture of overheated gases (steam-hydrogen or helium). The fuel power is adjusted in order to obtain the required temperature evolution.

The facility mainly consists of the PHEBUS driver core supplying the test fuel with nuclear power, a SFD loop (located on the vertical axis of the driver core) which reproduces the thermal-hydraulic conditions and a pressurized water loop (8 MPa, 533 K) working as an independent and external cooling circuit of the SFD loop.

A fairly flat axial profile of power (over 50 cm) is obtained with a neutronic filter of boron steel installed between the driver core and the test bundle.

The main component of the SFD loop is the test stringer (Fig. 1). It consists of three injection lines (steam, hydrogen, helium) for the gas supply, an electrical superheating device to increase the gas inlet temperature (max 1200 K) to the level required in the test scenario (not used during B9+), a test section, and an exit line which leads the gaseous flow to a pressure regulating system and then to a condenser and a storage tank.

3.2 - Bundle description and measurements

The test train cross-section and the longitudinal view show the bundle which consists of 21 unirradiated UO₂ fuel rods in a 12.6 mm pitch matrix (Fig. 2a and Fig. 2b). The total fissile height is 0.8 m. Two spacer-grids in Inconel 523 mm apart are located on either side of the mid plane at elevations 138 mm and 661 mm respectively from the bottom of the fissile column considered as the zero elevation. The implementation of fusible seals in the upper plugs of the rods (melting point : 1070 K) allows clad ballooning due to pressure effects during the tests to be avoided.

Rods are pressurized with helium at 0.7 MPa pressure in cold conditions.

The insulating shroud of the bundle is a multi-layer structure. The octagonal inner zircaloy liner 0.6 mm thick is surrounded by a thick porous ZrO₂ layer (94 mm ext. diameter and 69.5 mm between the faces of the inner octagonal surface), a dense ZrO₂ layer 1 mm thick and an external stainless steel tube 8 mm thick. Different kinds of thermocouples enable temperature measurements of the fuel centre, cladding, fluid and shroud at different radial locations and elevations (Fig. 3 and Fig. 4) to be made. The hydrogen concentration in the gas mixture at the loop outlet is measured continuously by means of a mass spectrometer. Detailed information on the facility is given in references [1], [2].

The rod numbering of the 21 rods bundle runs from 2 to 24 with omitted numbers 5 and 21 (Fig. 8).

3.3 - Objectives and experimental conditions of the B9+ test

3.3.1 - Objectives of the B9+ test

The objective of the PHEBUS SFD programme is to investigate the damage mechanisms acting on an uncovered PWR core. In order to avoid overly complicated integral experiments involving all the aspects of core degradation, the PHEBUS SFD tests have mainly been focussed on a few principal phenomena occurring during the core degradation [3].

In particular, the objectives of the B9+ test were to study the following phenomena.

- 1 - cladding oxidation.
- 2 - the mechanical behaviour of a variable thickness of the external zirconia layer of the cladding containing molten Zircaloy.
- 3 - the dissolution of UO_2 and ZrO_2 by molten Zircaloy.
- 4 - the relocation of the melt.

The test was performed with Inconel spacer-grids and also enables, under test conditions, the formation of low temperature eutectics with Zircaloy and the interaction with fuel pellets to be studied.

Absorber material rods were not included in the bundle and quenching effects on a hot bundle were not studied in this test.

3.3.2 - Scenario and T/H boundary conditions

The experimental scenario involves three parts (Fig. 5) :

- A first oxidation phase performed with a pure steam flow from 0 to 8370 s (closing time of steam injection). In fact steam probably remained present in the bundle up until 8378 s due to the delay between the closing time of the valve and the steam emptying of the bundle (Fig. 6).

The pressure, the mass flow rate and the inlet temperature were kept constant at the following values :

$$P = 1.9 \text{ MPa}$$

$$Q = 2 \cdot 10^{-3} \text{ kg/s}$$

$$T = 528 \text{ K}$$

Three power steps (4 KW, 8.8 KW and 11.5 KW) allowed rod temperature levels of 1000, 1350, 1600 K to be reached at the hottest level (Fig. 5). Then a slow power increase from 11.5 KW to 14.5 KW during about one hour resulted in slow heating from 1600 K to about 1800 K. A new power step from 14.5 KW to 18.0 KW allowed practically complete oxidation in the upper part of the bundle to be reached. The ballooning of the pressurized rods with He (0.7 MPa in cold conditions) was avoided by the low temperature melting of the fusible seal in the upper plug of each rod.

At the end of the oxidation phase the cooling gas was switched from steam to helium.

- The second heat-up phase was performed in pure helium starting at 8364 s (Fig. 6). A pressure of 1.9 MPa, a helium mass flow rate of 0.5 g/s and an inlet temperature of 528 K were maintained throughout this high temperature phase. Five power steps were performed leading to a maximum rod temperature of about 2750 K.
- During the final phase, which began at 13860 s, step reductions in nuclear power enabled a slow cooling down in order to keep the previous bundle geometry unchanged. The pressure was decreased to 0.4 MPa at 14135 s. During this phase a mean helium mass flow rate of 0.5 g/s with an inlet temperature of 528 K was maintained up to the final time of the test at 18000 s.

3.3.3 - Radial boundary conditions in the shroud

3.3.3.1 - Comments on the shroud

The analysis of previous PHEBUS-SFD tests showed that, due to the very low flow-rates used in these tests the main part of the power released in the bundle is transmitted to the external pressurized cooling loop through the shroud. The main parameter which controls this radial heat transfer is the thermal conductivity of the porous zirconia layer and uncertainties in this parameter dominates the uncertainty in calculating the temperature history of the fuel rods.

An effort was made in order to improve our knowledge of this parameter. The first PHEBUS-SFD tests showed a large change of thermal conductivity due to the progressive filling of the porosities with hydrogen arising from the oxidation of the inner Zry liner. This uncontrolled change was avoided in the B9+ test by the use of a continuous injection of helium in the porous zirconia during the first steam phase.

Laboratory tests were performed in order to measure the thermal conductivity of the porous ZrO_2 from different representative samples under a helium atmosphere, at atmospheric pressure and at temperatures in the range of 523 K to 2273 K. This conductivity was then extrapolated to the pressure conditions of the test (1.9 MPa) and this estimated value was recommended in the specifications [2] for the calculations.

$$\lambda = 0.302 \text{ W/m.K for } T < 1273 \text{ K}$$

$$\lambda = 0.374 - 1.31 \cdot 10^{-4} T + 5.85 \cdot 10^{-8} T^2$$

$$\text{for } 1273 < T < 2273 \text{ K}$$

As explained in section 7.2 this conductivity was non suitable due to an underprediction of the pressure effect.

3.3.3.2 - Thermal radial boundary conditions

Two kinds of radial Boundary Conditions (B.C.) were proposed in order to calculate the test.

1st approach :

It consists in representing as closely as possible the different layers of the shroud surrounding the 21 rod bundle (the internal octagonal liner in Zircaloy, a He gap, a porous ZrO_2 layer with a maximum thickness of 12.25 mm, a dense ZrO_2 layer 1 mm thick and the external stainless steel tube).

The external water cooling of the shroud maintained the steel tube surface at a constant temperature of 528 K all along the shroud for the entire test.

Grooves were provided in the porous ZrO₂ for the location of the thermocouples on the outer face of the Zry liner (Fig. 4) (Radius of the grooves 4 mm). Laboratory measurements on samples with a simulation of the grooves representative of the lower part of the insulator (- 27 cm to + 31 cm) showed that the heat flux increases by about 10 % at 1300 K, 20 % at 1800 K and 23 % at 2300 K due to the grooves.

2nd approach :

In order to avoid modelling of the actual shroud a simple surrounding structure involving only the internal octogonal liner was proposed. The following equivalent cylindrical geometry was proposed :

inner diameter	:	0.0733 m
outer diameter	:	0.0745 m
material	:	Zircaloy

Temperature histories were given at 10 different levels of the liner : 04/12/20/28/36/44/52/60/68/76 cm from the bottom of the fissile length [4].

These radial boundary conditions were defined by a best estimate ICARE2 calculation performed in modelling the actual shroud. This calculation was "adjusted" in order to find a correct thermal behaviour all along the bundle for the entire test. The parameter used so as to better match the measurements was the thermal conductivity of the porous zirconia.

It was pointed out that these radial boundary conditions were of course "ICARE 2 code dependent", for instance dependent on the physical models of the code. It was therefore recommended that the participants using a code able to represent the actual shroud, choose the 1st boundary conditions in making, if necessary, sensitivity studies on the shroud modelling (1st approach user-adjusted) to better fit the rod temperature measurements.

3.3.4 - Nuclear power history and distribution

3.3.4.1 - History

The nuclear power input in the test bundle is directly proportional to the neutron flux provided by the driver core. This latter is measured with two ionisation chambers which have been calibrated to directly indicate the driver core power level.

A comparison of the power signal as given by the ionisation chambers with a detailed thermal balance over the core cooling circuit showed very good linearity of the chambers' average signal (after correction for core inlet temperature) with the core power level.

The coupling factor between the driver core and the test bundle, that is the ratio between the chambers' signal and the actual power released in the bundle, was determined experimentally before each test. The average value is consistent with an analytical estimate of the same ratio.

Fig. 5 shows the bundle power evolution deduced from core power measurements as given by the ionisation chambers and the experimental coupling factor.

3.3.4.2 - Radial and axial distributions

Preliminary dosimetry tests on a PHEBUS SFD test bundle allowed the radial and axial power distributions to be determined. Fig. 8 gives the normalized radial distribution derived from dosimetry measurements.

Fig. 9 gives the axial power profile in the bundle at different times in the test transient corresponding to successive control rod positions.

This axial profile evolution results from a series of neutronic calculations with 4 successive control rod insertions, the zero power configuration being adjusted to the experimental dosimetry profile of the PHEBUS SFD bundle.

All of these curves refer to an intact bundle geometry. Neutronic calculations have shown that the coupling factor (ratio between driver core power and test bundle power) is very little dependent on the fuel mass distribution

in the test bundle. It means that the power axial profiles provided in Figure 9 may be considered as specific power profiles to be weighted by the UO₂ mass distribution at the different levels during fuel relocation (constant specific nuclear power for an unchanged control rod insertion).

3.3.5 - Experimental uncertainties

The following table summarizes the main estimated experimental uncertainties. More details are given in references [1] and [2].

Measurements	Uncertainties
Bundle Temperature	± 50 K above 2400 K
Pressure	3 %
Steam flow rate	5 %
Helium flow rate	5.10 ⁻⁶ kg/s
Nuclear Power	5 %
H ₂ mass generated	20 %

Among the 51 thermocouples which worked correctly at the beginning of the test, 31 failed sooner or later in the transient because they were exposed to too high a temperature or to material interactions. This was the case for all the fuel, cladding and liner thermocouples located between 30 cm and 75 cm, but the thermocouples located inside the porous ZrO₂ worked correctly up to the end of the test. These thermocouples have very similar histories to the one located at the same level in the bundle. This enabled the high temperature history of the rods to be evaluated with confidence by extrapolation from the temperature measurements inside the shroud. The consistency between the axial temperature profiles for each kind of structures enabled this extrapolation to be checked and confirmed.

4 - MAIN PHENOMENA OBSERVED

In this section a summary of the results related to the open part are given as well as the results from post test examinations [5] related to the blind part of ISP 28.

Figure 11 shows the two halves of the axial cutting of the bundle between 10 cm and 40 cm. Figures 12 to 16 show radial cutting at respectively 76, 58, 52, 44, 26, 17, 14, 5 cm from the bottom of the fissile length.

4.1 - Thermal behaviour

The first oxidation phase was characterized between 4000 and 8000 s by a mean slow heat-up of 0.06 K/s. At the end of this oxidation phase a rapid temperature increase was measured (> 3 K/s) at the hot zone (60-70 cm). The fuel temperature of an external rod reached about 2400 K at 60 cm. This temperature escalation was stopped by switching the cooling gas from steam to helium at 8364 s. Our analysis of this escalation showed that it was mainly due to enhancement of the oxidation kinetics at the temperature of the zirconia phase transition from a tetragonal to a cubic phase around 1850 K.

A detailed analysis of the thermal behaviour of the bundle at the 70 and 75 cm levels indicates that temperature escalations also occurred at these elevations on some cladding tubes.

It was deduced from ICARE2 sensitivity studies that the temperature peaks observed both on the liner and inside the shroud at the 70 and 75 cm levels could only be due to rod escalations occurring at the same levels in the bundle and not to a heat transfer from the 60 cm. Only the rods with a sufficient amount of remaining metallic Zry before the end of the oxidation phase were able to undergo a temperature escalation. Due to non-homogeneous oxidation observed on different rods at the same level, some other rods with less metallic Zry were not affected by an escalation, as shown by the only fuel TC01 located at 70 cm in the outer ring rods.

This escalation up to 75 cm was also confirmed by the limited fluid peak temperature observed on each of the 3 thermocouples (TC35, 75, 76) located at the outlet of the bundle at the 80 cm level.

On the whole, the oxidation escalation was limited either by the total oxidation of the remaining non-oxidized Zry or by the steam to helium switch injection. The melting temperature of the oxygen stabilized alpha Zry was reached for about 150 s, just before this injection switch. Then the resulting rapid stopping of the related oxidation power led to a local cooling of the rods with a temporary refreezing of the remaining non-oxidized Zry.

The second heat-up phase with He was characterized by pure steam starved conditions and melting or re-melting of the remaining Zry.

Thermocouple readings became unreliable at different times following the oxidation excursion due to interaction between the cladding sheaths and the molten materials. The unreliable part of the measurements has not been considered in this report.

A maximum temperature of about $2750 \text{ K} \pm 50 \text{ K}$ was reached at the hot zone at 13860 s. This value was estimated by extrapolation from the shroud and the lower bundle part temperature measurements (see § 3.3.5). Furthermore this value was confirmed by PIE results.

4.2 - Oxidation behaviour

Post-test examinations were performed on radial cuts of the bundle. Measurement of the cladding oxide thickness at different elevations was very difficult. At some levels the cladding had disappeared, at others the ZrO_2 layer was sometimes impossible to identify due to complex and non-uniform interaction between molten U-Zr-O materials and the remaining ZrO_2 layers (Fig. 13, 14).

In the upper part of the bundle, beyond 0.60 m, the cladding oxidation was complete or nearly complete and UO_2 dissolution was low. The general aspect of the bundle remained unchanged. However a strong distorsion of the array pitch due to the melting of the Inconel upper spacer grid (1650 K) at around 5500 s (Fig. 12) could be observed.

Between 25 and 60 cm, the cladding oxidation was partial (Fig. 13, 14). ZrO_2 dissolution by molten Zry occurred due to the diffusion of the oxygen from the oxide layer to the melt. This diffusion process appeared to have been localized near the Zr- ZrO_2 interface and led to a particular radial oxygen concentration profile inside the cladding.

At the lower levels where the metallic Zry remained solid during the He phase, an oxygen diffusion process also occurred at the levels characterized by a poor oxygen Zry sublayer. This process also led to a non-homogeneous radial oxygen profile which "kept in mind" the location of the initial ZrO₂ layer. The combination of visual examinations of micrographs and of the microprobe measurements of the local oxygen concentration profiles allowed an evaluation of the thickness of the ZrO₂ layer at the end of the oxidation phase. Uncertainties are believed to be less than the experimental range of the oxidation corresponding to the temperature differences between rods at the same elevation.

The axial profile (figure 25 of the individual comparisons) increased from a few percents (10 μm) below 20 cm to 40 % (350 μm at mid plane elevation) and complete (or nearly complete) oxidation in the upper part (60 to 70 cm).

4.3 - Hydrogen release

Hydrogen concentration in the gas mixture at the loop outlet was measured continuously with a mass spectrometer. The pressure evolution of uncondensable gases in a temporary storage tank also allowed the hydrogen produced to be measured. These two methods gave similar results. The measured total H₂ mass and production rate are given in figures 28 of the individual comparisons.

A total of 39,5 g of H₂ was released during the test. The uncertainty on this measurement was evaluated at 20 %.

4.4 - Inconel spacer grids

The two spacer-grids were located at 13.8 and 66 cm from the bottom of the active length. Post-test examinations on radial cuts performed at these elevations showed that the upper grid located in the hot bundle zone totally disappeared. Local interaction between Inconel and Zry cladding was not observed on the corresponding radial cut. The relocation of this grid occurred during the steam phase. Loss of thermocouple measurements just below this upper spacer-grid could indicate relocation temperatures of around 1550 K.

The lower spacer grid remained partially in place (Fig. 15b). Only the central part corresponding to the CR and 1R rods nearly disappeared and showed evidence of local Inconel-Zry interaction. The resulting melt led to local cladding failures followed by limited UO₂ dissolution during the He phase. Radial cutting of the bundle just above the lower spacer-grid (Fig. 15a) showed no evidence of any

significant catcher effect. Only little solid debris of oxidized Zry was observed on this grid. No evidence of refrozen melts was found on the remaining part of the grid. Visual observations of the radial cutting at 9.8 cm and 17.2 cm showed some gaps inside the cladding extending all over the Zry-UO₂ interface. These cavities could be due to local Inconel-Zry interaction. Globally no significant interaction was observed, probably on account of the protective effect of the ZrO₂ layer of the cladding.

4.5 - UO₂ dissolution by solid Zry

Due to the melting of the upper plug of the rods above 1070 K no differential pressure was applied across the cladding, enabling good UO₂ - solid Zry contacts. Nevertheless, due to a greater thermal expansion of the fuel than of the cladding, the PIE showed some evidence of local UO₂-solid Zry interactions on a few rods (level 26 cm, Fig. 14-b). Some (U, Zr) O₂-x globules were identified inside the cladding with an area-fraction less than 10 % of the total cladding section. But this interaction was very limited and did not lead to significant UO₂ dissolution (and relocation) that could be identified by a measurable fuel surface area decrease.

4.6 - UO₂ dissolution by molten Zry

Fuel dissolution was observed in radial cuts separated by about 2 cm in the zones of interest. Fuel dissolution was estimated from photographs by measuring the surface of the remaining fuel pellets.

$$D (\%) = 100 \cdot \frac{S_o - S}{S_o}$$

S : final surface area of the fuel
S_o : initial surface area of the fuel

These measurements were identified as the weight fraction of fuel dissolution. The uncertainty on these measurements was evaluated at 1.5 %. Only a mean value at each elevation seemed to be significant. At some elevations there was considerable spreading of the dissolution between the different rods particularly near the hot point - Figure 13-a - (from a few wt % up to 40 wt % at 56 cm). Visual observations of the different cuts showed that external rods (2nd ring rods) tended to be dissolved more than the internal ones.

The mean UO₂ dissolution profile is given in figures 29 of the individual comparisons. The dissolution was mainly limited to the zone between 28 and 60 cm. Limited mean dissolutions were found with a maximum of 14 wt % at 52 cm, in spite of considerable local dissolution on some rods. Between 60 and 70 cm only some particular rods were observed with significant local dissolution.

It was thought that local dissolutions could have occurred at the end of the oxidation phase during the 150 s period of the temperature escalation during which the remaining metallic Zry was molten and able both to dissolve the fuel and to be oxidized by the external steam. A second explanation concerned the Zry remaining at the end of the oxidation phase in the colder upper part of the rods. After melting during the He phase, this Zry could relocate internally into the slightly ballooned cladding of some rods, enabling more efficient local dissolution in pure steam-starved conditions, than during the first oxidation phase (Fig. 13 - Rod 6).

4.7 - ZrO₂ dissolution by molten Zry

Visual examinations of the cuts in the upper part of the bundle where oxidation exceeded 50 % showed significant azimuthal ZrO₂ layer thickness differences on some inner rods (minimum thickness about 3 times lower than the maximum thickness). Local ZrO₂ dissolution could partially explain these differences, but no quantitative evaluation could be made due to the difficulty of determining what was due to the azimuthal temperature differences, and what was due to ZrO₂ dissolution. The latter effect which seemed the more significant was mainly observed under the hot zone in the upper part of the cladding failure zone.

4.8 - Relocation of molten mixtures

Visual observations of the axial cuts of the bundle showed two main plugs. The lower one was very localized at the 5 cm level between rods 8, 9, 10, 13, 14, 15, 18. It was a metallic plug with Inconel (Fig. 16). Microprobe analysis of this frozen mixture gave the following mean atomic content :

55.4 % Zr ; 7.5 % U ; 23.6 % Ni ; 7 % Fe ; 1.5 % Cr ; 5 % O.

The external oxidation of this plug at the locations where microprobe analyses were performed was similar to that of the local cladding (~ 10 μm). This showed that relocation began during the steam phase from the liquefaction of the upper

spacer-grid. Part of the lower spacer-grid could also have been relocated in this zone later on during the He phase. At the level of the plug no evidence was found of interaction between the Inconel mixture with the surrounding rods.

The upper plug was larger and localized between 20 cm and 28 cm (Fig. 11, 14). It was a ceramic plug with two α -Zr(O) and (U, Zr) O₂ - x phases which formed during the cooling. Microprobe analysis gave the following mean atomic content :

$$65 \% \text{ Zr ; } 4 \% \text{ U ; } 31 \% \text{ O}$$

PIE observations showed that the ceramic phase (22 % of the surface area of the melt) was dispersed inside the α -Zr(O) phase.

Apart from these two plugs, local deposits on some external rod surfaces of small amounts of mixtures were mainly found between 28 and 40 cm. A few small deposits were also found locally on external rods as far as 60 cm.

The analysis of some of these small amounts of refrozen mixtures showed greater oxide phases. At level 40 cm the [α -Zr(O) ; (U, Zr) O₂ - x] two phase mixture had the following mean atomic content :

$$56 \% \text{ Zr ; } 6 \% \text{ U ; } 38 \% \text{ O}$$

The ceramic phase, richer in U (57 %) than the previous one, represented 33.5 % of the total surface area of the melt.

4.9 - Bundle blockage

Bundle blockage was determined from photographs by measuring all the surfaces of the different mixtures and sections of rods located inside the initial surface of the octogonal liner. This blockage was defined for the ISP 28 as the ratio between the solid surfaces and the internal surface of the liner.

$$B \% = 100 \frac{S_{oct} - S(t)}{S_{oct}}$$

S_{oct} = initial surface inside the octogonal liner (4000 mm²)

$S(t)$ = flow area section at the current time t

This definition had the advantage of giving a bundle blockage equal to 0 % in case of total dislocation of rods at one level and to 100 % in case of total flow blockage. This bundle blockage is equal to 38 % at time zero, due to undeformed rods. The blockage profile measured is given in figures 30 of the individual comparisons. The maximum blockage of 51 % was found in the upper plug zone at the 26 cm level in the upper plug zone. The minimum of 35 % was found at the 46 cm level. These bundle blockages corresponded respectively to hydraulic flow blockages of 21 % and - 4 %.

The cladding disappearance zone occurred for inner rods between 28 cm and 50 cm and up to 56 cm for external rods.

The fusible plug prevented fuel rod ballooning due to a pressure effect. No significant cladding "flowering" was observed, due to oxidation, as was observed in some CORA tests with unpressurized rods. Only a little deformation (a few %) was observed in the totally oxidized upper part of the bundle in the zone 70/80 cm (Fig. 12). These deformations could facilitate local zones of molten Zry relocation and accumulation with further local UO₂ dissolution (see § 4.6).

The liner configurations can be summarized as follows :

80 cm - 75 cm	:	in place - marked deformations nearly in contact with some rods. (Fig.12)
75 cm - 55 cm	:	partially in place - marked deformation - non-oxidized part relocated. (Fig.13)
56 cm - 34 cm	:	total disappearance. (Fig.13)
34 cm - 25 cm	:	partially in place - marked deformation. Some liner-rod contacts with frozen relocated mixtures are observed. (Fig.14)
25 cm - 0 cm	:	totally in place - slight deformation. (Fig.15,16)

5 - OVERVIEW OF PARTICIPANTS' MODELS

The 15 submissions to the ISP 28 are given in table 1 together with the names of the codes used for the analysis.

Eight codes with very different possibilities were used. SCDAP Mod1 stand-alone, SCDAP-RELAP5 Mod2 and Mod1, ICARE 2 V1 and V2p and MELCOR V 1.8.0 and V 1.8EA were able to take into account the main core degradation phenomena and the corresponding material relocation. KESS III, ATHLET SA, FRAS-SFD are under development concerning degradation - relocation processes and their calculations were mainly limited, as well as the MARCH3 calculation, to the prediction of the thermal and oxidation behaviour of the bundle.

The modifications of the codes carried out in order to calculate the PHEBUS B9+ test are summarized in table 2.

It must be pointed out that the ICARE2 modifications were mainly carried out in the framework of its development, and that the SCDAP Mod1 modifications were also carried out in the more general framework of its verification on the PHEBUS SFD experiments.

5.1 - Physical models of degradation

Some participants sent a short code description as was requested for this ISP concerning the physical models of the degradation phenomena involved during the B9+ test. Details of some of the implemented codes can be found in [6].

Tables 3 and 4 summarize the degradation models giving the user-specified parameters chosen by the participants. It must be noted that no specific spacer-grid involving a chemical interaction model exists in the eight codes used.

ZrO₂ dissolution by molten Zry is only considered by the ICARE2 code. The Hofmann kinetics law of ZrO₂ dissolution is used with the solubility of UO₂ deduced from an approximation of the ternary U-Zr-O phase diagram.

Great consistency is found as regards the oxidation kinetics correlations used. Cathcart up to 1853 K and Urbanic Heidrick correlations at higher temperature were the most often used.

Other differences between the codes involved cladding failure criteria (failure of the external ZrO_2 layer of the cladding) when the non oxidized Zry of the cladding melted and simultaneously dissolved the UO_2 pellets and the external ZrO_2 layer of the cladding. The resulting U-Zr-O mixture contained within a ZrO_2 shell was most often supposed to flow down after this ZrO_2 failure. Failure was supposed in the codes when an user specified temperature was reached ($2200\text{ K} < T_{\text{user limit}} < 2673\text{ K}$) provided that the oxide shell was not considered sufficiently thick to hold in the molten mixture. The user failure thickness limit was spread between $60\text{ }\mu\text{m}$ (USA) and $540\text{ }\mu\text{m}$ depending on the calculation.

5.2 - Nodalization of the PHEBUS bundle

There also existed a high degree of homogeneity between the different calculations concerning the total number of axial meshes for the active length of rods (80 cm). Most often eight to eleven meshes were chosen and 3 kinds of rods were selected representing respectively the Central Rod (CR), the 8 first Ring Rods (1R) and the 12 Second Ring Rods (2R). The 21 rods were put in one hydraulic channel except for SP-CSN and FRA-SP which chose 3 independent channels for each representative rod (Table 5). A typical modelling of the bundle is shown in Fig. 10.

5.3 - Shroud modelling

Shroud modelling was an important point because, as explained in the next section, the major heat loss from the fuel rods was through the multi-layering of the shroud to the subcooled surrounding cooling water (528 K). The most insulating layer was the porous ZrO_2 with an external cylindrical form and with an internal octogonal form (maximum thickness 12.25 mm). Table 6 summarizes the shroud modelling chosen by participants.

Four calculations were performed using the 2nd radial boundary condition approach : CZECHO, GER-IKE2, GER-GRS2 and TAIWAN.

Others calculations used different shroud modelling most often with the actual 4 shroud layers (Zr, porous ZrO_2 , dense ZrO_2 , SS) but FRA-SP and USA took into account a helium gap representing the 9 external liner thermocouple grooves which were made in the internal face of the porous ZrO_2 layer. This led to a variable porous ZrO_2 thickness with elevation [1].

It must be pointed out that each participant was free to choose the axial meshing in the bundle. Only 10 levels over the 80 cm of active length were required to give the calculational results - On the basis of our experience this choice which requires at least 10 meshes ensures numerical converged results even as regards melt relocations.

The conductivity of the porous ZrO_2 layer chosen by the participants is summarized in Table 6 and in Fig. 7. This point is discussed in the next sections.

5.4 - Nuclear power

Table 7 summarizes the modelling of the nuclear power for each submission.

6 - COMPARISONS OF INDIVIDUAL RESULTS WITH THE EXPERIMENT

Due to the important amount of data it was decided to compare in a first step each individual calculation with the experiment. The predictive capabilities of the codes involved in ISP 28 were analysed. The following parameters were chosen and are drawn in different Annexes given in volume 2 :

- UO_2 temp. versus time : lower and upper part : Fig. 1, 2
- Clad. temp. versus time : lower and upper part : Fig. 3, 4
- Fluid temp. versus time : lower and upper part : Fig. 5, 6
- Liner and shroud temp. versus time : Fig. 7, 8
- Temperature histories for different components at levels 50, 70 : Fig. 9, 10
- Axial temp. profiles at 7700 s, 9000 s, 12000 s, 14000 s : Fig. 11
- Heat flux through the shroud : Fig. 12
- Oxide, UO_2 , ZrO_2 dissolution profiles (CR) 9000 s and 14000 s : Fig. 13, 14, 15, 16
- Oxide, UO_2 , ZrO_2 dissolution profiles (1R) 9000 s and 14000 s : Fig. 17, 18, 19, 20
- Oxide, UO_2 , ZrO_2 dissolution profiles (2R) 9000 s and 14000 s : Fig. 21, 22, 23, 24
- Mean oxide profile / experiment : Fig. 25
- Oxidation and ZrO_2 dissolution versus time (cladding of 1R rods) : Fig. 26
- Oxidation profiles for the liner at 9000 s and 14000 s : Fig. 27
- H_2 release / experiment : Fig. 28
- Mean UO_2 dissolution profile / experiment : Fig. 29
- Flow blockage profile / experiment : Fig. 30
- Relocated material profile : Fig. 31

- Final picture of the bundle : Fig. 32
- Total UO_2 , ZrO_2 , Zry profiles at 9000 s : Fig. 33
- Total UO_2 , ZrO_2 , Zry profiles at 14000 s : Fig. 34

Annexes 1 to 15 contain, for each participation, the previous set of 34 figures. The plot identifiers used in these figures are described in Annex 17.

It must be pointed out that fourteen submissions were performed in SEMI BLIND conditions. The FRA-SP submission (joint CEA-Phebus Espana Consortium) was performed in OPEN conditions. This participant had to calculate the "2nd approach" boundary conditions on the shroud liner and was involved in the definition and the analysis of the post-test examinations. This submission, therefore, should be considered only as a reference calculation.

6.1 - FRA-SP (Annex 1) : ICARE2/V2p calculation

A good prediction of the rod temperatures was obtained in tuning the porosity of the porous ZrO_2 governing the heat conductivity. The temperature escalation (8200 s) was predicted at 60 and at 70 cm (as in the test). The maximum temperature was well predicted (2750 K) (A1 - Fig. 1 to 12). Total (CR, 1R) or near total oxidation (89 % is reached on 2R rods) was predicted at hot levels (60/70). Complete oxidation was not found in the upper part. These results are in agreement with the oxidation measurements (A1 - Fig. 25). The enhancement of oxidation when the temperature reaches 1853 K explains the temperature escalation at the hot level and the rapid ZrO_2 attaining nearly complete oxidation.

Limited ZrO_2 dissolution was calculated at levels 50 and 60 (maximum 13 % of the oxide layer calculated at the end of the steam phase. A1 - Fig. 26) but more significant ZrO_2 dissolution was found up to 60 % in the cladding failure zone. This important local reduction of the ZrO_2 thickness enabled the ZrO_2 failure thickness limit chosen by the user (300 μm) to be reached and contributed to a correct calculation of the cladding failure between 32 and 48 cm as observed in the test (A1 - Fig. 32). In spite of the correct oxidation prediction, H_2 production was slightly overestimated. The calculated fuel dissolution was limited to 12 % as in the test (A - Fig. 29). The bundle blockage profile showed a good prediction of the voiding and filling zones due to material relocation (A1 - Fig. 30).

The overall correct prediction of the fuel degradation was facilitated by the satisfactory prediction of the rod temperatures and by a correct calculation of the oxidation profile.

6.2 - SP-CSN (Annex 2) : SCDAP MOD1 Stand-alone code

The thermal behaviour of the bundle was greatly overestimated in spite of the use of a conductivity of the porous ZrO_2 (Fig. 7) calculated using the Missenard correlation (70 % constant porosity and He filled insulator). The temperature escalation was not calculated at 8200 s (as observed in the test) probably because the calculated oxidation was already complete at that time. The maximum rod temperature was overestimated, 2900 K instead of 2750 K in the test. Oxidation was overestimated : 100 % between 40 and 80 cm (A2, Fig. 25).

Extensive cladding deformation was calculated before the melting of the fusible seals in the upper plugs of the rods (1100 K) leading to a maximum blockage of 64 % at 60/70 cm.

Fuel dissolution was overpredicted (60 %) at lower levels only, between 16 cm and 40 cm, where cladding rupture was calculated. The relocation of the U-Zr-O mixture was partially frozen in the same zone and part of the molten material was predicted to flow down and to escape from the bundle.

6.3 - SP-UPM (Annex 3) : MELCOR V1.8.0 calculation

Temperatures were strongly overestimated mainly in the lower part of the bundle but cladding oxidation (A3 - Fig. 15, 19, 23, 25) and H_2 production (A3 - Fig. 28) were underestimated. (max oxidation of 62 %, 50 %, 27 % for CR, 1R, 2R rods). These contradictory results could be due to incorrect oxidation kinetics for $T > 1850$ K. The heat flux through the shroud (A3 - Fig. 12) was significantly underestimated during the He phase. This could be due to incorrect He properties. The heat exchange coefficients calculated by MELCOR in case of a pure He flow are to be checked.

Cladding failure by molten Zry occurred at level 20 cm on the 2R rods. When the melting point of ZrO_2 ($T > 2990$ K) was reached at 13500 s cladding failure occurred in the 48-64 cm zone for the CR and at the 60 cm level for 1R rods leading to a UO_2 debris bed formation. Part of the UO_2 was transported from the 20 cm and 60 cm levels. The ZrO_2 debris and the spacer-grids were relocated and

accumulated below the fissile length and at the 4 cm level. The total mass of relocated mixture (A3 - Fig. 31) represented in fact the total amount of dislocated UO_2 which had been produced at the 20 and 60 cm elevations when cladding failed. It did not represent a plug due to refrozen materials. Moreover, at these locations the bundle blockage decreased (A3 - Fig. 30).

6.4 - CZECHOSLOVAKIA (Annex 4) : FRAS - SFD calculation

ISP 28 was the first attempt made with the FRAS-SFD code to describe the severe fuel damage transient. No relocation can be calculated with the present version of the code and the calculation was stopped when cladding failure occurred.

The calculation was performed up to the steam-He switch at 8320 s where numerical instabilities were observed. Only one rod was calculated using a kind of 2nd BC approach applied to a surrounding rod instead of on the shroud liner. For this submission, therefore, all the 1R and 2R values corresponded in fact to the CR values.

Temperatures were overestimated mainly in the upper part. This led to an overestimation of the final oxidation profile (A4 - Fig. 25). At the upper levels a rapid oxidation versus time was anticipated (A4 - Fig. 26). The total oxidation was reached at 6000 s instead of 8000 s in the test. The H_2 produced for the central rod was converted to a complete bundle release (55 g) taking into account the ICARE2 calculated H_2 proportion between CR, 1R, 2R and liner (A4 - Fig. 28). Dissolution at the 80 cm level was calculated between 8200 and 8240 s (A4 - Fig. 14 and Fig. 29) just before the end of the calculation. Consequently the resulting molten mixture continued to be oxidized. A local dissolution of 10 wt % of UO_2 was calculated at 80 cm at the final time of the computation (8320 s).

6.5 - GER-IKE1 and IKE2 (Annex 5a, Annex 5b) : KESS III calculation

With the KESS III code, which is still being developed, IKE performed two calculations of ISP28. These calculations mainly focussed on the heat-up and oxidation processes.

IKE1 : 1st BC approach on the external face of the shroud :

The recommended heat conductivity values for the porous ZrO_2 resulted in a stronger temperature increase all along the whole length of the bundle than was

measured. This non-realistic prediction led to the use of the "first user-adjust BC approach" method with a ZrO_2 conductivity twice greater than the one measured. Under these conditions the overall calculation of the thermal behaviour was more correct but a general overestimation of the temperatures was still found during the oxidation phase. Just after the steam/He switch, the fluid temperature at the outlet (80 cm) (A5 - Fig. 6) was significantly underestimated. By comparison with the IKE2 calculation (2nd BC approach) it seems that this local trend was due to a local overestimation of the radial thermal leakage to the shroud. Oscillations of calculated temperatures were due to the use of too large time steps.

Oxidation and H_2 production (55 g) were also overestimated (A 5a - Fig. 25, 26). The temperature escalation at 60 cm was not predicted because oxidation was already calculated as complete at 8000 s, (A 5a - Fig 26) (The escalation was measured at 8200 s).

Due to the lack of the corresponding models in the current version of the KESS code no fuel dissolution results were transmitted and no relocation was allowed to occur in choosing a high value for the cladding failure (2673 K).

IKE 2 : 2nd BC approach on the shroud liner :

The application of the 2nd thermal BC on the liner led to a better prediction of the fuel rod temperature history but with a local underestimation by 75° at the hot level.

This was sufficient to prevent the calculation of the temperature escalation during which oxidation developed very fast. The total oxidation at hot levels, therefore, was not predicted due to the delayed threshold effect of the oxidation kinetics near 1850 K. The H_2 production was also too low (32 g instead of 39 g) (A 5b - Fig. 25 and 28).

In general, fluid temperatures seem to have been underpredicted but it must be pointed out that the fluid thermocouples were probably affected by the considerable radiative transfer in the bundle [A 5b - Fig. 5, 6]. Outlet fluid temperature was more correct than in the IKE1 case. Numerical instabilities on temperatures during the He phase were also reduced.

6.6 - GER - GRS1 and GRS 2 (Annex 6a, Annex 6b) : ATHLET SA calculation

With the ATHLET-SA code, which is still being developed, GRS performed two calculations of ISP28. These calculations mainly focussed on the core heat-up and oxidation processes.

GRS 1 : 1st BC approach on the external face of the shroud :

This calculation was performed after a first calculation run using the 2nd approach boundary condition (see the following GRS 2 calculation).

Results of this first calculation were used to calculate the porous ZrO_2 heat conductivity of the shroud composed of the main 3 layers (dense ZrO_2 omitted) versus time. Temperatures were overestimated in the lower part (up to 50 cm during the oxidation phase and up to 40 cm during the He phase). The reason for that could be an inadequate heat transfer coefficient in the shroud or the use of a constant power profile during the transient. Satisfactory agreement was obtained in the hot zone for the 2R rod (A 6a - Fig. 2) but the thermal radial gradient seems to have been overestimated between the 2R rods and the liner at 70 cm (A 6a - Fig. 10). In spite of very good 2R rod thermal behaviour, the temperature escalation was not predicted. Correct oxidation was obtained at the hot levels but overestimated under 40 cm. This explains the overestimation of H_2 by about 30 %. No fuel dissolution and no relocation results were available with the current version of the code.

GRS 2 : 2nd BC approach on the shroud liner :

GRS 2 and GRS 1 calculations were very similar because they are in fact two equivalent methods. Small differences were mainly due to the approximation performed to calculate the equivalent porous ZrO_2 conductivity from the GRS2 calculation (Fig. 6). This value was similar with the mean conductivity calculated with the Missenard model of ICARE2.

The final temperature plateau observed in Figs. 1 to 4 of Annex 6b corresponds to the formation of a U-Zr-O mixture which had to remain at its liquidus temperature of 2400 K up until the ZrO_2 layer was estimated to have melted.

6.7 - HUNGARY (Annex 7) : MARCH3 calculation

The calculation performed with MARCH3 was limited to the first oxidation phase. The He phase could not be calculated directly with the code. The shroud was taken into account by a fourth surrounding ring of 8 rods with zero nuclear power. The liner oxidation was taken into account by the cladding of these equivalent rods. Their properties were defined in order to find on these rods temperatures which could be used as reasonable boundary conditions for the inner 21 rods of the bundle. This method was presented as equivalent to the 1st BC approach.

The general behaviour of the rod temperature was correct, escalation was predicted at 8200 s (A7 - Fig. 2) but temperatures were overestimated in the hot zone where total oxidation was predicted from 45 cm to 80 cm. The H₂ production was 57 g instead of 39 g in the test.

The MARCH-3 code does not allow UO₂ and ZrO₂ dissolution. The calculation was stopped too soon to calculate rod relocation.

6.8 - I-PISE (Annex 8) : SCDAP/RELAP5 MOD2 calculation

A complete calculation was done with the SCDAP/RELAP5 MOD2 code. A correct thermal behaviour was obtained after adjustment of the heat conductivity of the porous ZrO₂ (Fig. 7) at a value about 3 times greater than the one measured.

A general slight overestimation was found except at the 70 and 80 cm levels where calculated temperatures fitted the measurements (A 8 - Fig. 2, 4, 6 and 10) very satisfactorily. A temperature escalation was found at level 70 cm on 2R rods but not at the 60 cm level as observed in the test, because oxidation was already nearly finished when the oxidation transition temperature of 1850 K was reached at this level. The calculated oxidation fitted the experiment (A8 - Fig. 25) very satisfactorily. The H₂ prediction was within the experimental uncertainty range (20 %). The non-active upper end of the fuel rods (7.3 cm long) gave an appreciable contribution to the oxidation (about 20 % of the cladding was oxidized at this level).

Fuel dissolution was obtained above and under the total oxidation zone. Dissolution was significantly overestimated (A8 - Fig. 29), 100 % was reached at

40 cm for the 3 kinds of rods instead of the 10 % in the test. Dissolution in the higher section of the active length (75/80 cm) was also calculated (45 %). In the test, only some local and weak UO₂ dissolution was also found above the hot zone.

The cladding oxide layer was correctly calculated to break, in the 35 - 55 cm zone at about 13050 s for the CR and 1R rods. But no cladding failure was calculated on the 2R rods which showed evidence of failure in the test.

Relocated U-Zr-O mixture was calculated to freeze at too low an elevation near the entrance of the bundle (5 cm) and below the active fuel column (52 % blockage at 5 cm) (A8 - Fig. 30) instead of the 20 - 28 cm zone in the test. Figure 32 summarizes the final bundle degradation. When the ZrO₂ cladding layer was calculated to break it was predicted not to relocate and remained in place.

The eutectic relocation at the 40 and 50 cm levels resulted in a reduction of the amount of fissile material and then of the nuclear heat generation. Temperature histories and profiles at these levels showed evidence of relocation (A8 - Fig. 1, Fig. 3, Fig. 11).

6.9 - ISPRA (Annex 9) : ICARE2 V1 calculation

The ICARE2 calculation was performed with a porous ZrO₂ conductivity greater than the one measured by a factor of three (Fig. 7). The overall thermal transient was correct with a slight underestimation of the rod temperatures in the hot zone (60 - 70 cm) (A9 - Fig. 11). Some parameters on the transmittal tape were incorrect due to writing errors and have not been given in the figures. (The shroud temperature, the heat flux through the shroud, the oxidation histories). Probably the non-prediction of the escalation at the hot level explains the too low oxidation value obtained (A9 - Fig. 25).

Fuel dissolution was found mainly between 15 and 25 cm where temperatures remained lower than the temperature failure criteria chosen by the user (2300 K). In the central zone where the cladding temperature exceeded 2300 K, the failure criteria was probably reached quickly because the oxide layer was always lower than the failure ZrO₂ thickness limit (500 μm). Molten Zry, therefore, could not be maintained in contact with the fuel for sufficiently long to lead to extensive UO₂ dissolution. All the rod cladding between 35 cm and 75 cm was relocated (A9 - Fig. 34). This led to an overestimated blockage in the lower part (93 % between

10 and 25 cm). Dissolution and relocation results were not in agreement with the experimental results mainly due to the considerable underestimation of the oxidation.

6.10 - JAPAN (Annex 10) : SCDAP/R5 MOD1 calculation

The first calculations performed with SCDAP/RELAP5/MOD1 led to cladding melt in the early phase of the test. The inner perimeter of the liner was therefore assumed to be three times longer than the real shroud, but the real geometry was kept unchanged for the flow area. Moreover it was not possible to take into account the pressure reduction during the final cooling phase.

The calculated thermal behaviour was greatly underestimated all along the bundle mainly during the oxidation phase (175 to 200° lower at the hot level just before the end of the oxidation phase). In these conditions oxidation and H₂ production were significantly underestimated.

A maximum of 40 % of oxidation at the hot level and 26 g of H₂ were calculated at the end of the steam phase. The code does not allow pure He, so during the helium phase a residual steam was maintained which explains the slow increase of oxidation and of H₂ production up to the end of the transient (A 10 - Fig. 26 and 28).

Fuel dissolution and molten mixture relocation did not appear in the results. The overestimation of the bundle blockage (A 10 - Fig. 30) could be due to the overestimation of the clad deformations.

6.11 - NETHER (Annex 11) : SCDAP/R5 MOD2.5 calculation

Due to an overestimation of the rod temperatures with the recommended thermal conductivity of the porous ZrO₂, sensitivity studies led to an increase of this value by a factor of 2. More correct temperatures were calculated, but still overestimated (A 11 - Fig. 1, 2, 10, 11). In particular the temperature escalation was predicted too early at 60, 70 and 80 cm (6800 s instead of 8200 s in the test) (A11 - Fig. 2, Fig. 7).

This early escalation was characterized by a run-away on the oxidation (A 11 - Fig. 26) and on the H₂ production (A 11 - Fig. 28). After this escalation, when the available zircaloy at hot level was fully oxidized the temperature decreased. The last peak in the H₂ rate was mainly due to the increase of the nuclear power which

led to an increase of the rod temperatures and of the oxidation at lower levels. After the steam/He switch a residual fraction of steam was maintained in order to avoid the code failure obtained when pure He is used. This explained the slow increase of oxidation in the He phase. Unexpected high oxidation was also found on the Zry liner at 70/80 cm. The strong oxidation run-away predicted on the rods in this zone explained the peak temperature calculated at the same elevation on the liner (A11 - Fig. 7). The overestimation of the temperature of the liner was also increased by a local run-away. This explained the overestimation of the liner oxidation in the upper part of the bundle.

A considerable overprediction of the fuel dissolution was found on the 3 kinds of rods between 25 and 55 cm (100 % at 40 cm) where non-oxidized Zr remained. (A 11 - Fig. 16, 20, 24, 29). Cladding failure of the CR and 1R rods was calculated as in the test at levels 30/40 cm when the failure temperature of 2500 K was reached at 13560 s. This was characterized by a loss of symmetry between the two total mass profiles of ZrO₂ and Zry at 14000 s (A 11 - Fig. 34). The corresponding U-Zr-O mixture was relocated and partially refrozen at level 5 cm. Second ring rod failure was not predicted because the temperature at the end of the He phase did not reach the chosen failure temperature of 2500 K. This indicates that this user-specified value was too large.

Around 13600 s the cladding of the 3 kinds of rods reached the melting temperature of ZrO₂ (2950 K) in the totally oxidized zone between 50 and 70 cm and a cohesive debris bed was predicted leading to a considerable 95 % bundle blockage at this level (A 11 - Fig. 30). This debris bed formation at 13600 s led to local unrealistic high temperatures (A 11 - Fig. 2, 4, 11) and to a code failure at 14000 s.

6.12 - SWEDEN (Annex 12) : SCDAP/R5 MOD2 calculation

The recommended heat conductivity of porous ZrO₂ was multiplied by about a factor 2 to obtain more reasonable predictions (Table 6). Rod temperatures were slightly overestimated under 30 cm, well-calculated between 30 and 50 cm and underestimated at the upper levels in the hot zone (A 12 - Fig. 2, 4, 11). The underprediction of the rod temperature was consistent with the underprediction of the liner temperature in spite of the SCDAP/R5 trend to overestimate the temperature difference between the outer row of rods and the liner. The temperature escalation observed at 60 cm, therefore, was not predicted, the oxidation of the 3 kinds of rods and the H₂ production were underestimated. A

maximum oxidation of 64 % was calculated on the central rod instead of the near 100 % observed and 27 g of H₂ was predicted instead of the 39 g measured in the test. The use of residual steam in the He phase explained the slow oxidation increase up to the end of the test (A 12 - Fig. 25, 26).

Due to the oxidation underestimation more non-oxidized Zr was available for the fuel dissolution which was overestimated (95 wt % instead of 14 wt % at 50 cm).

The overall underprediction of the fuel temperature and the choice of a high cladding temperature failure (2500 K - Table 4) prevented the prediction of a cladding rupture zone. The 2500 K limit was only exceeded at level 60 (A 12 - Fig. 2) where the calculated oxide layer thickness was greater than the ZrO₂ failure thickness limit (430 μm) chosen. No relocation occurred therefore and the bundle blockage (A 12 - Fig. 30) was only due to thermal rod deformations.

6.13 - TAIWAN (Annex 13) : MELCOR V1.8.0 calculation

The 2nd radial BC approach on the liner was chosen for this MELCOR calculation. In order to take into account the oxidation and relocation of the Zry liner, this structure was modelled as a canister (of a fuel BWR bundle) plus a surrounding heat structure. Radial heat flux was transmitted from rods to canister and then from the canister to this heat structure. The radiative steam absorption model was not used.

Very satisfactory agreement was obtained between the calculated and the measured temperatures (A 13 - Fig. 1 to 11). In spite of this accurate prediction, the temperature escalation observed at the 60 cm level was not calculated (A 13 - Fig. 2) and consequently the oxidation in the hot zone was underestimated (about 70 % instead of 100 %) and the calculated H₂ production was 32 g instead of the 39 g measured (inside the uncertainty experimental range) (A 13 - Fig. 25 and 28).

It must be pointed out that a constant mean axial power profile was used in the calculation. This could explain that the maximum temperature calculated was about 2600 K instead of about 2700 K in the test (the power profile was peaked in the hot zone due to the rising of the driver core control rods during the transient). No cladding failure was predicted due to the choice of a high failure temperature (2600 K) and due to an underprediction of the maximum temperature. Consequently no UO₂ and ZrO₂ material was transported.

The Zry liner (A 13 - Fig. 27) was calculated as melted and relocated. The corresponding failure criteria seemed different from those of the rods. All levels above 25 cm disappeared at 14000 s and liner relocation led to a maximum bundle blockage of 60 % at 20 cm. Refreezing location was correct (it must be pointed out that the Zry liner was equivalent concerning the initial mass of Zry to 8 rods).

The total mass profiles of UO₂, ZrO₂ and Zry material in the bundle also took into account the relocated materials (A 13 - Fig. 34). In the specifications [4] only non-relocated materials were required for the drawing of the total mass profiles.

6.14 - UK (Annex 14) : SCDAP/R5 MOD2.5 Version 361SC

The thermal conductivity recommended for the porous ZrO₂ gave rod temperatures in excess of those found in the test. Much better agreement was found when the much higher MATPRO values (Fig. 6) were used. The general thermal behaviour was well predicted for all the components, in particular at the hot 60 cm level (A 14 - Fig. 2). No further tuning of the shroud conductivity was made to better fit the measurements. The temperature escalation was well predicted at 60 cm and also at 70 cm.

Rod temperature histories at the 50 - 60 cm levels showed evidence of liquefied UO₂ relocation (A 14 - Fig. 1 to 3) in some upper axial nodes between 12000 s and 14000 s. The same evidence also appeared in the temperature profiles at 12000 s and 14000 s (A 14 - Fig. 11). Taking into account the evolution of the 5 power profiles versus time the maximum calculated temperature was about 2700 K as was estimated in the test. The fluid temperatures drawn at the 0 and 80 cm levels were in fact those at levels 4 and 76 cm (A 14 - Fig. 5,6).

At 60 cm, rapid oxidation during the run-away led to total oxidation on the CR and 1R rods and to 93 % on the 2R rods (A 14 - Fig. 15, 19, 23, 25). Oxidation was not complete in the upper part (70 - 80 cm) as measured in the test. Total H₂ production was also well calculated (36.8 g instead of 39 g in the test). Oxidation modelling was stopped during the He phase to avoid non-realistic oxidation due to residual steam (0.2 % imposed by the SCDAP/R5 code).

The fuel dissolution was excessive (100 % predicted at level 40 cm instead of 10 % in the test) (A 14 - Fig. 16, 20, 24, 29). It occurred where the Zry had not been completely oxidized, particularly at the upper level (70 - 80 cm) where dissolution was observed on some rods.

Cladding failure occurred on 2R rods at level 52 cm (11800 s) and later (13200/13640 s) at 44 cm (CR, 1R) and 36 cm (CR, 1R) roughly in the zone where failures were observed.

Relocated materials were calculated to freeze too far below the active fuel length. Only a small amount was located between 0 and 15 cm (A 14 - Fig. 30, 31). The shroud liner failure temperature was set to a high value so that no failure could occur.

A model for the hold-up of melt at the spacer-grids existed in the version of the code used but was effectively disabled due to an error of logic.

6.15 - U.S.A (Annex 15) : MELCOR V1.8EA calculation

The MELCOR calculation overestimated the rod temperatures with the recommended porous ZrO_2 conductivity. Sensitivity studies led to an improvement of the shroud modelling (Table 6) and an adjustment of the ZrO_2 conductivity in order to better fit the measurements (Fig. 6). The inlet steam flowrate (+ 5 %) and power (- 5 %) were changed in the experimental uncertainty range. Others parameters, in particular the flow distribution in the bundle, were also adjusted. Mixture properties were corrected (high quality of non-condensable gas) and cladding emissivity at high temperature imposed at 0.99 in order to improve rod temperature behaviour in the He phase.

In these conditions good thermal agreement was found and correct radial temperature gradients were calculated (A 15 - Fig. 9, 10). The temperature escalation was well predicted at 60 cm and also at 70 cm leading to the prediction of a temperature peak on the liner at 70 and 80 cm (A 15 - Fig. 2, 7, 8). Rod temperature dropped to zero at relocation because the cladding component relocated and was no longer present at 60 cm and 70 cm (A 15 - Fig. 4 and 10). Due to the use of a constant power profile, the maximum temperature was underestimated (2550 K instead of 2750 K in the test).

Oxidation run-away at hot levels (60 - 70 cm) led to a total oxidation on CR and on 1 R rods (78 % is reached on 2R rods) (A 15 - Fig. 13, 17, 21, 25). Oxidation was not found complete in the upper part as measured in the test. The total H_2 production was also well calculated (43 g instead of 39 g in the test).

No rod relocation was predicted until shortly before 14000 s. The CR failed at 50 and 60 cm (A 15 - Fig. 15) and the 1R rods failed at 60 cm (A 15 - Fig. 19) when the temperature reached the user-specified failure limit of 2500 K since the thickness of the oxide layer at these elevations was greater than the chosen limit of 60 μm . Due to the lack of support the remaining upper part of CR failed to form a debris bed. This rod failure process was not observed in the test.

No true UO_2 and ZrO_2 dissolution was calculated but a very small amount of UO_2 was transported as specified by the user in the input data deck when cladding failed at 50 and 60 cm (A 15 - Fig. 33 and 34). In a clad failure zone all the ZrO_2 was relocated with the remaining non oxidized Zr.

The axial profile of relocated materials (A 15 - Fig. 31) was characterized by 3 zones : a lower Inconel plug, a Zr - ZrO_2 - UO_2 plug at 20 cm and a pure UO_2 debris bed in the upper part (50 - 60 cm). The maximum bundle blockage of 45 % at 20 cm was mainly due to the freezing of cladding materials. This location was nearly in agreement with the test but the blockage was underestimated. All the grid spacers were relocated when the Inconel melting temperature of 1533 K was reached. They relocated on the core plate just below the active length and under the actual Inconel plug. The pure UO_2 debris bed in the upper part was not considered as a plug with a resulting blockage.

7 - OVERVIEW OF THE COMPARISONS

The aim of this section is to compare code predictions and to analyse the differences found using the same code. The ability to calculate the PHEBUS-SFD transient and the different thermal and degradation phenomena involved in the B9+ test will be examined in particular with regard to the choice of some user-specified input data. Modelling weaknesses and gaps will be identified and code performances with regard to the code running times will be discussed. A summary and an overview of the comparisons are given in [9].

Due to the large number of participants and to the difficulty in clearly showing the participants' results together, the submissions were classified into the following three groups :

GROUP I	GROUP II	GROUP III
FRA-SP SP-UPM ISPRA TAIWAN USA Measurements	FRA-SP I-PISE NETHER SWEDEN UK Measurements	FRA-SP SP CSN CZECHO GER IKE 1 GER GRS 1 HUNGARY JAPAN Measurements

The criteria for the classification were :

- Same code or same kind of codes :

- GROUP I - ICARE2 and MELCOR
- GROUP II - SCDAP/RELAP 5 Mod 2
- GROUP III - SCDAP Mod1 Stand Alone
- SCDAP/R5 Mod 1
- KESS III, ATHLET SA
- FRAS SFD, MARCH3

- Same phenomena calculated in the transient :

Degradation aspects are found mainly in GROUPS I and II.

The FRA-SP calculation with ICARE2 was quoted in the three groups in order to be used as a reference calculation (totally open submission).

For these comparisons a limited number of parameters were chosen.

TU2RZZ : Fuel temperature versus time at different elevations (30, 50, 60, 70 cm).

TSR160 and TSR360 : Liner and inner shroud temperatures

OX1RZZ : Oxidation histories at different levels (40, 50, 60, 70 cm).

HYDTOT	:	Total H2 release.
OX1RZZ	:	Oxidation profile on the first ring rods just after the end of the first steam phase
DUMEAN	:	The mean fuel dissolution profile for the 1R rods at 14000 s.
COBKZZ	:	The channel blockage profile at 14000 s showing material relocation with the main plugs. This parameter is defined as being equal to 38 % at the initial conditions of the transient due to the 21 intact rods inside the initial inner section of the octagonal Zr liner (see section 4.9).

All the comparisons are given in the Annex 16.

7.1 - The Modelling of the B9+ transient

7.1.1 - Nodalization

In general, a more or less common approach was used for the nodalization of the different components of the bundle (see section 5 and Fig. 10). One hydraulic channel and three different rods were often used. Two participants made use of 3 parallel and independent channels (FRA - SP, SP-CSN).

7.1.2 - Difficulties

The main problem encountered concerned the shroud modelling. Some codes were not able to directly take into account the multilayer shroud, therefore some modifications (MELCOR) or modelling compromises (FRAS-SFD, MARCH-3) had to be made by some participants even when the simplified 2nd BC approach was chosen. It must be pointed out that these codes were developed for reactor studies and have not been intensely used up to now for modelling small scale experiments.

A second difficulty encountered by some participants concerned the modelling of the pure He phase and the transition from steam to He. In general codes do not allow He as a cooling gas. H₂, air, or steam were therefore used in place

of He in conserving the enthalpy flow rate or in redefining gas properties in input. He gas was directly taken into account by some codes after modification of the fluid properties (MELCOR V 1.8EA, ICARE2 V2).

A pure non-condensable gas was not allowed by MELCOR V1.8.0 and SCDAP/R5 and a small fraction of steam (0.2 %) was necessary to avoid a code failure or inconsistencies. This led some participants who could not modify the code to calculate continuous weak oxidation during the He phase (I-PISE, JAPAN, NETHER, SWEDEN).

Some participants using MELCOR and SCDAP/R5 could not take into account the 5 specified power profiles due to the codes being limited respectively to 1 and 3 profiles. This limitation, which is only a problem for calculations of in-pile tests, can explain part of the underprediction of rod temperature during the He phase.

Others limitations were also mentioned concerning rod axial meshing (maximum 10 meshes) which could not be checked so as to study the effect on the results.

The majority of the users had difficulties as regards to printed outputs and drawing possibilities, particularly in representing the radial heat flux at some elevations or parameters related to material relocation (fuel dissolution and flow blockage profiles, profiles of non-relocated materials such as Zry, ZrO₂, UO₂ or profiles of relocated mixtures).

Lastly, during the switch from steam to He and afterwards, some numerical instabilities led to severe time step reductions (MELCOR, SCDAP/R5 Mod2, FRAS-SFD). Run statistics will be examined at the end of this section.

7.2 - Thermal behaviour

7.2.1 - Heat balance in the bundle

The thermal behaviour is controlled by the heat balance in the bundle. A calculated energy balance was given by some participants. (Fig. 17a, 17b, 17c). These curves show approximately that 70 % (during the steam phase) to 90 % (during the He phase) of the total nuclear power is transferred to the shroud.

The remaining energy is transferred to the fluid by convection and radiation absorption by steam. Rod temperatures therefore are mainly dependent on the prediction of the radial heat flux through the shroud [7].

The use of the recommended thermal conductivity of the porous ZrO_2 layer [2] always gave bundle temperatures in excess of those found in the experiment. All the participants who used the first approach had to choose higher conductivity, two to three times greater than the experimental recommended value (Fig. 7). The tuning of this parameter was performed by some participants (USA, I-PISE, FRA-SP) in order to fit the temperature measurements and obtain correct cladding oxidation conditions which have significant effect for later rod degradation at high temperature.

In particular, FRA-SP adjusted the conductivity of the porous ZrO_2 at each level by tuning the porosity calculated by the Missenard model. The dotted line in figure 7 shows the conductivity calculated by the Missenard model, assuming 70 % porosity and He-filled pores.

A detailed analysis of the heat transfer in a porous medium showed that the pressure effect was underestimated when the atmospheric pressure measurements of the conductivity were extrapolated to 1.9 MPa. This effect led to an increase of the conductivity by a factor consistent with the tuning factor of the participants.

Overall satisfactory agreement was generally obtained with the different codes concerning the thermal behaviour of the bundle (A16 - Fig. 1/1 to 6/3). The significant discrepancies are due to incorrect calculation of the shroud thermal leakage, underestimated by SP-CSN, NETHER and SP-UPM (only in the He phase) and overestimated by JAPAN and SWEDEN.

7.2.2 - Radial temperature profile

Table 8 summarizes the radial temperature gradients calculated at 7800 s at the hot point (60 cm). There was a general tendency to underestimate the temperature difference between 1 R and 2 R rods - Reasonable predictions were obtained with ICARE2V2p, SCDAP/RELAP5 Mod2 and ATHLET SA. Radial temperature differences in the shroud were in general well calculated. The overestimation by GER-IKE is due to too early a prediction of the temperature escalation. It must be pointed out that the use of a mean hydraulic

channel tends to reduce radial differences while the use of three independent channels (FRA-SP, USA) tends to increase them. Radial differences are also a function of cladding emissivity and decrease when the emissivity increases. From these comparisons performed with different cladding emissivities and different radiative heat transfer models it is therefore difficult to conclude as to the best hydraulic modelling. Degradation differences between each kind of rod result from the calculated radial temperature profile in the bundle.

7.2.3 - Temperature escalation

A rapid heat-up rate (> 3 K/s) occurred in the hot zone (60/70 cm) just after 8000 s. This resulted both in a rapid oxidation increase above 1850 K (tetragonal to cubic change of the ZrO_2 structure) and to a simultaneous nuclear power increase.

In general, participants who correctly calculated the heat balance and rod temperatures before 8000 s also predicted this temperature escalation : USA, UK, FRA-SP, I-PISE, HUNGARY (A16 - Fig. 3/2). In spite of an overall correct temperature prediction GER-GRS1 and GRS2, GER-IKE2, and TAIWAN did not predict this escalation. Due to the overprediction of the temperatures at the hot level, SP-CSN, GER-IKE1, NETHER and CZECHO calculated the escalation sooner than in the test (A16 - Fig. 3/3).

7.2.4 - Fluid temperature at the bundle outlet

The 3 fluid outlet thermocouples located at 80 cm indicated very similar temperature responses. They are suspected to have given a lower temperature than the local fluid temperature. This trend, which could be due to thermocouple heat losses by radiation towards the upper colder region of the test train, is confirmed by a general overestimation of the outlet fluid temperatures, mainly in the He phase (Figures 6 of Annexes 1 to 15).

7.2.5 - Maximum temperature

With a correct prediction of the heat flux through the shroud and by taking into account the specified evolution of the axial power profile in time, I-PISE, UK and FRA-SP with SCDAP/R5 and ICARE2 made a correct calculation of the maximum temperature estimated at 2750 K. This value was extrapolated from the internal shroud lower temperatures which could be measured

throughout the test (see section 3.3.5). This maximum temperature was underestimated by the MELCOR calculations (TAIWAN, USA) which were performed with a constant power profile less peaked in the hot zone than in the real case at 14000 s.

7.3 - Oxidation and H₂ production

The prediction of these parameters resulted directly from the prediction of the rod temperature (except for SP-UPM, see section 6-3).

7.3.1 - Cladding oxidation histories

These are shown at different elevations : 40, 50, 60, 70 cm (A16 - Fig. 7/1 to 10/3).

No prediction of steam starved conditions was mentioned during the steam phase but this could have occurred in the hot zone during the final and short oxidation escalation.

During this escalation at 8200 s, the remaining non oxidized Zry of the cladding in the hot zone (about 50 % of the initial value) was quickly consumed reaching nearly complete oxidation (A16 - Fig. 9/1 to 10/3). In these conditions a correct calculation of the oxidation excursion requires a very accurate calculation of the temperatures and energy balance in the bundle.

The considerable spreading of the cladding oxidation histories at 50 and 60 cm is mainly due to the temperature differences between the calculations. This spreading is greater at 50 cm in the axial "transition zone" of the escalation both in the experimental and calculation results.

Calculated axial oxidation profiles of the 1st ring rods were compared with the ZrO₂ measurements (A16 - Fig. 12/1 to 12/3). The minimum and maximum measurements of the outer and inner rods given in these figures are representative of oxidation at the end of the steam phase. Axial oxidation profiles were correctly predicted by ICARE2, MELCOR and SCDAP/R5 when both temperature histories and escalation were correctly predicted.

The total oxidation in the hot zone (60-70 cm) was found by nearly all the participants except for ISPRA, TAIWAN, SP-UPM, SWEDEN and JAPAN. Prediction of total oxidation does not necessarily indicate good thermal calculations but can be due to temperature overestimations (NETHER,

SP-CSN). Inversely, the non-prediction of total oxidation can result from a slight underestimation of the temperature which overly delays the beginning of the escalation (TAIWAN).

When a cladding failure is predicted with MELCOR and ICARE2, the dislocated ZrO₂ layer slumps with the molten Zry but is kept in place with SCDAP/R5. The ZrO₂ slumping which explains the sudden reductions of the calculated ZrO₂ layers (A16 - Fig. 7/1, 8/3, 9/1 and 9/3) occurs, in the B9+ test, during the He phase.

7.3.2 - H₂ production

Comparisons between calculations and measurements are shown in figures 11/1 to 11/3 (Annex 16). Only 4 calculations are within the experimental uncertainty range [32/47 g]. Hydrogen prediction results directly from the global calculation of the oxidation of the cladding tubes and liner, and the spreading of the calculated H₂ release sums up the uncertainties related to the release from these two structures.

In some calculations (FRA-SP, I-PISE, IKE1) part of the H₂ overestimation could be due to an overestimation of the liner temperature which results from an underestimation of the temperature difference between the external rods and the liner. (About 20 % of the total H₂ is produced by oxidation of the liner which is equivalent to about eight rods).

7.3.3 - Experimental and modelling uncertainties

Experimental uncertainties are related to different difficulties such as non-homogeneous cladding temperatures in the bundle and identification of a ZrO₂ thickness representative of the oxidation at the end of the steam phase. This ZrO₂ layer was in fact affected during the second He phase by the following interactions depending on the elevation : ZrO₂ reduction due to O₂ diffusion during the He phase (see section 4), ZrO₂ dissolution by molten Zry, strong UO₂-cladding chemical interaction, complete relocation for some levels. The spreading of the ZrO₂ thickness measurements results from these uncertainties (A16 - Fig. 12/1 to 12/3).

Modelling uncertainties are also related to different factors. During a significant oxidation phase as observed in B9+, the underlying metallic Zry is totally transformed into α -Zr(O) and then to ZrO₂. In these conditions the ZrO₂ layer increase kinetics leads to an underestimation of the oxidation. On the other hand, local α -Zr(O) melting during the escalation could lead to a relocation and/or simultaneous UO₂-ZrO₂ dissolution which could decrease oxidation. Most of the time these last limiting factors are not taken into account in the codes.

Finally, in spite of all these uncertainties and drawbacks, comparisons between calculations and data show that the oxidation prediction with the current models are within the experimental range when temperatures are correctly estimated.

7.4 - Inconel spacer-grids

There are no spacer-grid models in the code versions used able to take into account clad - Inconel spacer-grid interaction (see section 4.4). Only the MELCOR calculations (USA, SP-UPM) mentioned grid liquefaction and relocation predicted by a simple parametric model.

7.5 - Fuel dissolution by molten Zry

The second heat-up phase is characterized by extreme steam-starved conditions in order to facilitate simultaneous UO₂ and ZrO₂ dissolution by molten Zry. This phenomenon is significantly dependent on the temperature but also the oxidation profile which determines the mass of molten Zry available and its oxygen content. The UO₂ and ZrO₂ dissolutions are limited by the temperature dependent UO₂ solubility in the local U-Zr-O mixture or by the failure of the external ZrO₂ layer of the cladding (named in the following sections "cladding failure") which governs the flow-down of the mixture and the end of the dissolution.

Tables 3 and 4 summarize respectively the fuel dissolution models used and the conditions of cladding failure by molten Zry chosen by the users. Comparisons are shown in figures 13/1 to 13/3 of Annex 16.

Only ICARE2, SCDAP Mod1 and SCDAP/R5 Mod2 gave final results for the fuel dissolution. The FRAS-SFD code began a calculation of the UO₂ dissolution at the very end of the steam phase at 0.75 m, but the calculation could not be

continued in the He phase. There is no true dissolution model in MELCOR but a parametric model allows removal and transport of a user-specified fraction of the UO_2 when cladding failure by molten Zry is predicted.

Only ICARE2 V2p predicted a fuel dissolution in agreement with the test. In general, fuel dissolution was significantly overpredicted by SCDAP/R5 at each elevation where the non-oxidized Zry melted.

The ISPRA submission with ICARE2 V1 (with a different model) did not predict significant dissolution at the upper part of the bundle due to the failure criteria chosen ($500\ \mu\text{m}$, $2300\ \text{K}$) and due to oxidation underprediction. The oxide thickness calculated was always lower than the failure ZrO_2 thickness chosen ($500\ \mu\text{m}$) to maintain the molten Zry in place at a temperature greater than $2300\ \text{K}$. As a result, early cladding failure prevented significant duration of the fuel dissolution in the upper part of the bundle due to an early flow-down of the molten mixture.

SCDAP/R5 Mod2 and SCDAP Mod1 predicted considerable UO_2 dissolution at each elevation where some non-oxidized Zry remained and melted after the end of the oxidation phase. All the participants using these codes (SP-CSN, I-PISE, NETHER, SWEDEN and UK) chose the same cladding failure temperature of $2500\ \text{K}$ (and a failure thickness limit between 435 and $540\ \mu\text{m}$), so similar results were obtained. Due to a significant underestimation of the oxidation, particularly in the hot zone, SWEDEN over-predicted the fuel dissolution at these levels compared with the other SCDAP/R5 calculations.

Three main reasons related to the code models might explain the differences between ICARE2 V2p and SCDAP/RELAP5 Mod2 calculations, the cladding failure temperature ($2300\ \text{K}$ for ICARE2 and $2500\ \text{K}$ for SCDAP/R5), a lower solubility limit of UO_2 in the U-Zr-O mixture and a ZrO_2 dissolution by molten Zry considered in ICARE2. The first in the ICARE2 prediction tends to limit UO_2 dissolution in the central zone ($40\ \text{cm}$) due to early cladding failure, the second also tends to limit the prediction of UO_2 dissolution by ICARE2 due to a lower UO_2 solubility chosen as being the liquidus boundary of the U-Zr-O mixture. The third reason is related to the ZrO_2 dissolution discussed below.

7.6 - Zirconia dissolution by molten Zry

Only FRA-SP gave a calculation of the ZrO₂ dissolution. The ICARE2 V2p code simultaneously took into account UO₂ and ZrO₂ dissolution by molten Zry. This second dissolution phenomenon tends both to increase the oxygen content in the mixture (which decreases UO₂ solubility) and to reduce the ZrO₂ thickness. The calculated ZrO₂ dissolution calculated in the failure zone was able to attain up to 60 % of the ZrO₂ layer calculated at the end of the oxidation phase. When the melting temperature of α -Zr (O) was reached at about 10600 s, the calculated ZrO₂ thickness reduction observed in the oxidation histories at 50 cm (A.16 - Fig. 8/3) was due to this ZrO₂ dissolution. PIE showed local ZrO₂ reduction of up to 50 % in the upper part of the bundle, but it is not sure that this reduction resulted only from the ZrO₂ dissolution (see section 4.7).

7.7 - Relocation of molten materials and channel blockage

Nine submissions gave calculated results concerning material relocation

FRA-SP and ISPRA	with ICARE2
SP-UPM, TAIWAN, USA	with MELCOR
SP-CSN	with SCDAP Mod 1
I-PISE, NETHER, UK	with SCDAP/RELAP5 Mod2.

Predictions of the general trend of the relocation and the cladding failure zones are summarized in figure 15 of A16. The channel blockage calculated by the different codes is given in A16 - Fig. 14/1, 14/2, 14/3 (see definition in section 4.9).

There is considerable spreading of the calculated results even when calculations were performed with the same code. Relocation behaviour is in fact very sensitive to the following parameters :

- The final oxidation profile at the end of the steam phase. This profile determines the amount of non-oxidized Zry for the UO₂ and ZrO₂ dissolution and the thickness of the ZrO₂ shell which maintain the molten Zry in place,

- The thermal histories during the high temperature heat-up of the He phase. These histories determine the melting zone of the non-oxidized Zry, the UO_2 solubility limit in the U-Zr-O mixture (ternary phase diagram) and also the failure zone where the cladding failure temperature limit is exceeded,
- Cladding failure by molten Zry is governed by simple criteria. The user-specified failure parameters of these criteria are very important for relocation [7] [8]. Criteria usually include two parameters, a failure temperature limit and a ZrO_2 thickness limit. The axial failure zone increases when both the temperature limit decreases and when the ZrO_2 thickness limit increases. Additional criteria also govern debris bed formation (e.g. the melting temperature of ZrO_2).
- With the same conditions of oxidation, temperature and cladding failure, the amount of U-Zr-O mixture which can be formed before the cladding failure depends on the UO_2 dissolution model (UO_2 and ZrO_2 dissolution kinetics plus the UO_2 solubility limit).
- The final freezing of relocated material depends on the melt progression model and also on some user specified parameters such as the heat exchange (heat transfer coefficient and contact surface) between the molten material and the solid support or the mixture properties (solidus temperature).

Taking into account all the parameters involved in relocation prediction, it is very difficult to make an accurate analysis of the relocation and blockage results. This is a classic example of a domain in which compensation errors can lead to acceptable results.

The following comments can be made concerning the relocation predictions.

Only the reference calculation (ICARE2 V2p) which correctly predicted the UO_2 dissolution gave reasonable results concerning both the cladding failure zones and the bundle blockage (A16 - Fig. 15).

Whatever the prediction of the cladding failure zones, in general SCDAP/R5 and MELCOR predicted the refreezing zones at elevations that are either too low in the bundle or under the lower end of the rods. This trend was particularly followed by I-PISE and UK in spite of a correct prediction of the cladding failure zones. This disagreement with the test is mainly due to an overestimation of the UO_2 dissolution.

Using MELCOR V 1.8EA, the USA predicted a cladding failure zone by molten Zry (45 cm to 65 cm) for the inner rods higher than the experimental zone (28 cm to 50 cm) and a non-observed debris formation with cladding embrittlement between 65 and 80 cm on the central rod. A cladding failure criterion based on a temperature limit of 2500 K when the oxide layer thickness is greater than $60 \mu\text{m}$ was applied to a transient which underestimated the temperature during the He phase (power profile constant). This explains the incorrect prediction of the failure zone above the actual one. The use of a different failure condition based on the usual ZrO_2 thickness limit condition would have avoided the failure prediction in the upper part of the bundle, and the prediction of higher temperatures would have led to a failure prediction lower in the bundle.

The location of the blockage near 20 cm is in agreement with the test but the corresponding bundle blockage (ZrO_2 -Zr mixture with 0.3 % of UO_2) is slightly underestimated and too poor in UO_2 . It results from the first cladding failure process by molten Zry. The cladding failure of the CR therefore spreads up to 80 cm due to lack of support from below. This leads to a UO_2 debris bed formation which remains located in the 50/60 cm zone. A solid debris bed was not observed in the B9+ test where the complete oxidized cladding maintained the UO_2 pellets in place.

No liner relocation was predicted.

The SP-UPM calculation with MELCOR V 1.8 predicted incorrect cladding failure and relocation zones. Two kinds of cladding failure were calculated. The first was due to molten material when the ZrO_2 thickness limit was lower than $100 \mu\text{m}$ whatever the temperature of the molten Zry. Due to this too low a value corresponding to an oxidation of only 11 %, the lower zone of the bundle could fail (zone 16 to 24 cm for 2R rods) whereas no failure could be predicted in the zone where clad failures were observed in the test. A second kind of cladding failure occurred in the 48-64 cm region to form a pure UO_2 debris bed. The corresponding criteria were based on the melting of ZrO_2 ($T > 2990 \text{ K}$) which

was reached at the end of the heating phase (just before 14000 s) because the rod temperatures were significantly overpredicted in spite of a power profile that was kept constant. (Maximum temperature estimated in the test : 2750 K). No debris bed formation would have been calculated with a more correct prediction of the rod temperatures. The main part of the relocated molten materials dripped outside the active fuel length (including all the spacer grids and the molten Zry and ZrO₂). These results are not in agreement with the test. The percentage of UO₂ and ZrO₂ transported by means of the molten Zry relocated after the cladding failure was imposed at 20 % by the user.

No cladding relocation was predicted by MELCOR V 1.8 in the TAIWAN submission due to the choice of too high a failure temperature of 2600 K, greater than the maximum temperature calculated (underestimation of the temperatures due to the use of a constant power profile). Only the Zry liner was relocated but the failure zone was overestimated (25-80 cm instead of 25-56 cm in the test). The freezing zone of the liner was well calculated with a blockage of 60 % instead of 52 % in the test (A16 - Fig. 14/1).

The UK and I-PISE calculations performed with SCDAP/RELAP5 Mod2 were similar, the rod temperatures were well predicted and the cladding failure parameters were the same (2500 K and about 520 μm). The results are in agreement with the test concerning the CR and the 1 R rods. In the two calculations, the cladding failure results were different as regards the 2R rods which were only predicted to fail in the UK calculation at 52 cm. The non-prediction of the 2 R rod failure in the I-PISE calculation was due to the cladding temperatures which remained below the failure temperature of 2500 K. The excessive amount of eutectic resulting from the UO₂ dissolution could explain part of the overestimation of the melt relocation distance (too large an amount of energy in the melt). Only part of the melt was therefore refrozen within the test train in the lower 0-8 cm zone leading to a limited bundle blockages (41 % in the UK submission and 52 % for I-PISE) in spite of the overestimation of the UO₂ dissolution.

The NETHER calculation was performed with the same cladding failure criteria as the UK, but the relocation results were very different. The overprediction of the temperatures led to an overestimation of the oxidation in the central 40-56 cm zone which prevented cladding failure. With overestimated temperature and oxidation conditions, the CR and 1R rods could only fail in the lower zone

30-40 cm. The melting temperature of ZrO_2 was also reached in the upper part (50-65 cm). This led to cladding failure with a debris bed formation around 60 cm and a nearly complete blockage of 96 % (A16 - Fig. 14/2) not observed in the test. The mixture resulting from the fuel dissolution was frozen too far, as in the UK and I-PISE calculations, in spite of a smaller amount of mixture. Only part of this mixture was refrozen in the lower 0-8 cm zone in the bundle.

The SCDAP-Mod1 calculation of SP-CSN was characterized by an overestimation of the rod temperatures and the oxidation (nearly complete oxidation above 40 cm). In spite of an overprediction of the fuel dissolution zone under 40 cm (A16 - Fig. 13/3), part of the predicted cladding failure zone and the frozen material distribution is in agreement with the test (A16 - Fig. 15). With cladding failure criteria based only on a temperature limit of 2500 K, and with overestimated temperature and oxidation conditions, the failure zone could only be found in the upper part of the remaining not completely oxidized zone (24 - 40 cm for CR and 1R rods). This calculated zone corresponds to the cladding failure zone observed in the test but is characterized by different temperature and oxidation conditions. The first part of the molten material was frozen in the failure zone in spite of the too high temperatures obtained in this zone and led to a correct channel blockage of 54 %. The second part was dripped outside the active fuel length (not observed in the test). Only compensation effects between the different degradation models can explain the noted agreements. The maximum flow blockage of 62 % at 60 cm (A16 - Fig. 14/3) was due to the prediction of considerable cladding deformation before rod plug melting (not observed in the test).

In the SWEDEN submission, no cladding failure was predicted because the cladding temperatures were always below the failure temperature limit (2500 K) chosen by the user.

For JAPAN, the same reason probably explains the non-prediction of cladding failure (too large a failure temperature of 2700 K was chosen). The calculated channel blockage of more than 50 % above 20 cm (A16 - Fig. 14/3) could be due to the prediction of considerable cladding deformation.

7.8 - Mixture compositions

The few mixture compositions which were transmitted are summarized in Table 9. These compositions are given in percentage of UO_2 , Zr , ZrO_2 and steel or

Inconel. The codes have no models that take into account chemical reactions in the mixtures except molten Zry oxidation. The final composition results only from the addition of the different relocated melts. There is poor agreement except with the ICARE2 code as regards the main plug at 20 - 28 cm.

7.9 - Code run time statistics

Table 10 summarizes the information concerning the computational times needed for the B9+ calculations. The lack of relative computer speeds for all the computers used does not allow a correct code performance comparison. Nevertheless the following comments can be made :

- The average time step size can give a rough idea of code performance. There is considerable spreading of this value. The largest time steps of about 1 to 10 s were used by ICARE2, FRAS, KESS, ATHLET and MELCOR (USA and TAIWAN). The SCDAP/R5 Mod 1 and Mod 2 and MARCH 3 codes were run with very small time steps in the range of 10^{-1} to 10^{-2} s. The CPU time of the MELCOR calculation performed by SP-UPM was also very long (8 times the MELCOR calculations of TAIWAN and USA). The main reason for this is that two control volumes in the core region were used, with too small a volume for the entrance of the rods which control the time step throughout the Courant condition. It must be pointed out that the KESS, ATHLET and FRAS codes did not perform dissolution and relocation calculations which are time consuming.
- The same trend is observed as regards the CPU-time per second problem time and per cell. The number of cells was deduced from Table 5 using the number of rods and the axial meshing for the total rod length or active length. (The shroud was considered as a rod). The largest minimum step (5 s) was used with KESS and this could explain the temperature oscillations found in the He phase. (A5a - Fig. 5, 6).
- The transition period from steam to helium and the following pure helium phase was CPU time consuming due to numerical instabilities. The minimum time step was often divided by a factor greater than 5 or 10 (MELCOR, SCDAP/RELAP5) No reduction was really necessary with SCDAP Mod1, ICARE2, ATHLET and KESS,

- Whatever the computer used, excessive CPU times are a real handicap for sensitivity studies. In particular it was indicated that the CPU times needed with SCDAP/RELAP5 Mod2 or SCDAP Mod1 ranged from 36 h (CRAY XMP14) to 75 h (SUN4/330). These very long CPU times were mainly due to numerical instabilities in the He phase calculation which took up 80 % to 90 % of the total CPU time. The first pure vapour phase was less time-consuming (more than 5 hours) but the CPU time still remained significant.

8 - CONCLUSIONS

The PHEBUS SFD B9+ test, selected as International Standard Problem n° 28 was calculated by a large number of participants using the main existing SFD codes. In spite of experimental uncertainties, unavoidable for tests performed with severe thermal-hydraulic conditions, the ability of these codes to predict the main governing phenomena of the early phase of a PWR core degradation was able to be assessed.

Above all, the semi-blind nature of ISP 28 must be considered as regards the comparisons with the experiment. The thermal-hydraulic behaviour was given to the participants. The degradation aspect of the bundle was the blind part of the exercise, so "user-tuning" to better predict degradation was not performed. One exception concerned the FRA-SP submission (joint CEA - Phebus Espana Consortium) which was performed in open conditions. These participants were closely involved in the PHEBUS Programme and their submission was considered as a reference calculation.

Substantial experimental data were obtained from the PHEBUS B9+ test. Different axial oxidation states, UO_2 and ZrO_2 dissolutions and relocations of the liquefied mixtures on the lower part of the bundle were characterized. Experimental boundary conditions such as the nuclear power, the thermal-hydraulic conditions at the bundle entrance, and the sink temperature on the outer surface of the shroud were well defined.

Thermal behaviour :

The main uncertainty of the test concerned the radial thermal leak through the shroud. Participants could not calculate correct rod temperatures using the recommended thermal conductivity of the porous ZrO_2 layer of the shroud. The porous ZrO_2 conductivity value deduced from laboratory measurements performed at 0.1 MPa

was extrapolated to the pressure condition of B9+ (1.9 MPa). This extrapolated value, recommended for performing the exercise was not suitable due to an underestimated pressure effect. Consequences on the thermal rod prediction were as follows.

- Using the 1st approach for the radial BC, all the calculations showed that to obtain a correct general tendency of the rod temperatures it was required a "user-adjusted" ZrO₂ conductivity value greater than the one recommended by a factor 2 to 3. Few participants seem to have performed accurate tuning of this very sensitive parameter for calculating the thermal conditions of the bundle.
- Using the 2nd approach for the radial BC, all the participants found correct rod temperatures with the MELCOR, ATHLET SA and KESS III codes.

In general, participants who performed a correct calculation of the thermal behaviour of the first steam phase were able to calculate the final oxidation and temperature escalations : the UK and I-PISE with SCDAP/R5-MOD2, the USA with MELCOR, FRA-SP with ICARE2. A slight tendency to overestimate oxidation in the upper part of the bundle and the corresponding H₂ release was observed. Only four participants predicted H₂ production inside the experimental uncertainty range.

In spite of the difficulty in predicting cladding oxidation with a local and strong escalation suddenly stopped by steam starved conditions, code to data comparisons show that the current models based on kinetics correlations of Cathcart up to 1853 K and Urbanic Heidrick at higher temperature are sufficient to predict oxidation within the experimental uncertainty range providing that a correct calculation of the energy balance in the bundle is performed.

UO₂-Cladding interactions and resulting melts relocation :

Except for the reference calculation with ICARE2V2p, degradation processes such as UO₂ and ZrO₂ dissolutions, cladding failure by molten Zry, and relocation and freezing of molten mixtures were not well predicted. Nearly all the codes showed the same trend in the deviation with the PTE. Discrepancies in rod temperatures and related sensitive effects on melt progression cannot totally explain the discrepancies found for rod degradation. Discrepancies also resulted from areas with weaknesses and gaps in the following aspects of core damage modelling.

UO₂ dissolution by molten Zry and solubility limit

- Fuel dissolution by molten Zry was significantly overestimated except with version V2p of ICARE2. The maximum mean dissolution observed in B9+ test was in fact

limited to 14 %. This chemical interaction is highly dependent on the temperature and oxidation conditions. In addition, a correct prediction needs correct modelling of UO_2 solubility in the resulting U-Zr-O mixture. This limiting factor of the interaction is given by rough models of the ternary phase diagram of the mixture which should be verified, particularly at high temperature.

ZrO₂ dissolution by molten Zry

- ZrO_2 dissolution by molten Zry, which could not be quantified in the PIE, determines the chemical effect on the cladding failure process (reduction of the ZrO_2 layer) and increases the O_2 content in the U-Zr-O melt resulting from the simultaneous UO_2 and ZrO_2 dissolutions. These two effects tend to limit UO_2 dissolution by molten Zry. Modelling of ZrO_2 dissolution by molten Zry is recommended.

External ZrO₂ cladding layer failure

- Mechanistic models of mechanical failure of the external ZrO_2 cladding layer by molten Zry are currently lacking. Only simple parametric models based on one or two criteria using parameters defined by the user are available. These important user-specified conditions determine the end of UO_2 dissolution at the failure location, and the flow-down and relocation of the U-Zr-O mixture. The diversity of the conditions and parameters used clearly shows a lack of data in this field and modelling deficiencies. From the B9+ experimental results, the failure criteria which would have defined a better cladding failure zone in the case of a correct thermal and oxidation prediction are :

$$T_{\text{clad}} > 2300 \text{ K and } e^{\text{OX}} < 400 \text{ to } 500 \mu\text{m.}$$

These criteria remain applicable for a code which does not have a cladding ZrO_2 dissolution model. For codes modelling ZrO_2 dissolution, the oxide thickness limit related to mechanical effects only is reduced.

Melts relocation

- Calculated melts relocate and refreeze too far or out of the bundle (SCDAP/RELAP5 - Mod2, MELCOR, SCDAP Mod1). In addition to an overestimated amount of melts resulting from UO_2 dissolution, which leads to an overestimated amount of transported energy and relocation distance, incorrect relocation parameters or incorrect mixture material properties are also suspected.

Inconel spacer-grid

- Effective Inconel spacer-grid models including interaction with rods do not exist or are not able to work. Only MELCOR described spacer-grid melting and relocation. Modelling of spacer-grid effects is recommended.

User effects :

As shown in previous ISP exercises different results were produced by different participants using the same code. In this ISP28, user influence on the predicted results mainly originated from the possibility of defining degradation parameters in the input data deck. The main ones are the cladding failure parameters which can have tremendous effects on relocation going from a total relocation to no relocation at all with similar thermal and oxidation conditions. Some parametric models allow relocation of fuel and ZrO₂ in quantities specified by user input parameters (MELCOR). In that case, final relocation results, particularly flow blockage, are therefore user-dependent.

Degradation results were calculated using different nodalizations and representations. The resulting differences could not be identified except as regards multi channel modelling which tended to increase radial temperature gradients and differences between the second ring rods and the inner rods for degradation prediction.

User effects could be reduced if more mechanistic models were available, or if more detailed information and recommendations were given in the user guide-lines, including the sensitivity of some user-specified parameters strongly affecting rod degradation (cladding failure limits).

Results also depend to a large extent on user experience and on the time and means devoted to performing the necessary sensitivity studies. Some participants acknowledged that they were not familiar with the code used and with the sensitivity of some of the parameters for degradation. A good knowledge of the phenomena governing rod degradation and of the related physical models of the codes would help the user to better prepare code input data with relevant values assigned to the more sensitive user-specified parameters.

Finally this exercise illustrates the importance of the code user, the need for improved user-guidelines, as well as the need for experts in core degradation in order to make code utilization more effective with valuable judgements on predictions especially in these areas where code modelling deficiencies have been identified.

Running times :

Excessive running times were communicated by some participants, well in excess of a few hours (SCDAP/RELAP5 Mod2). Whatever the computer used, such long computing times are a real handicap for sensitivity studies. Efficient calculations were performed with MELCOR and ICARE2 with more reasonable CPU times.

Codes validation :

In addition to the modelling improvements suggested above, code validation efforts must be maintained. The significant differences obtained in the code-to-data, or code-to-code comparisons illustrate a considerable need for SFD code validation focussing on core degradation phenomena which govern major aspects of safety studies : H₂ release and quantification of the remaining non oxidized Zry, early UO₂ dissolution with change of core geometry, core channel blockage, high temperature and fuel morphology histories which are key parameters governing the release of fission products.

Codes versatility :

Codes have been developed for reactor calculations, but verification and validation need more code versatility so as to take into account some peculiarities of small-scale experiments : power profiles versus time, surrounding structures with imposed boundary conditions, pure non-condensable flow, models to calculate view factors - in particular experimental geometries - and more output and drawing convenience.

Recommendation for reactor calculations :

Complete validation of degradation models for reactor plant calculations should take into account code-to-data comparison results obtained from a larger set of conditions, e.g. irradiated and cracked fuel concerning the UO₂ dissolution. Similarly, different conditions, from a steam-rich atmosphere to pure steam-starved conditions, as in the B9+ test, including different heating rates should be considered as regards cladding failure conditions before final recommendations for plant calculations are given.

Next ISPs on SFD experiments like CORA13 and FLHT-6 should provide a complementary and valuable contribution to SFD code validation.

REFERENCES

- [1] C. GRANDJEAN - C. GONNIER
Preliminary specifications for the International Standard Problem ISP 28.
C.E.A report - PHEBUS CSD 112/90 - March 1990.
- [2] C. GRANDJEAN - C. GONNIER
Technical specifications - Complementary report.
C.E.A report - PHEBUS CSD 117/90 - September 1990.
- [3] C. GONNIER - G. GEOFFROY - B. ADROGUER
PHEBUS Severe Fuel Damage Programme - Main results.
A.N.S. meeting - Portland - 21, 25 July 1991.
- [4] B. ADROGUER
International Standard Problem ISP 28.
SFD PHEBUS test B9+ - Final specifications for calculations and reported results.
C.E.A report - PHEBUS CSD 115/90 - September 1990.
- [5] R. GEOFFROY - J.M. BOYER - M. PERROT
PHEBUS B9+ . Examens après essais.
C.E.A report - DMT 91/346 - Juillet 1991.
- [6] S.R. KINNERSLY and al.
State-of-the-Art Report (SOAR) on In-Vessel Core. Degradation in LWR Severe Accidents.
OECD/CSNI report. NEA/CSNI/R (91) 12-NOV. 1991.
- [7] S. BOURDON - P. VILLALIBRE - B. ADROGUER - G. GEOFFROY
Analysis of the severe fuel damage test PHEBUS B9+ using ICARE code.
27th National Meeting, AIChE Minneapolis (1991).

- [8] B. ADROGUER, S. BOURDON, R. GONZALEZ.
Analysis of the fuel-cladding chemical interaction in PHEBUS SFD tests using ICARE2 Code.
AIEA meeting on "Behaviour of Core Materials and Fission Product Release in Accident Conditions in LWRs".
Aix-en-Provence - March 1992.
- [9] B. ADROGUER, S. BOURDON, C. RONGIER.
Results of the International Standard Problem 28 on the PHEBUS SFD test B9+.
AIChE meeting on Heat Transfer and Fuel Behaviour in Nuclear Reactor Accidents.
San Diego - August 1992.

LIST OF ANNEXES (VOLUME 2)

All these annexes are given in the volume 2 of this report.

- Annex 1 : FRA-SP. Joint CEA-Phebus España submission
- Annex 2 : SP-CSN submission
- Annex 3 : SP-UPM submission
- Annex 4 : CZECHOSLOVAKIA-NRI submission
- Annex 5a : GER-IKE 1 submission (1st BC approach)
- Annex 5b : GER-IKE2 submission (2nd BC approach)
- Annex 6a : GER-GRS1 submission (1st BC approach)
- Annex 6b : GER-GRS2 submission (2nd BC approach)
- Annex 7 : HUNGARY-CRIP submission
- Annex 8 : I-PISE UNIVERSITY submission
- Annex 9 : ISPRA submission
- Annex 10 : JAPAN-JAERI submission
- Annex 11 : NETHERLANDS-ECN submission
- Annex 12 : SWEDEN-SN submission
- Annex 13 : TAIWAN-AEC submission
- Annex 14 : UK-AEA Technology submission
- Annex 15 : USA-NRC submission
- Annex 16 : Comparisons between codes
- Annex 17 : Plot identifiers

LIST OF TABLES (VOLUME 1)

Table 1	:	List of participants and codes
Table 2	:	Code modifications
Table 3	:	Physical models used
Table 4	:	Cladding failure criteria and relocation models used
Table 5	:	Nodalization schemes
Table 6	:	Shroud modelling
Table 7	:	Nuclear power
Table 8	:	Radial temperature differences at 60 cm - Time 7800 s
Table 9	:	Mixture composition at 18000 s
Table 10	:	Run statistics.

LIST OF FIGURES (VOLUME 1)

- Fig. 1 : Test stringer
- Fig. 2a : Bundle cross section
- Fig. 2b : Longitudinal view of the bundle
- Fig. 3 : Thermocouple locations
- Fig. 4 : Shroud thermocouples
- Fig. 5 : Experimental scenario
- Fig. 6 : Steam to helium switch
- Fig. 7 : Porous ZrO₂ conductivity
- Fig. 8 : Radial power profile
- Fig. 9 : Axial power profiles
- Fig. 10 : Bundle modelling
- Fig. 11 : Axial cut of the lower end of bundle
- Fig. 12 : Cross cutting at elevation 0.76 m
- Fig. 13a : Cross cutting at elevation 0.58 m
- Fig. 13b : Cross cutting at elevation 0.52 m
- Fig. 14a : Cross cutting at elevation 0.44 m
- Fig. 14b : Cross cutting at elevation 0.26 m
- Fig. 15a : Cross cutting at elevation 0.17 m
- Fig. 15b : Cross cutting at elevation 0.14 m
(Lower spacer - grid location)
- Fig. 16 : Cross cutting at elevation 0.05 m
- Fig. 17a : Bundle power distribution
SCDAP/R5/Mod2 calculation (USA)
- Fig. 17b : Bundle power distribution
SCDAP/R5/Mod2 calculation (UK)
- Fig. 17c : Bundle power distribution
ICARE2 V2p calculation (FRA-SP)

**LIST OF FIGURES FOR EACH CODE-TO-DATA ANNEX
ANNEX 1 TO ANNEX 15 (VOLUME 2)**

Page 1 : UO₂ temperature

- Fig. 1 : UO₂ temperature of the second ring rods versus time at levels 20, 30, 40 and 50 cm (TU2R20, TU2R30, TU2R40, TU2R50).
- Fig. 2 : UO₂ temperature of the second ring rods versus time at levels 60 and 70 cm (TU2R60, TU2R70).

Page 2 : Cladding temperature

- Fig. 3 : Cladding temperature of the first ring rods versus time at levels 20, 30, 40 and 50 cm.
- Fig. 4 : Cladding temperature of the first ring rods versus time at levels 60 and 70 cm.

Page 3 : Fluid temperature

- Fig. 5 : Fluid temperature of the mean channel versus time at levels 0, 30 and 40 cm.
- Fig. 6 : Fluid temperature of the mean channel versus time at levels 50 and 80 cm.

Page 4 : Liner and shroud temperature

- Fig. 7 : Liner temperature versus time at levels 40, 60 and 80 cm.
- Fig. 8 : Shroud temperature versus time at levels 30, 40, 60 and 70 cm.

Page 5 : Radial temperature histories at 50 and 70 cm

- Fig. 9 : Temperature versus time at level 50 cm.
- Fig. 10 : Temperature versus time at level 70 cm.

Page 6 : Axial temperature profiles and radial heat flux

Fig. 11 : Axial temperature profiles at 7700, 9000, 12000 and 14000 s.

Fig. 12 : Heat flux to the shroud versus time at levels 20, 40 and 60 cm.

Page 7 : Central rod : Oxidation, UO₂ and ZrO₂ dissolution profiles

Fig. 13 : ZrO₂ profile at 9000 s.

Fig. 14 : UO₂ and ZrO₂ dissolution profiles at 9000 s.

Fig. 15 : ZrO₂ profile at 14000 s.

Fig. 16 : UO₂ and ZrO₂ dissolution profiles at 14000 s.

Page 8 : First ring rods : Oxidation, UO₂ and ZrO₂ dissolution profiles

Fig. 17 : ZrO₂ profile at 9000 s.

Fig. 18 : UO₂ and ZrO₂ dissolution profiles at 9000 s.

Fig. 19 : ZrO₂ profile at 14000 s.

Fig. 20 : UO₂ and ZrO₂ dissolution profiles at 14000 s.

Page 9 : Second ring rods : Oxidation, UO₂ and ZrO₂ dissolution profiles

Fig. 21 : ZrO₂ profile at 9000 s.

Fig. 22 : UO₂ and ZrO₂ dissolution profiles at 9000 s.

Fig. 23 : ZrO₂ profile at 14000 s.

Fig. 24 : UO₂ and ZrO₂ dissolution profiles at 14000 s.

Page 10 : Clad oxidation profiles and ZrO₂ layer histories

Fig. 25 : Clad oxidation profiles for central rod and second ring rods at 9000 s.

Fig. 26 : ZrO_2 layer increase and dissolution versus time for the first ring rods at levels 20, 30, 40, 50, 60, 70 and 75 cm.

Page 11 : ZrO_2 profile in the liner and total H_2 production

Fig. 27 : ZrO_2 mass fraction versus level for the liner at 9000 and 14000 s.

Fig. 28 : Total H_2 production and H_2 mass flow rate.

Page 12 : Mean profiles of UO_2 dissolution and bundle blockage

Fig. 29 : Mean UO_2 dissolution profile at 18000 s.

Fig. 30 : Blockage (defined as being equal to 38 % at initial conditions).

Page 13 : Bundle pictures

Fig. 31 : Total mass of relocated mixtures at 9000 s and 18000 s.

Fig. 32 : Final picture of the bundle.

Page 14 : Axial distribution of core materials

Fig. 33 : Total mass of UO_2 , ZrO_2 , Zr at 9000 s.

Fig. 34 : Total mass of UO_2 , ZrO_2 , Zr at 18000 s.

TABLE 1 : LIST OF PARTICIPANTS AND CODES

INSTITUTION	COUNTRY	EXPERT	CODE	IDENTIFIER (*)
Spanish PHEBUS Consortium and CEA	SPAIN and FRANCE	P. VILLALIBRE S. BOURDON	ICARE2 V2p	FRA-SP
Spanish PHEBUS Consortium - CSN	SPAIN	A. ALVAREZ J. MARTINEZ	SCDAP MOD1	SP-CSN
Universidad Politecnica de Madrid C.T.N. - UPM	SPAIN	S.A. ENCISO JV.L MONTERO J.G. PINDADO C.S. SANTAMARINA	MELCOR V 1.8.0	SP -UPM
Nuclear Research Institute N.R.I. - REZ	CZECHOSLOVAKIA	F. PAZDERA M. VALACH L. BELOVSKY	FRAS - SFD	CZECHO
IKE, University of Stuttgart	GERMANY	K.D. HOCKE S. KRETSCHMER K. MULLER	KESS - III	GER-IKE1 GER-IKE2 (**)
GRS, Garching	GERMANY	A. BALL K. TRAMBAUER	ATHLET-SA	GER-GRS1 GER-GRS2 (***)
Central Research Institute for Physics C.R.I.P.	HUNGARY	G. GYENES B. TOTH P. VERTES	MARCH 3	HUNGARY
Pise University and ENEA	ITALY	G. FRUTTUOSO F. ORIOLO	SCDAP/RELAP5 MOD2	I-PISE
ISPRA J.R.C.	ISPRA	J.A. CAPITAO I. SHEPHERD	ICARE 2 V1	ISPRA

TABLE 1 : LIST OF PARTICIPANTS AND CODES (continued)

INSTITUTION	COUNTRY	EXPERT	CODE	IDENTIFIER (*)
JAERI CSK Corp.	JAPAN	K. HASHIMOTO K. SODA E. MATSUMOTO (*)	SCDAP/RELAP5 MOD1/C22	JAPAN
Energ. Centrum Nederland E.C.N.	NETHER- LANDS	L.WINTERS	SCDAP/RELAP5 MOD2-V3F1	NETHER
STUDSVIK NUCLEAR	SWEDEN	J. ERIKSSON	SCDAP/RELAP5 SRL-C/V3f	SWEDEN
Institute of Nuclear Energy Research A.E.C.	TAIWAN	SHIH-KUEI CHENG LAINSU KAO	MELCOR V 1.8.0	TAIWAN
AEA Technology WINFRITH	UK	T.J. HASTE J.N. LILLINGTON A.J. LYONS	SCDAP/RELAP5 MOD2.5 SRL-C/V 361sc	U.K.
SANDIA Nat. Lab. and NRC	USA	G.M. MARTINEZ	MELCOR V 1.8. EA	U.S.A

(*) IDENTIFIER for comparisons between the different codes and the measurements

(**) IKE 1 : identifier for the calculation performed in using the 1st shroud boundary condition approach

IKE 2 : for the 2nd shroud boundary condition approach

(***) GRS1 : identifier for the calculation performed using the 1st shroud boundary condition approach

GRS2 : for the 2nd shroud boundary condition approach

TABLE 2 : CODE MODIFICATIONS

PARTICIPANT	CODE	ORIGINAL CODE OR MODIFICATIONS
FRA-SP	ICARE 2 V2p	<ul style="list-style-type: none"> - New UO₂ dissolution model - New ZrO₂ dissolution model - Solubility limits in U-Zr-O mixtures - Oxidation when β-Zr is consumed
SP-CSN	SCDAP MOD1 stand alone	<ul style="list-style-type: none"> - Modelling of the melting seal of rod plenum - He as coolant gas - Fuel gap model for fresh fuel - Oxidation release energy at the steam temp. - Missenard model for conductivity of porous ZrO₂
SP-UPM	MELCOR V 1. 8. 0	No
CZECHO	FRAS-SFD	Adaptation for the B9+ calculation and for SFD conditions
GER-IKE	KESS III	<ul style="list-style-type: none"> - Oxidation of the shroud liner - Adaptation for the 2nd approach B.C
GER-GRS	ATHLET-SA	No
HUNGARY	MARCH3	<ul style="list-style-type: none"> - Imposed steam flow rate at the entrance instead of steam controlled by a water level - Modelling of the shroud with 2 methods (core barrel and fictitious outer ring rods)
I. PISE	SCDAP/RELAP5	No

TABLE 2 : CODE MODIFICATIONS (continued)

PARTICIPANT	CODE	ORIGINAL CODE OR MODIFICATIONS
ISPRA	ICARE 2 V1	No
JAPAN	SCDAP/RELAP5 MOD1	No
NETHER	SCDAP/RELAP5 MOD2	<ul style="list-style-type: none"> - Imposed cladding failure at 1073 K to avoid overpressurization of rods - Remove double side oxidation - Setting He void fraction to 0.998 to avoid code failure during the steam/He switch
SWEDEN	SCDAP/RELAP5 SRL	Increase the number of points of the axial power profile
TAIWAN	MELCOR V 1.8.0	No
U.K.	SCDAP/RELAP5 MOD2	<ul style="list-style-type: none"> - Increase the number of different axial power profiles and the total number of points - Melt temp. of ZrO₂ imposed to 3000 K to avoid debris bed formation (has no effect in the base case)
U.S.A.	MELCOR V 1.8. EA	<ul style="list-style-type: none"> - Time dependant pressure as boundary condition - Failure temperature versus elevation for structures - Fluid viscosities corrections for non condensable gas - Add a conduction transfer in the helium gap between the shroud liner and porous ZrO₂ - Correction of radiation transfer between components and liner instead of a canister structure - Correction of the mixture gas viscosity

TABLE 3 : PHYSICAL MODELS USED

PARTICIPANT	CODE	RADIATIVE MODEL	OXIDATION AND TRANSITION T	UO ₂ DISSOLUTION BY MOLTEN Zr SOLUBILITY LIMITS (SL) IN THE U-Zr-O MIXTURE	ZrO ₂ DISSOLUTION BY MOLTEN Zr	SPACER GRID MODEL
FRA-SP	ICARE2 V2p	- Hotel method - Fij per rod (*) - absorption by H ₂ O	Urbanic-H 1853 K	Kim diffusion model SL : Liquidus Temp. from a ternary U-Zr-O phase diagram model	Hofmann diffusion model	No
SP-CSN	SCDAP Mod1	- Net radiative method - Fij per rod - absorption by H ₂ O	Cathcart-Pawel Urbanic-H 1850 K	Turk dissolution model SL : pseudo-binary Politis diagram	No model	No
SP-UPM	MELCOR V 1.8.0	- Fij per adjacent representative rod (constant) - absorption by steam - axial Fij	Cathcart-Pawel Urbanic-H 1853 K modified constant	- No specific model - User parametric model to impose the fraction of UO ₂ transported when candling occurs (20 %)	Same comment than for UO ₂ (20 %)	Relocation when melting
CZECHO	FRAS-SFD (1 rod)	Simple model Fij between cylinders	Diffusion model for solid and liquid Zr	Time-independent model SL : a ternary U-Zr-O phase diagram model	Same comment than for UO ₂	
GER-IKE	KESS III	Fij = f (pinch, rod \emptyset) Fij = 0.45 (rod/rod)	Urbanic-H	Not used	No	No
GER-GRS	ATHLET-SA	- Fij per rod - no absorption by steam	Cathcart Urbanic-H 1853 K	Not used	No	

TABLE 3 : PHYSICAL MODELS USED (continued)

PARTICIPANT	CODE	RADIATIVE MODEL	OXIDATION AND TRANSITION T	UO ₂ DISSOLUTION BY MOLTEN Zr SOLUBILITY LIMITS (SL) IN THE U-Zr-O MIXTURE	ZrO ₂ DISSOLUTION BY MOLTEN Zr	SPACER GRID MODEL
HUNGARY	MARCH-3	Fij between cylinders	Urbanic-H	No model	No	No
I-PISE	SCDAP/ RELAP5 Mod2	- Net radiative approach - Fij per rod calculated by the code - absorption by H ₂ O	Cathcart-Pawel Urbanic-H (1850 K)	Hofmann-Uetsuka diffusion model SL : liquidus limit given by MATPRO model	No specific model	No
ISPRA	ICARE2 V1	See FRA-SP	Urbanic-H 1853 K	Time-independent model SL : pseudo binary diagram of Politis	No	No
JAPAN	SCDAP/ RELAP5 Mod1		Cathcart-P Urbanic-H 1820 K	See I-PISE	No	No
NETHER	SCDAP/ RELAP5 Mod2	See I-PISE	See I-PISE	See I-PISE	No	No
SWEDEN	SCDAP/ RELAP5 SRL	Fij given by a Studsvik code (8 zones per rod)	"	"	"	"

TABLE 3 : PHYSICAL MODELS USED (continued)

PARTICIPANT	CODE	RADIATIVE MODEL	OXIDATION AND TRANSITION T	UO ₂ DISSOLUTION BY MOLTEN Zr SOLUBILITY LIMITS (SL) IN THE U-Zr-O MIXTURE	ZrO ₂ DISSOLUTION BY MOLTEN Zr	SPACER GRID MODEL
TAIWAN	MELCOR V 1. 8. 0	Fij between representative rods imposed to 1	Urbanic-H	See SP-UPM	See SP-UPM	No
U.K.	SCDAP/RELAP5 Mod2	Fij given by the view code (true geometry)	See I-PISE	See I-PISE	No	No
U.S.A	MELCOR V 1. 8. EA	Fij between components (axial $F_{ij} = 0.25$) (radial $F_{ij} = 1.0$) absorption by H ₂ O	Urbanic-H 1853 K	See SP-UPM 20 % of UO ₂ transport when candelung occurred	See SP-UPM 100 % of ZrO ₂ transport	See SP-UPM

(*) Fij view factor between 2 surfaces i and j

**TABLE 4 : CLADDING FAILURE CRITERIA (CFC)
AND RELOCATION MODEL USED**

PARTICIPANT	CFC due to molten Zr Tc, eOX, eZr (*)	CFC for solid debris formation	Relocation model for molten mixtures
FRA-SP (ICARE2 V2p)	Tc > 2300 K eOX < 300 μm	Criteria to define dislocated mate- rial (not used)	Candling model with an user specified velocity (0.6 m/s). Mass and energy equations.
SP-CSN (SCDAP MOD1)	Tc > 2500 K (criteria only tempera- ture dependent)		Mechanistic candling model with calcula- tion of velocity and Temp. of the mix- ture.
SP-UPM (MELCOR V 1. 8. 0)	2200 K < Tc < 2990 K and eOX < 100 μm or T > 2990 K	eZr < 100 μ m (gravitational setting by logical processes)	Candling model with user imposed heat transfer (1000 W/m ² K) and based on mass/energy equations.
CZECHO (FRAS-SFD)	Tc > 2400 K eOX < 300 μm		No model Calculations stops when clad failure occurs
GER-IKE (KESS III)	Tc > 2673 K eOX has no retention effect		Not used
GER-GRS (ATHLET SA)	no explicit criteria based on Tc and eOX		Not used
HUNGARY (MARCH 3)	Melting temp. of α-Zr (O)		Not used
I. PISE (SCDAP/RELAP5)	Tc > 2500 K eOX < 540 μm		Model based on mass momentum and energy equations

**TABLE 4 : CLADDING FAILURE CRITERIA (CFC)
AND RELOCATION MODEL USED (continued)**

PARTICIPANT	CFC due to molten Zr T_c, e^{OX}, e_{zr} (*)	CFC for solid debris formation	Relocation model for molten mixtures
ISPRA (ICARE2 V1)	T _c > 2300 K e ^{OX} < 500 μm		See FRA-SP
JAPAN (SCDAP/R MOD1)	T _c > 2700 K e ^{OX} < 360 μm	T _c > 2950 K (melting T of ZrO ₂)	
NETHER (SCDAP/R. MOD2)	T _c > 2500 K e ^{OX} < 520 μm	T _c > 2950 K	Model based on mass momentum and energy equations.
SWEDEN (SCDAP/R. SRL)	T _c > 2500 K e ^{OX} < 435 μm	T > 2950 K	See NETHER
TAIWAN (MELCOR V 1. 8. 0)	T _c > 2600 K e ^{OX} < 100 μm	e _{zr} = 0	See SP-UPM h = 1000 W/m ² .K
U.K. (SCDAP/R. MOD2)	T _c > 2500 K e ^{OX} < 520 μm	T > 2950 K	See NETHER
U.S.A. (MELCOR V 1. 8. EA)	if e ^{OX} < 60 μm T _c > 2200 K if E ^{OX} > 60 μm T _c > 2500 K	e _{zr} < 0.1 μm (not used)	See SP-UPM Candling heat transfer coefficient = 300 W/m ² K

- (*) T_c : failure cladding temperature
e^{OX} : failure ZrO₂ thickness limit
e_{zr} : failure Zr thickness limit

TABLE 5 : NODALIZATION SCHEMES

PARTICIPANT	NUMBER OF HYDRAULIC CHANNELS	NUMBER OF DIFFERENT KIND OF RODS	AXIAL MESHING (active length)	AXIAL MESHING (total rod)	RADIAL MESHING OF RODS
FRA-SP	3	3	10 Cst	13	2
SP-CSN	3	3	10 Cst		4
SP-UPM	1	3	10 Cst	12	
CZECHO	1	1	40 ≠		17
GER-IKE	1	3	20 Cst	22	
GER-GRS1	1	3	9 ≠	11	
GER-GRS2	1	3	10 Cst	12	
HUNGARY	1	3	10 Cst		1
I-PISE	1	3	8 ≠	10	5
ISPRA	1	5	16 Cst		2
JAPAN	1	3	10 Cst		
NETHER	1	3	11 ≠	13	3
SWEDEN	1	3	8 Cst		5
TAIWAN	1	3	9 ≠	10	
U.K.	1	3	10 Cst	10	5
U.S.A.	1	3	9 ≠	11	

Cst : constant meshing

≠ : different ΔZ

TABLE 6 : SHROUD MODELLING

PARTICIPANT	RADIAL DIFFERENT LAYERS	POROUS ZrO ₂ RADIAL MESHING	POROUS ZrO ₂ THICKNESS (mm)	CONDUCTIVITY OF THE POROUS ZrO ₂ LAYER
FRA-SP	5 Zr/He/pZrO ₂ dZrO ₂ /SS	4 (bottom) 6 (top)	8.3 (bottom) 9 (top)	Missenard model - pure helium Porosity tuned : 40 % < p < 80 %
SP-CSN	4 Zr/pZrO ₂ / dZrO ₂ /SS	5		Missenard model - pure helium Porosity constant : p = 70 %
SP-UPM	4	12	10.72	$\lambda' = 2 \times \lambda_{mes}$
CZECHO	2nd BC way			non used
GER-IKE1		11		$\lambda' = 2 \times \lambda_{mes}$
GER-IKE2	2nd BC way			non used
GERf-GRS1	3 Zr/pZrO ₂ /SS	4	10.7	λ deduced from the 2nd approach case
GER-GRS2	2nd BC way			non used
HUNGARY				fictitious shroud with λ adjusted
I-PISE	4	10	11.65	$\lambda' > 2 \times \lambda_{mes}$ - see Fig. 6
ISPRA	4	3		$\lambda' = 3 \times \lambda_{mes}$
JAPAN	4	3	10	$\lambda' \sim 3 \times \lambda_{mes}$
NETHER	4	5	10.7	$\lambda' = 2 \times \lambda_{mes}$
SWEDEN	4 same SP-CSN		9.23	$\lambda' = 2 \times \lambda_{mes} \times (1 + 0.0005 (T - 300))$
TAIWAN	2nd BC way			non used
U.K.	4 Zr/ZrO ₂ / dZrO ₂ /SS	10	11.65	MATPRO - see Fig. 6
U.S.A.	5 Zr/He/pZrO ₂ dZrO ₂ /SS	3	9.72 (bottom) 10.69 (top)	Similar to the Missenard model - see Fig. 6

λ_{mes} : measured heat conductivity (recommended)

pZrO₂ : porous ZrO₂ - dZrO₂ : dense ZrO₂ - SS : Stainless Steel

TABLE 7 : NUCLEAR POWER

PARTICIPANT	CODE	AXIAL PROFILE VERSUS TIME / POWER
FRA-SP	ICARE 2 V2p	- 5 recommended axial profiles - Recommended radial profile on 3 rods
SP-CSN	SCDAP MOD1	- 3 recommended axial profiles (B, C, D) - Recommended radial profiles on 3 rods
SP-UPM	MELCOR V 1. 8. 0	- One mean axial profile (based on A and E profiles) - Recommended radial profile on 3 rods - + 5 % on the Nuclear Power
CZECHO	FRAS-SFD	- 5 recommended axial profiles - central rod
GER-IKE	KESS III	- 4 interpolated axial profiles - Recommended radial profile on 3 rods
GER-GRS	ATHLET SA	- One axial profile (D profile at 11940 s) - Recommended radial profile on 3 rods
HUNGARY	MARCH 3	- Mean axial profile - Recommended radial profile on 3 rods
I-PISE	SCDAP/RELAP5 MOD2	- 3 recommended axial profiles (C, D, E) - Recommended radial profile on 3 rods
ISPRA	ICARE2 V1	- Mean axial profile - Recommended radial profile on 5 rods
JAPAN	SCDAP/RELAP5 MOD1	- 3 recommended axial profile (A, B, D) - Recommended radial profile on 3 rods
NETHER	SCDAP/RELAP5 MOD2	- 5 recommended axial profiles - Recommended radial profile on 3 rods
SWEDEN	SCDAP/RELAP5 SRL	- 3 recommended axial profiles (A, C, E) - Recommended radial profile on 3 rods
TAIWAN	MELCOR V 1. 8. 0	- One axial mean profile - Recommended radial profile on 3 rods
U.K.	SCDAP/RELAP5 MOD2	- 5 recommended axial profiles - Recommended radial profile on 3 rods
U.S.A.	MELCOR V 1.8.0 EA	- One axial profile (C profile at 9370 s) - Recommended radial profile on 3 rods - - 5 % on the Nuclear Power

TABLE 8 - RADIAL TEMPERATURE DIFFERENCES AT 60 cm - TIME 7800 s

PARTICIPANT	TUIR-TCIR	TUCR-TUIR	TUIR-TU2R	TC2R-TSRI	TSRI-TSR3
EXPERIMENT	50 to 60	<10	60 to 90	150 to 180	650
FRA-SP (ICARE V2p)	54	5	66	151	600
SP-CSN (SCDAP Mod1)	50	5	115	220	600
SP-UPM (MELCOR V1.8.0)	70	72	160	219	450
CZECHO (FRAS-SFD)	50	-	-	-	-
GER-IKE (KESS III)	25	7	26	68	1000
GER-GRS (ATHLET SA)	25	17	58	200	620
HUNGARY (FRAS-SFD)	Same	~	25	-	-
I-PISE (SCDAP/R5/M2)	50	10	50	~ 190	600
ISPRA (ICARE2V1)	50	1	16	136	640
JAPAN (SCDAP/R5/M1)	42	7	24	100	600
NETHER (SCDAP/RD/M2)	42	25	40	193	560
SWEDEN (SCDAP/R5/M2)	41	5	40	195	575
TAIWAN (MELCOR V1.8.0)	44	13	50	100	-
UK (SCDAP/R5/M2)	45	10	20	155	550
USA (MELCOR V1.8EA)	40	42	113	143	660

TABLE 9 : MIXTURE COMPOSITION AT 18000 s

PARTICIPANTS	ELEVATION (cm)	UO2 (WT %)	ZrO2 (WT %)	Zr (WT %)	INCONEL (WT %)	U (A %)	O (A %)	Zr (A %)	INCONEL NI Fe Cr
Experiment	40 20-28 5	(U, Zr) O2-x (U, Z) O2-x	ZrO2 ZrO2	α -Zr(O) α -Zr(O)		6 4 7.44	38 31 4.9	56 65 55.4	23.6 7. 1.5
FRA-SP (ICARE2)	28 (1R) 20 (1R) 12 (2R)	13.5 23.9 23.3	43.8 29.9 24.4	42.7 46.2 52.2	0 0 0	3 6 6	48 44 40	49 50 54	-- -- --
SP-UPM (MELCOR V 1.8.0)	- 7 - 16 - 26	10.5 68.1 33.4	6.6 0.4 7.5	83.2 0 0.9	0 31.5 58.1	3.3	15.5	81.2	
USA (MELCOR V 1.8EA)	60/50 20 5 0	100 0.3 3 0.5	98 76.9 7.4	1.7 20.1 7.8	0 0 0 84.3	~ 0 0.52	66.2 59.75	33.8 39.73	

TABLE 10 : RUN STATISTICS

PARTICIPANT	CODE	TIME CALCULATED (s)	COMPUTER	CPU TIME (s)	Δt min (s)		Δt max (s)		MEAN Δt (s)	NUMBER TIME STEPS	CPU / Cell / Problem time (ms)
					p1	p2	p1	p2			
FRA-SP	ICARE2 V2p	18000	SUN 4/60	6340	10	5	20	10	11.3	1593	6.8
SP-CSN	SCDAP MOD1	18000	CDC Cyber 180	432918	0.1		20	0.1			600
SP-UPM	MELCOR V1.8.0	18000	VAX STATION 3100	376200	0.6	0.03	1	0.6	0.1	178614	435
CZECHO	FRAS-SFD	8320	PC-INTEL 386/7	18000	3.410 ⁻⁴		40		7	1200	27
GER-IKE1	KESS III	18000	VAX 6000-410	7200	5	5	20	10	6.4	2800	4.5
GER-GRS1	ATHLET SA	18000	Amdahl 5870	7240	2	1	2	1	1.3	13828	8.4
HUNGARY	MARCH 3	8364	mVAX TPA-11	52200	0.12		3		1.45 10 ⁻²	575000	72
I-PISE	SCDAP/RELAP5/2	18000	CRAY MXP 14	131623		0.01	0.5		1.45 10 ⁻²	1243002	114
ISPRA	ICARE2 V1	18000	SUN Sparcl	7610	0.5	0.5	50	50	15.9	1133	7
JAPAN	SCDAP/RELAP5/1	18000	FACOM M780	25800	0.12	0.03	1	0.12	0.07	256023	36
NETHER	SCDAP/RELAP5/2	14000	CONVEX C220S	222000	0.025	.01	0.3	0.05	2.85 10 ⁻²	491912	237
SWEDEN	SCDAP/RELAP5/2	18000	SUN 4/330	100800		0.025		0.5	0.14	125755	176
TAIWAN	MELCOR V1.8.0	18000	VAX 6310	21260	0.5	0.4	1	1	0.94	19160	39
U.K.	SCDAP/RELAP5/2	18000	SUN 4/330	270000	0.2	.025	1	0.025	0.043	416721	416
U.S.A.	MELCOR/V1.8EA	18000	VAX 8700	22197	1.5	0.3	5	1.5	0.8	22119	28

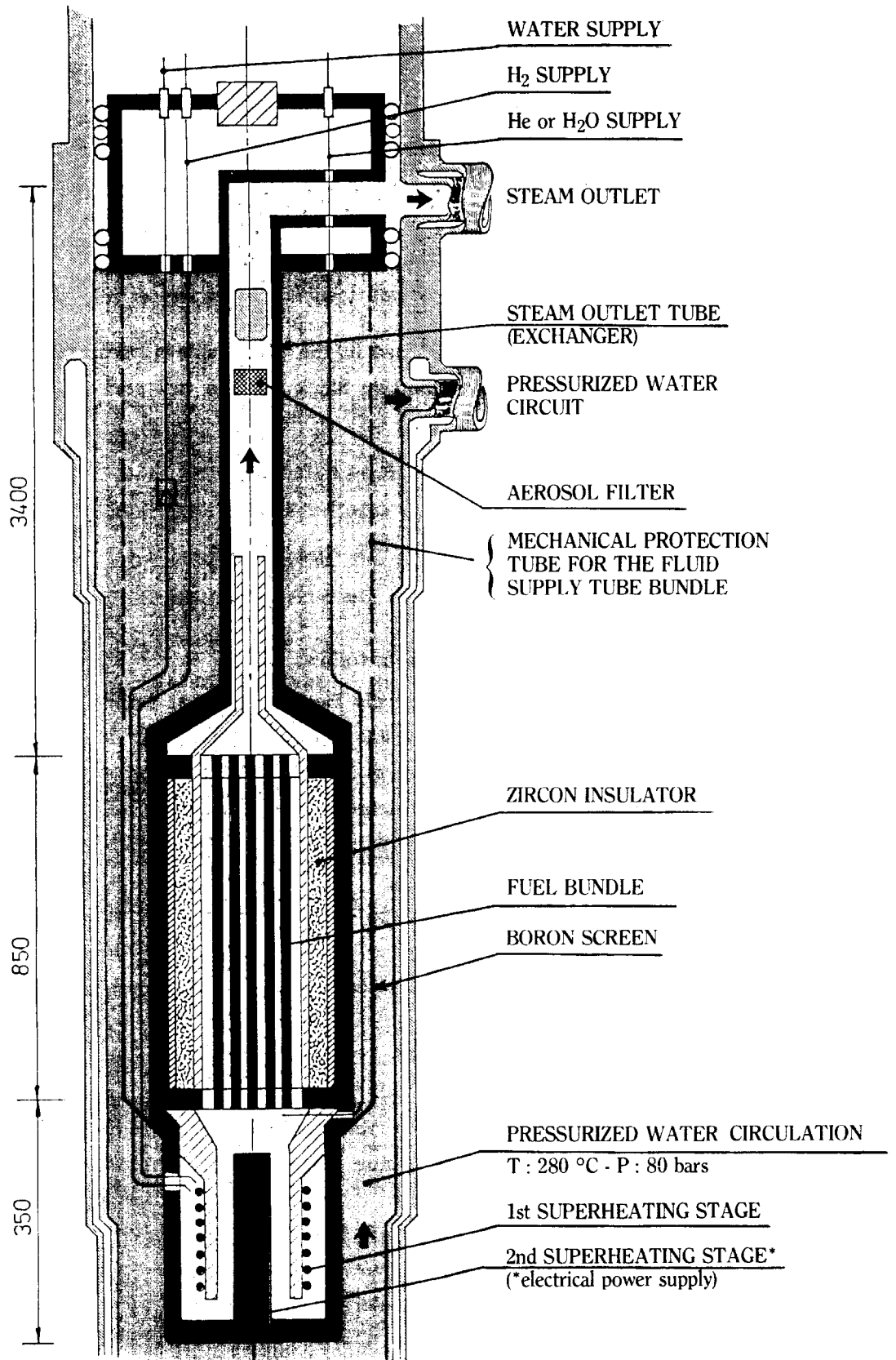
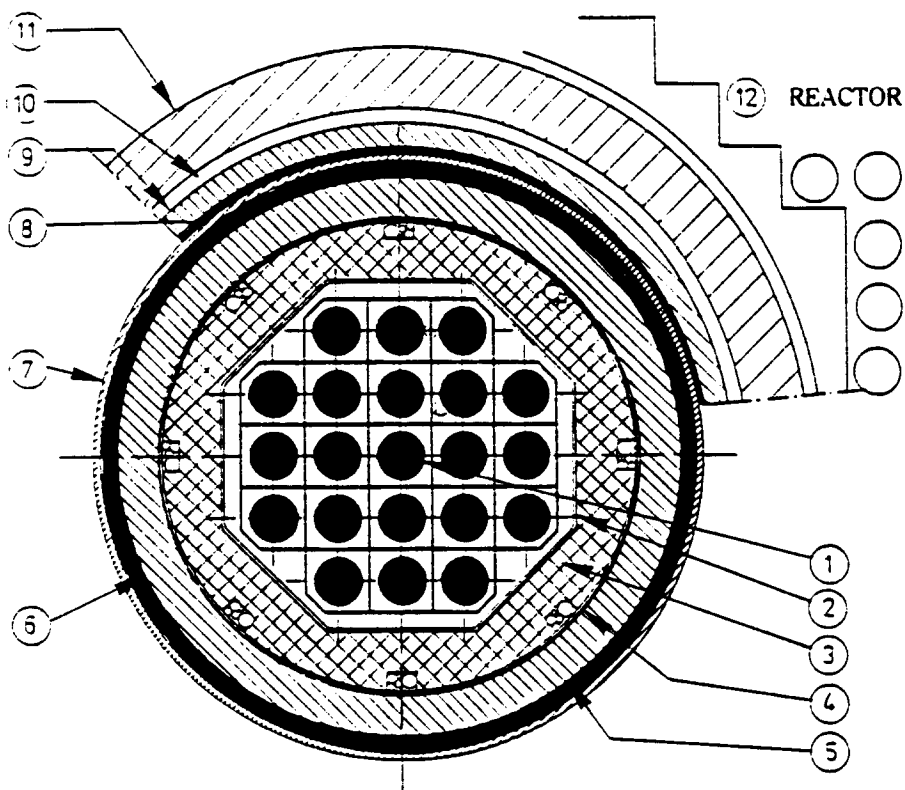


FIG. 1 : TEST STRINGER



	DESIGNATION (materials)	Int. radius (mm)	Ext. radius (mm)	Thickness (mm)
Test device pressurized water loop	1 21 pins test bundle : UO ₂ , Zr			
	2 Octagonal tube : Zircaloy	34.75	35.35	0.6
	3 Thermal insulation : porous ZrO ₂	35.35	47.	
	4 Dense zirconia flame sprayed layer	47.	48.	1.
	5 Test device tube : stainless steel	48.	56.	8.
	6 Pressurized water : - H ₂ O, 80 bar, 260°C	56.	59.25	3.25
	7 Neutronic screen : boron steel	59.25	60.75	1.5
	8 Pressurized water : - H ₂ O, 80 bar, 260°C	60.75	62.	1.25
Cell in pile	9 Inconel pressure tube	62.	67.	
	10 Vacuum	67.	70.	3.
	11 Zircaloy safety tube	70.	82.	12.
Reactor	12			

FIG. 2a : BUNDLE CROSS SECTION

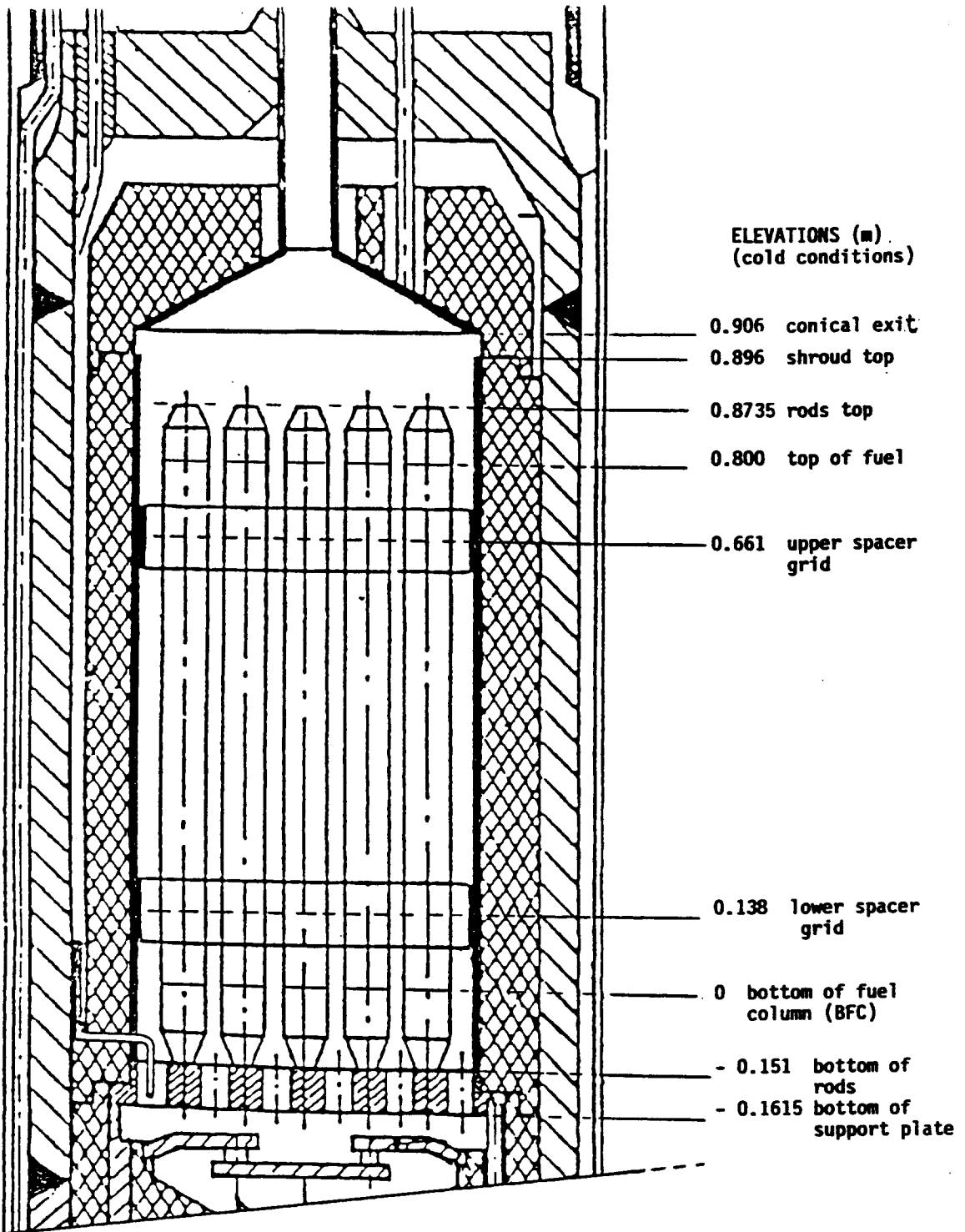


FIG. 2b : LONGITUDINAL VIEW OF THE BUNDLE

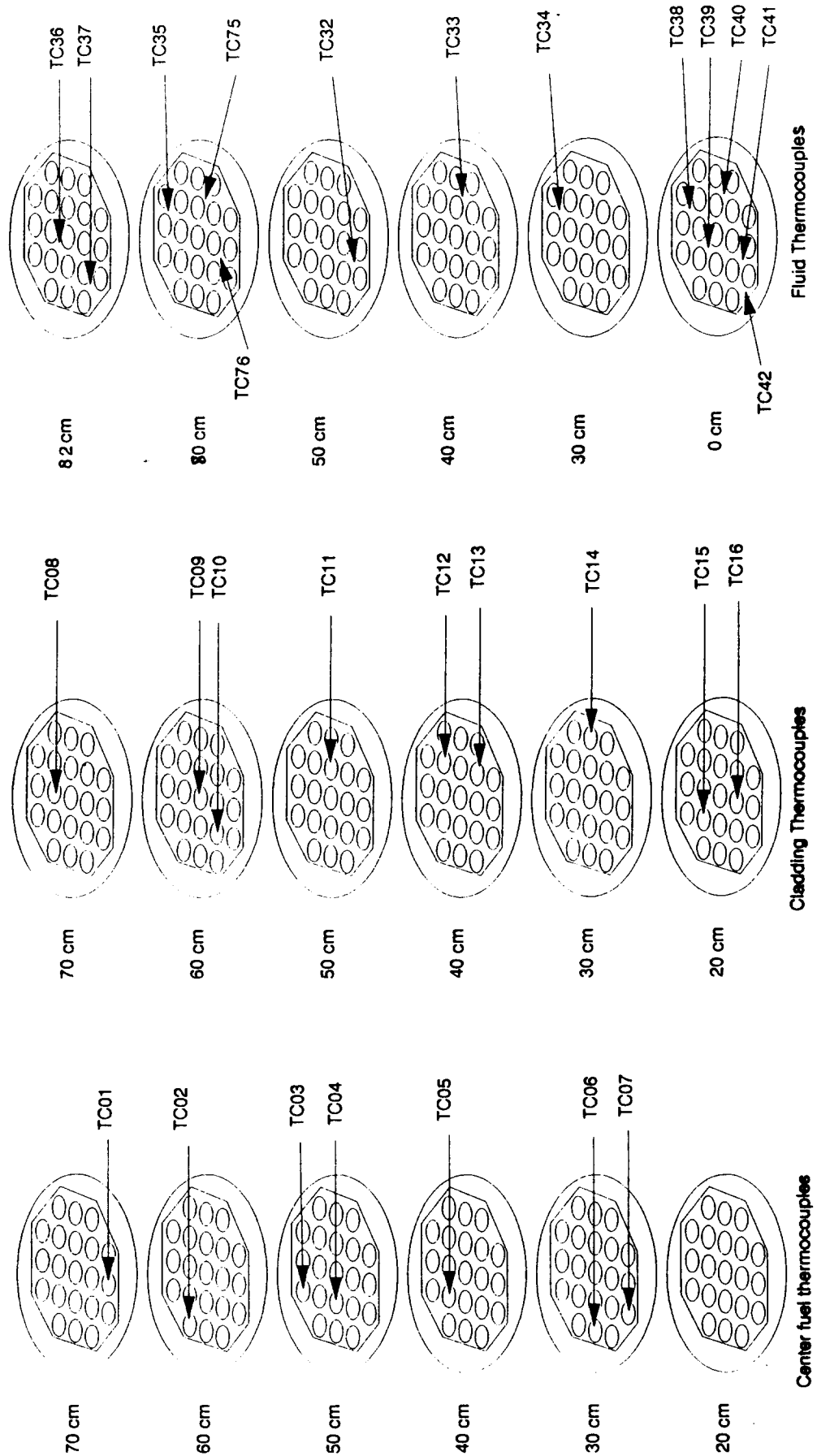


FIG. 3 : THERMOCOUPLE LOCATIONS

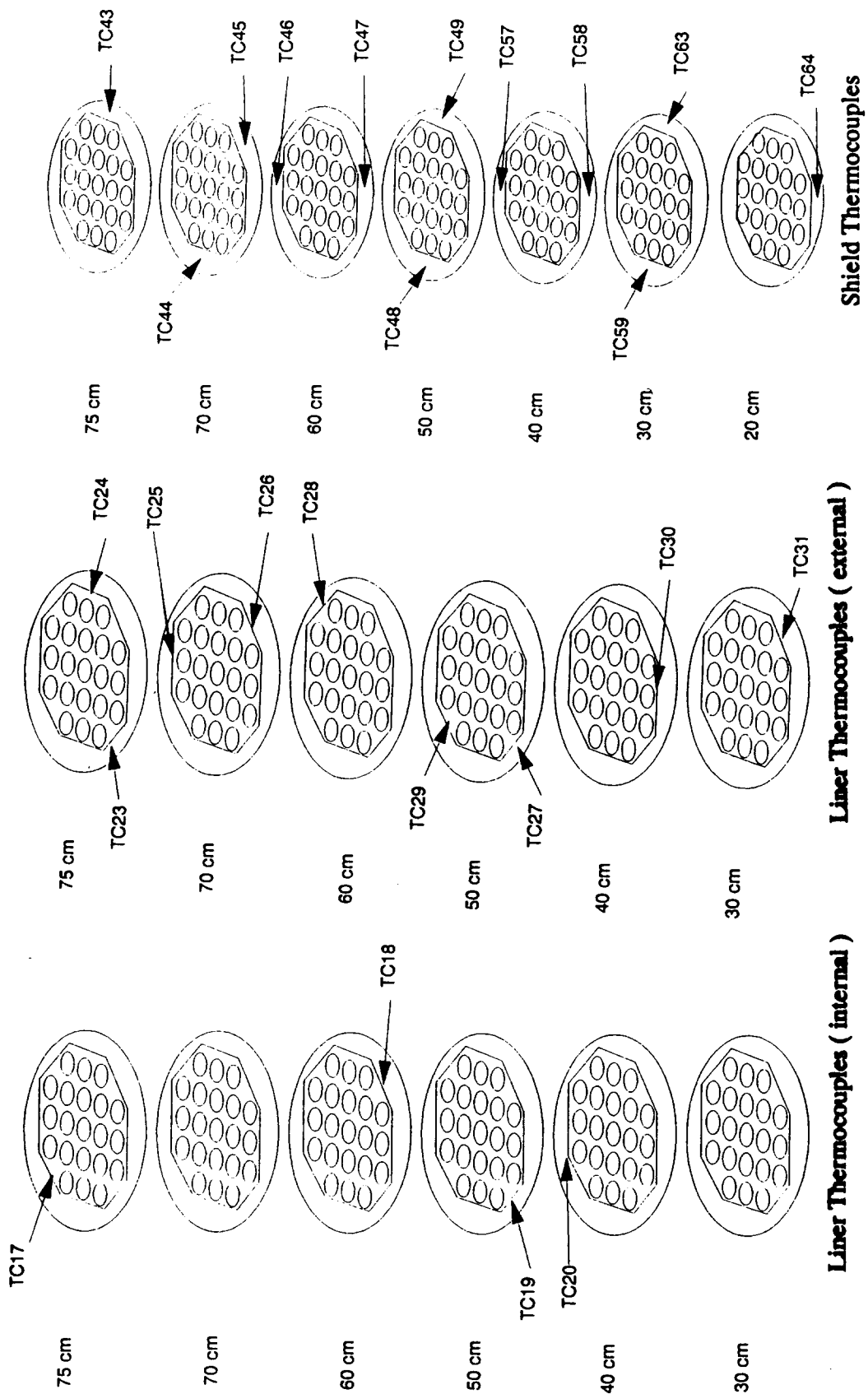


FIG. 4 : SHROUD THERMOCOUPLES

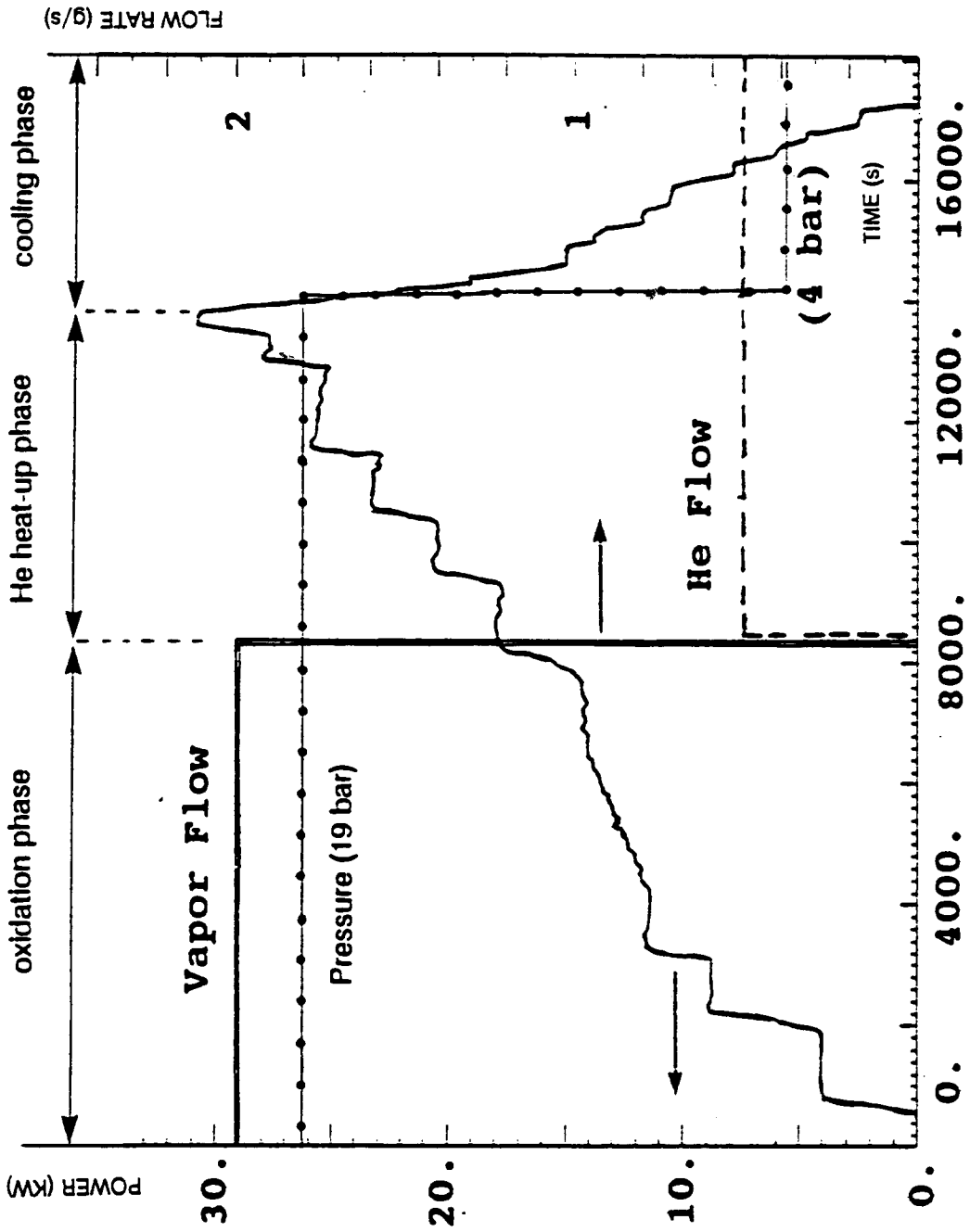


FIG. 5 : EXPERIMENTAL SCENARIO

**PHEBUS SFD B9+
SWITCH H2O/HE**

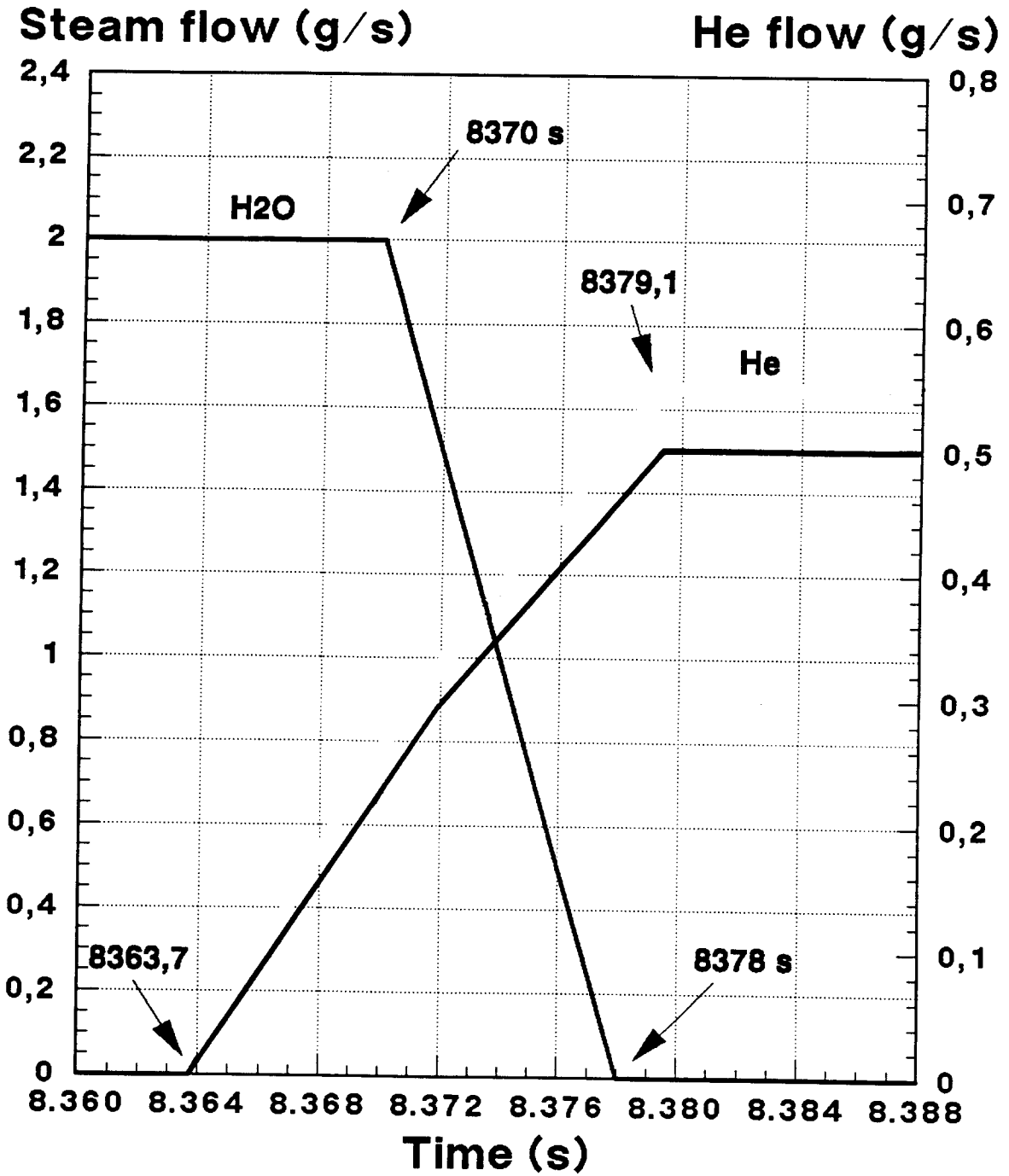


FIG. 6 : STEAM TO HELIUM SWITCH

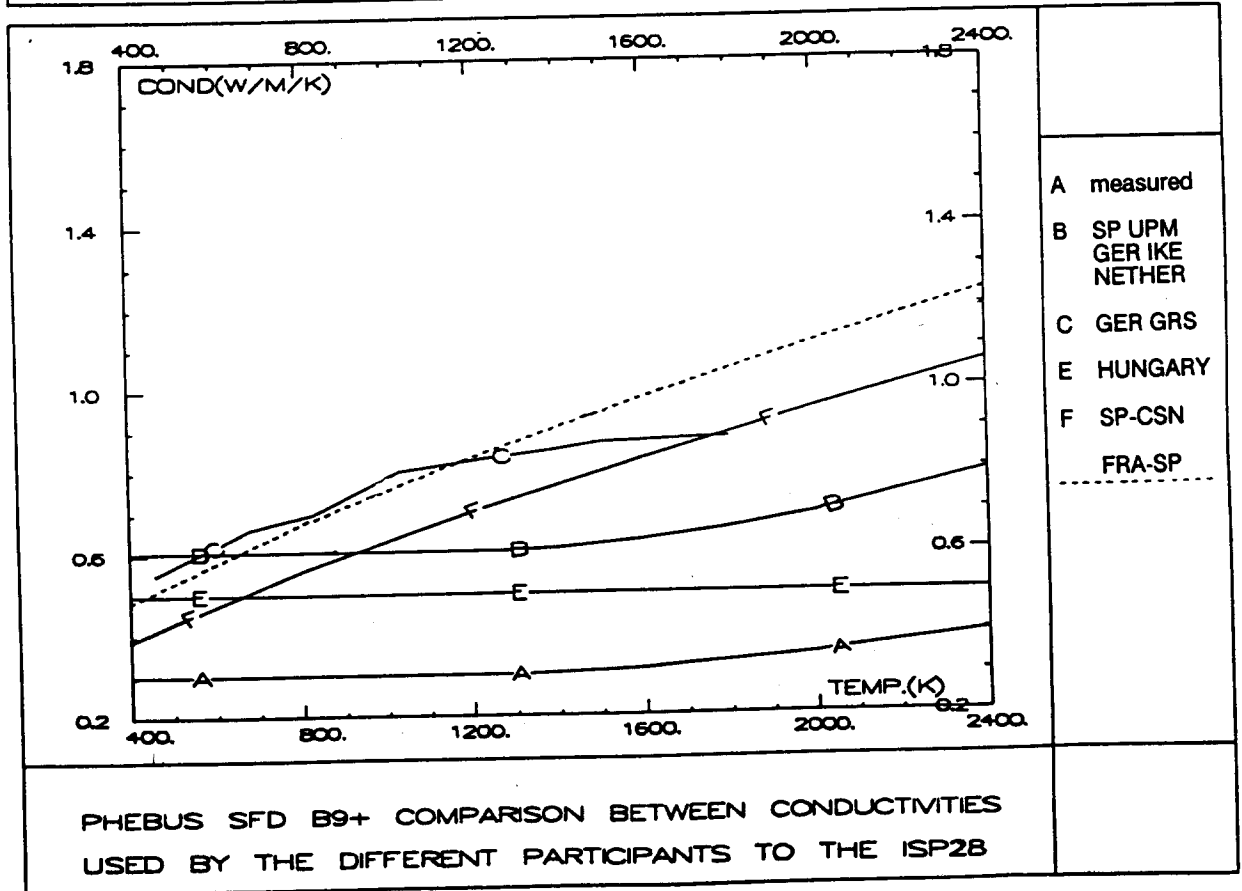
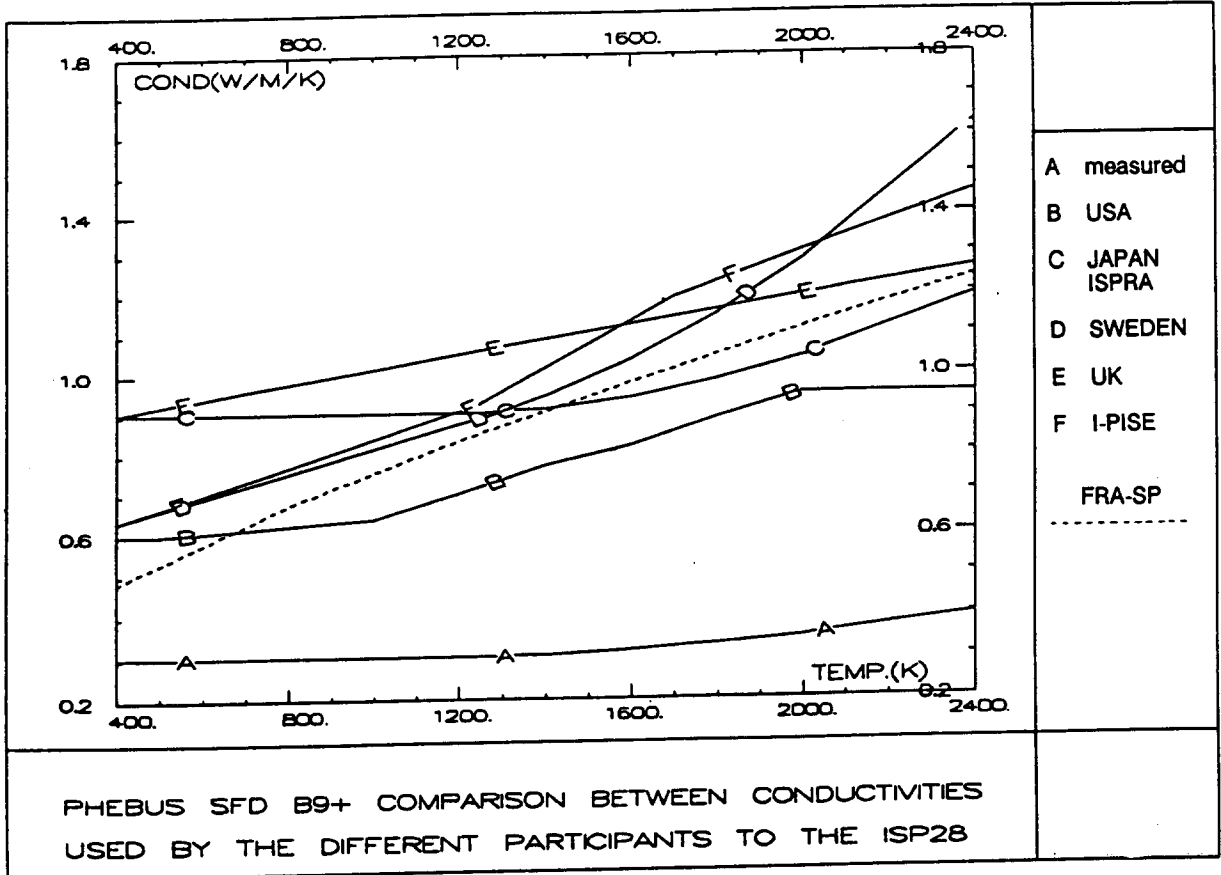


FIG. 7 : POROUS ZRO2 CONDUCTIVITY

Rod numbering and radial power distribution in the bundle

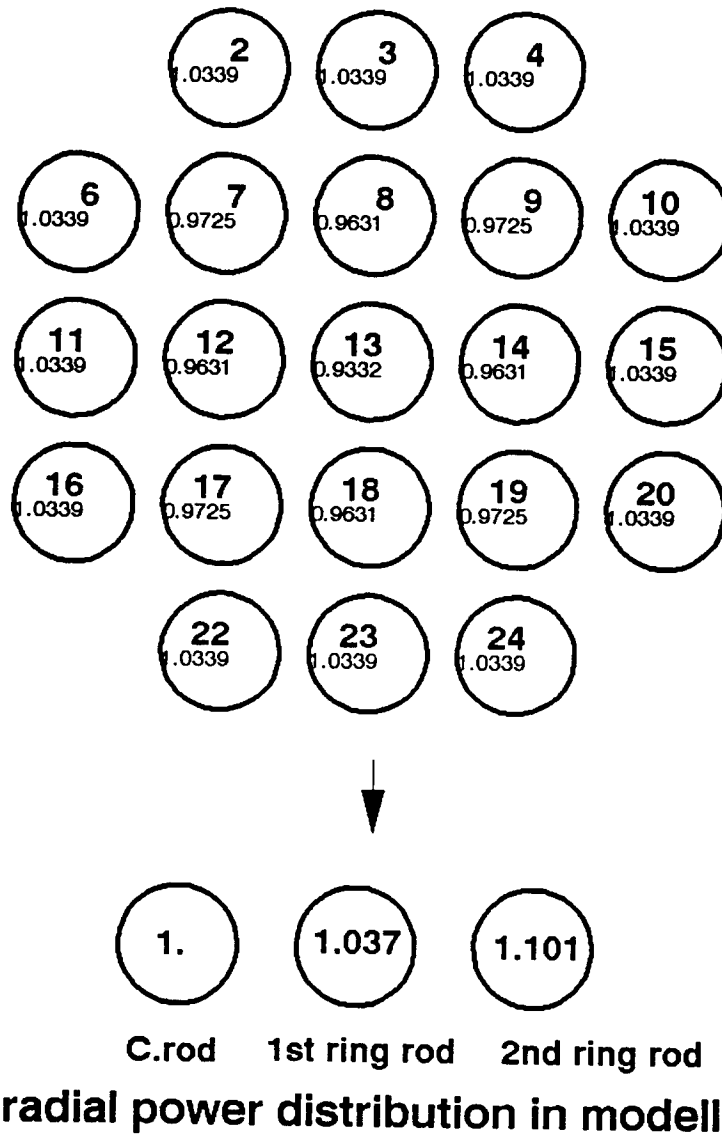


FIG. 8 : RADIAL POWER PROFILE

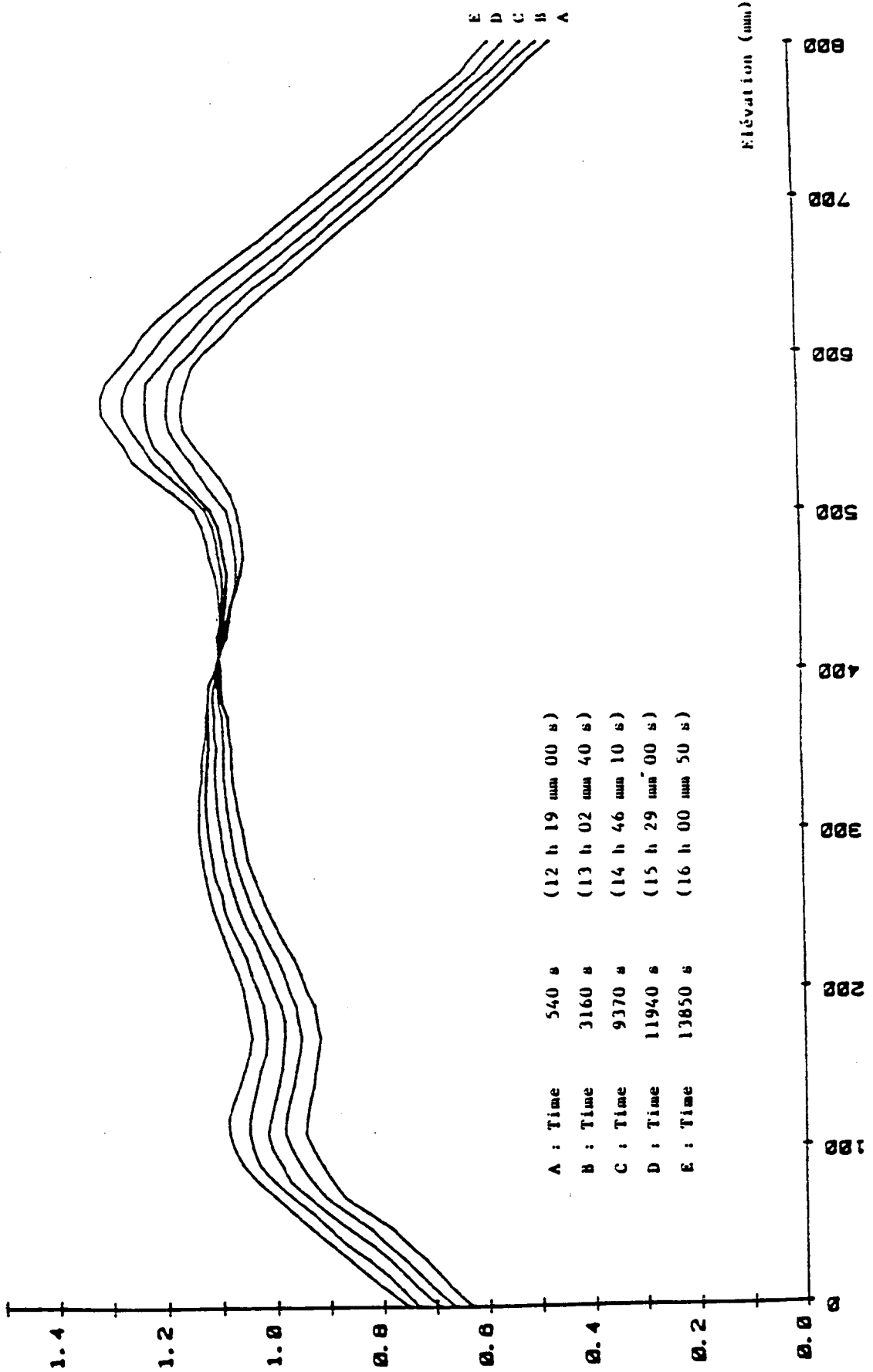


FIG. 9 : AXIAL POWER PROFILE

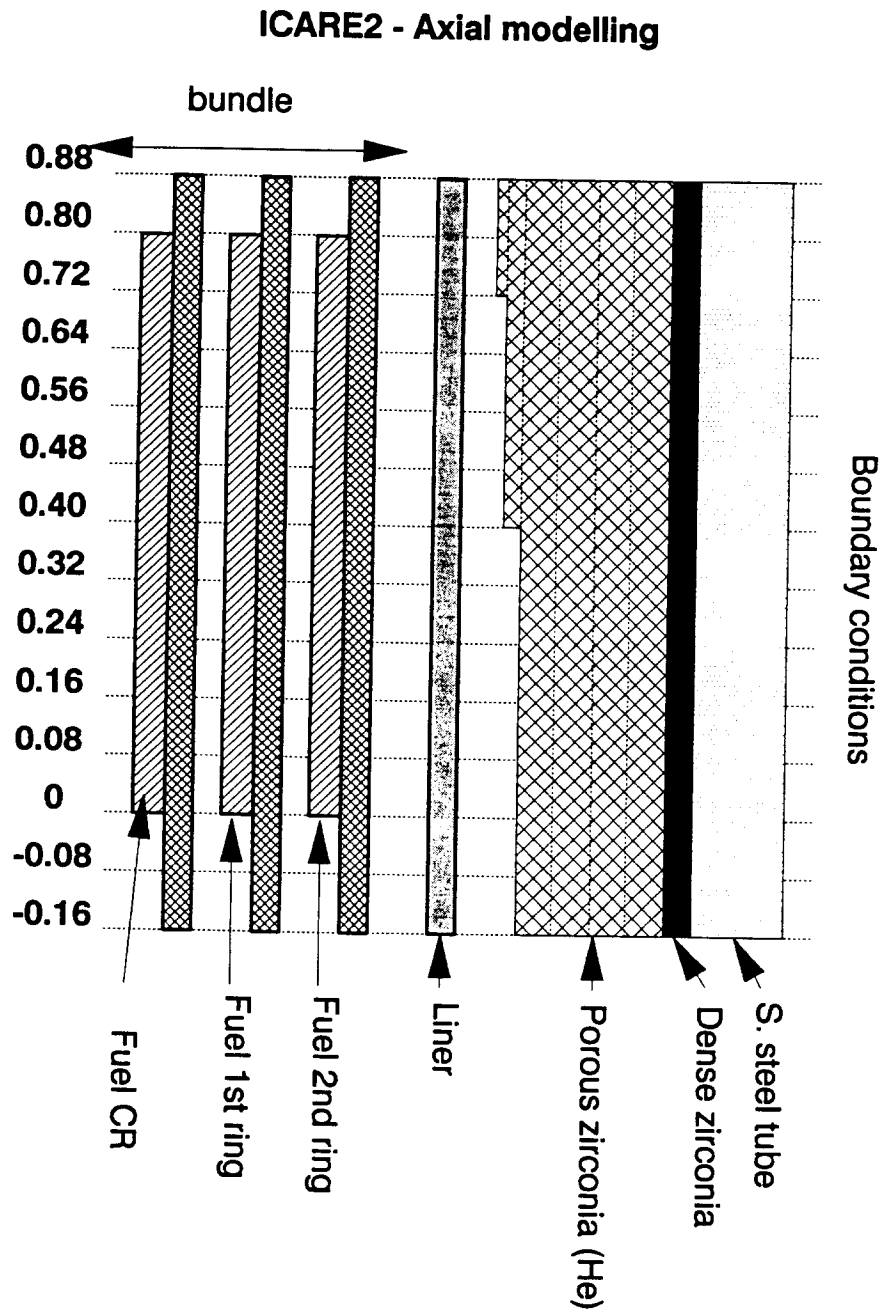


FIG. 10 : BUNDLE MODELLING

PHEBUS TEST B9+

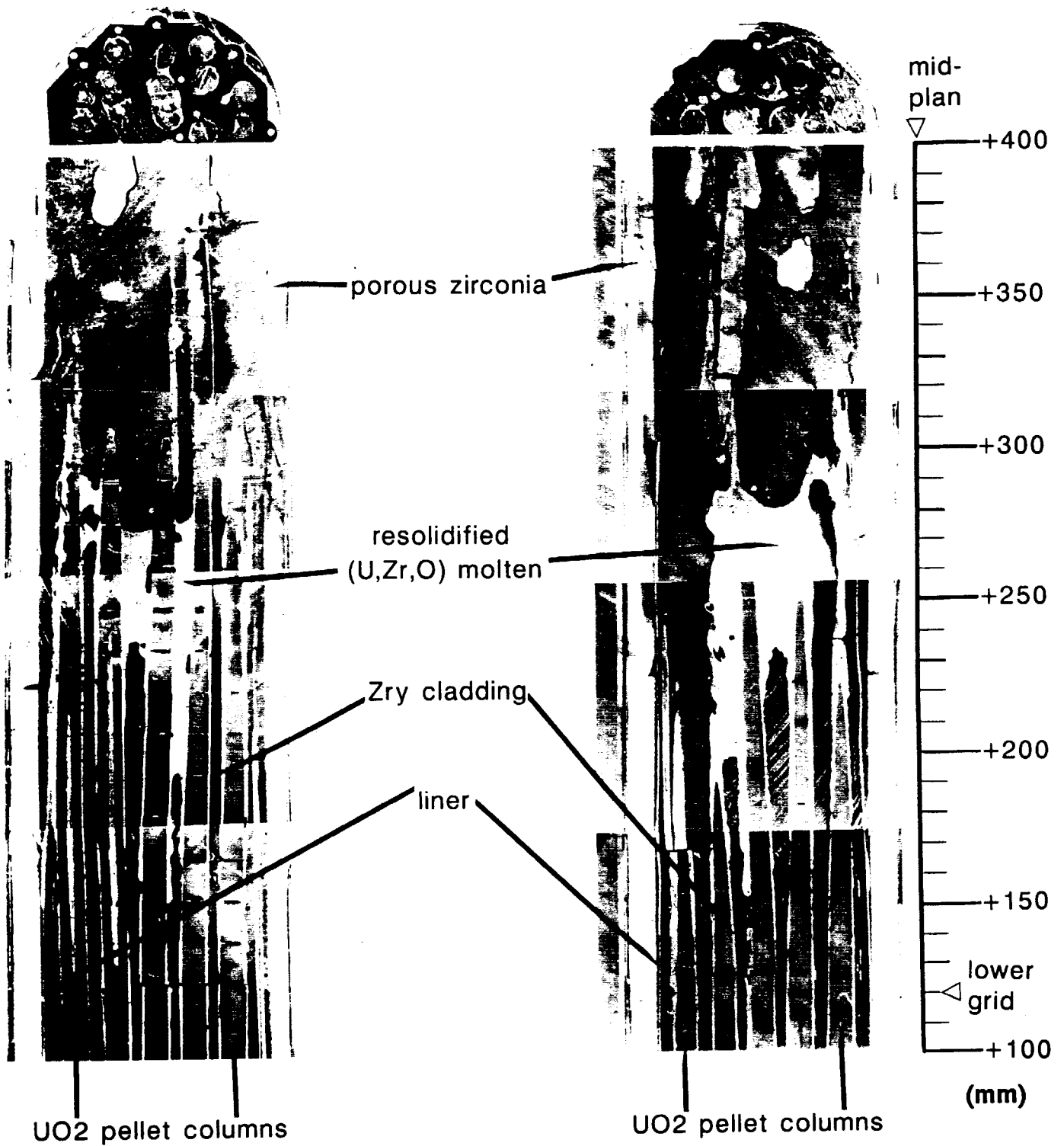
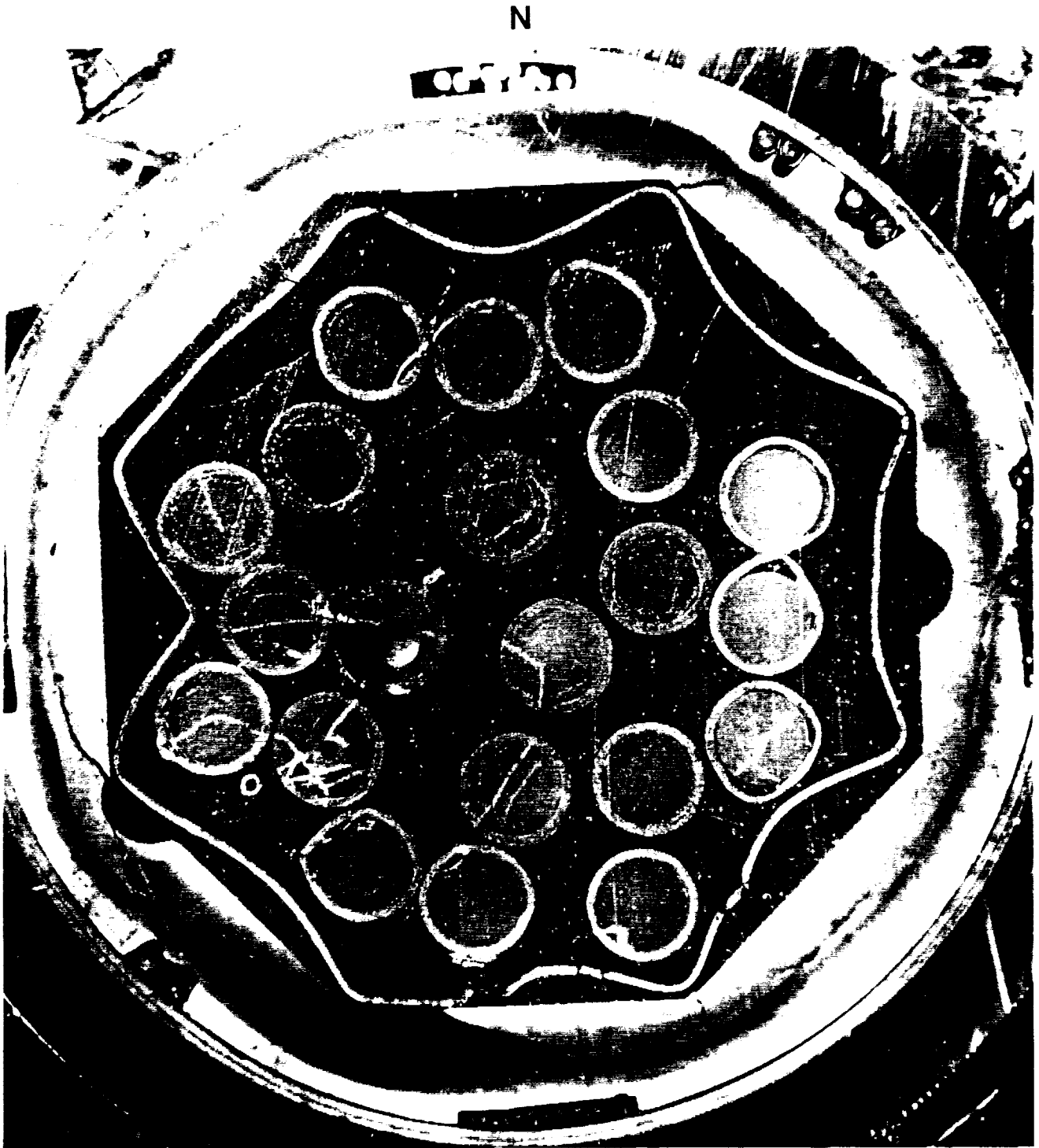


Fig. 11 : Axial cut of the lower end of bundle



10mm

Fig. 12 : Cross cutting at elevation 0.76m

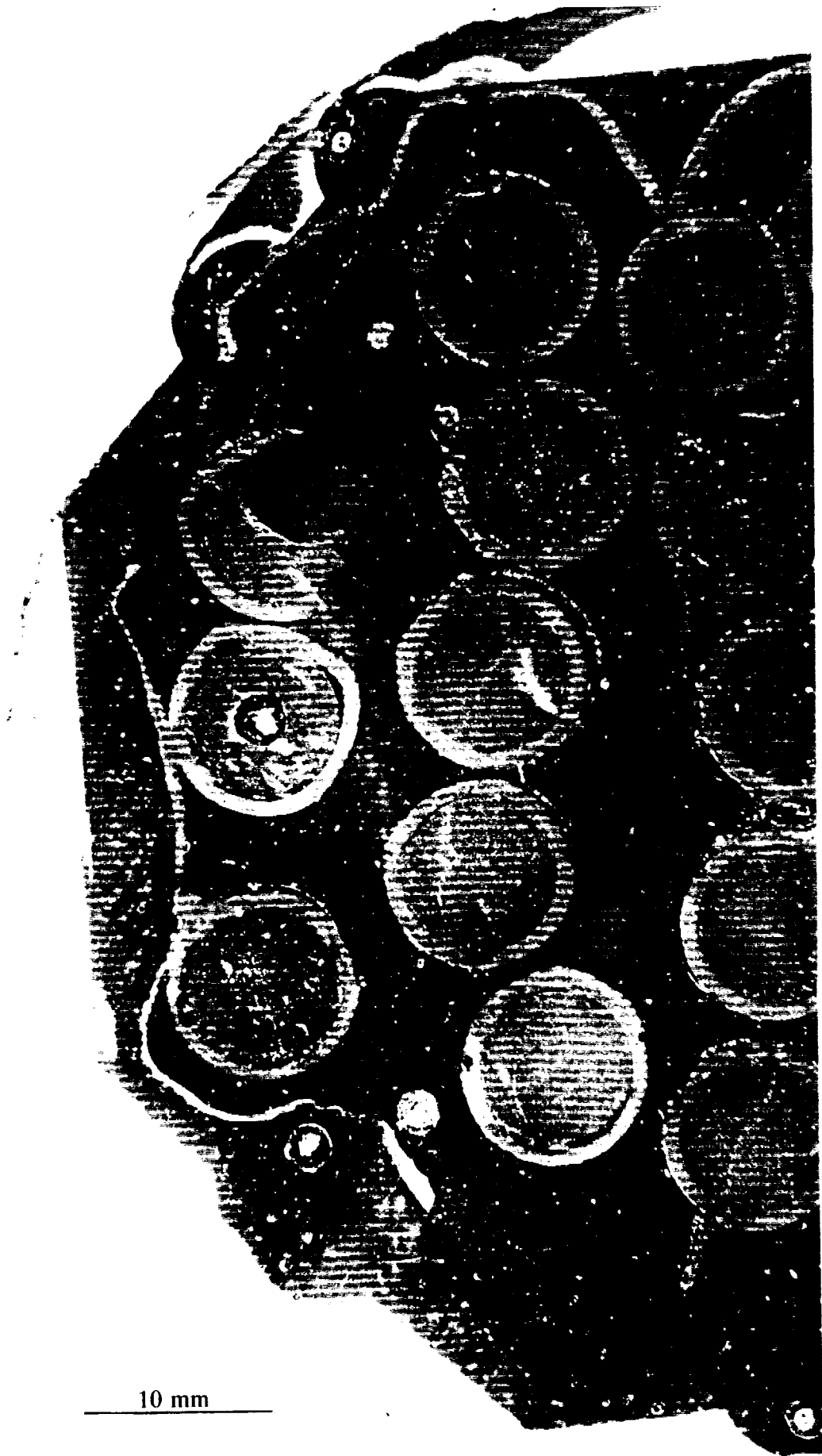


Fig. 13a : Cross cutting at elevation 0.58m

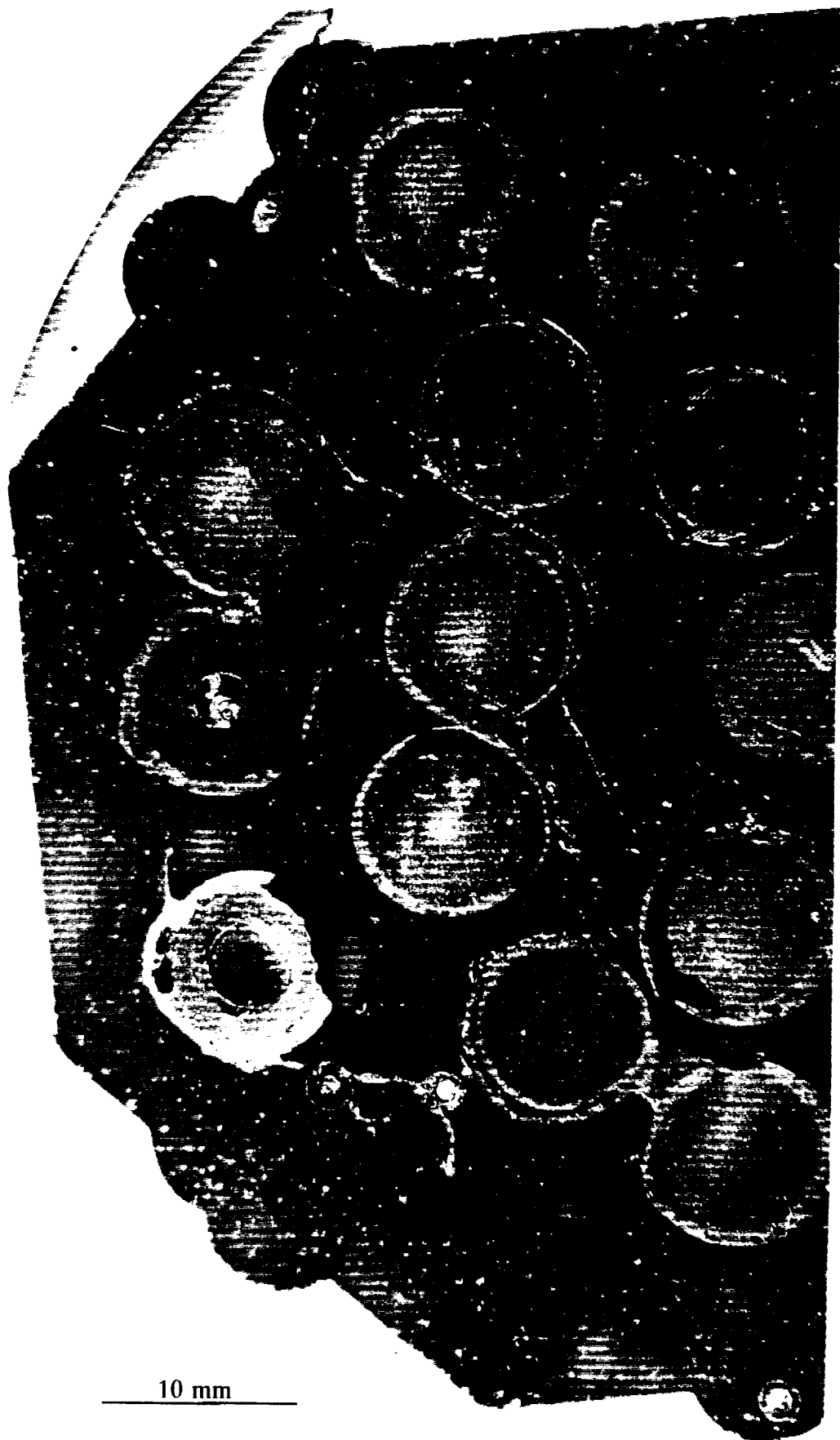


Fig. 13b : Cross cutting at elevation 0.52m

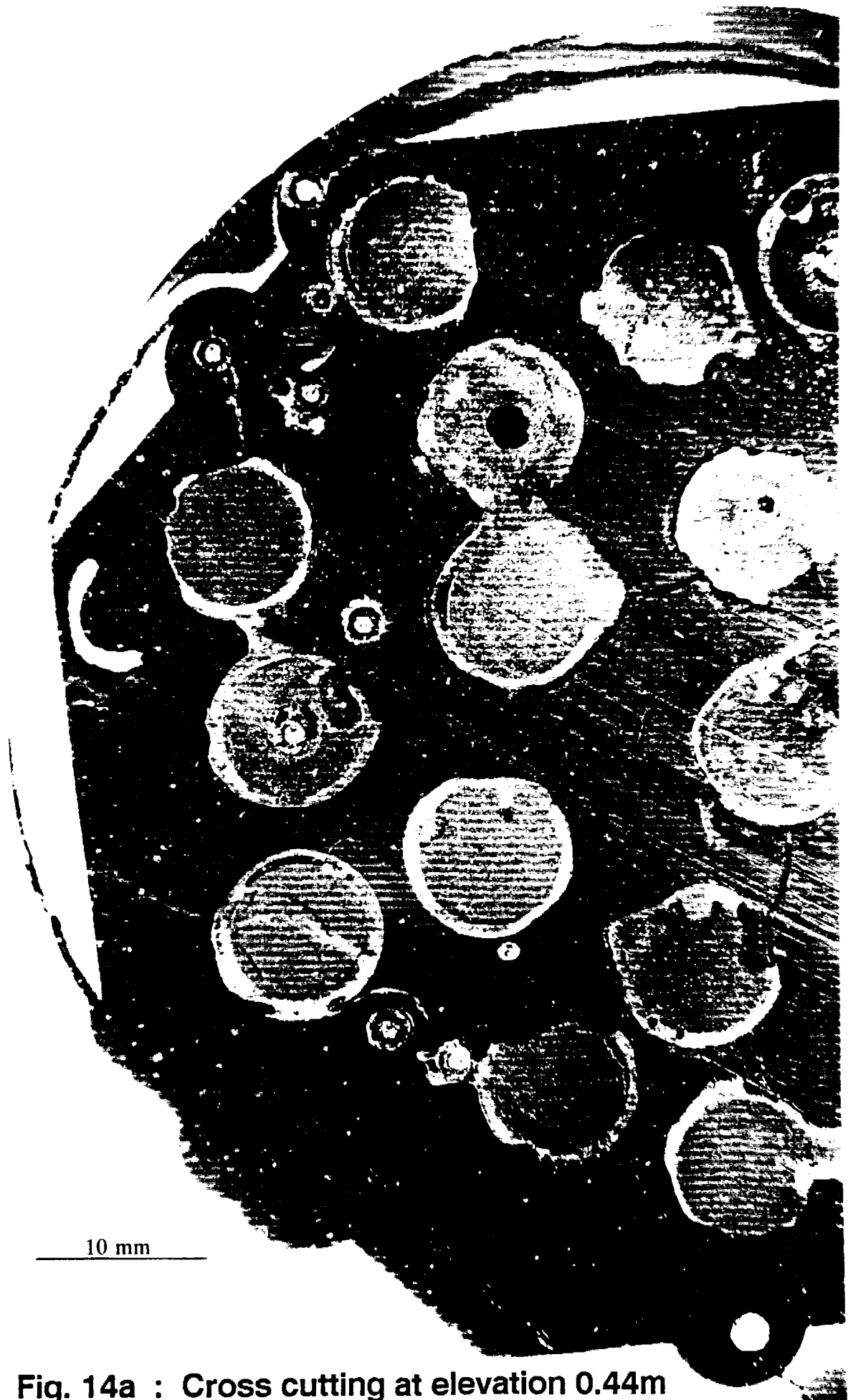


Fig. 14a : Cross cutting at elevation 0.44m

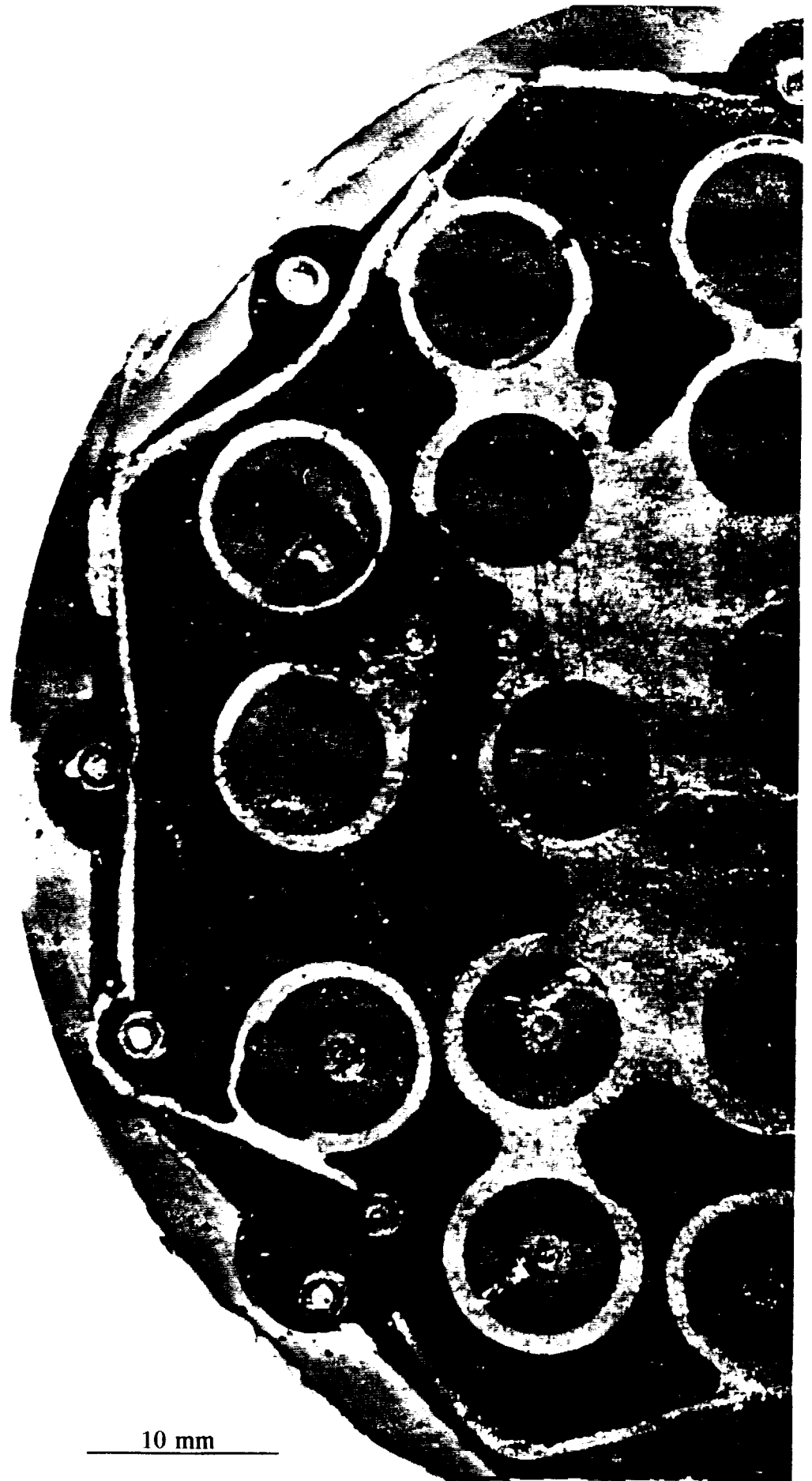


Fig. 14b : Cross cutting at elevation 0.26m

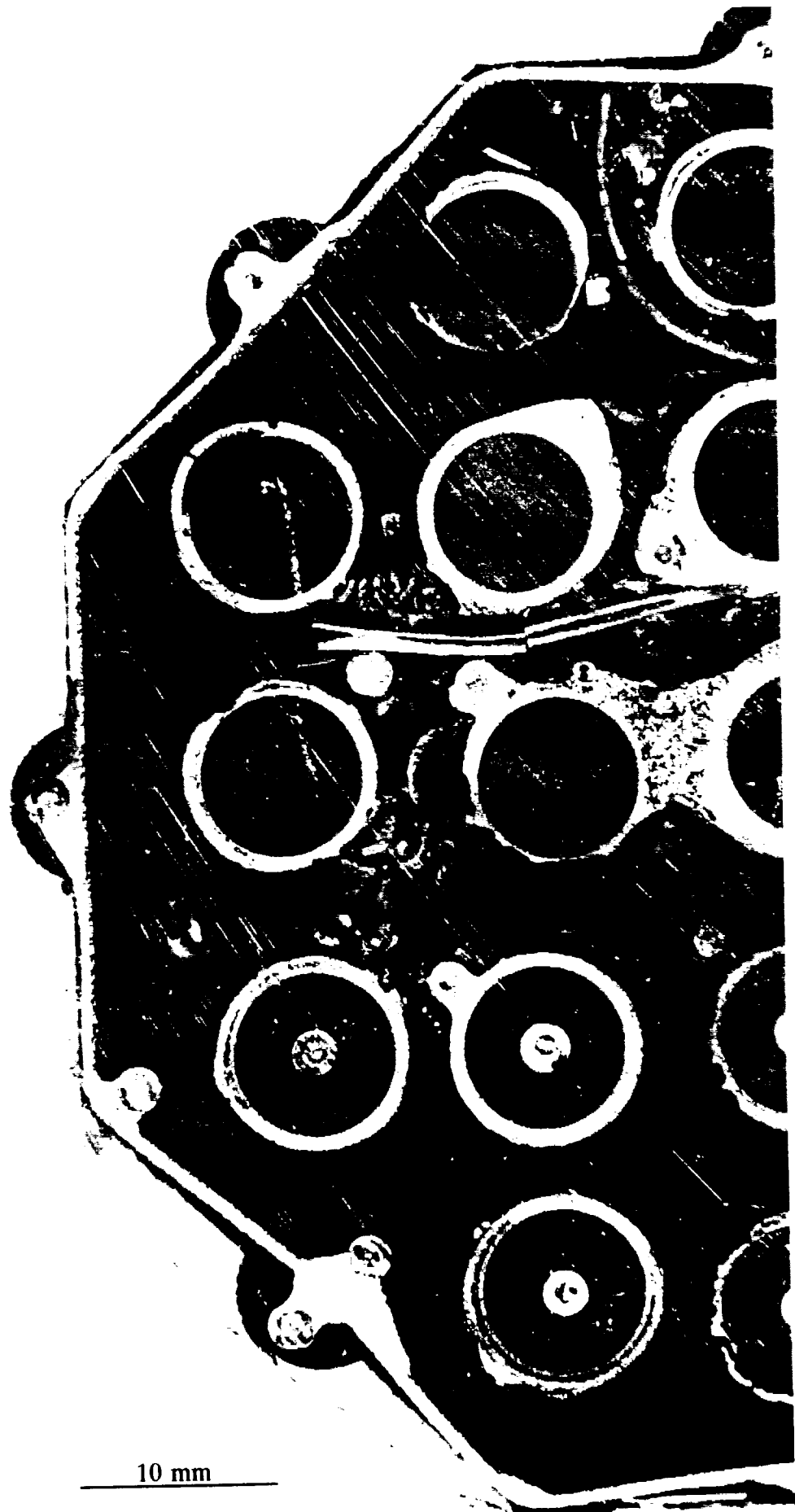
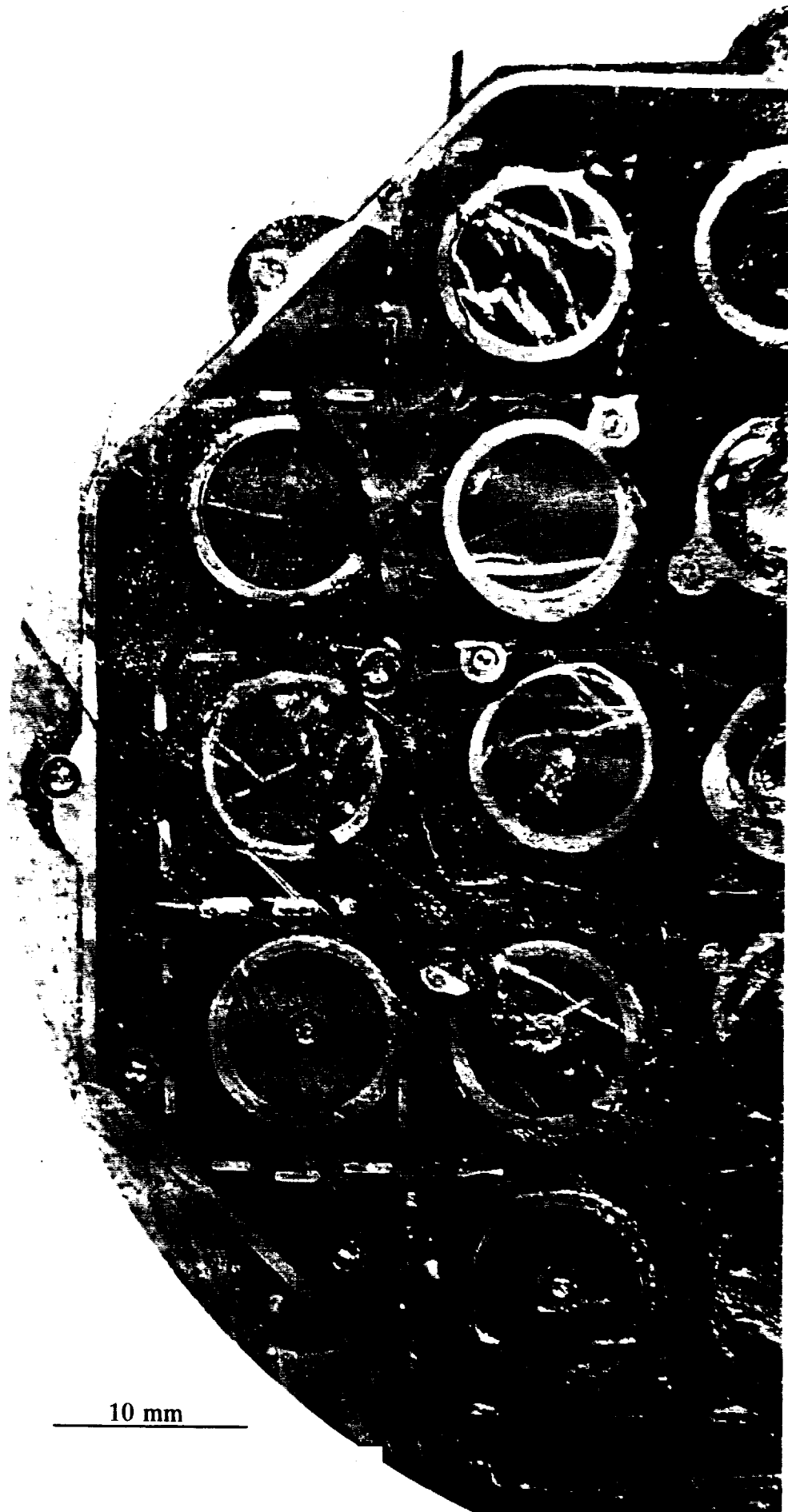


Fig. 15a : Cross cutting at elevation 0.17m



**Fig. 15b : Cross cutting at elevation 0.14m
(Lower Spacer-Grid Location)**

N

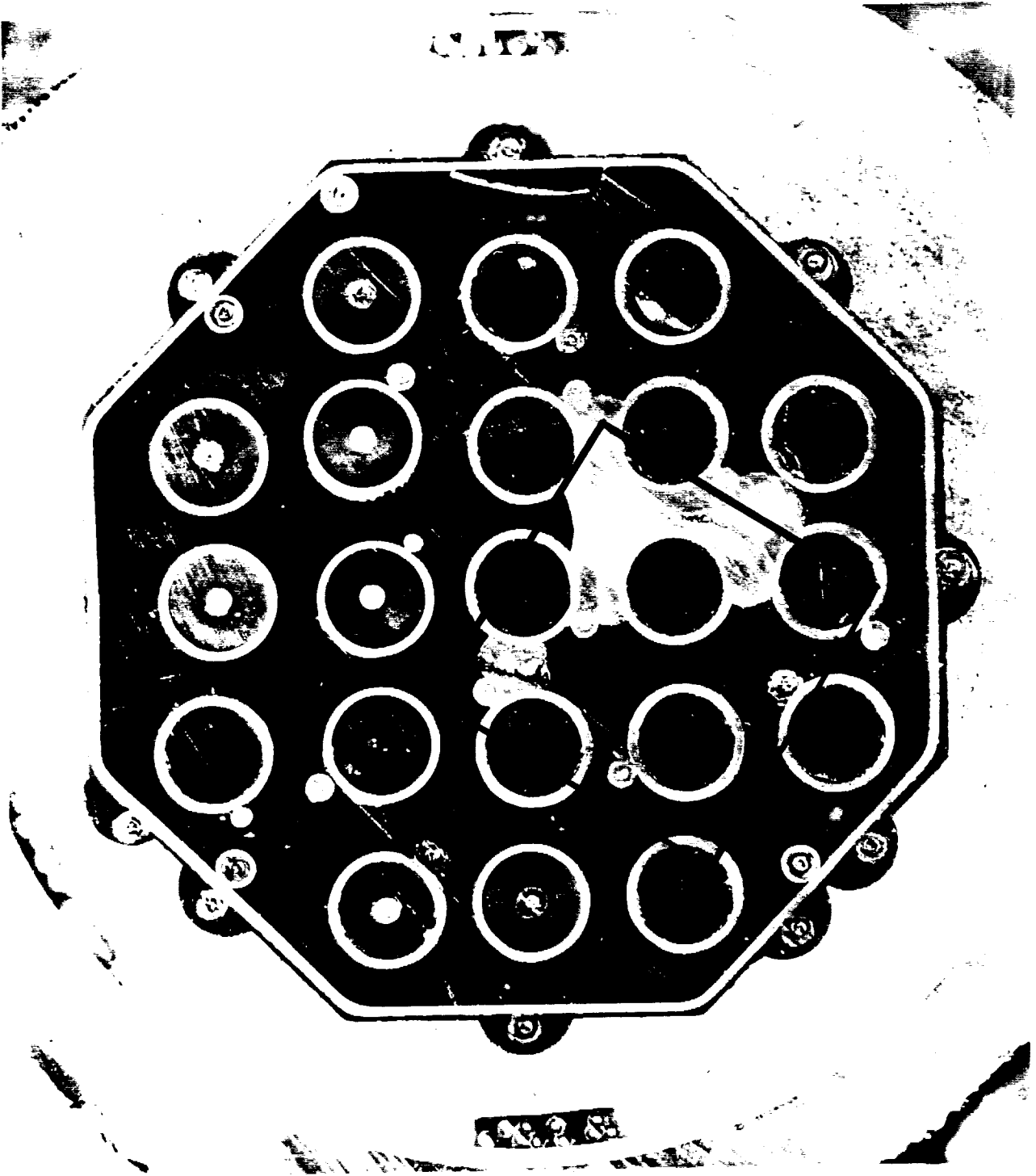


Fig. 16 : Cross cutting at elevation 0.05m

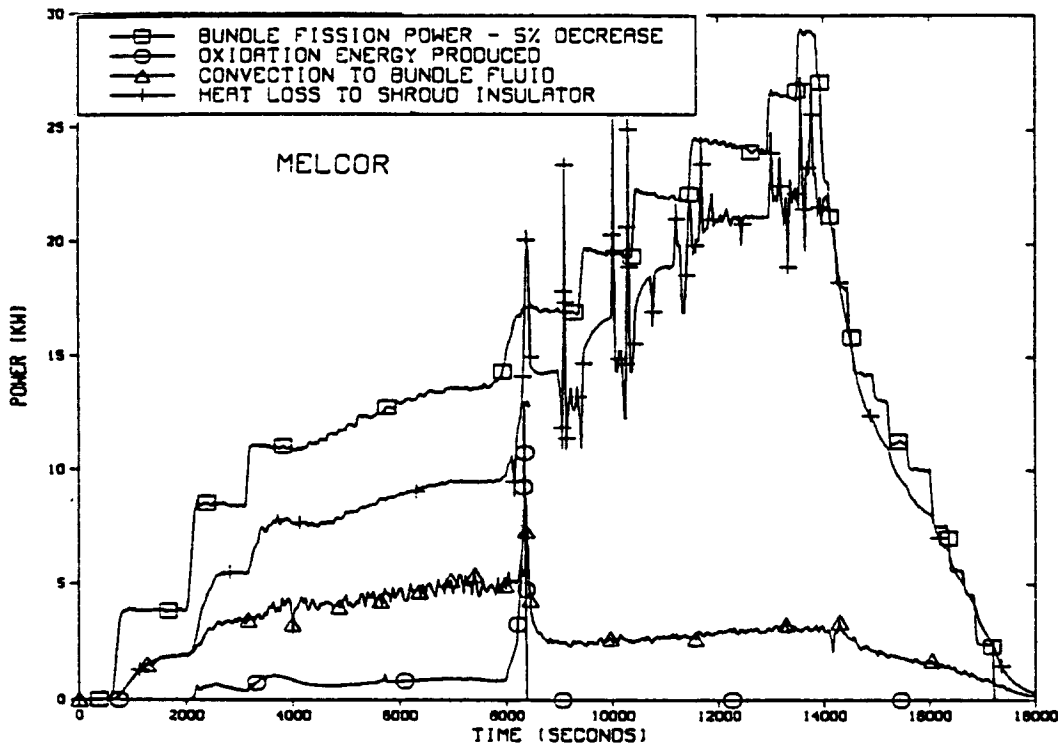


FIG. 17a : BUNDLE POWER DISTRIBUTION
MELCOR CALCULATION (USA).

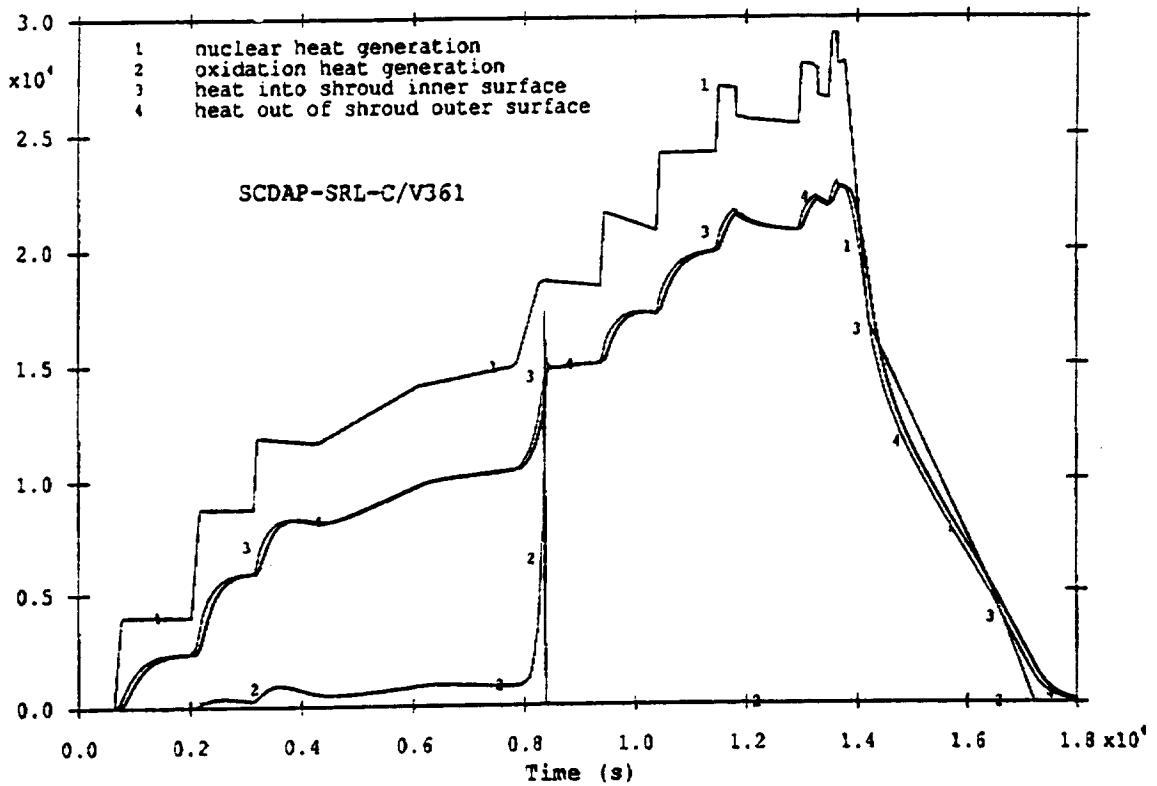
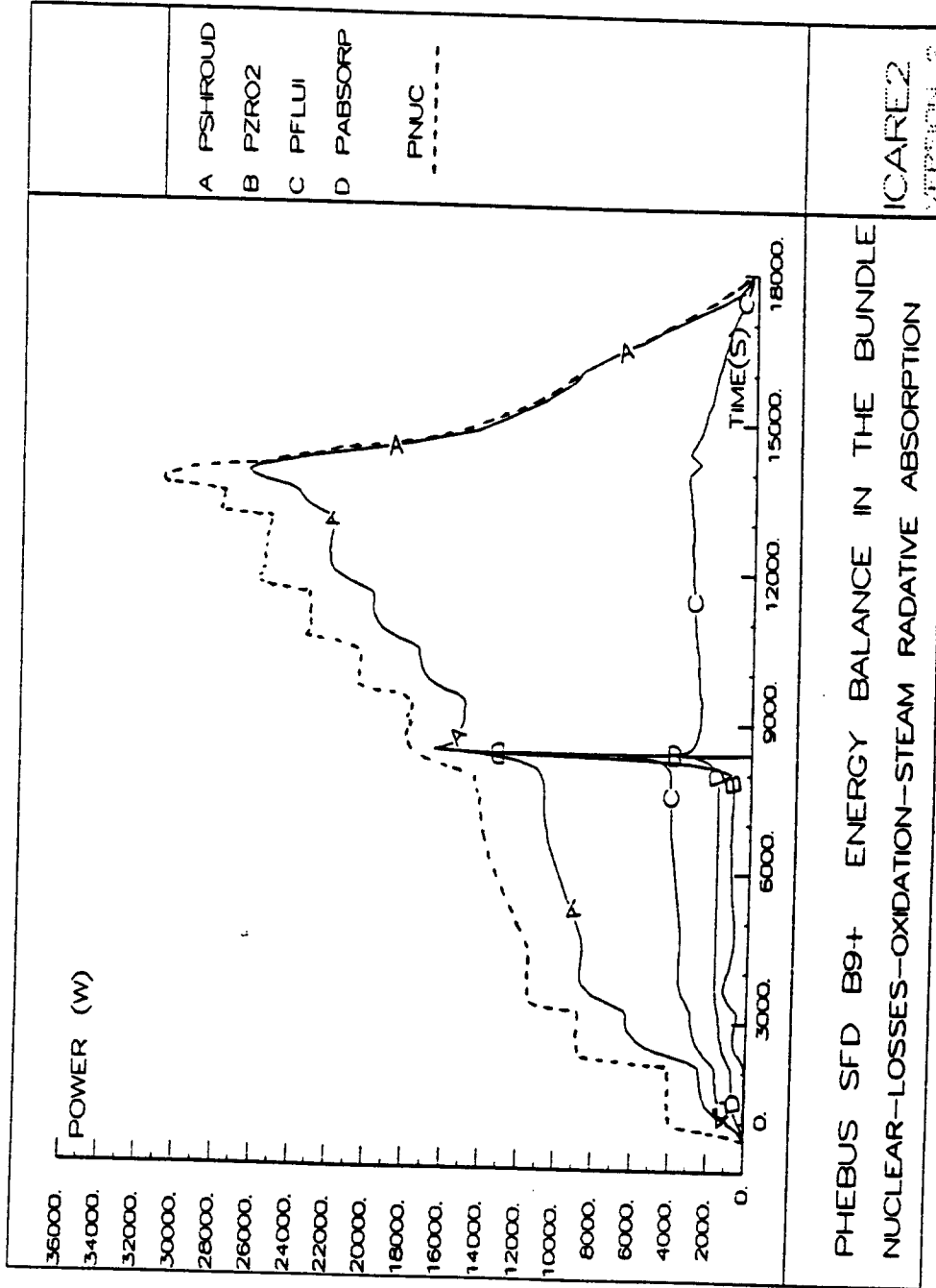


FIG. 17b : BUNDLE POWER DISTRIBUTION
SCDAP/R5/Mod 2 CALCULATION (UK)



PHEBUS SFD B9+ ENERGY BALANCE IN THE BUNDLE
 NUCLEAR-LOSSES-OXIDATION-STEAM RADATIVE ABSORPTION

ICARE2
 VERSION 2

FIG. 17c : BUNDLE POWER DISTRIBUTION
 ICARE2V2p CALCULATION (FRA-SP)

DISTRIBUTION LIST
ISP 28 PARTICIPANTS

ISP 28 PARTICIPANTS	ORGANIZATION	NAME
CZECHOSLOVAKIA	NRI/REZ	F. PAZDERA M. VALACH L. BELOVSKY
FRANCE and SPAIN	CEA/IPSN Spanish PHEBUS Consortium	S. BOURDON P. VILLALIBRE
GERMANY	GRS/GARCHING	A. BALL K. TRAMBAUER
GERMANY	IKE/STUTT GART	K.D. HOCHE S. KRETSCHMER K. MULLER
HUNGARY	C.R.I.P./BUDAPEST	G. GYENES B. TOTH P. VERTES
E.C.	ISPRA/JRC	J.A. CAPITAO I. SHEPHERD
ITALY	ENEA and PISE Univ.	G. FRUTTUOSO F. ORIOLO
JAPAN	JAERI and CSK Corp.	K. HASHIMOTO K. SODA E. MATSUMOTO
NETHERLANDS	E.C.N./PETTEN	L. WINTERS
SPAIN	U.P. Madrid - C.T.N.	S.A. ENCISO J.V.L. MONTERO J.G. PINDADO C.S. SANTAMARINA
SPAIN	Spanish PHEBUS Consortium and CSN	A. ALVAREZ J. MARTINEZ
SWEDEN	Studsvik Nuclear/NYOPKING	J. ERIKSSON
TAIWAN	INER/AEC/LUNG-TAN	S.K. CHENG L. KAO
UNITED KINGDOM	AEA-Tech./WINFRITH	T.J. HASTE J.N. LILLINGTON A.J. LYONS
UNITED STATES	SANDIA Nat. Lab. and NRC	G.M. MARTINEZ

PARTICIPANTS OUT OF THE FRAMEWORK OF ISP 28

KOREA	KAERI/DAEDUK-DANJI	H.P. PARK Y. JIN C.K. PARK
POLAND	IAE/OTWOCK/SWIERK	S. STEMPNIEWICZ P. MARKS
RUSSIA	IBRAE/NSI	A. KIESELEV G. SAMOLIOVA